THE FORMATION
OF ACOUSTICAL
FIELDS
IN OCEANIC
WAVEGUIDES

Nizhny Novgorod
1995

THE FORMATION OF ACOUSTICAL FIELDS IN OCEANIC WAVEGUIDES

Collected scientific papers

The papers collected in this book are focused on the interrelated problems of low-frequency acoustic fields synthesis and analysis in oceanic waveguides. Wave fields formed by the underwater sources of different origin (localized sources and antennas, regular and random scatterers, random inhomogeneities of the oceanic medium itself) are examined to develop new approaches and techniques of remote acoustic sensing of the ocean, acoustic tomography techniques included. The results of theoretical studies and experiments carried out both in laboratory and in the ocean are presented and discussed. Particular attention is paid to the reconstruction of oceanic inhomogeneities and estimating the related performances of underwater receiving systems aimed at practical applications.

The book is intended for the researchers and students engaged in the fields of underwater acoustics, wave propagation, remote sensing and antennas.

CONTENTS

PREFACE

The collected papers present recent works of the leading researchers engaged in the area of acoustic field formation in oceanic waveguides. Considerable interest in such phenomena arises due to their numerous applications in remote acoustic probing and acoustic tomography of the ocean. In these applications, it is necessary to solve a number of interrelated problems of acoustic field synthesis, sound diffraction and scattering by various inhomogeneities in underwater channels, inverse problems of the ocean diagnostics, and the problems aimed at developing adequate methods and algorithms of space-time acoustic signal processing in underwater antenna systems.

It should be mentioned that the term "the formation of fields" included in the title is not widely used in acoustics and has a more optical origin. We employ this term here to emphasize the intrinsic relationship and analogies of adaptive ocean acoustics discussed in the book with adaptive optics. The noted analogies permit us to hope that these areas will enrich each other. Thus, study of the formation of ocean acoustic fields as the methods of synthesis and analysis of wave fields adapted to the conditions of underwater sound propagation and scattering may be interpreted in a wider sense as the development of hydroacoustic information/measuring systems.

In general, the topics covered in the book may be divided into three key parts. First, the problems related to the sound fields synthesis and optimum source excitation for remote sensing of the ocean at different spatial scales. Second, the problems of acoustic fields diffraction and scattering by the ocean inhomogeneities, random and regular ones included. And, finally, the problems of sound fields analysis performed by antenna systems of underwater observation. For solution of all these problems, it is necessary to take into account the intrinsic features of sound propagation in refractive oceanic waveguides.

Particular attention of the authors is focused on the problems of the reconstruction of oceanic medium inhomogeneities by using

tomographic techniques. The majority of them considered here were tested successfully by experiments both in laboratory and in the ocean.

Obviously, it is difficult to embrace all the particular related problems in several papers collected in one book. Meanwhile, we hope that the papers presented as well the references cited in them help a reader to form a general notion of the level of current research in this modern area of ocean acoustics.

Vladimir Talanov,

Vitaly Zverev

INTERRELATED PROBLEMS OF ACOUSTIC FIELD SYNTHESIS AND ANALYSIS IN LONG–RANGE OCEAN ENVIRONMENTS

E. Yu. Gorodetskaya, A. I. Malekhanov and V. I. Talanov

INTRODUCTION

The problems of acoustic field synthesis and analysis in long-range ocean environments are of particular interest in low--frequency acoustic sounding of the ocean and ocean acoustic tomography. The well-known intrinsic features of such environmets are (i) waveguiding propagation in underwater sound channels which leads to the finite discrete spectrum of acoustic field normal modes, and (ii) random (volume and/or surface) inhomogeneities of a channel which perturb the intermodal phase shifts and cause a degradation of modal covariances and acoustic coherence loss over long distances. These propagation features lead to substantial complexity of the indicated problems. On the other hand, the environmental constraints on the spatial spectrum of radiated/received wave fields permitted us to formulate an adaptive approach to antenna synthesis [1, 2]. The word "adaptive" is used here to indicate that the source antenna is optimized in dependence on the statistical effects of propagation and the criterion of signal processing in receiving array. In short, the problem of interest is to excite the modes which turn out to be the most "effective" from the point of view of spatial signal processing at long distances from the sources.

In this paper, we give the most essential aspects of adaptive approach to the wave field synthesis in random-inhomogeneous channels, and illustrate them by computer simulation using some typical models of long-range underwater propagation, shallow-water and deep-water environments included. We focus here on the particular adaptive algorithms maximizing the received signal coherence which are based on the multimode signal eigenspectrum analysis and criteria related. All the signals are assumed to refer to a fixed frequency of the Fourier spectra of radiated/received spatial-temporal fields.

We address the problems by brief considering the eigenvector expansion in source array synthesis (Sec. 1) and spatial signal analysis (Sec. 2) in a multimode waveguide. Also, in Sec. 2 we define some integral characteristics of multimode signal related intrinsically with its coherence, which are suitable for the further formulations. Next,

in Sec. 3 we formulate an adaptive approach to the problem of acoustic field synthesis in long-range underwater channels and show the algorithms which are effective to control the signal coherence at the long-distanced receiving array. Some significant results of computer simulation are given in Sec. 4. The final Sec. 5 presents a summary of the results.

1. SOURCE ANTENNA SYNTHESIS: BASIC EQUATIONS

The first step is to outline the antenna synthesis problem in a two-dimensional regular waveguide. In the papers [3, 4], the synthesis problem was formulated by using a general variational approach which is widely used in the antenna theory to restrict the superdirectivity and related effects. The synthesis algorithms derived in these papers have been shown to be the most effective to control the modal spectrum of excited wave field.

For a waveguide supporting M normal modes far enough from a source, and a vertical array consisting of N sources (M, N arbitrary), the ($M \times 1$) vector $\mathbf{a}$ of mode the excitation coefficients is given by

$$\mathbf{a} = \mathbf{U}^H \mathbf{y}, \quad a_m = \sum_{n=1}^{N} y(n) u_m^*(n), \quad m = 1, 2, \ldots, M. \tag{1}$$

Here $\mathbf{y}$ is the ($N \times 1$) vector of source excitation coefficients with the entries $y(n)$; $\mathbf{U}$ is the ($N \times M$) matrix of modal structure on the N-source array; the entries $u_m(n)$ are the regular modal shapes over array; the superscript H and the asterisk denote the Hermitian transposition and the complex conjugation, respectively. The modal indices m correspond to the respective eigenvalues of the Sturm–Liouville boundary problem. The vector $\mathbf{a}$ can be physically interpreted as the array modepattern by using a close analogy with the beampatterm in a free space.

We define the criterion of antenna synthesis optimization as to maximize the ratio μ of the power P_M, radiated to the discrete spectrum modes, to the total radiated power P_0 (P_0 is fixed):

$$\mu = \frac{P_M}{P_0}, \quad P_M = \sum_{m=1}^{M} |a_m|^2, \quad P_0 = \sum_{m=1}^{\infty} |a_m|^2 = \text{const}, \tag{2}$$

when the second sum P_0 includes the continuous spectrum modes ($M < m \leq \infty$) forming the near-field pattern.

The stated variational problem reduces to the two eigenvalue–eigenvector problems in the N-dimensional source space and the M-dimensional mode space which permit one to obtain the orthogonal

bases of eigendecomposition in the source space and mode space, respectively [3, 4]. The first (antenna) basis is given by

$$\mu_p \mathbf{y}_p = (\mathbf{U}\mathbf{U}^H)\mathbf{y}_p, \quad p = 1, 2, \ldots, R. \tag{3}$$

The second (modal) basis is given by

$$\mu_p \mathbf{a}_p = (\mathbf{U}^H\mathbf{U})\mathbf{a}_p, \quad p = 1, 2, \ldots, R. \tag{4}$$

Here the eigenvalues μ_p are the coefficients of energetic "linkage" of the eigenvectors $\mathbf{y}_p$ with the discrete spectrum modes ($\mu_p = |\mathbf{a}_p|^2/P_0$), and

$$R = \text{rank}(\mathbf{U}\mathbf{U}^H) = \text{rank}(\mathbf{U}^H\mathbf{U}) \leq \min\{M, N\}$$

(in practice, $R \ll \min\{M, N\}$ for $M \gg 1$ [4]). The basis $\{\mathbf{y}_p\}_{p=1}^R$ can be regarded as the basis of "antenna modes", and the basis $\{\mathbf{a}_p\}_{p=1}^R$, as the corresponding basis of antenna modepatterns.

As a result, the optimal source excitation vector $\mathbf{y}_{opt}$ for the most effective (as regards the criterion used) excitation of a desired modal spectrum, or modepattern $\mathbf{a}_0$ (arbitrary), is obtained by the following eigenvector expansion:

$$\mathbf{y}_{opt} = \sum_{p=1}^{R} \frac{(\mathbf{a}_0^H \mathbf{a}_p)}{\mu_p} \mathbf{y}_p. \tag{5}$$

According to Eq. (5), the expansion of arbitrary source vector $\mathbf{y}$ in the basis $\{\mathbf{y}_p\}_{p=1}^R$ permits one to evaluate its efficiency from the point of view of waveguide excitation and radiated power transportation by normal modes. This efficiency is seen to increase with the weight coefficient of the eigenvector $\mathbf{y}_1$ which corresponds to the largest eigenvalue μ_1 (for ordered eigenvalues: $\mu_1 \geq \mu_2 \geq \ldots \mu_R > 0$). By the special source arrangement we have an opportunity to increase considerably the energetic "linkage" of the sources with a desired group of normal modes. In its turn, the modal spectrum $\mathbf{a}_0$ is chosen in dependence on the particular problem of application (in remote sensing, communication, and so on).

Thus, the particular problem of antenna synthesis in a waveguide stated to maximize the radiated power transformation into the desired spectrum of normal modes is solved by using the weighted eigenvector expansion (5) which depends on both the modal shapes and source arrangement. It should be emphasized that the sharp reduction of the total number of the basis components (3), (4) in comparison with the total number of modes, $R \ll M$, limits the sensitivity of

the synthesized multimode fields to mismatch effects. This property is a principal advantage of the synthesis technique outlined above.

2. MULTIMODE SIGNAL ANALYSIS FORMULATIONS

2.1. Karhunen–Loeve expansion in mode space

The second step is to consider the optimal eigenvector expansion of the multimode signal to be processed at a large distance from sources. Recently we have used this expansion to analyze the performances of optimal array signal processors in random-inhomogeneous waveguides, with application to long-range underwater acoustics [5–8].

For the waveguide considered above, the signal vector s from an K-element receiving array and its spatial covariance matrix $\mathbf{M}$ defined by $\mathbf{M} = <\mathbf{s}\mathbf{s}^H>$, are expressed by the modal decomposition:

$$\mathbf{s} = \sum_{m=1}^{M} \tilde{a}_m \mathbf{v}_m, \quad \mathbf{M} = \mathbf{V}\mathbf{R}\mathbf{V}^H. \tag{6}$$

Here, $\mathbf{v}_m$ are the $(K \times 1)$ vectors of modal shapes and $\mathbf{V}$ is the $(K \times M)$ matrix of modal structure on the array, $\tilde{\mathbf{a}}$ is the $(M \times 1)$ vector of modal spectrum, and $\mathbf{R} = <\tilde{\mathbf{a}}\tilde{\mathbf{a}}^H>$ is the $(M \times M)$ matrix of modal covariances. The vectors $\mathbf{v}_m$ and the matrix $\mathbf{V}$ are determined by the waveguide eigenfunctions and the array element arrangement, similar to the vectors $\mathbf{u}_m$ and the matrix $\mathbf{U}$ in Eq. (1).

The random amplitudes $\tilde{a}_m(t)$ are related to the excited components a_m (1) by

$$\tilde{a}_m(t) = A_m a_m \epsilon_m(t) \exp\left(-i h_m \rho\right), \quad m = 1, 2, \ldots, M, \tag{7}$$

where A_m are the regular coefficients of spherical decreasing (not of vital importance), h_m are the radial wavenumbers, ρ is a distance, and $\epsilon_m(t)$ are the random complex functions describing stochastization of modal amplitudes in a random-inhomogeneous channel.

The key point of the model (6), (7) is that the signal is assumed to be a superposition of regular modal shapes multiplied by random amplitudes. Generally, this model can be refered to the signal consisting of the discrete spectrum spatial harmonics (modes) with arbitrary intermodal covariances.

We use as the basic technique the signal orthogonal decompositions in the sensor space and mode space, similar to the approach (3), (4). The first of them is the well-known Karhunen–Loeve expansion (KLE) in the eigenbasis $(\lambda_p, \mathbf{m}_p)$ of the signal spatial covariance

matrix $\mathbf{M}$ [9], and the second, the signal modal spectrum decomposition in the basis determined by the following eigenvalue-eigenvector problem [5]:

$$\lambda_p c_p = \mathbf{RQ} c_p, \quad p = 1, 2, \ldots, r. \tag{8}$$

Here, $\mathbf{Q} = \mathbf{V}^H \mathbf{V}$ is the $(M \times M)$ matrix of modal shape orthogonalities with the entries

$$Q_{mn} = \sum_{k=1}^{K} v_m^*(k) v_n(k),$$

the $(M \times 1)$ eigenvectors c_p are the modal spectra of the $(K \times 1)$ eigenvectors $\mathbf{m}_p$ (i.e. $\mathbf{m}_p = \mathbf{V} c_p$), and the eigenvalues λ_p are assumed to be ordered and normalized:

$$\lambda_1 \geq \lambda_2 \geq \ldots \lambda_r > 0, \quad \sum_{p=1}^{K} \lambda_p = 1, \tag{9}$$

and

$$r = \mathrm{rank}(\mathbf{M}) = \mathrm{rank}(\mathbf{RQ}) \leq \min\{M, K\}.$$

According to Eqs. (8), (9), the multimode signal $(\mathbf{s}, \mathbf{a})$ is incoherent superposition of the orthonormal eigencomponents $(\lambda_p, \mathbf{m}_p, c_p)$ with the intensities λ_p, spatial shapes $\mathbf{m}_p$ and modal spectra c_p. Decomposition in the basis $\{\lambda_p, \mathbf{m}_p, c_p\}_{p=1}^r$ is the KLE generalized for the discrete spectrum signals, or the modal KLE. Two intrinsic factors, the modal covariances and mode orthogonalities affect mutually the signal expansion. The number r of components is considerable, $1 \ll r \leq M$, if the signal-carrying modes are weakly correlated and the array length is large enough for their orthogonality, or spatial resolution. This case corresponds to the coherence-degraded signal when the coherence length $K_c \ll K$, and the multimode signal processor need to be substantially complicated.

It should be emphasized that the modal spectra c_p (8) are only determined by the modal orthogonality factors Q_{mn}, if the modal covariances are substantially degraded owing to statistical effects of long-range propagation in a random-inhomogeneous channel. In turns, the modal orthogonalities depend on the waveguide eigenfunctions and arrangement of the array elements, so these two factors should be taking into account in *a priori* estimating the signal eigenvalues λ_p and the modal spectra c_p which "form" the eigenvalues in accordance with Eq. (8).

Figure 1 illustrates the absolute values of modal spectra $|c_p(m)|$ for the horizontal array in two different cases of equidistant (a) and
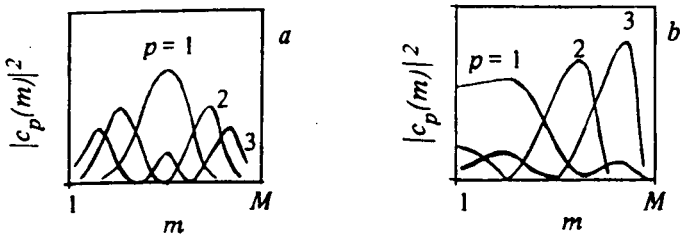
Fig. 1. The modal spectra $|c_p(m)|$ for the horizontal receiving array in the cases of equidistant (a) and nonequidistant (b) spectra of the radial wavenumbers.

nonequidistant (b) spectra of the radial wavenumbers [2, 6–8] (the intermodal correlation scale, or the number of modes correlated with some arbitrary mode. is less than "modewidth" of the patterns $Q_m(n)$ in both cases). For the vertical arrays, the modal spectra of the signal eigencomponents can be more complicated owing to oscillating modal shapes $v_m(k)$ and more complicated structure of the matrix $\mathbf{Q}$.

The optimal quadratic processor maximizing the deflection criterion [9] in a special case of the signal (6) and spatially white noise background has been shown [5–8] to be obtained by incoherent λ_p-weighted combination of the linear modal filters matched to the signal eigencomponents. The additional quadratic gain over the optimal linear filter matched to the most powerful component $(\lambda_1, \mathbf{m}_1, \mathbf{c}_1)$, is equal to the ratio:

$$ G = \frac{(\sum_{p=1}^{r} \lambda_p^2)^{1/2}}{\lambda_1}, \quad 1 \leq G \leq r^{1/2}. \tag{10} $$

Thus, the modal KLE is a proper technique for the multimode signal analysis in dependence on the signal propagation and scattering, with particular application in long-range underwater acoustics. An essential advantage of this decomposition consists in a possibility of effective exploiting the close relation of spatial coherence to modal covariances to examine the array processor performance/complexity.

2.2. Integral characteristics of multimode signals

The quantity G (10) is one of the integral characteristics of the signal eigenvalue spectrum (8), (9) suitable for the processor performance/complexity consideration.

In addition to the analysis outlined above, a partially coherent multimode signal may be considered by using a general informational

approach. According to this approach which is well-known in statistical optics [10], each component $(\mathbf{m}_p, \mathbf{c}_p)$ is interpreted as the coherent eigenstate of the signal $(\mathbf{s}, \mathbf{a})$, and the corresponding eigenvalue λ_p (9), as the probability of signal localization in that eigenstate. Then, the number r is the total number of degrees of freedom and characterizes the spatial "disorder" caused by modal covariance degradation. Obviously, an increase of the spatial disorder physically corresponds to a decrease of the ratio K_c/K, or loss of the signal coherence.

Following the informational approach, we define the entropy H of the spectrum λ_p as the integral characteristic of the signal disorder, and the normalized quantity I as the inverse characteristic:

$$H = -\sum_{p=1}^{r} \lambda_p \ln \lambda_p, \qquad I = 1 - \frac{H}{H_{\max}}. \tag{11}$$

The entropy $H_{\min} = 0$ corresponds to the case of deterministic, or perfectly coherent multimode signal, while the entropy

$$H_{\max} = \ln [\, \min\{M, K\}\,]$$

corresponds to the maximum signal disorder. On the contrary, the quantity I decreases monotonically with broadening of the spectrum λ_p from $I_{\max} = 1$ (order) to $I_{\min} = 0$ (disorder), so I can be defined as the order index.

An essential point of the informational approach consists in the fact, that the maximum available number of the signal eigenstates is intrinsically limited by the total number of modes: $r_{\max} = M$, $H_{\max} = \ln M$. This entropy value corresponds to the special case of uncorrelated and perfectly resolvable modes with the uniform intensity spectrum, when all the eigenvalues $\lambda_p = 1/M$. Since the mode resolution can be achieved only in overdetermined case $(K \geq M)$, the latter $(K - M)$ eigenvalues are zero. So generally, the signal can be partially coherent (not spatially white) in spite of the condition $I = 0$. For a free space, however, always $H_{\max} = \ln K$, so the signal is incoherent if and only if the order index $I = 0$.

Thus, the integral characteristics of the multimode signal (6) which are intrinsically related with the eigenvalue spectrum (9) of its spatial covariance matrix, are the quadratic gain G (10), the entropy H and the order index I (11). These characteristics are useful for the formulation of adaptive synthesis approach which will be given in the next section.

The particular dependences of the integral eigenspectrum characteristics G, H, and I on the key patameters, such as number of modes M, number of array elements K and intermodal correlation

scale, were analyzed in details in our recent paper [2]. Of the most importance is the fact that the signal eigenvalues are "formed" by the different modes (see Fig. 1) so the signal-carrying modes have the essentially different effects on the signal eigenspectrum. Therefore, we can (i) estimate the modes which are the most effective to control the eigenvalues and integral characteristics, and (ii) formulate some adaptive algorithms of modal spectrum correction.

3. AN ADAPTIVE APPROACH TO ACOUSTIC FIELD SYNTHESIS IN UNDERWATER CHANNELS

3.1. Basic idea

An interrelated consideration of the optimal source antenna synthesis and signal processing in an underwater channel makes it possible to state the different problems of active remote sensing, target detection, and communication. The signal coherence is the key factor in all of these problems which restricts the system performances. In particular, from the point of view of the detection problem, the source optimization is to form the multimode signal s with essentially nonuniform eigenspectrum λ_p on the receiving array. In this case, the reduced-complexity suboptimal processing is achieved by the low-rank spatial filtering as it follows from Eqs. (8)–(10). Following the informational interpretation, the problem is to form the signal with the minimum entropy, or the maximum order index.

Thus, the basic idea consists in the most effective correction of the excited modal spectrum to maximize the received signal coherence. This correction is achieved by optimizing the source array excitation as it was shown in Sec. 1. Using the concept developed in the previous section, the problem is physically formulated as that of source radiation focusing into the eigencomponent (λ_1, c_1) of the signal to be processed at a large distance from the sources. The presented approach is considered to be adaptive one since the correction pointed out intrinsically depends on (i) the modal covariances, (ii) the receiving array arrangement in a channel, and (iii) desired scheme and criterion of the array signal processor. The key point of waveguide propagation leading to the adaptive synthesis formulation, is the discrete spectrum of normal modes which permits one to select the most effective modes to control the signal coherence and, therefore, to achieve the "matched" wave field synthesis.

Taking into account the statistical effects of coherence degradation, the perfectly coherent signal $(\lambda_1 = 1, \ G = 1, \ I = 1)$ can be

synthesized only at one (arbitrary) mode. Meanwhile, if the mode orthogonality matrix $\mathbf{Q}$ (8) is not diagonal, then the resolution "mode-width" incorporates a considerable number of modes exceeding the intermode correlation scale. The synthesized wave field may be multimodal and, simultaneously, the received signal will satisfy to the desired eigenvalue distribution. The *a priori* estimate of modal resolution (orthogonalities) determines the requirements on the receiving array arrangement for increasing the signal coherence at the given eigenvalues μ_p (3), (4).

3.2. Adaptive algorithms

Using the approach formulated above, we can define the interrelated criteria of adaptive wave field synthesis by the following equations [2]:

$$\lambda_1 = \lambda_0, \quad G = G_0, \quad I = I_0, \tag{12}$$

where the quantities λ_0, G_0 and I_0 are desired values of the corresponding characteristics. Generally, these criteria can be used for any model of signal propagation in random-inhomogeneous environments. However, the key propagation feature in a mutimode wavegude that was emphasized above is the principal possibility to control the signal eigenspectrum by the optimal modal excitation.

A particular adaptive algorithm can be shown as the following iteration procedure [1, 2]. As the first step, evaluation of the eigenbasis $(\lambda_p, c_p)_0$ (8) under the initially excited modal spectrum $\mathbf{a}_0$ (for example, with the uniform intensity spectrum $|a_0(m)|^2 = \mathrm{const}(m)$) makes it possible to obtain the source vector $\mathbf{y}_{opt}$ (5) so as to synthesize the signal with the intensity spectrum $< |a_m|^2 > = |c_1(m)|_0^2$. Since this correction leads to the effective excitation of the first (most powerful) signal eigencomponent, the modes that forming the high-order ones are suppressed. Iteration of the same step results in subsequent narrowing of the eigenvalue spectrum, and the total number of steps is determined by the desired values (12). Asymptotically $\lambda_1 \to 1$, and the signal coherence length $K_c \gg K$. As the result, the quadratic gain $G \to 1$ according to Eq. (10), and the order index $I \to 1$ according to Eq. (11). In the opposite case, if the modes of high-order components are the most excited ones, the signal coherence only degrades.

Thus, the adaptive algorithm is expressed by

$$|a_0(m)|_j^2 \sim |c_1(m)|_{j-1}^2, \quad \sum_{m=1}^{M} |a_0(m)|_j^2 = \mathrm{const}(j), \tag{13}$$

where the iteration index $j = 1, 2, \ldots J$, and J is the total number of iterations. The second equation fixes the total power radiated to the normal modes during the iterations.

The essential point is estimation of the modal spectra $|c_1(m)|^2_{j-1}$ which requires elaboration of special signal processing techniques (see, for example, [11, 12]). So the other iterative spectra are of particular interest to be exploited in a more simple scheme. For example, the spectrum $|F_1(m)|^2_{j-1}$, where the entries $F_1(m)$ are determined by

$$F_1(m) = \sum_{k=1}^{K} v_m(k)m_1(k).$$

The vector $\mathbf{F}_1$ is the first eigencomponent modepattern which is obtained by using only modal shapes and the first signal eigenvector. In this case, the adaptive algorithm is expressed by

$$|a_0(m)|^2_j \sim |F_1(m)|^2_{j-1}, \quad \sum_{m=1}^{M} |a_0(m)|^2_j = \text{const}(j). \qquad (14)$$

The algorithms (13), (14) are interrelated due to the close relation of the iterative spectra, which is clear from $\mathbf{F}_1 = \mathbf{Qc}_1$. However, they have the different efficiency and, in particular, the different value of J for the given values of the criteria (12).

Incorporating the effects of range-dependent modal intensity spectrum and/or the range-dependent modal structure leads to an increased complexity of the source optimization problem. In these cases the synthesis of additional multimode signals are required to correct the adaptive algorithms.

4. RESULTS OF COMPUTER SIMULATION

The adaptive algorithms are examined here by simulations for:

(1) horizontal $\lambda/2$-array in an isovelocity shallow-water channel with perfectly rigid bottom and free surface, and

(2) vertical $\lambda/2$-array in a deep-water channel with Munk's sound-speed profile.

The main goal of simulations is to illustrate the effect of increasing the received signal coherence by the adaptive correction of excited modal spectrum in accordance with the algorithms (13), (14) under the condition of substantially degraded intermodal covariances.

For the intermodal correlations (6), a simple exponential model is used:

$$r_{mn} = \exp\left(-|m-n|/\Delta\right), \quad 0 \le \Delta \le \infty, \qquad (15)$$

where the parameter Δ denotes the intermodal correlation scale, or the coherence "length" in mode space, which is a function of the distance to source and depends on ocean environment. In accordance

with some theoretical results [13, 14], a physical foundation for this model can be the random phase modulation $\epsilon_m(t)$ (7) in an underwater channel with large-scale random inhomogeneities (see also the paper by *A. G. Sazontov* in this issue). We note that the typical distances of modal covariance degradation (when $\Delta \ll M$) for sound frequency ≥ 100 Hz may be up to ~ 100 km in shallow-water channels and up to ~ 300 km in deep-water channels (the degradation is caused mainly by acoustic scattering by wind-induced surface waves and internal waves, respectively) [13, 14]. The regular modal phase shifts which should be generally written in Eq. (15) are not of vital importance and omitted for the sake of simplicity.

It is clear that the adaptive algorithms discussed are of the most interest exactly for the small scales $\Delta \ll M$ since the large scales $\Delta \sim M$ lead to rather high spatial coherence.

Following the algorithm (13), the matrix $\mathbf{R}(j)$ is simulated by using the iterative procedure:

$$\mathbf{R}_j = (\ diag|c_1(m)|_{j-1}\ )\,\mathbf{R}_{j-1}\,(\ diag|c_1(m)|_{j-1}\ ) \tag{16}$$

under the constraint $Tr(\mathbf{R}_j) = M$. The initial matrix $\mathbf{R}_0$ is expressed by Eq. (15), i.e. the initial modal spectrum is simulated to be uniform (all the modes are excited).

In its turn, the algorithm (14) leads to the following iterative procedure for the matrix $\mathbf{R}(j)$:

$$\mathbf{R}_j = (\ diag|F_1(m)|_{j-1}\ )\,\mathbf{R}_{j-1}\,(\ diag|F_1(m)|_{j-1}\ ). \tag{17}$$

under the same constraint and initial condition.

4.1. Horizontal array in a shallow-water channel

In this example of the receiving array arrangement, the modal vectors $\mathbf{v}_m$ are the plane-wave vectors, and the entries of matrix $\mathbf{Q}$ coincide with the convenient beampattern factors of the phased array:

$$v_m(k) = \exp\left(i\pi\kappa_m(k-1)\right), \quad \kappa_m = h_m \sin\theta,$$

$$Q_{mn} = \frac{\sin(Kx_{mn})}{\sin(x_{mn})}\exp\left(i(K-1)x_{mn}\right), \quad x_{mn} = \frac{\pi(\kappa_m - \kappa_n)}{2k_0}.$$

Here h_m are the radial wavenumbers, θ is the angle of arrival in the horizontal plane of the receiving array arrangement, k_0 is the wavenumber in a free space. Nonequidistant spectrum of the isovelocity channel eigenvalues h_m [15] leads to considerable difference (by $\sim M^{3/2}$ times) in spatial "density" of the lower-order ($m \sim 1$) and the higher-order ($m \sim M$) modes. Following the noted analogy with the
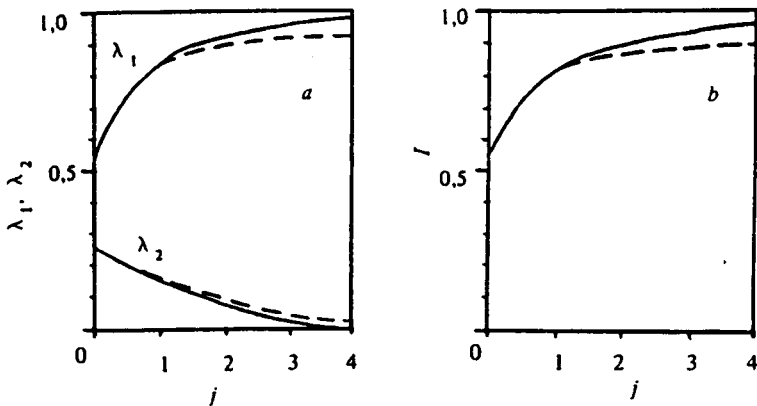
Fig. 2. The dependences $\lambda_1(j)$, $\lambda_2(j)$ (a) and $I(j)$ (b) using the algorithms (13), (16) (the solid curves) and (14), (17) (the dashed curves) for the values $M = 16$, $\Delta = 0.1$ and $K \sin \theta = 8$.

phased array operation in a free space, or the mode–angle analogy, the multimode signal can be interpreted here as superposition of the plane waves with the angular spectrum corresponding to the radial wavenumber spectrum.

Figures 2 and 3 illustrate the adaptive algorithms (13)–(17) for the following values of parameters: $M = 16$, $\Delta = 0.1$ (uncorrelated modes), $K \sin \theta = 8$. The dependences $\lambda_1(j)$, $\lambda_2(j)$ and $I(j)$ are shown in Fig. 2, and the iterative spectra, in Fig. 3. As can be easily seen, the eigenspectrum localizes rapidly in the largest eigenvalue, so the signal "forgets" its initial coherence degradation and spatial disorder. The rather effective localization ($\lambda_1 \simeq 0.9, I \simeq 0.9$) is achieved even for $J = 2$. It should be pointed out (see Fig. 3) that the first eigencomponents are essentially not single-modal.

The dependence $G(j)$ which is determined solely by the largest eigenvalues, is more steep: $G(1) \simeq 1.0$. Therefore, one cycle is quite sufficient to achieve high-performance linear processing matched to the first eigencomponent (which is carried here by the lower-order modes).

Nonoptimal correction of the modal spectrum does not lead to the required localization of the eigenspectrum. For example, the excitation of high-order modes ($m \geq 10$) leads to a more uniform spectrum of the signal eigenvalues in spite of the considerable decreasing of the total number of signal-carrying modes [1]. Therefore, the criteria
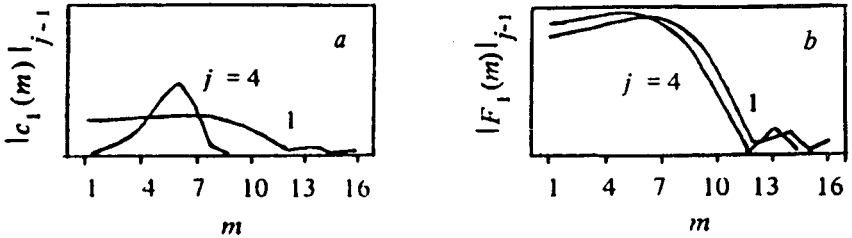
18

Fig. 3. The iterative spectra $|c_1(m)||_{j-1}$ (a) and $|F_1(m)||_{j-1}$ (b) for the algorithms (13), (16) and (14), (17), respectively.

(12) are achieved not simply as the result of decreasing number of the excited signal modes but due to the optimal source power focusing to the modes that carry the first signal eigencomponent.

4.2. Vertical array in a deep-water channel

In this example, we use well-known Munk's model for the sound-speed profile in a deep-water channel [15, 16]. The values of the model parameters are as follows: $H = 4$ km (the depth), $B = 1$ km (the depth of the sound-speed minimum), and $M = 212$ for a cw source of 230 Hz.

The key dependences of the eigenspectrum characteristics on the vertical array arrangement, large-aperture and short-aperture arrays included, have been analyzed previously [2] with an emphasis on the most important case of weak intermodal correlations (the scale $\Delta \ll M$). In this section, we restrict ourselves only by simulation showing the adaptive algorithms for the case of degraded modal covariances ($\Delta = 0$) and relatively short $\lambda/2$-array of $K = 32$ elements ($z_1 = 100$ m and $z_K = 208.5$ m when z_k denotes the array element depth). This type of hydrophone arrays is widely used in underwater acoustic applications.

Figure 4 illustrates the dependences of the first three eigenvalues $\lambda_{1,2,3}$ (a), the quadratic gain G and order index I (b) on the iteration index j for the algorithm (13), (16) (the solid curves), and for the modified algorithm (the dashed curves) using the following iterative spectrum:

$$\tilde{c}_1(m) = |c_1(m)| \ (100 \leq m \leq 130), \quad \tilde{c}_1(m) = 0 \ (m < 100, \ m > 130). \ (18)$$

Figure 5 illustrates the iterative spectra for these algorithms. The modified algorithm (18) is synthesized to correct the modal spectrum so that the main lobe of the spectrum $c_1(m)$ is maintained but the "tail"(corresponding to the high-order modes) is suppressed. This
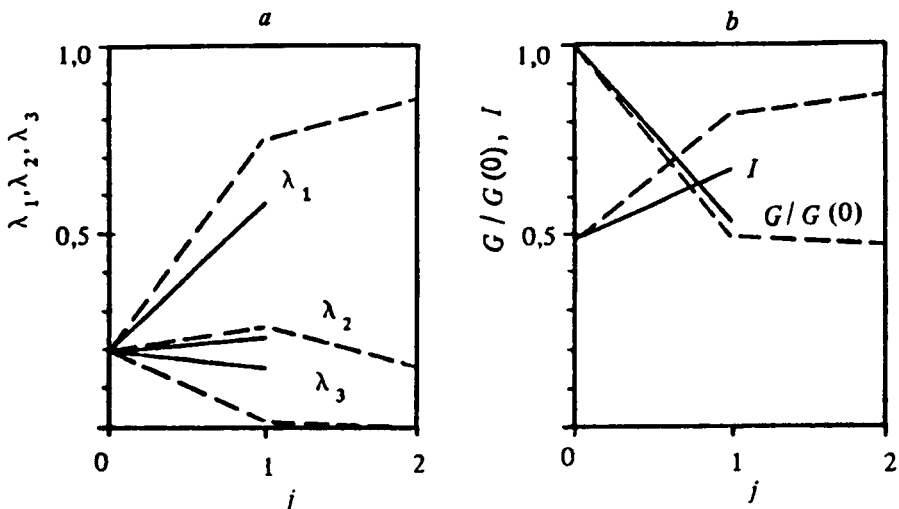
19

Fig. 4. The dependences $\lambda_1(j)$, $\lambda_2(j)$ and $\lambda_3(j)$ (a), $G(j)/G(0)$ and $I(j)$ (b) using the algorithms (13), (16) (the solid curves) and (13), (18) (the dashed curves).

additional narrowing of the modal spectrum leads to a more effective iterations as it is shown in Fig. 4.

Thus, the simulation results exhibit a principal possibility to control the acoustic coherence in random-inhomogeneous underwater channels by adaptive correction of the signal modal spectrum. The algorithm efficiency is shown to be dependent on the rate of the signal eigenvalue localization desired in accordance with the criteria (12).
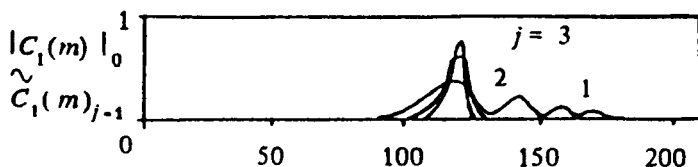

Fig. 5. The iterative spectra $|c_1(m)||_{j-1}$ (for $j = 1$) and $\tilde{c}_1(m)$ (for $j = 2, 3$) for the algorithms (13), (16) and (13), (18), respectively.

5. SUMMARY

In this paper, an adaptive approach to the problem of acoustic field synthesis in long-range ocean environments was considered. The optimal source excitation and spatial signal analysis were shown to be obtained by using similar techniques of the eigenvalue–eigenvector expansion associated with the normal-mode model of propagation in an underwater channel. This fact was exploited to formulate the adaptive acoustic field synthesis which was shown to be the iterative correction of the excited modal spectrum depending on the modal covariances and the receiving array arrangement.

Two particular adaptive algorithms were presented and compared. They were proposed to optimize the modal signal spectrum so that the signal coherence is increased considerably in spite of modal covariance degradation in a channel. The computer simulation results exhibited distinctly a rather high efficiency of the algorithms in the most interesting case of small ratios of the intermodal correlation scale to the total number of signal-carrying normal modes.

ACKNOWLEDGEMENTS

REFERENCES

1. *A. I. Malekhanov and V. I. Talanov*, An adaptive approach to antenna synthesis in multimode waveguides // Proc. 1992 URSI Internat. Symp. Signals, Systems and Electronics (Paris, 1992), pp. 596–599.

2. *E. Yu. Gorodetskaya, A. I. Malekhanov and V. I. Talanov*, Adaptive acoustic fields monitoring in ocean waveguides // in: Acoustic Fields Formation in Ocean Waveguides. Reconstruction of Inhomogeneities, ed. by V. A. Zverev (Niznhy Novgorod, 1994), pp. 9–43 (in Russian).

3. *V. I. Talanov*, On antenna synthesis in multimode waveguides // Izv. vuzov — Radiofizika, 1985, vol. 28 (7), pp. 872–879 (in Russian).

4. *N. K. Vdovicheva, V. I. Talanov, I. Sh. Fiks and I. A. Shereshevsky*, A variational approach to antenna synthesis in multimode waveguides // Proc. 1989 URSI Internat. Symp. Electromagn. Theory (Stockholm, 1989), pp. 246–248.

5. *A. I. Malekhanov and V. I. Talanov*, On the signal reception in multimode waveguides // Akust. Zhur., 1990, vol. 36 (5), pp. 891–897 (in Russian).

6. *E. Yu. Gorodetskaya, A. I. Malekhanov and V. I. Talanov*, Modeling of the optimal array signal processing in underwater sound shannels // Ibid., 1992, vol. 38 (6), pp. 1044–1051 (in Russian).

7. *A. I. Malekhanov*, Optimal spatial signal processing in nonstationary waveguides // Proc. 14th GRETSI Sypm. on Signal and Image Processing (Juan les Pins, 1993), pp. 293–296.

8. *E. Yu. Gorodetskaya and A. I. Malekhanov*, The theoretical gain limitations of array signal processing in underwater sound channels // Proc. 2nd Europ. Conf. on Underwater Acoustics, ed. by L. Bjørno (Copenhagen, 1994), pp. 665–670.

9. *H. L. Van Trees*, Detection, Estimation and Modulation Theory, Part I (Wiley, New York, 1968).

10. *E. L. O'Neill*, Introduction to Statistical Optics (Addison–Wesley, London, 1963).

11. *T. C. Yang*, Effectiveness of mode filtering: A comparison of matched-field and matched-mode processing // J. Acoust. Soc. Am., 1990, vol. 87 (5), pp. 2072–2084.

12. *H. M. Chouhan and G. V. Anand*, A new technique of acoustic mode filtering in shallow water // Ibid., 1991, vol. 89 (2), pp. 735–744.

13. *A. G. Nechaev*, Acoustic field interference degradation in random-inhomogeneous ocean // Akust. Zhur., 1987, vol. 33 (3), pp. 535–538 (in Russian).

14. *A. L. Virovlyansky, A. G. Kosterin and A. N. Malakhov*, Fluctuations of normal modes in the canonical underwater sound channel // Ibid., 1989, vol. 35 (2), pp. 229–235 (in Russian).

15. *L. Brekhovskikh and Yu. Lysanov*, Fundamentals of Ocean Acoustics (Springer, New York, 1982).

16. *S. Flatte* (editor), Sound Transmission through a Fluctuating Ocean (Cambridge, London, 1979).

FORMATION OF ACOUSTICAL FIELDS
BY LEAK MODES AND SHEAR AND SIDE WAVES
IN LAYERED OCEANIC WAVEGUIDES

E.L. Borodina, A.I. Khil'ko, V.N. Shirokov

Anomalous high losses of hydroacoustical field may often be observed in natural oceanic waveguides [1]; to describe this phenomenon it is necessary to study the effect of mode energy leakage. This problem can be solved. for example, by choosing of sound speed profiles and density stratification in the waveguide [2] with the exception of shear vibration in the ground or the ice layer. Inclusion into the propagation model the shear oscillations allows to calculate accurately the leak mode absorption and requires to study the behavior of normal modes caused by an interference of reflected transversal and longitudinal waves and also Rayleigh and Stonely waves propagating along the ground surface [3,4]. The elastic ice covering in the oceanic shallow waveguide leads both to a change of the critical frequencies of hydroacoustical modes [5] and an appearance of symmetrical and antisymmetrical zero-order modes of the ice layer. An influence of the antisymmetrical or flexural mode on the interference structure of hydroacoustical field near the ice layer was shown in papers [6,7]. The contribution of symmetrical zero ice mode also can be appreciable (even dominant, for example, in a mode shadow zone appeared due to the high decay of hydroacoustical normal modes).

Examine now the contribution of leak modes, side waves, Rayleigh and Stonely waves to the hydroacoustical field in various waveguides. All modes of the oceanic waveguide are leak due to the influence of sediment layers of low sound speeds and upper air boundary. Corrections to the mode wavenumber caused by the leakage of the acoustical energy (for example, to the air layer) are relatively small and can be calculated by method of disturbances. Determination of the mode characteristics in the waveguide with sediment bottom is more difficult, it requires a solution of the dispersion equation in a complex domain. We will consider the field structure according to the complication of the waveguide model: from the Pekeris waveguide covered by a liquid half-space of low sound speed (the model of air covering) to the elastic half-space composed of three iso-velocity layers (as the model of ice-covered shallow sea).

As stated above, the account of the air does not change appreciably the sound field characteristics, but the difference appears due to the air side wave caused by acoustical wave propagating in the

air. When the source is situated in the air half-space, this difference becomes significant.

THE WAVEGUIDE COVERED BY THE AIR HALF-SPACE

Observe now the waveguide composed of a horizontal liquid layer between two liquid half-spaces. The acoustical field characteristics in this model proceed to those of the Pekeris waveguide when the density of the upper medium tends to zero. The point monotone source is situated in upper medium on the height h_s (the origin of the cylindrical coordinate system is on the upper boundary, and the vertical axis z is directed to the air). Then, satisfying the continuity conditions of fields and those derivatives on boundaries and the condition on the infinity one can obtain the decision of wave equation for the pressure in the layer:

$$p_1(r, z, t) = \rho_1 \omega^2 \exp(i\omega t) \int_0^\infty k \; J_0(kr) \; g_1(k, z)/d_1(k) \; dk \; , \qquad (1)$$

where

$$g_1(k, z) = 2q_0(\rho_1/\rho_0) \exp(-ik_1 h_s) \{-\alpha_0 \cos[\alpha_0(h - z)] +$$
$$i(\rho_0/\rho_1)\alpha_2 \sin[\alpha_0(h - z)]\} \; ,$$

$$d_1(k) = \sin(\alpha_0 h)[(\rho_1/\rho_0)\alpha_0^2 + (\rho_0/\rho_2)\alpha_1\alpha_2] + i \cos(\alpha_0 h)[\alpha_1 + (\rho_1/\rho_2)\alpha_2]\alpha_0 \; ,$$

$$k_1 = \omega/c_1 \; , k_0 = \omega/c_0 \; , k_2 = \omega/c_2 \; ,$$

$$\alpha_1 = \sqrt{k_1^2 - k^2} \; , \alpha_0 = \sqrt{k_0^2 - k^2} \; , \alpha_2 = \sqrt{k_2^2 - k^2} \; ,$$

h - is the layer thickness, c_1, c_0, c_2 - are the sound speeds in upper half-space, layer and down half-space, respectively, ρ_1, ρ_0, ρ_2 - are the densities of corresponding media, q_0 - is the source power.

Present the integral in equation (1) as a contour integral by closed path in upper half of a six-sheets Riemann surface [8]. On condition that $kr \gg 1$ using residue theorem one can obtain:

$$p_1(r, z, t) = \sum_{n=1}^N Res(k_n) - \sum_{m=1}^3 I_m \; , \qquad (2)$$

where the first item presents the sum of residues of integrated function in poles inside the contour, and the second item is the sum of integrals by Pekeris cut sides in the plane of complex k.
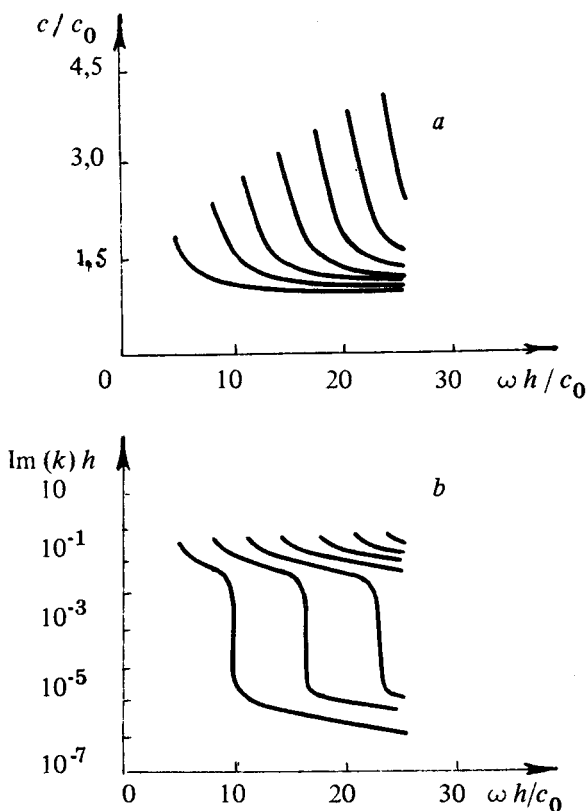
24

Fig. 1. Dispersion curves of phase velocity amplitudes (a) and wavenumber imaginary parts (b) of waveguide modes in the model of three liquid layers

Examine now the case of rare air half-space: $c_1/c_0 = 0.2, \rho_1/\rho_0 = 0.001$, where only modes with complex wavenumber take place. Substitution of the wavenumber k in the form $k = k_p + s$ to the expression for $d_1(k)$ (here k_p - is complex wavenumber determined in Pekeris model [8,9]) yields $Re(s) \approx (\rho_1/\rho_0)^2$ and $Im(s) \approx (\rho_1/\rho_0)$, i.e. the normal mode parameters of this waveguide and Pekeris model differ slightly. Fig. 1 shows amplitudes of mode phase velocities (a) and imaginary parts of wavenumbers (b) versus normalized frequency for $c_2/c_0 = 1.13, \rho_2/\rho_0 = 1.5$. Unlike Pekeris waveguide, the wavenumbers in studied model have small imaginary corrections visible when the frequency exceeds the critical mode frequencies of the waveguide.

Integrals I_m in (2) by sides of vertical cuts in a complex plane to points $k = k_1, k = k_0, k = k_2$ can be presented as

$$\sum_{m=1}^{3} I_m = \int_{i\infty}^{k_2} k\, H_0^{(1)}(kr)\, F_2(k)\, dk + \int_{i\infty}^{k_1} k\, H_0^{(1)}(kr)\, F_1(k)\, dk +$$

$$\int_{i\infty}^{k_0} k\, H_0^{(1)}(kr)\, F_0(k)\, dk \ , \tag{3}$$

$$F_2(k) = \left.\frac{g_1(k,z)}{d_1(k)}\right|_{+\alpha_2} - \left.\frac{g_1(k,z)}{d_1(k)}\right|_{-\alpha_2} ,$$

$$F_1(k) = \left.\frac{g_1(k,z)}{d_1(k)}\right|_{+\alpha_1} - \left.\frac{g_1(k,z)}{d_1(k)}\right|_{-\alpha_1} ,$$

$$F_0(k) = \left.\frac{g_1(k,z)}{d_1(k)}\right|_{+\alpha_0} - \left.\frac{g_1(k,z)}{d_1(k)}\right|_{-\alpha_0} ,$$

The sign $+$ on α_i denotes integration by the left side of the cut, the sign $-$ corresponds to the right side. The first and second items in (3) describe bottom and surface side waves, respectively. The third item turns to zero because integrals by two sides of the cut by path $Re(k) = k_0$ are equal in magnitude and opposite. In approach

$$2 \tan^2\left[k_0 h \sqrt{1 - (c_0/c_1)^2}\right] \ll (c_2/c_0 - c_0/c_2)\, k_0 r$$

the first integral yields

$$I_1(r,z) = 2(\rho_1/\rho_2)/r^2 \ \exp\left[ik_2 r - k_1 h_s \sqrt{1 - (c_1/c_2)^2}\right]$$

$$[i\alpha_0(\rho_1/\rho_0)\cos(\alpha_0 z) + \alpha_1 \sin(\alpha_0 z)] \ /$$

$$\left\{\alpha_0[\alpha_0(\rho_1/\rho_0)\sin(\alpha_0 h) + i\alpha_1 \cos(\alpha_0 h)]^2\right\} \ . \tag{4}$$

Evidently, the function $I_1(r,z)$ oscillates along the depth and depends on a distance as $1/r^2$. When

$$(\rho_1/\rho_0)^2 \ (c_0/c_1 - c_1/c_0)\, k_0 r \ll 1 \ ,$$

the second integral turns to

$$I_2(r,z) = 2(\rho_1/\rho_0)/r \ \exp\left[ik_2 r - k_0 z \sqrt{(c_0/c_1)^2 - 1}\right] \ .$$

The function $I_2(r, z)$ exponentially decreases with the depth increase, and it is inversely proportional to the distance.

At frequencies lower than the first critical frequency of the first waveguide mode the total field consists of side waves only. When the frequency goes up, the contribution of first quasi-propagating modes becomes predominant, but only near the source, because this field exponentially depends on a distance. Fig. 2 illustrates this phenomenon showing amplitude-frequency characteristics of side waves and the total field for $h_s = 0, z = -0.1h$. In the region below the critical frequency one can see a predominance of side waves (curves 2 and 3) over the normal mode field (curve 1) at large distances. Inclusion of dissipation losses to the model increases this effect. As it was obtained, in contrast to the bottom side wave the surface wave exponentially decreases with the increase of a distance to air boundary or a frequency.

As a result, one can conclude, that for studied waveguide in absence of propagating modes the spatial-frequency form of the acoustical field is complicated by the side waves; and the main peculiarity of this waveguide appears the surface side wave, especially for the excitation of the waveguide from the air.

ICE-COVERED WAVEGUIDE

Consider the system composed of a liquid layer between an elastic layer and an elastic half-space. The corresponding limiting process transforms this waveguide to the well-known model of a liquid layer with the elastic bottom. If the point monotone source is situated in the liquid layer on the depth h_s, then the corresponding solution for the field pressure can be written as:

$$p_2(r, z, t) = \rho_0 \omega^2 \exp(i\omega t) \int_0^\infty k \, J_0(kr) \, g_2(k, z)/d_2(k) \, dk \, , \qquad (5)$$

where

$$g_2(k, z) = q_0 \begin{cases} D(h_2 - h_s) \, Q(z + h_1), & z \geq -h_s \\ \\ D(h_2 + z) \, Q(h_s - h_1), & z \leq -h_s \end{cases}$$

$$d_2(k) = \alpha_l(\rho_0/\rho)k_t^4 \left[(\rho_0/\rho') \alpha_l' k_t'^4 \sin(\alpha_0 \Delta h) + i \, \alpha_0 \, R'(k) \cos(\alpha_0 \Delta h) \right] \times$$

$$P_1(k) + \alpha_0 \left[(\rho_0/\rho') \alpha_l' k_t'^4 \cos(\alpha_0 \Delta h) + i \, \alpha_0 \, R'(k) \sin(\alpha_0 \Delta h) \right] \times \ P_2(k) \, ,$$
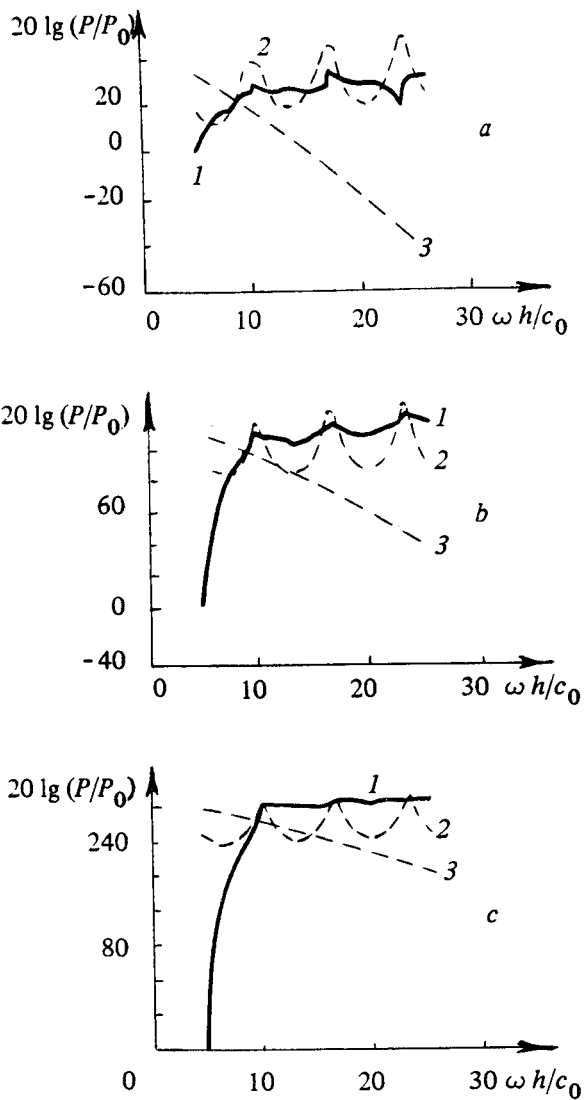
Fig. 2. Components of the total acoustical field in the waveguide: 1 - the sum of normal modes, 2 - the bottom side wave, 3 - the surface side wave; a) $r = 2h$, b) $r = 8h$, c) $r = 20h$

$$D(z) = (\rho_0/\rho') \, \alpha_l' \, k_t'^4 \, \sin(\alpha_0 z) + i\,\alpha_0 \, R'(k) \, \cos(\alpha_0 z) \, ,$$

$$Q(z) = (\rho_0/\rho') \, \alpha_l \, k_t^4 \, P_1(k) \, \sin(\alpha_0 z) - \alpha_0 \, P_2(k) \, \cos(\alpha_0 z) \, ,$$

$$P_1(k) = (2k^2 - k_t^2)^2 \cos(\alpha_l h_1) \sin(\alpha_t h_1) + 4k^2 \alpha_l \alpha_t \sin(\alpha_l h_1) \cos(\alpha_t h_1) \, ,$$

$$P_2(k) = 8k^2 \alpha_l \alpha_t \, (2k^2 - k_t^2)^2 \, [1 - \cos(\alpha_l h_1) \cos(\alpha_t h_1)] +$$

$$[(2k^2 - k_t^2)^4 + 16k^4 \alpha_l^2 \alpha_t^2] \sin(\alpha_l h_1) \sin(\alpha_t h_1) \, ,$$

$$R'(k) = (2k^2 - k_t^2)^2 + 4k^2 \alpha_l \alpha_t \, ,$$

$$k_l = \omega/c_l \ , \ k_t = \omega/c_t \ , \ k_0 = \omega/c_0 \ , \ k_l' = \omega/c_l' \ , \ k_t' = \omega/c_t' \ , \ \alpha_l = \sqrt{k_l^2 - k^2} \ ,$$

$$\alpha_t = \sqrt{k_t^2 - k^2} \ , \ \alpha_0 = \sqrt{k_0^2 - k^2} \ , \ \alpha_l' = \sqrt{k_l'^2 - k^2} \ , \ \alpha_t' = \sqrt{k_t'^2 - k^2} \ ,$$

h_1 - is the thickness of the solid layer, $h_2 - h_1 = \Delta h$ - is the thickness of the liquid layer, c_l, c_t, ρ - are the propagation velocities of longitudinal and shear waves and the density of the elastic layer, respectively, c_l', c_t', ρ' - are the corresponding values in the elastic half-space, c_0, ρ_0 - are the sound speed and the density of the liquid layer. Integration of (5) in the domain of complex k when $kr \gg 1$ yields the expression similar to (2), but with five integrals by cuts. Observe now the mode structure of the acoustical field and compare the contributions of different normal waves.

As stated above, the sound field structure in a given model is complicated by additional modes caused by elastic oscillations in the upper layer and the bottom half-space. Fig. 3 shows the dispersion curves of phase velocities (a) and wavenumber imaginary parts (b) for $h \to \Delta h$, $c_2 \to c_l'$, $\rho_2 \to \rho'$, $c_2/c_0 = 1.53$, $c_t/c_0 = 0.67$, $c_t'/c_0 = 0.61$, $\rho/\rho_0 = 0.9$, $h_1/\Delta h = 0.02$, that corresponds to the experimental characteristics of the ground, where shear wave speed is less then sound speed in the ocean, and the elastic properties of season shelf ice. As seen from a comparison of Fig. 3a and Fig. 1a, critical frequencies of normal waveguide modes in the second model are shifted to high region due to the change of impedance boundary conditions. These modes (see curve 1) are leak in all frequency band, and those attenuation constants exceed the corresponding values of the Pekeris model (Fig. 3b, 1b). At high frequencies (HF) ($\omega \gg c_l'/\Delta h$, $\Delta \omega \gg c_l/h_1$) the dispersion equation $d_2(k) = 0$ proceeds to three expressions:

$$\alpha_l' \, (\rho_0/\rho') \, k_t'^4 + \alpha_0 \, R'(k) = 0 \ , \ \alpha_l \, (\rho_0/\rho) \, k_t^4 + \alpha_0 R(k) = 0 \ , \ R(k) = 0 \ ,$$

where $R(k) = (2k^2 - k_t^2) + 4k^2\alpha_l\alpha_t$. The first and second expressions present Stonely dispersion equation of the systems water-ground and water-ice, respectively, and the third one is Rayleigh equation on the ice surface [10]. Al low frequencies (LF) ($\omega \ll c_t'/\Delta h$, $\Delta\omega \ll c_t/h_1$) the dispersion equation has two solutions: $k_n = k_t^2/(2\sqrt{k_t^2 - k_l^2})$ and Rayleigh wavenumber for sealed ground (derived from $R'(k) = 0$).

As seen from Fig. 3a, one mode (curve 2) called below the ground wave corresponds the solution of Rayleigh equation for the ground at low frequencies ($c = c_r'$) [4] and the solution of Stonely equation for the system water-ground at high frequencies ($c = c_s'$). The Stonely wave is leak in this model and, as follows from [3], becomes noticeable at transversal wave speeds $c_t' > 0.65c_0$. The LF asymptotics $c_n = \omega/k_n$ characterizes the symmetrical zero mode of the ice layer (curve 3). Phase velocity of this mode is almost invariable in the observed frequency band, the expended dependence is given in [7]. Rayleigh wave velocity is the HF asymptotics of antisymmetrical zero or flexural mode of ice layer (curve 4), the phase velocity of which goes to zero at LF.

The ground mode is propagating (with zero losses) for any parameters, because both of phase velocity asymptotes do not exceed the bottom share wave velocity [11]. For the given conditions the flexural mode is propagating too, and high-velocity symmetrical wave with low attenuation is leak at all frequencies (see curve 3 at Fig. 3b). As wavenumber vertical projections α_0 of flexural and ground modes are imaginary, these modes appear inhomogeneous in the liquid layer, i.e. exponentially decreasing with an increase of the distance from interface surfaces. On the contrary, the symmetrical mode oscillates with the depth change.

The limiting process of (5) when $h_1 \to 0$ or $\rho \to \rho_0$, $c_1 \to \infty$ yields the expression for the pressure in absence of the elastic layer:

$$p_3(r, z, t) = \rho_0\omega^2 \exp(i\omega t) \int_0^\infty k\, J_0(kr)\, g_3(k, z)/d_3(k)\, dk\,, \qquad (7)$$

where

$$g_3(k, z) = q_0 \begin{cases} D(h_2 - h_s)\, \sin(\alpha_0 z), & z \geq -h_s \\ \\ D(h_2 + z)\, \sin(\alpha_0 h_s), & z \leq -h_s \end{cases}, \qquad d_3(k) = D(h_2)\,.$$

The dispersion curves of this waveguide are given in Fig. 4. A small shift of critical frequencies occurs relatively to the previous case, and the phase velocity curve of the ground mode is practically
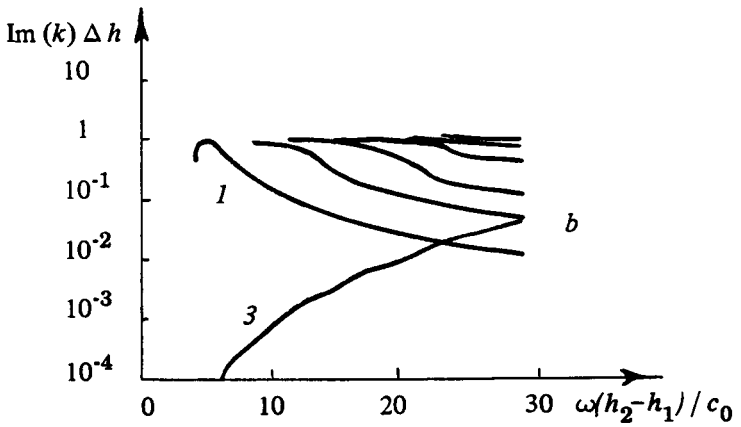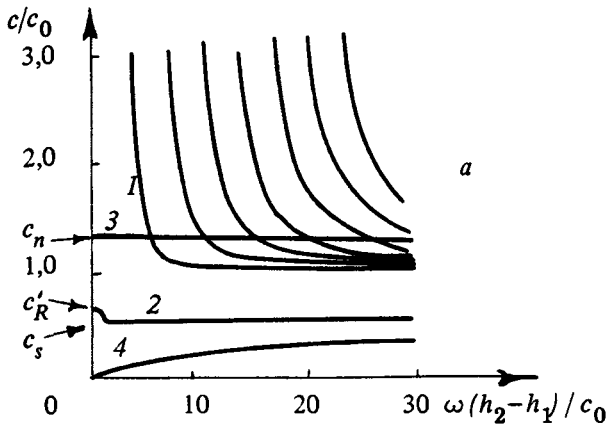
Fig. 3. Dispersion curves of mode phase velocities (a) and wavenumber imaginary parts (b) in the model of three elastic layers
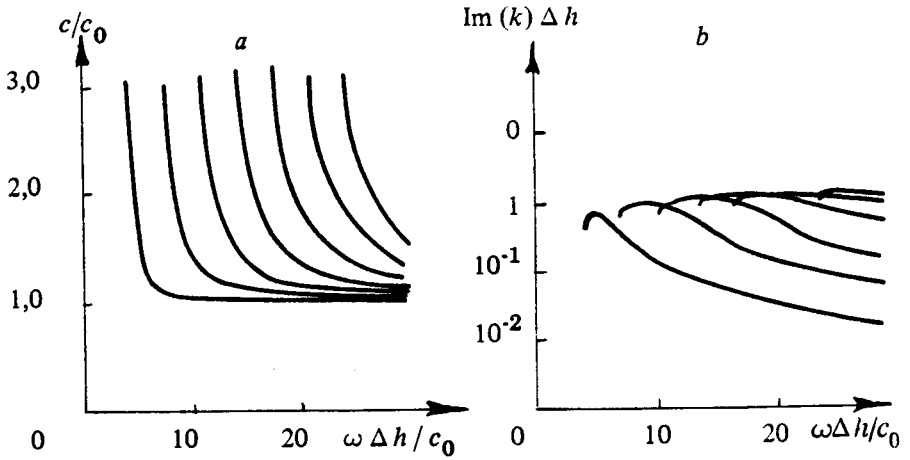
Fig. 4. Dispersion curves of mode phase velocities (a) and wavenumber imaginary parts (b) in the model of two layers with the elastic bottom
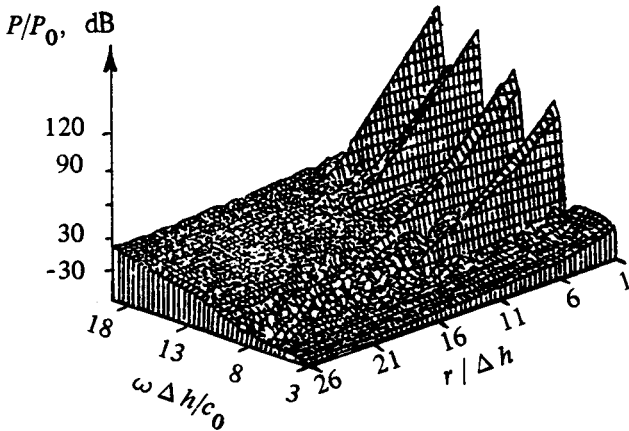

Fig. 5. The pressure amplitude versus the frequency and the distance: at the depth $z = -5h_1$ $(h_s = 2h_1)$
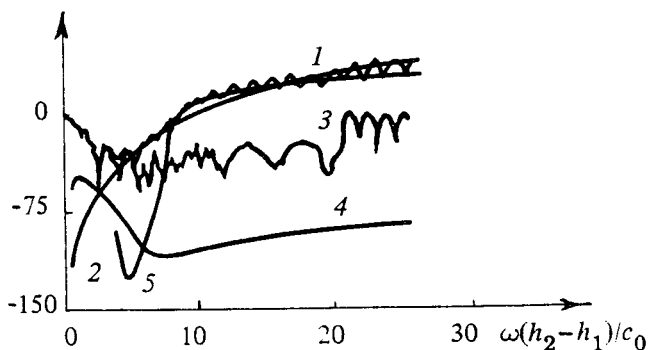
20 lg (P/P_0), dB

Fig. 6. Amplitude-frequency characteristics of the sound pressure: 1 - the total field; 2 - the symmetrical wave; 3 - the flexural mode; 4 - the ground mode; 5 - the first hydroacoustical mode ($z = -15h_1$, $h_s = 15h$, $r = 20\Delta h$)

the same as shown in Fig. 3, i.e. the elastic layer does not influence on this mode; elastic layer modes are lacking.

Compare numerically the contributions of various modes into the total field $p_3(r, z, t)$. Fig. 5 shows the pressure amplitude at the depth $z = -5h_1(h_s = 2h_1)$ versus a distance to the source and a frequency. At frequencies below the first mode critical frequency of liquid layer the flexural mode is predominant, at above frequencies the total field consists of two main waves: flexural and first hydroacoustical modes. Four exponentially decreasing resonance peaks coincide in critical frequencies of the second and the next modes of the liquid layer. At distances $r \geq 10\Delta h$ the field is defined by propagating and weakly leak modes. As mentioned above, besides the first hydroacoustical mode at frequencies $\Delta\omega \geq 10c_0/\Delta h$, the symmetrical zero ice mode also is weakly leak. Comparative amplitude-frequency characteristics of these and other modes at $r = 20\Delta h(z = -5h_1, h_s = 15h_1)$ given in Fig. 6 show the largest contribution of the flexural wave al LF ($\omega \leq 5c_0/\Delta h$). With the frequency increase the excitation coefficient increases, and the symmetrical mode becomes predominant. At ($\omega \leq 10c_0/\Delta h$) the attenuation of the first hydroacoustical mode goes down, so that its influence becomes significant; and the total field is the sum of this mode and the symmetrical mode. One can expect the decrease of the attenuation of the second and the next modes with the further increase of the frequency or the liquid layer depth, i.e. these modes will take part in the total field. The numerical estimation of the ground wave shows its visible contribution when
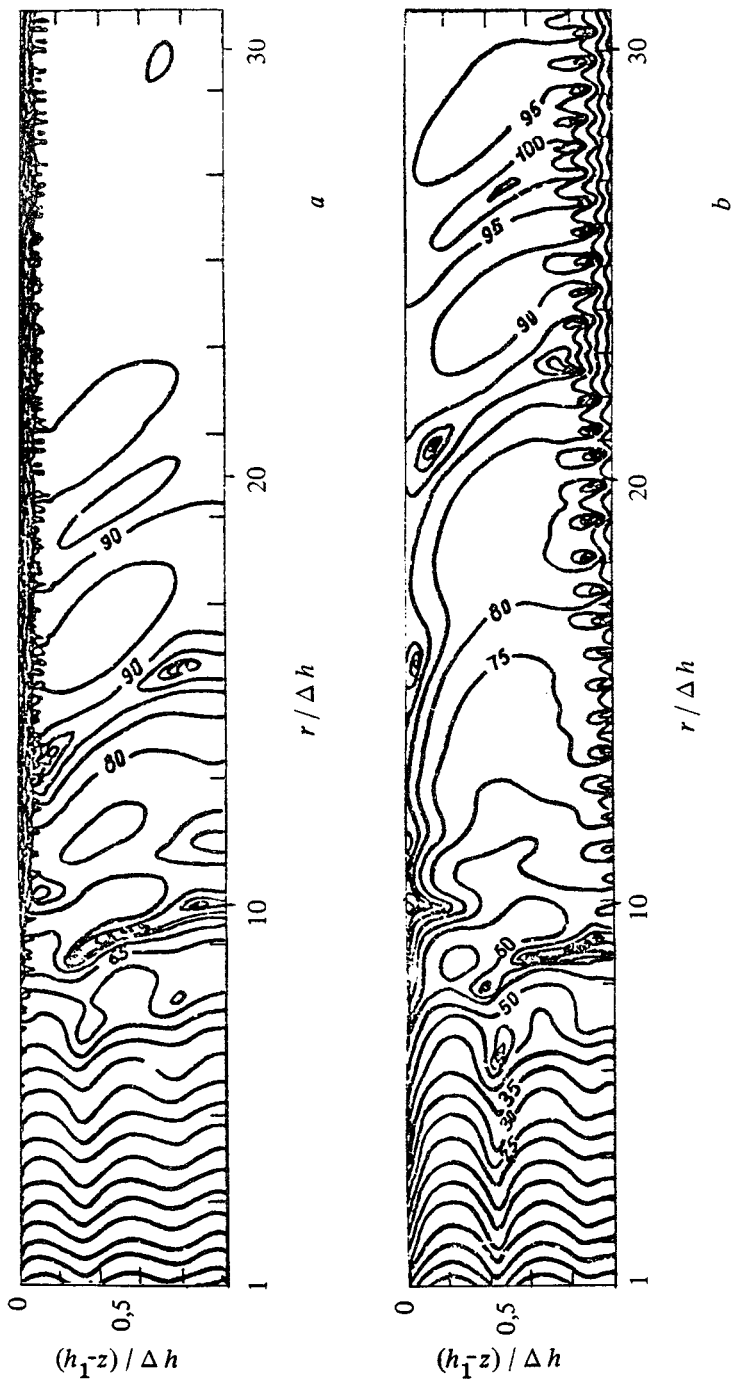
33

Fig. 7. The pressure amplitude versus the frequency and the depth: a - $h_s = 2h_1$,; b - $h_s = 45h_1$

the source is situated near the bottom or the frequency is below the critical one in the absence of an elastic layer.

Fig. 7 shows isolines of the field pressure versus a frequency and a distance for two positions of the source: near the surface and the bottom at frequency $\omega = 8.5c_0/\Delta h$. In the first case we obtain the sound field of so-called near-surface character formed mainly by propagating near the elastic layer flexural wave; and, on the contrary, in the second case the source near the bottom excites effectively the ground mode exceeding other waves especially at large distances ($r \geq 10\Delta h$). Thus, the numerical calculations show, that in shallow sea, where the shear wave velocity is less then the sound speed in the water at distances $r \geq 10\Delta h$ and frequencies $\omega \geq 10c_0/\Delta h$, the total field is formed by shear waves in the ground and in the ice layer and also side waves predominant near the bottom and the surface of the waveguide. Moreover, far from the boundaries this field is getting visibly weaker. At frequencies $\omega \geq 10c_0/\Delta h$ the field within liquid layer is composed of one or two weakly leak hydroacoustical modes. The symmetrical zero ice mode also can significantly raise the field at these frequencies when the leak waves are strongly attenuated.

At presented calculations we did not take into account the mode decay due to a dissipation and an energy absorption. This decay depends on various factors: the age of the ice, its large-scale inhomogeneities (ice-hummocks, cracks, erosions, etc.), characteristics of sediment layer. All these factors can result in a significant decay of the surface propagating and leak modes. Mention in the conclusion, that an account of various inhomogeneities complicates the field structure by reciprocal excitation and transformation of hydroacoustical modes and Rayleigh-Stonely waves.

REFERENCES

1. *Hastrup O.F.* Anomalies of losses near small glancing angles and those influence on the propagation in the shallow sea// Bottom-interacting ocean acoustics/ Ed. by W.A. Kuperman, F.B. Jensen. Moscow: Mir, 1984. P.105-119. (in Russian)

2. *Ageeva N.S., Krupin V.D.* Behavior of mode frequency characteristics in the shallow sea depending on longitudinal wave speed of the sediment layer and the sound speed profile in the water layer// Acoust. Journ. 1984. V.30, N5. P.577-584 (in Russian).

3. *Grudskaya O.N., Grudskii S.M. and Kravtsov Yu.A.* Propagation of the sound in the simplest hydroacoustical waveguides with liquid and elastic bottom. Pre-print IOF AN SSSR N57, Moscow, 1989, 62 P. (in Russian).

4. *Lobanov V.N., Petukhov Yu.V.* Peculiarities of the spatial-frequency

distribution of wide-band sound intensity in shallow oceanic waveguide. Pre-print NIRFI N321, Nizhny Novgorod. 1991. 49 P. (in Russian).

5. *Grachev G.A., Rivelis E.A., Rozenberg A.V.* On influence of the thin ice layer on propagation of low-frequency sound in the shallow sea// Math. methods of applied acoustics/ Ed. by I.B. Simonenko. RGU, Rostov-na-Donu. 1990, 176 P. (in Russian).

6. *Khil'ko A.I., Shirokov V.N.* Structure of seismoacoustical field in the ice-covered shallow sea with the elastic bottom at different conditions of the excitation// Waves and diffraction - 90/ Ed. by B.E. Kinber. Phys. Soc., Moscow. 1990. V.2. P.362-365. (in Russian).

7. *Khil'ko A.I., Shirokov V.N.* Amplitude-frequency characteristics of the sound field in the waveguide with elastic boundaries// Vestnik Kiev. politech. inst. Elektronika i zvukotechnika, V.15, Kiev: Izd-vo KGU, 1991. (in Russian).

8. *Pekeris K.L.* Theory of sound propagation in shallow water// Sound propagation in the ocean/ Ed. by L.M. Brechovskich. Moscow: Izd. Inostr. Lit. 1951. P.48-156. (in Russian).

9. *Kujama T., Kikuchi T.* Calculation of complex wavenumbers of virtual modes in Pekeris's model// Underwater acoustics/ Ed. by L. Bjorno. Moscow: Mir. 1985. P.155-160. (in Russian).

10. *Brechovskich L.M.* Propagation of waves in layered media. M.: Nauka. 1973. 343 P. (in Russian).

11. *Brechovskich L.M., Godin O.A.* Acoustics of layered media. Moscow: Nauka. 1989. 416 P. (in Russian).

ACOUSTIC COHERENCE
IN A DEEP RANDOM OCEANIC WAVEGUIDE

A.G. Sazontov

Introduction

The study of the combined effects of scattering and regular refraction on acoustic coherence is of great importance in understanding statistical behavior of oceanic sound transmission. From the theoretical point of view analysis of this problem reduces to evaluating the mutual coherence function (MCF) of space and time. There have been many theoretical treatments of this subject. Recently, the systematic investigations examining the propagation of the MCF in a refractive oceanic waveguide containing random inhomogeneities have been carried out in a ray oriented approach using the path integral formalism developed for this situation by Dashen [1]. The predictions of acoustic coherence from the path integral theory and its comparisons with single–receiver measurements are fairly well summarized in the book by Flatte *et al.* [2]. It should be noted that a solution for MCF equivalent to that obtained by path integral methods can be derived as the first approximation of the second moment equation when only one path of multipath configuration is treated [3,4]. Wilson and Tappert [5] have employed the Monte–Carlo technique for obtaining the MCF from the acoustic transport equation that allows to simulate the fluctuation phenomena in a deep sound channel where rough surface and volume scattering effects are important.

There is an alternative method to describe the statistical properties of acoustic signal based upon mode coupled treatment which is more suitable for the important case of low–frequency long–range propagation. Applied to ocean acoustics this approach has been developed in a series of publications (see, e.g. [6–16]). Most of the research to date using a normal mode decomposition has dealt with the average wavefield intensity evolution which was obtained by numerical integration of coupled mode power equations [8,9] or by means of a diffusion approach [6,7,14,15] when a discrete set of guided modes is regarded as a continuum. The analytical works concerning the correlation characteristics of a miltimode signal have also been tried by use of a matrix analog of the Rytov approximation, although their results are applicable only to the case of short propagating distances [13,16].

The aim of the present paper is to provide an efficient method for solving the radiation transport equation for a multimode oceanic waveguide

and to find in a closed form an useful approximate expression for the total MCF which is valid for a wide range of refractive index profiles and types of scattering irregularities. It is important to have such a solution since it enables one to study acoustic propagation and loss of coherence in realistic underwater environments. The body of this paper is organized as follows. Section 1 contains a brief discussion of the radiation transport equation in a randomly inhomogeneous oceanic waveguide and related theory. The analytical method used to solve the transport equation is based on quasi–classical approximation and generation function technique and is described in Section 2. Section 3 addresses the validity limits of the theory. Section 4 derives a simplified asymptotic version of the total MCF and comments on its relation to the results obtained by using geometrical optics. Section 5 shows how the method proposed may be extended to consider rough surface scattering effects. Calculations of the expected spatial and temporal acoustic coherence from oceanic internal waves and fully developed wind seas are presented in Section 6. In Section 7, we summarize the key results.

1   Formulation of the propagation model

Consider an underwater sound channel of depth H, in which the refractive index is the sum of the deterministic background profile $n_0(z)$ depending on vertical coordinate z and the stochastic field $\mu(\mathbf{r}, z, t)$ modeling the acoustic medium fluctuations. Here, $\mathbf{r} = (x, y)$ is the horizontal two–dimensional position vector and t is the time. (The coordinate system is chosen with the z-axis downward.) The perturbation μ is assumed to be Gaussian random variable with zero mean, and can be described by its autocorrelation function

$$< \mu(\mathbf{r}_1, z_1, t_1)\mu(\mathbf{r}_2, z_2, t_2) >= B_\mu(|\mathbf{r}_1 - \mathbf{r}_2|, z_1, z_2, t_1 - t_2).$$

The angular brackets $< \cdots >$ indicate ensemble averaging.

Let a nondirectional acoustic source be located at coordinates $(0, z_0)$ and emit a cw signal of a carrier frequency ω_0. The waveguide with the background medium is described by the normal mode functions, $\varphi_n(z)$, defined by the eigenvalue problem

$$\frac{d2}{dz^2}\varphi_n(z) + \left[k^2 n_0^2(z) - \kappa_n^2\right]\varphi_n(z) = 0$$

together with appropriate boundary conditions and an orthonormality

38

relation, i.e., $\int_0^H dz\, \varphi_n(z)\varphi_m(z) = \delta_{nm}$. The eigenvalue corresponding to the n-th modal function is designated by κ_n^2, and $k = \omega_0/c_0$, where c_0 is some reference sound speed. The complex envelope of the acoustic pressure field $p(r,z,t)$ in an irregular oceanic channel can be formally represented by

$$p(r,z,t) = \sum_{n=1}^{M} p_n(r,t)\,\varphi_n(z). \tag{1}$$

Here, M is the number of propagation modes and $p_n(r,t)$ is the random normal mode amplitudes. The time factor $\exp(-i\omega_0 t)$ has been suppressed. In writing (1) we ignored the possibility of radiation modes and associated continuous spectrum using the fact that these modes make a very small contribution to the farfield. The expansion coefficients $p_n(r,t)$ satisfy the coupled wave equations:

$$\left(\nabla_\perp^2 + \kappa_n^2\right)p_n(r,t) = -\sum_m V_{nm}(r,t)p_m(r,t), \tag{2}$$

where

$$V_{nm}(r,t) = 2k^2 \int_0^H dz\, n_0(z)\,\mu(r,z,t)\varphi_n(z)\varphi_m(z)$$

and $\nabla_\perp^2$ stands for the two-dimensional Laplacian. The matrix $V_{nm}(r,t)$ appearing in (2) is real and symmetric. At this stage we make the quasistatic approximation, that is, the temporal variations of the envelope function caused by volume inhomogeneities are small compared to the harmonic oscillations.

We will be interested in the behavior of the second moment of the sound wave that has passed through a scattering medium with regular refraction:

$$\Gamma(r_1,z_1,t_1|r_2,z_2,t_2) = <p(r_1,z_1,t_1)\,p(r_2,z_2,t_2)>. \tag{3}$$

Inserting Eq. (1) into Eq. (3), one finds that

$$\Gamma(r_1,z_1,t_1|r_2,z_2,t_2) = \sum_{n,m} \Gamma_{nm}(1,2)\,\varphi_n(z_1)\varphi_m(z_2), \tag{4}$$

$$\Gamma_{nm}(1,2) = <p_n(r_1,t_1)\,p_m^*(r_2,t_2)>,$$

where labels 1 and 2 refer to two different horizontal position points and times. Thus, the problem of finding a result for Γ in an oceanic waveguide now reduces to evaluating the cross–modal coherence functions $\Gamma_{nm}(1,2)$.

We define sum and difference coordinates as $\mathbf{r} = (\mathbf{r}_1 + \mathbf{r}_2)/2$, $\rho = \mathbf{r}_1 - \mathbf{r}_2$ and introduce the angular distribution function $J_{nm}(\mathbf{r}, \mathbf{s}, \tau)$ of propagating radiation:

$$\Gamma_{nm}(1,2) \equiv \Gamma_{nm}(\mathbf{r}, \rho, \tau) = \oint d\mathbf{s}\, J_{nm}(\mathbf{r}, \mathbf{s}, \tau)\, \exp(i\kappa_{nm}^+ \rho\mathbf{s}), \qquad (5)$$

where $\mathbf{s}$ is the two–dimensional unit vector, the symbol $\oint$ denotes integration over all $\mathbf{s}$ directions, $\tau = t_1 - t_2$ and $\kappa_{nm}^+ = (\kappa_n + \kappa_m)/2$. The equation governing the change of $J_{nm}(\mathbf{r}, \mathbf{s}, \tau)$ as a result of the scattering can be derived from the Bethe–Salpeter equation and has the form

$$\left[\mathbf{s}\nabla_{\mathbf{r}} - i(\kappa_n - \kappa_m) \right] J_{nm}(\mathbf{r}, \mathbf{s}, \tau) = -\frac{1}{2} \Big[\sum_{n'} \sigma_{nn'}(\mathbf{s}) J_{n'm}(\mathbf{r}, \mathbf{s}, \tau) +$$

$$+ \sum_{m'} \sigma_{m'm}(\mathbf{s}) J_{nm'}(\mathbf{r}, \mathbf{s}, \tau) \Big] + \sum_{n'} \sum_{m'} \oint d\mathbf{s}'\, \sigma_{nn'}^{mm'}(\mathbf{s}, \mathbf{s}', \tau) J_{n'm'}(\mathbf{r}, \mathbf{s}', \tau).$$

This equation is a radiation-transport–type equation in which the scattering kernel $\sigma_{nn'}^{mm'}(\mathbf{s}, \mathbf{s}', \tau)$ is given by

$$\sigma_{nn'}^{mm'}(\mathbf{s}, \mathbf{s}', \tau) = B_{nn'}^{mm'}(\kappa_{nm}^+ \mathbf{s} - \kappa_{n'm'}^+ \mathbf{s}', \tau); \qquad (6)$$

$$B_{nn'}^{mm'}(\mathbf{æ}, \tau) = \frac{\pi}{2\kappa_{nm}^+} \int\!\!\!\int\limits_{-\infty}^{\infty} \frac{d^2\rho}{(2\pi)^2} < V_{nn'}(\mathbf{r} + \rho/2, t_1) V_{mm'}(\mathbf{r} - \rho/2, t_2) > e^{i\mathbf{æ}\rho}.$$

The function σ_{nm} describes the rate at which the energy is lost from the n-th acoustic normal mode due to coupling to the m-th mode, and it is related to $\sigma_{nn'}^{mm'}(\mathbf{s}, \mathbf{s}', \tau)$ by

$$\sigma_{nm}(\mathbf{s}) = \sum_{n'} \oint d\mathbf{s}'\, \sigma_{nn'}^{mn'}(\mathbf{s}, \mathbf{s}', \tau = 0).$$

In the case of large–scale inhomogeneities, i.e., $k l_\perp \gg 1$ and $l_\perp \gg l_\parallel$, where $l_\perp$ and $l_\parallel$ are, respectively, the characteristic horizontal and vertical correlation length, the matrix scattering cross section $\sigma_{nn'}^{mm'}(\mathbf{s}, \mathbf{s}')$ is sharply peaked at $\kappa_{nm}^+ \mathbf{s} \approx \kappa_{n'm'}^+ \mathbf{s}'$. In what follows, where the forward scattering is assumed to be essential, we shall use the spatial coordinate system $\mathbf{r} = (x, R)$ with the x-axis taken in the main direction of wave propagation, and also put $\mathbf{s} = (s_\parallel, s_\perp)$ where $s_\perp \ll 1$ and $s_\parallel = \sqrt{1 - s_\perp^2} \approx 1 - \frac{1}{2} s_\perp^2$. To eliminate the rapid phase variation in J_{nm} we turn to slowly varying cross–modal angular correlation functions $\overline{J}_{nm}$ as follows

$$J_{nm}(\mathbf{r}, \mathbf{s}, \tau) = \overline{J}_{nm}(\mathbf{r}, \mathbf{s}, \tau)\, e^{i\kappa_{nm}^- x}, \qquad (7)$$

40

where $\kappa_{nm}^- = \kappa_n - \kappa_m$. The resulting system of equations for $\overline{J}_{nm}$ then becomes

$$\left[(1 - \frac{1}{2}s_\perp^2)\frac{\partial}{\partial x} + s_\perp\frac{\partial}{\partial R} - \frac{i}{2}\kappa_{nm}^- s_\perp^2\right]\overline{J}_{nm}(\mathbf{r}, s_\perp, \tau) =$$

$$= -\frac{1}{2}\left[\sum_{n'}\overline{\sigma}_{nn'}(x)\overline{J}_{n'm}(\mathbf{r}, s_\perp, \tau) + \sum_{m'}\overline{\sigma}_{m'm}(x)\overline{J}_{nm'}(\mathbf{r}, s_\perp, \tau)\right] + \qquad (8)$$

$$+ \sum_{n',m'}\int_{-\infty}^{\infty}ds'_\perp\overline{\sigma}_{nn'}^{mm'}(x; s_\perp, s'_\perp, \tau)\overline{J}_{n'm'}(\mathbf{r}, s'_\perp, \tau),$$

where $\overline{\sigma}_{nm}(x) = \sum_{n'}\int_{-\infty}^{\infty}ds'_\perp\overline{\sigma}_{nn'}^{mn'}(x, s_\perp, s'_\perp, \tau = 0)$ with $\overline{\sigma}_{nn'}^{mm'}(x; s_\perp, s'_\perp, \tau) =$
$= B_{nn'}^{mm'}(\kappa_{nm}^+ - \kappa_{n'm'}^+, \kappa_{nm}^+ s_\perp - \kappa_{n'm'}^+ s'_\perp, \tau)\exp[i(\kappa_{n'm'}^- - \kappa_{nm}^-)x]$,
and integration over $s'_\perp$ is extended from $-\infty$ to ∞.

In addition to (8), initial conditions in x must be imposed. These conditions, dictated by the source, may be obtained by a matching procedure to give

$$\overline{J}_{nm}(x = 0, R, s_\perp) = \frac{1}{8\pi\sqrt{\kappa_n\kappa_m}}\varphi_n(z_0)\,\varphi_m(z_0)\,\delta(R). \qquad (9)$$

In the small angle approximation Eq. (5) reduces to

$$\Gamma_{nm}(\mathbf{r}, \rho, \tau) = \exp(i\kappa_{nm}^+\rho_\parallel)\int_{-\infty}^{\infty}ds_\perp J_{nm}(\mathbf{r}, s_\perp, \tau)\exp(i\kappa_{nm}^+\rho_\perp s_\perp), \qquad (10)$$

where $\rho = (\rho_\parallel, \rho_\perp)$. The functions $\Gamma_{nm}(\mathbf{r}, \rho, \tau)$ depend on the variable $\rho_\parallel$ only through the trivial factor $\exp(i\kappa_{nm}^+\rho_\parallel)$. By taking it into account we can set in Eq. (10) $\rho_\parallel = 0$ considering instead of $\Gamma_{nm}(\mathbf{r}, \rho, \tau)$ the "transverse" coherence functions $\Gamma_{nm}^\perp$ defined as

$$\Gamma_{nm}(\mathbf{r}, \rho, \tau)\big|_{\rho_\parallel = 0} \equiv \Gamma_{nm}^\perp(1,2)e^{i\kappa_{nm}^- x} = \int_{-\infty}^{\infty}ds_\perp J_{nm}(\mathbf{r}, s_\perp, \tau)\exp(i\kappa_{nm}^+\rho_\perp s_\perp).$$

$$(11)$$

Note that $\Gamma_{nm}^\perp(1,2)$ correspond to slowly varying forward propagating cross-modal coherence functions, where $\mathbf{r}_1 = (x, y_1)$ and $\mathbf{r}_2 = (x, y_2)$. For simplicity of notation we will henceforth drop the subscript "$\perp$".

Equations (7)–(11) are the main equations in this section. If we approximate $(1 - s^2/2)$ by 1 and take the Fourier transform of Eq. (8) with respect

to s, then for $\Gamma^{\perp}_{nm}(1,2)$ we find

$$\left[\frac{\partial}{\partial x} - \frac{i}{\kappa^+_{nm}}\frac{\partial^2}{\partial\rho\partial R} + \frac{i}{2}\frac{\kappa^-_{nm}}{\kappa^{+2}_{nm}}\frac{\partial^2}{\partial\rho^2}\right]\Gamma^{\perp}_{nm}(1,2) =$$

$$= -\frac{1}{2}\left[\sum_{n'} A_{nn'}(1,1)\,\Gamma^{\perp}_{n'm}(1,2) + \sum_{m'} A_{m'm}(2,2)\,\Gamma^{\perp}_{nm'}(1,2)\right] + \qquad (12)$$

$$+ \sum_{n'}\sum_{m'} A^{mm'}_{nn'}(1,2)\,\Gamma^{\perp}_{n'm'}(1,2)$$

with

$$\Gamma^{\perp}_{nm}(1,2)\big|_{x=0} = \frac{1}{4\kappa^+_{nm}\sqrt{\kappa_n\kappa_m}}\,\varphi_n(z_0)\,\varphi_m(z_0)\,\delta(\rho)\,\delta(R), \qquad (12a)$$

where $A_{nn'}(1,1) = \sum_{m'} A^{n'm'}_{nm'}(1,1)$ and

$$A^{mm'}_{nn'}(1,2) = \frac{\pi\exp\left[i(\kappa^-_{n'm'} - \kappa^-_{nm})x\right]}{2\kappa^+_{nm}\kappa^+_{n'm'}}\int_{-\infty}^{\infty} d\varkappa_y\, B^{mm'}_{nn'}(\kappa^+_{nm} - \kappa^+_{n'm'}, \varkappa_y)e^{i\varkappa_y\rho}.$$

Equation (12) is obviously equivalent to the second moment equation derived from parabolic wave equation under the Markov approximation, and the latter equation has been exclusively used by previous authors. With regard to Eq. (12) the following point should be noted. If one is interested in the long range propagation, then only nonoscillatory terms contribute appreciably to the equation system (12). So, in the limit of large x Eq. (12) reduces to

$$\left[\frac{\partial}{\partial x} - \frac{i}{\kappa^+_{nm}}\frac{\partial^2}{\partial\rho\partial R} + \frac{i}{2}\frac{\kappa^-_{nm}}{\kappa^{+2}_{nm}}\frac{\partial^2}{\partial\rho^2}\right]\Gamma^{\perp}_{nm}(1,2) =$$

$$= -\frac{1}{2}\left[A_{nn}(1,1) + A_{mm}(2,2)\right]\Gamma^{\perp}_{nm}(1,2) + \sideset{}{'}\sum_{n',m'} A^{mm'}_{nn'}(1,2)\,\Gamma^{\perp}_{n'm'}(1,2), \quad (13)$$

where the symbol $\sum'_{n',m'}$ means the summation over all couples of modes satisfying the synchronism condition

$$\kappa_n - \kappa_m = \kappa_{n'} - \kappa_{m'}. \qquad (14)$$

In these circumstances the diagonal elements of the matrix $\Gamma^{\perp}_{nm}$ decouple from the off–diagonal elements, since at $n = m$ the condition (14) will be justified when $n' = m'$. Note also, that the behavior of the off–diagonal elements Γ_{nm} $(n \neq m)$ depends essentially on the type of an oceanic

waveguide. In particular, for waveguides having quasi–equidistant spectrum of the wavenumbers κ_n the condition (14) can be satisfied for a large number of modes n, m and n', m' such that $n - m = n' - m'$. In the opposite case, when the spectrum κ_n is nonequidistant, the contribution to the double sum gives only terms $n = n'$ and $m = m'$.

2 Quasi–classical derivation of the cross–modal mutual coherence functions from the matrix transport equation

The general solution of Eq. (8) corresponding to an arbitrary initial distribution on the plane $x = 0$: $\overline{J}_{nm}(\mathbf{r}, s, \tau)\big|_{x=0} = J_{nm}^{00}(R, s)$ can be expressed as

$$\overline{J}_{nm}(\mathbf{r}, s, \tau) = \sum_{\nu} \sum_{\lambda} \iint_{-\infty}^{\infty} ds' dR' g_{n\nu}^{m\lambda}(x, R, s | 0, R', s') J_{\nu\lambda}^{00}(R', s'), \quad (15)$$

where $g_{n\nu}^{m\lambda}(\cdot | \cdot)$ are the Green–matrix elements which obey the equation

$$\left[\left(1 - \frac{1}{2}s^2\right)\frac{\partial}{\partial x} + s\frac{\partial}{\partial R} - \frac{i}{2}\kappa_{nm}^{-}s^2 \right] g_{n\nu}^{m\lambda}(x, R, s | x', R', s') =$$

$$= \sum_{n',m'} \int_{-\infty}^{\infty} ds'' \overline{U}_{nn'}^{mm'}(x, \tau; s, s'') g_{n'\nu}^{m'\lambda}(x, R, s'' | x', R', s') \quad (16)$$

with

$$g_{n\nu}^{m\lambda}(\cdot | \cdot)\big|_{x=0} = \delta_{n\nu}\, \delta_{m\lambda}\, \delta(s - s')\, \delta(R - R').$$

In writing (16) the parametrical dependence $g_{n\nu}^{m\lambda}$ on τ has been omitted for brevity and it has been put

$$\overline{U}_{nn'}^{mm'}(x, \tau; s, s') = -\frac{1}{2}\left[\delta_{mm'}\overline{\sigma}_{nn}(x) + \delta_{nn'}\overline{\sigma}_{m'm}(x) \right] \delta(s - s') + \overline{\sigma}_{nn'}^{mm'}(x, s, s', \tau). \tag{17}$$

The set of coupled integrodifferential Eqs. (16) is very hard to solve exactly and numerical simulations are needed. If M becomes too large, the numerical integration of these equations becomes impractical. However, in the quasi–classical approximation, when for $\varphi_n(z)$ the WKB formulae are valid, it is possible to construct the analytical solution for $g_{n\nu}^{m\lambda}$ and to obtain an useful, approximate representation for the total MCF.

The approach employed is based on the following basic assumptions that reinforce each other:

(i) The first one concerns the structure of the coupling matrix elements and consists in the possibility of presentating $\sigma_{nn'}^{mm'}$ in the form:

$$\sigma_{nn'}^{mm'} = f(n, m, n - n', m - m'), \tag{18}$$

where the function f tends rapidly to zero as the difference indices $n - n'$, $m - m'$ increase, and undergoes relatively slow variations of n and m (at given $n - n'$, $m - m'$). The physical basis for this assumption is the fact that by definition, Eq. (6), the cross–section matrix is proportional to the product of the coupling elements V_{nm}. But, in compliance with the well–known Landau result [17], the matrix element of quantity $\mu(z)$ calculated in the WKB–approximation transforms to the Fourier components μ_{n-m} of the series expansion of the function $\mu(z_n(x))$, where $z_n(x)$ is the classical trajectory of motion (specified in (36)).

(ii) In addition to large mode numbers $(M \gg 1)$, the theory is restricted by the requirement that the coupling mechanism involves predominantly near neighbors, so that the Green matrix elements $g_{n\nu}^{m\lambda}$ differ from zero when n and ν, m and λ are such that

$$\left| \frac{n - \nu}{\nu} \right| \ll 1 \quad , \quad \left| \frac{m - \lambda}{\lambda} \right| \ll 1. \tag{19}$$

(iii) To simplify the problem we replace the factor $(1 - s^2/2)$ appearing in the left–hand side of Eq. (16) by 1 and drop the term proportional to $s^2 \overline{J}_{nm}$ since $s_\perp \ll 1$.

Now, we turn to direct discussion of the procedure for theoretical evaluation of the cross–modal MCF. In order to solve (16) it is convenient to introduce a generating function $F_{\nu\lambda}^{\alpha\beta}$ that contains two new independent variables α and β:

$$F_{\nu\lambda}^{\alpha\beta}(x, R, s | x', R', s') = \sum_n \sum_m g_{n\nu}^{m\lambda}(x, R, s | x', R', s') e^{i(n-\nu)\alpha - i(m-\lambda)\beta}. \tag{20}$$

It follows from Eq. (20) that $F_{\nu\lambda}^{\alpha\beta}$ is a periodic function with period 2π, i.e., $F_{\nu\lambda}^{\alpha\beta} = F_{\nu\lambda}^{\alpha+2\pi \, \beta+2\pi}$ and, therefore, the segment $0 \leq \alpha, \beta \leq 2\pi$ may be taken as the main region of the definition of $F_{\nu\lambda}^{\alpha\beta}$ over the variables α and β. The relation between $g_{n\nu}^{m\lambda}(\cdot|\cdot)$ and $F_{\nu\lambda}^{\alpha\beta}(\cdot|\cdot)$ is given by the Fourier inversion

$$g_{n\nu}^{m\lambda}(\cdot|\cdot) = \frac{1}{(2\pi)^2} \int_0^{2\pi} d\alpha \, e^{-i(n - \nu)\alpha} \int_0^{2\pi} d\beta \, e^{i(m - \lambda)\beta} F_{\nu\lambda}^{\alpha\beta}(\cdot|\cdot). \tag{21}$$

Multiplying (16) by $\exp\left[\,i(n-\nu)\alpha - i(m-\lambda)\beta\,\right]$ and performing the double summation over all n and m lead to the result

$$\left(\frac{\partial}{\partial x} + s\frac{\partial}{\partial R}\right)F^{\alpha\beta}_{\nu\lambda}(x,R,s|x',R',s') = \qquad (22)$$

$$= \frac{1}{(2\pi)^2}\int\limits_0^{2\pi}d\alpha\int\limits_0^{2\pi}d\beta\int\limits_{-\infty}^{\infty}ds''K^{\alpha\beta|\alpha'\beta'}_{\nu\lambda}(x,\tau;s,s')F^{\alpha'\beta'}_{\nu\lambda}(x,R,s|x',R',s'),$$

where

$$K^{\alpha\beta|\alpha'\beta'}_{\nu\lambda}(\cdot) = \sum_{n,m}\sum_{n',m'}\overline{U}^{mm'}_{nn'}(\cdot)e^{-i\nu(\alpha-\alpha')+i\lambda(\beta-\beta')}f^{\alpha\alpha'}_{nn'}f^{*\beta\beta'}_{mm'}; \quad (23)$$

$$f^{\alpha\alpha'}_{nn'} = \exp\left[\,in\alpha - in'\alpha'\,\right].$$

The specific presentation of the coupling matrix $U^{mm'}_{nn'}$ calculated in the quasi–classical approximation, Eq. (18), together with conditions (19) allow one to simplify the shape of the kernel $K^{\alpha\beta|\alpha'\beta'}_{\nu\lambda}$ and to reduce Eq. (22) to more convenient form. In view of the fact that $U^{mm'}_{nn'}$ is a function mainly of difference indices, we change the summation variables in (23) from n, n' and m, m' to n, m and $q = n' - n$, $p = m' - m$. Owing to the properties of the quasi–classical elements, the function $U^{m\,m+p}_{n\,n+q}$ falls off rapidly as q and p increase. It means that the quantities $U^{m\,m+p}_{n\,n+q}$ differ from zero only if the labels q and p do not exceed a definite number of effective interacting modes $\triangle M_{eff}$. Hence, if

$$\left|U^{m\,m+p}_{n\,n+q}\right| \approx 0 \quad \text{at } q,p > \triangle M_{eff} \quad \text{and} \quad \triangle M_{\text{eff}} \ll M, \qquad (24)$$

then the summation over q and p can be extended to infinity with negligible error. In these circumstances and when (19) is taken into account we can expand the phase factor in $\overline{U}^{mm'}_{nn'}$ in Taylor series in both differences $n - n'$, $m - m'$ and $n - \nu$, $m - \lambda$ to give

$$arg\overline{U}^{mm'}_{nn'} = x\left[\frac{d\kappa_n}{dn}(n-n') + \frac{1}{2}\frac{d^2\kappa_n}{dn^2}(n-n')^2 - \right. \qquad (25)$$

$$\left. - \frac{d\kappa_m}{dm}(m-m') - \frac{1}{2}\frac{d^2\kappa_m}{dm^2}(m-m')^2 + \cdots\right]$$

with

$$\frac{d\kappa_n}{dn} = \frac{d\kappa_\nu}{d\nu} + \frac{d^2\kappa_\nu}{d\nu^2}(n-\nu) + \cdots \quad ; \quad \frac{d\kappa_m}{dm} = \frac{d\kappa_\lambda}{d\lambda} + \frac{d^2\kappa_\lambda}{d\lambda^2}(m-\lambda) + \cdots$$

Equation (25) is a good approximation of $\arg \overline{U}_{nn'}^{mm'}$ provided that $d\kappa_n/dn$ and $d\kappa_m/dm$ vary slowly over the group of effective interacting modes considered. Then, in accordance with (18), the quantities $U_{n\,n+q}^{m\,m+p}$ are smooth functions of n and m, so that we can use the following expansion

$$U_{n\,n+q}^{m\,m+p} = U_{\nu\,\nu+q}^{\lambda\,\lambda+p} + \left[(n-\nu)\frac{\partial}{\partial\nu} + (m-\lambda)\frac{\partial}{\partial\lambda}\right] U_{\nu\,\nu+q}^{\lambda\,\lambda+p} + \cdots \quad (26)$$

If we retain only terms involving the fist–order derivatives with respect to ν and λ in Eq. (25) and keep only the first term in Eq. (26), then for $K_{\nu\lambda}^{\alpha\beta|\alpha'\beta'}$ we get

$$K_{\nu\lambda}^{\alpha\beta|\alpha'\beta'}(\cdot) = H_{\nu\lambda}^{\alpha'\beta'}(\cdot)\triangle_{\mathrm{M}}(\alpha-\alpha')\,\triangle_{\mathrm{M}}(\beta-\beta')e^{-i\nu(\alpha-\alpha')+i\lambda(\beta-\beta')},$$

where

$$H_{\nu\lambda}^{\alpha\beta}(\cdot) = \sum_{q,\,p=-\infty}^{\infty} U_{\nu\,\nu+q}^{\lambda\,\lambda+p}(\cdot)e^{iq\left(\alpha-\frac{d\kappa_\nu}{d\nu}x\right)-ip\left(\beta-\frac{d\kappa_\lambda}{d\lambda}x\right)} \quad (27)$$

and

$$\triangle_{\mathrm{M}}(\phi) = \frac{1}{2\pi}\sum_{l=1}^{\mathrm{M}}\exp(il\phi) = \frac{\sin \mathrm{M}\phi/2}{2\pi\sin\phi/2}\,e^{i(\mathrm{M}+1)\phi/2}.$$

An approximate attempt to include the effects of higher order terms in (25) is discussed in section 5.

The characteristic scale of the function $H_{\nu\lambda}^{\alpha\beta}$ over the variables α and β is $\sim 1/\triangle M_{eff}$, while the function $(\sin \mathrm{M}\phi/2)/(\sin\phi/2)$ has the scale $\sim 1/\mathrm{M}$. Since we have already used the fact that $\triangle M_{\mathrm{eff}} \gg \mathrm{M}$, therefore $H_{\nu\lambda}^{\alpha'\beta'}$ change only slightly over scales that are large compared to $1/\mathrm{M}$ and we can regard $H_{\nu\lambda}^{\alpha'\beta'}$ as nearly constant. Then, the integration over α' and β' in the right–hand side of Eq. (22) can be carried out with the help of the formula

$$\int_0^{2\pi}\frac{d\alpha'}{2\pi}e^{-i\nu(\alpha-\alpha')}\int_0^{2\pi}\frac{d\beta'}{2\pi}e^{i\lambda(\beta-\beta')}\triangle_{\mathrm{M}}(\alpha-\alpha')\triangle_{\mathrm{M}}(\beta-\beta')F_{\nu\lambda}^{\alpha'\beta'}(\cdot) = F_{\nu\lambda}^{\alpha\beta}(\cdot)$$

which is easy to prove using the definitions of $F_{\nu\lambda}^{\alpha\beta}$ and $\triangle_{\mathrm{M}}(\phi)$.

Thus, under the assumption made above the final version of Eq. (22) is

$$\left(\frac{\partial}{\partial x} + s\frac{\partial}{\partial R}\right)F_{\nu\lambda}^{\alpha\beta}(x,R,s|x',R',s') = \int_{-\infty}^{\infty}ds''H_{\nu\lambda}^{\alpha\beta}(x;s,s'',\tau)\times \quad (28)$$

$$\times F_{\nu\lambda}^{\alpha\beta}(x,R,s''|x',R',s').$$

Later, in terms of the parameters characterizing the refractive and scattering properties of the oceanic waveguide we shall establish the necessary conditions allowing one to reduce the starting Eq. (22) to Eq. (28).

Equation (28) coincides formally with the equation governing the propagation of the MCF in free space. Such an analogy allows one to use in analyzing (28) the well-known methods developed as applied to the wave scattering theory in nonstratified media (see, e.g. [18]). This has the advantage of offering the possibility of obtaining solutions in a closed form for waveguides.

The equation for the generating function, (28), can be solved exactly by the Fourier transform method or by the method of characteristics. The result is

$$F^{\alpha\beta}_{\nu\lambda}(x, R, s|x', R', s') = \int\!\!\!\int\limits_{-\infty}^{\infty} \frac{d\rho\, d\rho'}{(2\pi)^2} e^{-i\kappa^+_{\nu\lambda}(s\rho - s'\rho')} \hat{F}^{\alpha\beta}_{\nu\lambda}(x, R, \rho|x', R', \rho');$$

$$\hat{F}^{\alpha\beta}_{\nu\lambda}(1,2|1',2') = \hat{g}^0_{\nu\lambda}(1,2|1',2') \exp\left[-T^{\alpha\beta}_{\nu\lambda}(1,2|1',2')\right] \tag{29}$$

with

$$\hat{g}^0_{\nu\lambda}(1,2|1',2') = \frac{\kappa^+_{\nu\lambda}}{2\pi(x-x')} \exp\left\{\frac{i\kappa^+_{\nu\lambda}(\rho-\rho')(R-R')}{(x-x')}\right\}$$

and

$$T^{\alpha\beta}_{\nu\lambda}(1,2|1',2') = \int\limits_{x'}^{x} d\xi \int\limits_{-\infty}^{\infty} d\text{\ae}_y H^{\alpha\beta}_{\nu\lambda}(x,\tau;\text{\ae}_y) \exp\left\{\frac{i\text{\ae}_y\left[\rho(\xi-x') + \rho'(x-\xi)\right]}{(x-x')}\right\}.$$

This solution has the nature of a Green function solution of the radiation transport equation in the absence of regular refraction and in such a form it was first obtained by Dolin [19]. Equation (29) can be used to express the "transverse" coherence function (11) in terms of $\hat{F}^{\alpha\beta}_{\nu\lambda}$ as

$$\Gamma^\perp_{nm}(1,2) = \sum_\nu \sum_\lambda \int\limits_{-\infty}^{\infty} d\rho' \int\limits_{-\infty}^{\infty} dR'\, \hat{g}^{m\lambda}_{n\nu}(x,\rho,R|0,\rho',R')\, \Gamma^{00}_{\nu\lambda}(\rho',R') \tag{30}$$

with

$$\hat{g}^{m\lambda}_{n\nu}(1,2|1',2') = \frac{1}{(2\pi)^2} \int\limits_0^{2\pi} d\alpha\, e^{-i(n-\nu)\alpha} \int\limits_0^{2\pi} d\beta\, e^{i(m-\lambda)\beta}\, \hat{F}^{\alpha\beta}_{\nu\lambda}(1,2|1',2').$$

$$\tag{31}$$

Equations (29) — (31) constitute our central results. In conjugation with (4), (11) they give explicit rules for calculating both the correlation function and the wavefield intensity in a random oceanic waveguide. For a point source situated at $(0, z_0)$ from (30) with $\Gamma_{nm}^{00}(R, \rho)$ given by (12a), we get

$$\Gamma_{nm}^{\perp}(1,2) = \frac{1}{(2\pi)^2} \sum_{\nu,\lambda} \int_0^{2\pi} d\alpha \, e^{-i(n-\nu)\alpha} \int_0^{2\pi} d\beta \, e^{i(m-\lambda)\beta} \, \Gamma_{\nu\lambda}^{\alpha\beta}(1,2), \quad (32)$$

with

$$\Gamma_{\nu\lambda}^{\alpha\beta}(1,2) = \Gamma_{\nu\lambda}^{0}(1,2) \exp\left[-\frac{1}{2} D_{\nu\lambda}^{\alpha\beta}(1,2)\right], \quad (33)$$

and

$$\Gamma_{\nu\lambda}^{0}(1,2) = \frac{1}{4\kappa_{\nu\lambda}^{+}\sqrt{\kappa_\nu \kappa_\lambda}} \, \varphi_\nu(z_0) \, \varphi_\lambda(z_0) \, g_{\nu\lambda}^{0}(1,2|0,0);$$

$$D_{\nu\lambda}^{\alpha\beta}(1,2) = 2 T_{\nu\lambda}^{\alpha\beta}(1,2|0,0).$$

It is seen from (33) that the multiply scattering effects give rise to the exponential term $\exp\left[-\frac{1}{2} D_{\nu\lambda}^{\alpha\beta}(1,2)\right]$ describing the loss of coherence. The characteristic decorrelation scales depend somewhat on the inhomogeneity spectrum parameters entering into $D_{\nu\lambda}^{\alpha\beta}(1,2)$. Now we will focus our attention at evaluating $D_{\nu\lambda}^{\alpha\beta}(1,2)$ in quasi–classical approximation and on establishing the relationship between $D_{\nu\lambda}^{\alpha\beta}(1,2)$ and the phase–structure function calculated along two different equilibrium rays connecting the source to the receiver. In order to obtain $D_{\nu\lambda}^{\alpha\beta}$ it is necessary to find a result for the coupling matrix $U_{nn'}^{mm'}$ whose elements appearing in the definition of $H_{\nu\lambda}^{\alpha\beta}$, according to (27), that requires, on the other hand, the knowledge of the matrix elements $V_{nn'}$. In the WKB approximation for normal modes

$$\varphi_n(z) = \left(\frac{4a_n}{\Lambda_n}\right)^{1/2} \left[n_o^2(z) - a_n^2\right]^{-1/4} \cos\theta_n(z); \quad z_n^{\min} < z < z_n^{\max}, \quad (34)$$

where $a_n = \kappa_n/k$, Λ_n is the mode cycle distance, $\theta_n(z) = k \int_{z_n^{\min}}^{z} dz' [n_0^2(z') - a_n^2]^{1/2}$ $- \pi/4$ is the phase integral, $z_n^{\min}$ and $z_n^{\max}$ denote the turning points, the universal formula for the quasi–classical matrix element may be obtained [17] (see also [20] for detail). In our notation it has the form

$$V_{nn'}(\mathbf{r}, t) = \frac{4k^2}{\Lambda_n} \int_0^{\Lambda_n/2} dx' n_0[z_n(x')] \mu(\mathbf{r}, z_n(x'), t) \cos\left(\frac{2\pi}{\Lambda_n}(n-n')x'\right), \quad (35)$$

48

where $z_n(x)$ is the modal ray trajectory satisfying the equation

$$\frac{d^2 z_n(x)}{dx^2} = \frac{1}{2a_n} \frac{d}{dz} n_0^2[z_n(x)]$$ (36)

with

$$\frac{dz_n(x)}{dx} = \frac{1}{a_n}\sqrt{n_0^2(z) - a_n^2} \equiv \text{tg}\,\chi_n(x) \; ; \; n_0[z_n(x)]\cos\chi_n(x) = a_n,$$

and $\chi_n(x)$ is the angle the modal ray makes with the horizontal at the point x.

Applying (35) to (17) with subsequent performing the necessary calculations in (27) enable us to rewrite $D_{\nu\lambda}^{\alpha\beta}(1,2)$ as

$$D_{\nu\lambda}^{\alpha\beta}(1,2) = \int\limits_0^x dx' \Big[d_{\nu\nu}^{\alpha\alpha}(x,1|x',1) + d_{\lambda\lambda}^{\beta\beta}(x,2|x',2) - 2d_{\nu\lambda}^{\alpha\beta}(x,1|x',2) \Big]; \quad (37)$$

$$d_{\nu\lambda}^{\alpha\beta}(x,1|x',2) = 2\pi k^2 \int\limits_{-\infty}^{\infty} d\Omega \int\limits_{-\infty}^{\infty}\int\limits_{-\infty}^{\infty} \frac{d\ae_y d\ae_z}{\cos\chi_\nu(x')\cos\chi_\lambda(x')} \Phi_\mu\Big(\ae_{\nu\lambda}(x'),\Omega,z_{\nu\lambda}^{\alpha\beta}(x')\Big)\times$$

$$\times \cos\Big(\ae_y\rho\frac{x'}{x}\Big)\cos\Big(\ae_z\xi_{\nu\lambda}^{\alpha\beta}(x')\Big)\cos(\Omega\tau).$$

Here, $\Phi_\mu(\ae,\Omega,z)$ is the local spectrum of the sound–speed fluctuations taken at $\ae = \ae_{\nu\lambda}^{\alpha\beta}(x)$, where the wave number $\ae_{\nu\lambda}^{\alpha\beta}(x)$ has components

$$\ae_{\nu\lambda}^{\alpha\beta}(x) = \big(-0.5(\text{tg}\,\chi_\nu^\alpha(x) + \text{tg}\,\chi_\lambda^\beta(x)),\ae_y,\ae_z\big),$$

$\text{tg}\,\chi_\nu^\alpha(x) = dz_\nu^\alpha(x)/dx$ is the inclination of a modal ray with the path $z_\nu^\alpha(x) \equiv z_\nu(x - \alpha\Lambda_\nu/2\pi)$, and $z_{\nu\lambda}^{\alpha\beta}(x) = 0.5\big(z_\nu^\alpha(x) + z_\lambda^\beta(x)\big)$; $\xi_{\nu\lambda}^{\alpha\beta}(x) = z_\nu^\alpha(x) - z_\lambda^\beta(x)$. The expression for $D_{\nu\lambda}^{\alpha\beta}(1,2)$, Eq. (37), is immediately recognized as the phase–structure function with the only difference that the integral in (37) is taken along modal ray instead of usual geometric ray. The combination $d_{\nu\nu}^{\alpha\alpha}(x,1|x',1) + d_{\lambda\lambda}^{\beta\beta}(x,2|x',2) - 2d_{\nu\lambda}^{\alpha\beta}(x,1|x',2)$ can now be regarded as a density of the phase–structure function. Note, that precisely the same result for $D_{\nu\lambda}^{\alpha\beta}(1,2)$ can be obtained by using geometrical optics to compute the random phase of modal rays $\Psi_{\nu\alpha}(x,y,t)$ associated with the path in the presence of fluctuations [21]

$$\Psi_{\nu\alpha}(x,y,t) = \frac{k^2}{a_n} \int\limits_0^x dx' n_0[z_\nu^\alpha(x')]\,\mu\big(x',y\frac{x'}{x},z_\nu^\alpha(x'),t\big)$$ (38)

and the quantity of interest can be expressed directly in terms of $\Psi_{\nu\alpha}(x,y,t)$ as $\quad D_{\nu\lambda}^{\alpha\beta}(1,2) = < \big(\Psi_{\nu\alpha}(1) - \Psi_{\lambda\beta}(2)\big)^2 >.$

49

3 Limitations and validity

We examine the validity of the basic assumption made during the derivation of Eq. (28). First, to obtain Eq. (28) the small angle approximation was invoked. This requires that the scale size of the irregularities is much large than the wavelength of the acoustic field, i.e., $kl_\perp \gg 1$.

Then, we assumed that the number of effective interacting modes ΔM_{eff} must be significantly less than the number of propagating modes M. The quantity ΔM_{eff} is the characteristic scale of the function $\sigma_{\nu\,\nu+q}^{\lambda\,\lambda+p}$ over the index variables q and p. With the help of (35) and using the definition (6), it is easy to estimate that a mode with label ν can effectively couple to

$$\Delta M_{eff}(\nu) = \sqrt{\left(\Lambda_\nu \operatorname{tg}\chi_\nu / l_\parallel\right)^2}$$

modes. Here, the overline denotes a weighted average over the spectrum. Since ΔM_{eff} is independent of ω_0, while $M \sim \omega_0$, there will be a lower limit on acoustic frequency below which the criterion (24) will fail.

The other assumption implicit in Eq. (28) is that the second order derivatives with respect to ν and λ in the series expansion (25) as well as the term proportional to $s^2 \overline{J}_{nm}$ in the left–hand side of (16) are small enough to justify neglect of them. The contribution of the higher order derivatives to $H_{\nu\lambda}^{\alpha\beta}$, Eq. (27), is easy shown to be

$$H_{\nu\lambda}^{\alpha\beta}(\cdot) = \sum_{q,\,p\,=\,-\infty}^{\infty} U_{\nu\,\nu+q}^{\lambda\,\lambda+p}(\cdot) f_{\nu\alpha}(x,q)\, f_{\lambda\beta}^*(x,p),$$

where $f_{\nu\alpha}(x,q) = \exp\left[iq\left(\alpha - \frac{d\kappa_\nu}{d\nu}x\right) - \frac{i}{2}q^2\frac{d^2\kappa_\nu}{d\nu^2}x\right]$. This correction in conjugation with the term $\sim s^2\overline{J}_{nm}$ in Eq. (16) modifies the result for $D_{\nu\lambda}^{\alpha\beta}$ leading to the appearance in $d_{\nu\lambda}^{\alpha\beta}$ of an additional multiplicative factor $Q_{\nu\lambda}^{\alpha\beta}(x, x', \ae_y, \ae_z)$ of the form

$$Q_{\nu\lambda}^{\alpha\beta}(x, x', \ae_y, \ae_z) = \exp\left\{-\frac{i}{2}\left[\frac{\kappa_{\nu\lambda}^{-}\ae_y^2 x'(x - x')}{\kappa_{\nu\lambda}^{+2}x} + \right.\right.$$

$$\left.\left. + \ae_z^2\left(\varrho_{f_\parallel}^2(x', \nu, \alpha) - \varrho_{f_\parallel}^2(x', \lambda, \beta)\right)\right]\right\},$$

where

$$\varrho_{f_\parallel}(x, \nu, \alpha) = \operatorname{tg}\chi_\nu^\alpha(x)\left[\frac{2\pi}{k}\left|\frac{d}{da_\nu}\int_{z_\nu^{\min}}^{z_\nu^\alpha(x)}\frac{a_\nu dz}{\sqrt{n_0^2(z) - a_\nu^2}}\right|\right]^{1/2}$$

can be interpreted as the modal analog of the vertical radius of the first Fresnel zone [22]. Therefore, our consideration will be valid if

$$\left|\varrho_{f\perp}^2(x,\nu)-\varrho_{f\perp}^2(x,\lambda)\right|\ll l_\perp^2 \quad ; \quad \left|\varrho_{f\|}^2(x,\nu,\alpha)-\varrho_{f\|}^2(x,\lambda,\beta)\right|\ll l_\|^2, \quad (39)$$

where $\varrho_{f\perp}(x,\nu)=\sqrt{2\pi/\kappa_\nu}\,x$ has the sense of the horizontal radius of the Fresnel zone. It is important to emphasize that the conditions (39) are much less rigorous in comparison with the traditional Fresnel conditions for individual geometric ray provided that $\varrho_{f\|}\ll l_\|$, $\varrho_{f\perp}\ll l_\perp$.

Finally, the assumed smoothness of the change of $U_{nn'}^{mm'}$ versus indices n and m enabled us to truncate (26) keeping only the first term in this series. Such approximation will be justified if

$$\left|\Phi_{\nu\alpha}(x)\varrho_{f\|}^2(x,\nu,\alpha)-\Phi_{\lambda\beta}(x)\varrho_{f\|}^2(x,\lambda,\beta)\right|\ll l_\|^2, \quad (40)$$

where $\Phi_{\nu\alpha}^2(x)=<\Psi_{\nu\alpha}^2(x)>$ is the phase variance (38).

4   Asymptotic behavior of the total MCF. Interpretation of the results

The evaluation of the total MCF requires a double summation and twofold integration in (32) and subsequent double summation of the result obtained according to (4). It is a very difficult computational task and in order to make the problem manageable we shall assume, that for sufficiently large propagation distances, the structure function $D_{\nu\lambda}^{\alpha\beta}$ depends mainly on difference argument $\varphi=\alpha-\beta$. As a result the Eq. (32) takes the form

$$\Gamma_{nm}^\perp(1,2)=\frac{1}{2\pi}\sum_{\nu\lambda}\int_0^{2\pi}d\varphi\,e^{-i(n-\nu)\varphi}\Gamma_{\nu\lambda}^\varphi(1,2)\,\delta_{n-m\,;\,\nu-\lambda}.$$

Hence, under the assumption made above the diagonal elements of the matrix $\Gamma_{nm}^\perp(1,2)$ decouple from the off–diagonal elements, that agree exactly with the discussion given at the end of Sec. 1. It should be emphasized that the off–diagonal elements as we can see from $D_{\nu\lambda}^{\alpha\beta}(1,2)$, Eq. (37), are exponentially decaying functions of range. Therefore, these terms will be particularly important in describing the evolution of the total MCF at relatively short propagating distances. With increasing range, the diagonal elements Γ_{nm} in (4) becomes increasingly important and exclusively these terms play a dominant role in modeling the asymptotic behavior of the MCF.

The further simplification of the expression for the total MCF occurs when we again use the WKB approximation for the normal modes. To see the physical implication of this we rewrite Eq. (4) with the help of Eq. (32) as

$$\Gamma(\mathbf{r}_1, z_1, t_1 | \mathbf{r}_2, z_2, t_2) = \frac{1}{(2\pi)^2} \sum_{n,m} \sum_{\nu,\lambda} \int\!\!\!\int_0^{2\pi} d\alpha \, d\beta \, \Gamma_{\nu\lambda}^{\alpha\beta}(1,2) \, J_{n\lambda}^{\alpha}(z_1) \, J_{m\lambda}^{*\beta}(z_2),$$

$$(41)$$

where

$$J_{n\nu}^{\alpha}(z) = \varphi_n(z) \exp\left[i\kappa_n x - i(n - \nu)\alpha \right].$$

Then, we present the cosines in (34) in terms of exponentials

$$\varphi_n(z) = \varphi_n^+(z) + \varphi_n^-(z),$$

where

$$\varphi_n^{\pm}(z) = \left(a_n/\Lambda_n\right)^{1/2} \left[n_0^2(z) - a_n^2\right]^{-1/4} \exp\left(\pm i\theta_n(z)\right)$$

and change the summation variables n, m and ν, λ in (41) to: ν, λ and $q = n - \nu$, $p = m - \lambda$. Using the same analysis as given previously in deriving at (28) we find

$$\Gamma(\mathbf{r}_1, z_1, t_1 | \mathbf{r}_2, z_2, t_2) = \sum_{\nu,\lambda} \left[\Gamma_{\nu\lambda}^+(1,2)\varphi_\nu^+(z_1)\,\varphi_\lambda^-(z_2) + \Gamma_{\nu\lambda}^-(1,2)\varphi_\nu^-(z_1)\,\varphi_\lambda^+(z_2)\right],$$

$$(42)$$

where $\Gamma_{\nu\lambda}^{\pm}(1,2) = \Gamma_{\nu\lambda}^0(1,2) \exp\left[i(\kappa_\nu - \kappa_\lambda)x - \frac{1}{2}D_{\nu\lambda}^{\pm\pm}(1,2)\right]$, and

$$D_{\nu\lambda}^{\pm\pm}(1,2) = D_{\nu\lambda}^{\alpha\beta}(1,2) \text{ at } \alpha = \frac{2\pi}{\Lambda_\nu}x \mp \frac{d\theta_\nu(z_1)}{d\nu}, \beta = \frac{2\pi}{\Lambda_\lambda}x \mp \frac{d\theta_\lambda(z_2)}{d\lambda}.$$

The formula (42) has a direct physical interpretation: each term entering (42) can be identified with the ray contribution to the total MCF propagating in a multipath oceanic channel.

5 Rough surface scattering effects on ocean acoustic coherence

In certain circumstances, for example, when the propagation takes place in an upper sound channel, surface interactions play a predominant role in acoustic signal fluctuations. The formalism developed in the previous sections may be extended to the analysis of acoustic coherence after long range multiple surface scatterings. This can be done as follows.

In the presence of a soft boundary $z = \zeta(\mathbf{r}, t)$, where ζ represents the random displacements of the ocean surface, in addition to the wave equation the following condition on the acoustic pressure field is imposed

$$p(\mathbf{r}, \zeta(\mathbf{r}, t), t) = 0.$$

Concerning the statistics of $\zeta(\mathbf{r}, t)$ we assume the usual hypothesis that $\zeta(\mathbf{r}, t)$ is a Gaussian homogeneous and stationary field with zero mean and is characterized by the spatial–temporal correlation function B_ζ:

$$B_\zeta(\rho, \tau) = \, < \zeta(\mathbf{r}, t) \zeta(\mathbf{r} + \rho, t + \tau) > \, .$$

For a small Rayleigh parameter the explicit boundary condition can be expanded at the mean ocean surface $z = 0$ in powers of ζ to give

$$p(\mathbf{r}, 0) = -\zeta(\mathbf{r}, t) \left. \frac{\partial p(\mathbf{r}, z)}{\partial z} \right|_{z=0} .$$

In the case considered, it is straightforward to derive that the normal mode amplitudes $p_n(\mathbf{r}, t)$ in the representation (1) formally obey the set of stochastic equations (2) in which the coupling coefficients V_{nm} are now defined according to [6]

$$V_{nm}(\mathbf{r}, t) = \varphi_n'(0) \varphi_m'(0) \zeta(\mathbf{r}, t),$$

where the prime denotes differentiation with respect to depth z. Hence, rough surface and volume scattering effects can be formally described in the framework of united approach and the particular scattering mechanism specifies the concrete form of the coupling elements V_{nm}. Therefore, the equations governing the propagation of the MCF in a waveguide with a rough surface are thus the same as before except that the scattering kernel $\sigma_{nn'}^{mm'}$ must be replaced by

$$\sigma_{nn'}^{mm'}(s, s', \tau) = \frac{\pi}{2\kappa_{nm}^+} \left[\varphi_n'(0) \varphi_{n'}'(0) \varphi_m'(0) \varphi_{m'}'(0) \right] F_\zeta(\kappa_{nm}^+ s - \kappa_{n'm'}^+ s', \tau),$$

where $F_\zeta(\ae, \tau)$ is the Fourier transform of the surface autocorrelation with respect to ρ.

A considerable simplification occurs when we deal with long range propagation. In this case, as was mentioned in Sec. 1, for the upper–sound channel having a nonequidistant spectrum of the wavenumbers κ_n, the Eq. (13) at $n \neq m$ reduces to

$$\left[\frac{\partial}{\partial x} - \frac{i}{\kappa_{nm}^+} \frac{\partial^2}{\partial \rho \partial R} + \frac{i}{2} \frac{\kappa_{nm}^-}{\kappa_{nm}^{+2}} \frac{\partial^2}{\partial \rho^2} \right] \Gamma_{nm}^\perp(1,2) =$$

$$= \left[-\frac{1}{2} \left(A_{nn}(1,1) + A_{mm}(2,2) \right) + A_{nn}^{mm}(1,2) \right] \Gamma_{nm}^\perp(1,2). \qquad (43)$$

Thus, as a consequence of (43) we obtain the following representation [23]:

$$\Gamma_{nm}^{\perp}(1,2) = \frac{1}{8\pi\sqrt{\kappa_n\kappa_m}x}\varphi_n(z_0)\,\varphi_m(z_0)\,\exp[-R_{nm}(1,2)],$$

where

$$R_{nm}(1,2) = \big(A_{nn}(1,1) + A_{mm}(2,2)\big)x - \int_0^x dx'\,A_{nn}^{mm}(\rho\frac{x'}{x},\tau).$$

For the diagonal elements $\Gamma_{nn}^{\perp}(1,2)$ a similar procedure as given in Sec. 2 leads to the expression [23]:

$$\Gamma_{nn}^{\perp}(1,2) = \frac{1}{8\pi x}\sum_{m=1}^{M}\frac{1}{\kappa_m}\varphi_m^2(z_0)\int_0^{2\pi}\frac{d\alpha}{2\pi}\,e^{-i(n-m)\alpha - \frac{1}{2}D_{m\alpha}(1,2)}$$

and

$$D_{m\alpha}(1,2) = \sum_{q=1}^{M}\int_0^x dx'\int_{-\infty}^{\infty}d\ae_y\,B_{mq}^{mq}(\kappa_m-\kappa_q,\ae_y,\tau)\Big[1-\cos(\ae_y\rho\frac{x'}{x})e^{i(q-m)\alpha}\Big].$$

6 Evaluation of the intensity and acoustic coherence from oceanic internal waves and fully developed wind seas

To illustrate the effects of random volume and surface scattering on acoustic transmission we consider the realistic deep ocean environments from the North–West Pacific and assuming the Garret–Munk spectrum for B_μ and the Pierson–Moskowitz spectrum for B_ζ. The two sound–speed profiles chosen for our calculations are shown in Fig. 1. They represent summer and winter seasonal averages at latitude 45°N and buoyancy frequency. The summer profile differs from the winter one in possessing an added surface layer of warm water, strengthening the sound channel without greatly changing its deeper regions.

We begin with observing the effect of internal wave scattering on the wavefield intensity as a function of range and depth. The quantity of interest is

$$I(r,z) = <|p(\mathbf{r},z,t)|^2> = \sum_{n,m}\Gamma_{nm}^{\perp}(1,1)e^{i(\kappa_n-\kappa_m)x}\,\varphi_n(z)\varphi_m(z).$$

For many purposes one is interested only in the long range average intensity. In this case as mentioned above the diagonal elements $\Gamma_{nn}^{\perp}$ make the main contribution to $I(r,z)$.
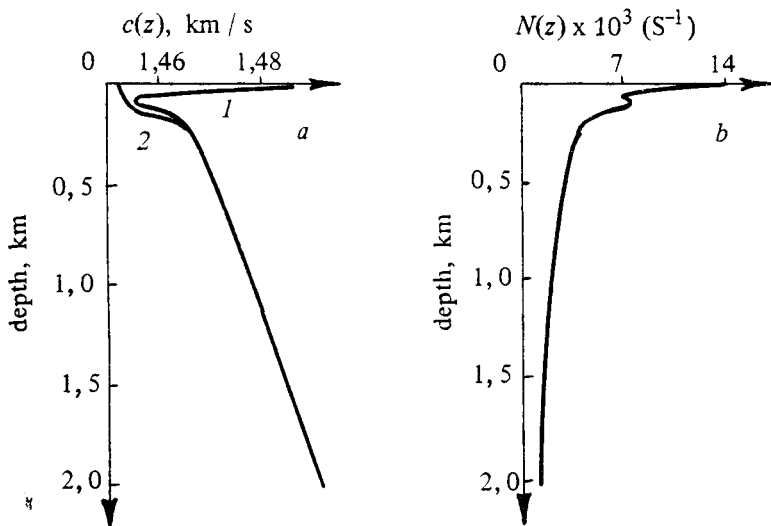
Fig. 1: Sound–speed profiles (a) and buoyancy–frequency distribution (b) from the North–West Pacific. The profiles are: 1 – summer; 2 – winter

Figure 2 shows the behavior of the function $I(r, z)$ (in decibel notation) for fixed r and variable z, or for fixed z and variable r with cylindrical spreading factor removed.

Calculations have been carried out for summer profile, for source frequency of 250 Hz and source depth of 50 m. It is seen from this figure that multiply scattering effects are responsible for redistributing the initial intensity distribution. Distinctly it is observed from Fig. 2a where the initial major peaks at the source and reciprocal depths ($r = 0$) after long range ($r = 1000$ km) become diminished.

In Fig. 3 we plot the normalized MCF in the case of time, transverse horizontal and vertical separations. The theoretical curves in Fig. 3 have been used the results of the work of Esswein and Flatte [24] for the phase–structure density from internal waves.

Analogous graphs for wavefield intensity and correlation functions are presented in Figs. 4 and 5 for winter sound–speed profile assuming that the fully developed wind seas are the dominant source of transmission fluctuations.
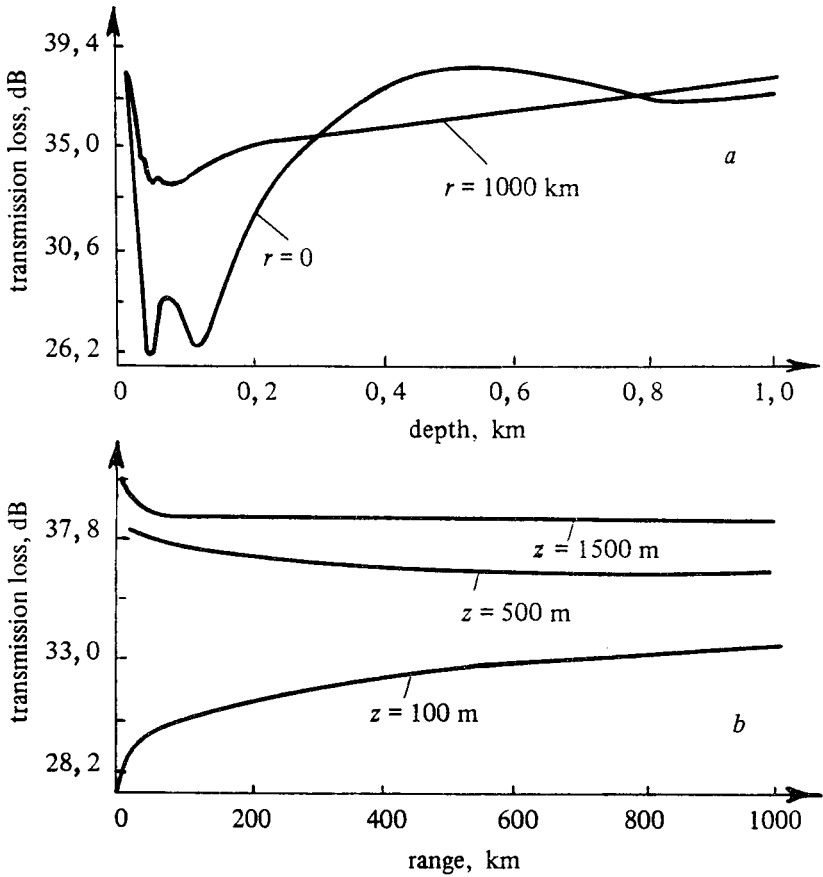
Fig. 2: Reduced intensity as a function of depth (a) and range (b), with cylindrical spreading factor removed, for summer profile. Source frequency is 250 Hz, source depth is 50 m
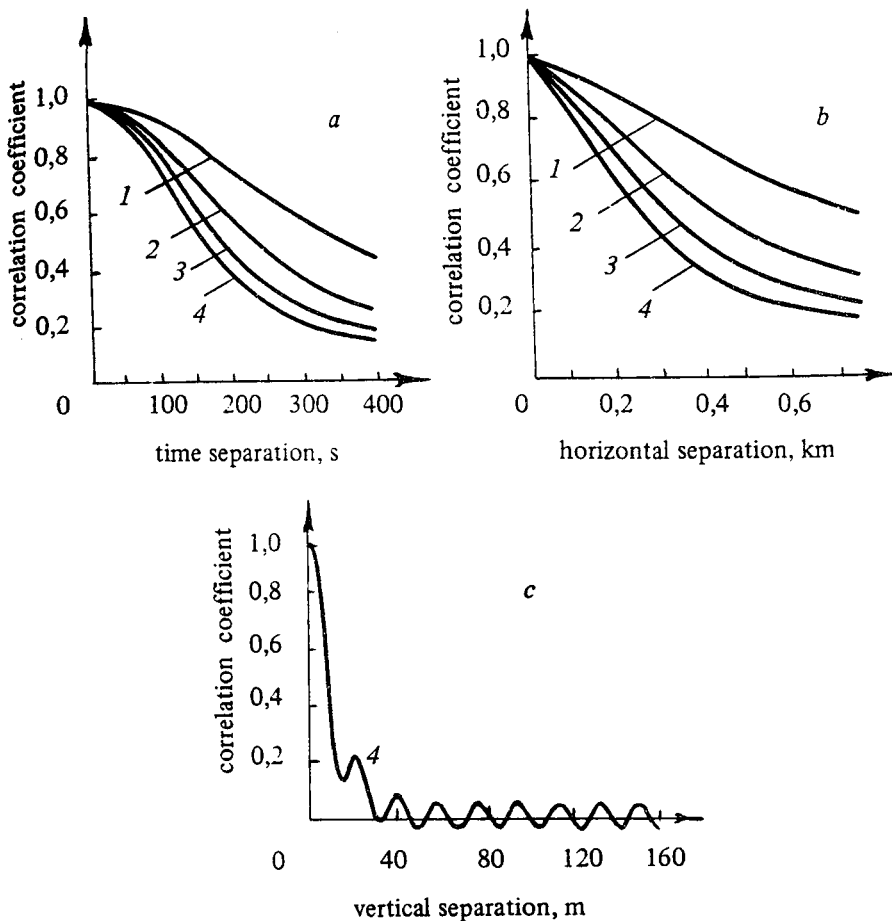
Fig. 3: The normalized MCF of time (a), horizontal position (b) and vertical position (c) for summer sound–speed profile and various ranges: 1 – 250 km, 2 – 500 km, 3 – 750 km, 4 – 1000 km. Source frequency is 250 Hz and source depth is 100 m
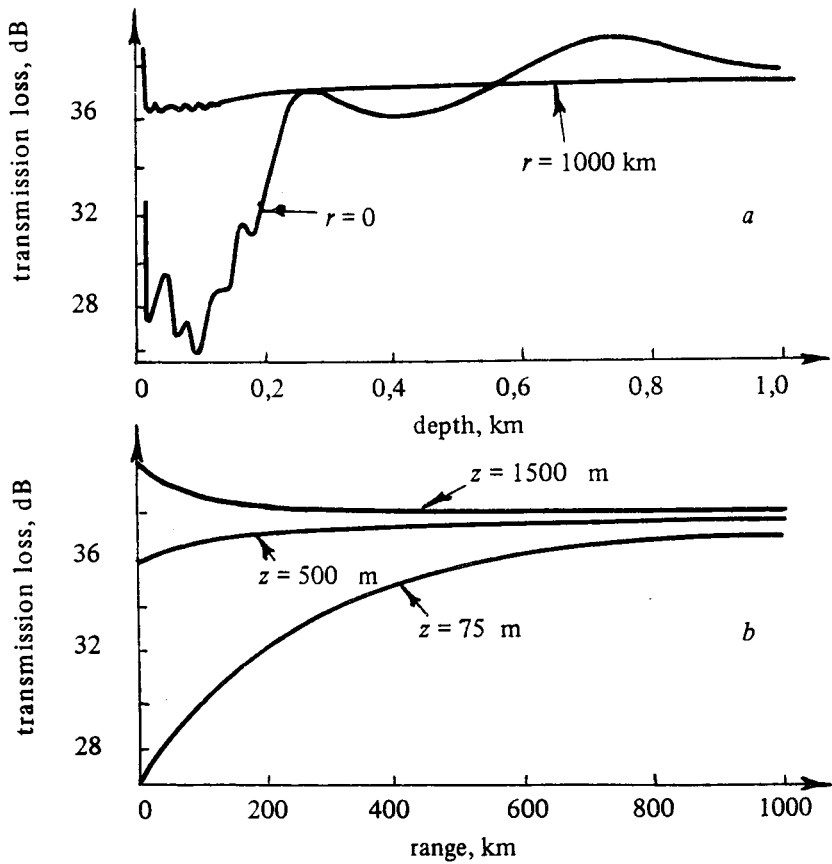
Fig. 4: Reduced intensity as a function of depth (a) and range (b), with cylindrical spreading factor removed, for winter profile. Source frequency is 250 Hz, source depth is 100 m and wind speed v is 15 m/s
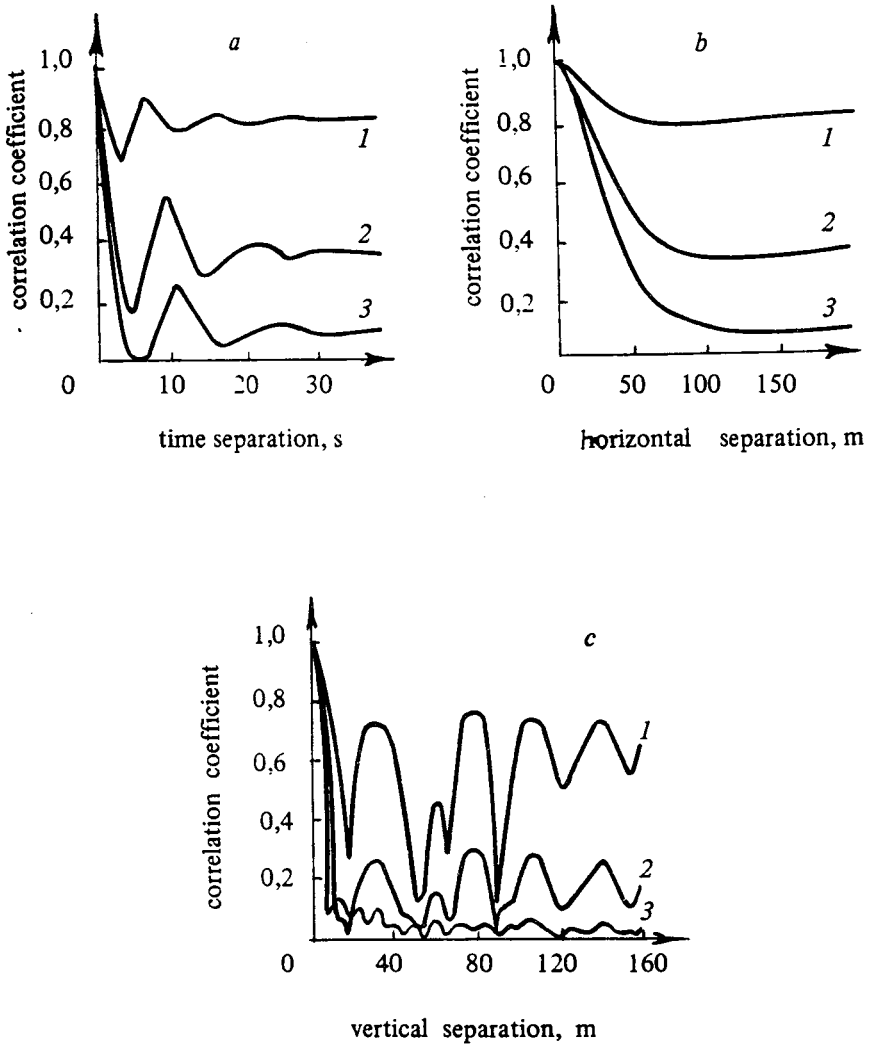
Fig. 5: The normalized MCF of time (a), horizontal position (b) and vertical position (c) for winter sound–speed profile at $r = 500 \; km$ and various surface roughnesses: $1 - v = 10 \; m/s$, $2 - v = 13 \; m/s$, $3 - v = 15 \; m/s$. Source frequency is 250 Hz and source depth is 100 m

7 Summary and conclusions

The mutual coherence function is of great importance in understanding statistical behavior of ocean acoustic transmission. It has been shown in this paper how to efficiently derive an asymptotic expression for the MCF in terms of modal structure of the acoustic pressure field using the radiation transport equation. The method for solving the corresponding matrix equation is based on combined use of the WKB approximation and generating function technique. The procedure elaborated allows one to reduce the problem of the wavefield coherence calculation in a refractive sound channel with random volume inhomogeneities to the analogous problem in free space. The validity conditions for the given formalism are formulated. The method employed was also extended to include rough surface scattering effects. The application is illustrated by numerical computation of the expected acoustic coherence for realistic environments from the North–West Pacific under the assumption that the random field of internal waves or fully developed seas are the dominant source of transmission fluctuations.

Several conclusions may be drawn from the above analysis. First, the volume and surface scattering serve to redistribute the initial intensity distribution as a function of depth. After sufficiently long range, the initial intensity peaks at depth corresponding to the source depth and reciprocal depth become diminished. Rough surface scattering has been established to cause the most significant effects on ocean acoustic coherence. In particular, as observed in the results of Sec. 5, for a source of 250 Hz, at a range of 500 km and wind speed of 15 m/s, the characteristic horizontal coherence length and coherence time have an order of magnitude of 50 m and of 2 s, respectively. For comparison, the corresponding scales computed from the Garrett–Munk spectrum and summer profile in Fig. 1 are of order 400 m and 200 s.

It should be pointed out that the above calculational methods will be useful in the design and analysis of experiments whose purpose is ocean tomography.

References

1. *Dashen R.* Path integrals for waves in random media // J. Math. Phys. 1979. V. 20, № 5. P. 894–920.

2. *Flatte S.M., Dashen R., Munk W.H., Watson K.M., and Zachariasen F.* Sound Transmission Through a Fluctuating Ocean, edited by S.M. Flatte // (Cambridge U.P., New York, 1979).

3. *Macaskill C.C., Uscinski B.J.* Propagation in waveguides containing random irregularities: the second moment equation // Proc. R. Soc. Lond. 1981. A 377. P. 73–98.

4. *Beran M.J., Whitman A.M., and Frankenthal S.* Scattering calculations using the characteristic rays of the coherence function // J. Acoust. Soc. Amer. 1982. V. 71, № 5. P. 1124–1130.

5. *Wilson H.L., Tappert F.D.* Acoustic propagation in random oceans using the radiation transport equation // Ibid. 1979. V. 66, № 1. P. 256–274.

6. *Bass F.G., Fuks I.M.* Wave Scattering From Statistically Rough Surface // (Pergamon, Oxford, U.K., 1979).

7. *Kohler W.E., Papanicolau G.C.* Wave propagation in a random–inhomogeneous ocean // In: Lecture Notes in Physics. V. 70. Wave Propagation and Underwater Acoustics, edited by J.B. Keller and J.S. Papadakis (Springer–Verlag, Berlin, 1977).

8. *Dozier L.B., Tappert F.D.* Statistics of normal mode amplitudes in a random ocean // J. Acoust. Soc. Amer. 1978. V. 64, № 1. P. 533–547.

9. *Beilis A., Tappert F.D.* Coupled mode analysis of multiply rough surface // Ibid. 1979. V. 66, № 3. P. 811–826.

10. *Sutton G.R.* Application of a stochastic waveguide propagation model to ocean acoustics // J. Math. Phys. 1981. V. 22, № 12. P. 974–976.

11. *Kryazhev F.I., Kudryashov B.M., and Petrov N.A.* Propagation of low–frequency sound waves in a waveguide with irregular boundaries // Sov. Phys. Acoust. 1976. V. 22, № 3. P. 21–24.

12. *Dolin L.S., Nechaev A.G.* Mode description of the acoustic field interference structure in a waveguide with statistically rough wall // Izv. VUZov. Radiofizika. 1981. V. 24, № 11. P. 1337–1344 (in Russian).

13. *Moiseev A.A.* On the evaluation of field coherence function in a randomly inhomogeneous waveguide // Dokl. Akad. Nauk USSR. 1984. V. 279, № 6. P. 1339–1344 (in Russian).

14. *Sazontov A.G., Farfel' V.A.* On the calculation of low–frequency sound attenuation in the ocean due to scattering by internal waves // Akusticheskii Zhurnal. 1986. V. 32, № 4. P. 492–498 (in Russian).

15. *Artel'nyj V.V., Kukushkin V.D., Raevskij M.A.* On energy and correlation characteristics of low–frequency acoustic waves in underwater sound channels // Ibid. 1986. V. 32, № 4. P. 591–597 (in Russian).

16. *Sazontov A.G.* Calculation of the two–frequency mutual coherence function and the time pulse moments in a random–inhomogeneous ocean // Ibid. 1989. V. 35, № 5. P. 908–916 (in Russian).

17. *Landau L.D., Lifshitz E.M.* Quantum Mechanics // (Nauka, Moscow, 1989) (in Russian).

18. *Isimaru A.* Wave Propagation and Scattering in Random Media // (Academic Press, New York, 1978).

19. *Dolin L.S.* On the light scattering in a layer of turbid medium // Izv. VUZov. Radiofizika. 1964. V. 7, № 2. P. 61–68 (in Russian).

20. *Migdal A.B.* Qualitative Methods in Quantum Theory // (Nauka, Moscow, 1975) (in Russian).

21. *Sholin D.V., Kosterin A.G.* Analysis and calculation of statistical characteristics of mode amplitudes in waveguides with volume random inhomogeneities // Akusticheskii Zhurnal. 1991. V. 37, № 5. P. 956–964 (in Russian).

22. *Virovlyanskij A.L., Kosterin A.G.* Fresnel volumes in multimode waveguides // Izv. VUZov. Radiofizika. 1989. V. 32, № 4. P. 478–486 (in Russian).

23. *Sazontov A.G., Farfel' V.A.* Calculation of the coherence degree and the shape of an acoustic pulsed signal in an oceanic waveguide with a rough surface // Akusticheskii Zhurnal. 1995. V. 41, № 1. P. 128–133 (in Russian).

24. *Esswein R., Flatte S.M.* Calculation of the phase–structure function density from oceanic internal waves // J. Acoust. Soc. Amer. 1981. V. 70, № 5. P. 1387–1396.

SOUND SCATTERING BY SPATIAL-LOCALIZED INHOMOGENEITIES IN OCEANIC WAVEGUIDES: CALCULATION AND MEASUREMENT METHODS

S.M.Gorsky, V.A.Zverev and A.I.Khil'ko

Diffraction of the acoustic fields by spatially localized inhomogeneities in oceanic waveguides is investigated by analytical methods using numerical experiments on the basis of physical modelling and by the way of field measurements. The possibilities of numerical simulation and measurement under the conditions of physical modeling1 are discussed. It was shown that from the point of view of studying the diffraction phenomena in the ocean, the significance of these methods is due to the difficulties in performing hydroacoustic experiments. Provisional calculations and measurements under the model conditions can noticeably increase the efficiency of sophisticated field observations. Besides using the results obtained by different authors, a systematic concept of the structure of perturbed signals in the waveguides and a brief analysis of the possibility of the formulation and measurement of diffracted fields in layered waveguides are proposed.

INTRODUCTION

Field diffracted by inhomogeneity in an oceanic waveguide is formed by interference of normal waves. In this context, the field structure can be much more complicated than the similar structures observed in free space. In particular, the inhomogeneity - produced perturbations can noticeably exceed the similar perturbations in free space, owing to the field concentration by the waveguide with respect to depth. Meanwhile, local attenuation of the acoustic field will be observed because of the destructive interference. The problem considered is an internal boundary-value problem of diffraction for irregular waveguides. When bodies have an arbitrary form or a complex internal structure, the numerical methods which allow solutions to be found with finite accuracy are used for solving such problems. These methods include the technique based on the Rayleigh hypothesis of the diffraction field representation in the form of a set of divergent waves [1], the techniques using the solutions of integral equations [2,3], the T-matrix procedure [4] and other methods [5,6,7]. All these methods can be used for solving the internal problem of diffraction for irregular waveguides. However, the problem becomes more complicated since it is rather problematic to find an appropriate, coordinate

system that can easily satisfy the boundary conditions on the perturbing body as well as at the boundaries of the waveguide. There is a number of methods of solution of this problem based on the assumption of smallness of the multiply, scattered fields as well as of the weak variability of the waveguide properties to the inhomogeneity scales [8,9,10]. Besides that, the methods using either a long-wave or a short-wave approximation of the diffraction due to inhomogeneities are used for solving the internal problem of diffraction in irregular waveguides [9,10]. On the whole, it should be mentioned that the papers mentioned above have one feature in common. They all try to divide the general problem into two separate problems of acoustic wave propagation and scattering defining an algorithm in a certain range of parameters (dimensions, frequency, etc.) for construction of a general solution by using the well-known solutions for acoustic fields in irregular waveguides and for acoustic wave scattering in free space. Such an approach makes it possible to use the results obtained earlier to analyze the problem.

ANALYSIS OF THE METHODS OF SOLUTION

The internal boundary-value problem for irregular waveguides is formulated as follows: the perturbed field, which represents a sum of the unperturbed Ψ_0 field and the diffracted Ψ_s field (where Ψ is the displacement velocity potential) must satisfy the scalar wave equation, the initial conditions, the conditions of emission and the boundary conditions at the boundaries of the waveguide and on the surface of the perturbing body. All these conditions, together with the wave equation (with variable coefficients in the case of irregular waveguides), can be represented as a relation which includes the Green is function. We thus arrive at an equivalent but a different formulation of internal boundary-value problem

$$\Psi(\vec{R}) = \frac{1}{4\pi} \int_S [G(\vec{R}, \vec{R}_s)\nabla_s \Psi(\vec{R}_s) - \Psi(\vec{R}_s)\nabla_s G(\vec{R}, \vec{R}_s)]d\vec{A}_s +$$

$$+ \int_V \rho(\vec{R}_\rho)G(\vec{R}, \vec{R}_\rho)dv_\rho, \qquad (1)$$

where S is the surface of the perturbing body, $\vec{R}, \vec{R}_s, \vec{R}_\rho$ are the radius-vector is of the points of observation, of the surface of the body and of the extended source $\rho(\vec{R}_\rho)$, respectively (Fig.1). The function $G(\vec{R}, \vec{R}_i)$ is the Green's function. From Eq.(1) it follows that knowledge of the field and its derivative normal to the perturbing body surface is required to define the perturbed field. Equation (1)

64

$$\vec{e}=\{\,\zeta,\eta\,\}, \quad \vec{R}_0=\{\vec{r}_0,z_0\}, \quad \vec{R}=\{\vec{r},z\}$$
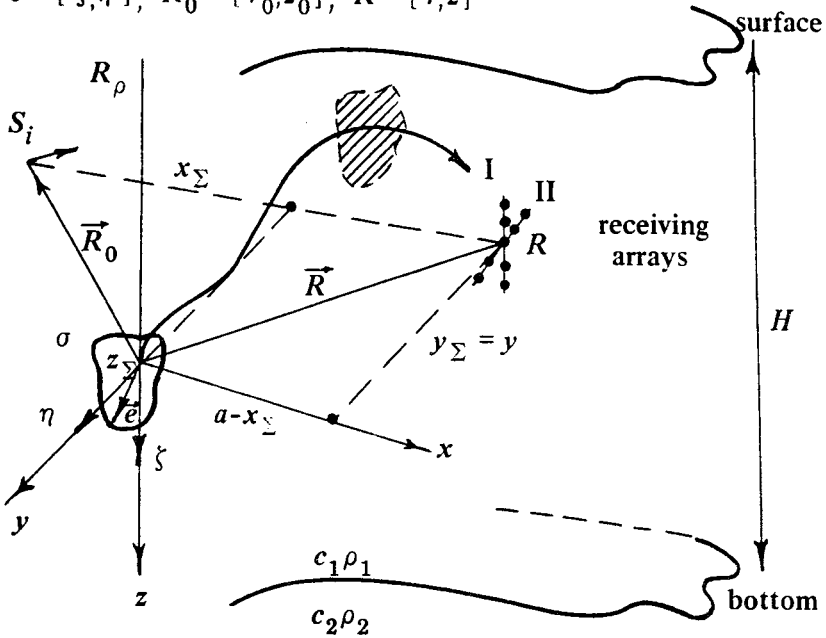
Fig. 1. The disposition of source, scatterer and receiving system.

includes the impedance of the body surface in implicit form, which relates the field and its normal derivative. For closure of Eq.(1) we must, in general, solve the body oscillation problem.

In a case, when perturbing body can be characterized by a local impedance, the integral equation for the acoustic field and its derivative on the body surface, which follows from Eq.(1) when the point of observation is dropped to the surface S, becomes re-defined and can be reduced to the Fredholm integral equation of the first or second kind. For solving the problem of diffraction in free space one generally uses the methods reducing the integral equations to an infinite system of algebraic equations [3,4]. At the attempt to use these methods for solving the internal problem of diffraction, besides the difficulties due to the resonance phenomena, the difficulties associated with the multiple scattering effects and with an adequate description of the transformation of various modes in waveguides with elastic walls are

added. Nevertheless, solution of Eq.(1) can be found by different methods defining differently the Green's function.

Appoximations of the waveguide Green's function. The Green's function in a waveguide has rather a complex structure and the contribution of its different components changes considerably when receding from the source. In particular, the traveling waveguide modes contribute most when they are spaced well from the source. Rather often, contributions from the leaky modes and the continuous spectrum modes can be neglected under the conditions of smallness of the multiple scattering effects. For analysis of diffracted fields in the waveguides at large distances from the source the waveguide Green's function is generally used in the form of a sum of undamped traveling modes:

$$G(\vec{R}, \vec{R}_s) = \sum_{n=0}^{N} \varphi_n(z_\rho)\varphi_n(z_s)e^{ih_n|\vec{r}_\rho - \vec{r}_s|}(h_n|\vec{r}_\rho - \vec{r}_s|)^{-1/2}, \qquad (2)$$

where $\varphi_n(z)$ and h_n are the eigenfunctions and the eigenvalues of the Sturm-Louiville problem for an unperturbed waveguide, $\vec{r} = (x, y)$ are the horizontal coordinates and N is a number of propagating waveguide modes. Expression (2) defines $G(\vec{R}, \vec{R}_s)$ for horizontally uniform waveguides of various types including a refraction waveguide. Analytical solutions for $\varphi_n(z)$ are found for some simple dependencies of the refractive index. In particular, such solutions are found for oceanic waveguides, such as an isovelocity waveguide in the liquid and elastic half-spaces, a surface waveguide with a linear dependence of sound velocity on depth, a bilinear waveguide and a waveguide with parabolic profile. In many cases, however, the numerical methods have to be used to find the eigenvalues. Note that the use of the Green's function in form (2) for solution (1) has become widespread for solving the internal boundary-value problems of diffraction both in electrodynamics and in acoustics [5,7,9]. In these papers, $G(\vec{R}, \vec{R}_s)$ in form (2) is used for solving the integral equation for bodies of arbitrary form by reducing the integral equation to a set of linear algebraic equations using the Krylov-Bogolyubov method (the piece-constant approximation). Since the function $G(\vec{R}, \vec{R}_s)$ has algorithmic singularity, the latter is at first singled out in explicit form when the matrix elements of the set of equations are calculated and then the solutions of these equations become stable.

We have discussed some methods for solving the internal boundary-value problem of diffraction for irregular waveguides of universal nature, which permit a rigorous and consistent substantiation. Meanwhile, certain difficulties are encountered when using such methods.

66

which are due to the estimation of accuracy and validity of the results obtained. All these methods are based on rather complicated algorithms of calculations. In this relation, of much interest are the investigations of the internal boundary-value problem of diffraction in waveguides based on the evristic methods. In particular, we should mention the papers using the approximations of short-wave [5,7,9] diffraction. Characteristic of this approximate method is that it can be used only in a limited range of parameters of the problem. However, practice shows that the approximate method possess a higher efficiency, relative simplicity of the algorithms and physical clarity. These features have an importance in the analysis of this problem applied to refraction oceanic waveguides where the structure of unperturbed fields is rather complicated.

Short-wave approximation. A different approach was proposed [5,7] where the dimensions of the perturbing body were assumed to be much more than the wave length. Assigning the boundary conditions on the surface of the body and making use of the Kirchhoff approximation in the small-angle approximation one can obtain a simple expression for the scattering matrix of the waveguide modes S_{nm} [5,7]:

$$S_{nm} = ih_n \int_\xi T(\xi)\varphi_m(\xi + z_\Sigma)\varphi_n(\xi + z_\Sigma)d\xi \int_\eta L(\eta)e^{i[\frac{h_n y_{so}}{S'} + \frac{h_m y_r}{r'}]\eta}d\eta, \quad (3)$$

where $\sigma(\xi, \eta) = T(\xi)L(\eta)$ is a function describing the form of the screen limited by the shadow-forming line of the body; y_{so} and y_r are the horizontal displacements of the source and the receiver from the horizontal line normal to the screen and passing through the screen center; $S' = (x_\Sigma^2 + y_{so}^2)^{1/2}$, $r' = ((a - x_\Sigma)^2 + y_r^2)^{1/2}$; x_Σ and a are the distances from the illumination field source to the body and the distance between the source and the point of observation respectively. Unlike the scattering matrix, expression (3) (obtained in [5]) does not permit to show explicitly the scattering diagram on the body, corresponding to the scattering in free space, but S_{nm} in form (3) allows calculations to be performed when h_n and φ_n change on scales less than the dimensions of the body.

This approximate method mentioned above is based on the assumptions that play an important role in physics and which were proved many times in the experiments in an appropriate range of parameters. In particular, the calculations of diffracted fields in a hydroacoustic waveguide in the short-wave approximation were compared with the experimental results. The comparison showed high efficiency and good accuracy of the calculations [5]. Besides the method of comparing the calculations with the measurements, there is another method which compares the calculations based on the approxi-

mate methods with the results obtained by using more rigorous methods and compares the results obtained by different methods if they apply in the same range of parameters.

THE STRUCTURE OF PERTURBED ACOUSTIC FIELDS

Below we analyze the structure of perturbations by a localized inhomogeneity in a waveguide of an oceanic type in the short-wave approximation. First of all, we should note that when the hydroacoustic field perturbations far from the inhomogeneity (specifically a perfect solid of arbitrary shape) are analyzed, the leaky modes and the continuous spectrum modes can be assumed to be small. In this case, the matrix elements S_{nm} (Eq. (3)) in the small-angle approximation are the refractive indices of the waveguide modes. From expression (3) it is seen that the integral over a plane, limited by a shadow-forming line, can accurately be represented in the form of a product of two integrals defining the diffraction along the respective coordinate for many configurations of perturbing bodies and it can be represented like this approximately for other configurations. Diffraction with respect to depth leads to transformation of the mode spectrum, and the energy transformation from a mode with number n into a mode with number m is defined by the matrix element:

$$T_{nm} = \int_{\xi} T(\xi)\varphi_m(z_{\Sigma} + \xi)\varphi_n(z_{\Sigma} + \xi)d\xi \qquad (4)$$

If the screen dimensions d are much less than the characteristic dimension of the function $\varphi_n(z)$, then each incident mode will be uniformly transformed into all diffracted modes. As the vertical dimensions of the screen increase, the number of modes, into which effective energy rescattering will occur, will decrease. The conditions for (d_{max}, z_r^{max}) under which T_{nm} takes the maximum value, was considered in paper [7]. In smoothly inhomogeneous waveguides Eq.(4) can be represented as a mode filter:

$$T_{nm} = \mp\frac{\pi}{2}[\widehat{T}_{n\pm m} - \widehat{T}_{n\mp m}], \qquad (5)$$

where $\widehat{T}_{n\pm m} = \frac{1}{2\pi}\int_{-\infty}^{\infty} T(\xi)e^{i\xi(q_n \pm q_m)}d\xi$, q_m is a vertical projection of the wave vector for a mode with index m. Assigning the excitation coefficients of the incident modes a_n, the diffracted modes can, in view of (5) and (3), be described by a relation

$$a_m = -\sum_{n=0}^{N} \frac{\pi}{2} \quad a_n \quad [\widehat{T}_{n+m} - \widehat{T}_{n-m}] \quad L_{nm}, \qquad (6)$$

68

which represents contraction of the mode spectrum with the frequency response of the space filter. In approximate calculations, where the mode spectrum has greatly nonequidistant frequencies and the screen has large dimensions, one can retain only the term $\widehat{T}_{n-m}$ in Eq.(6).

According to Eq.(6), the diffracted field represents a superposition of horizontally diffracted structures $L_{nm}(y_r)$, having depth-dependent complex coefficients defined by set of T_{nm} and a_n. The integral L_{nm} represents an analog to the expression defining diffraction on the screen in free space, which is well known in radiophysics and in optics [11]. Characteristic of this integral is the presence of an expression $-ih_n\eta y_{so}(S')^{-1}$ in the exponent and the dependence of the space frequency $h_m y_r (r')^{-1}$ on the diffracted mode number. In the particular case of normal incidence of the field, where $y_{so} = 0$ and $L(\eta) = 1$ at $|\eta| \le \eta_0$ and 0 at $|\eta| > \eta_0$, the horizontal distribution in each of the partial diffracted structures will be described by the relation:

$$L_{nm} \sim \eta_0 \sin(\frac{h_m}{r'} y_r \eta_0)(\frac{h_m}{r'} y_r \eta_0)^{-1}, \tag{7}$$

as the intermode dispersion and the distance from the screen to the reception domain increase, the differences in the scales of partial diffraction structures will grow. Deviation of the observation point from the line normal to the screen and passing through the screen center causes distortions due to the interference of mode partial diffraction structures. The condition of intersection of space variation spectra owing to the mode interference and the diffraction of each mode can be written in the form:

$$(4\pi r_0' \Delta h_{ij}^{-1})^{1/2} \approx r_0' \pi (< h_{ij} > \eta_0)^{-1}, \tag{8}$$

where $r_0 = a - x_\Sigma$, Δh_{ij} is the difference of the horizontal projections of the mode wave numbers, $< h_{ij} >$ is the mean value of the wave numbers, and η_0 is the horizontal dimension of the inhomogeneity. Figure 2 shows qualitative dependencies of the perturbed field intensity at different distances behind the screen. In the first case (Fig. 2a), the field variations due to the mode interference occur at the lower frequencies while in the second case (Fig. 2b), at the higher frequencies as compared to the diffraction-produces field variations.

When the horizontal dimensions of the screen are sufficiently large, one can observe space division of the partial diffraction structures of separate modes with the side illumination:

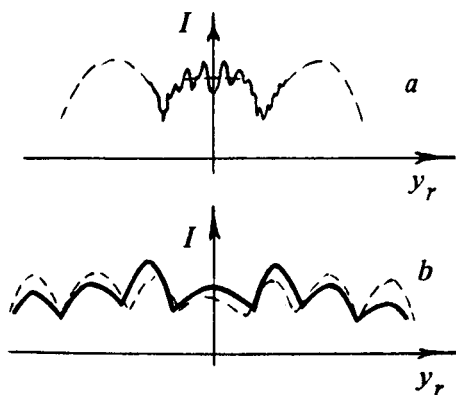$$y_{so}\eta_0(h_i - h_j)(2\pi x_\Sigma)^{-1} \ge 1. \tag{9}$$

Fig. 2. The field variations due to the mode diffraction and interference (variations without inhomogeneities is shown by dashed line).

In order to reconstruct the resultant spatial-temporal distribution of the perturbed field in oceanic-type waveguides one should summate the waveguide modes with the overexcitation coefficients a_m (see Eq. (6)). Since oceanic waveguides are most often multimodal ones, this summation has to be performed by a computer, which is reasonable also because solving the waveguide eigenvalue problem often reduces to solving the higher-order transcendent equations. Figure 3 shows the numerical structure of perturbation for an oceanic waveguide which represents a layer of liquid on a liquid half-space, for a rectangular screen on the case when four modes were excited in the layer of liquid ($H = 130\,m$, $c_1 = 1500m/s$, $c_2 = 1505m/s$, $2\eta_0 = 20\lambda$, $d = 2.4\lambda$, $a = 1.4x10^4\lambda$, $x_\Sigma = 4x10^3\lambda$, $z_0 = 2\lambda$, $z_\Sigma = 10\lambda$). It is seen that the variations developing along the horizontal coordinate y are considerably smoother. Unlike the free space, where perturbations in the far zone are close to the unperturbed field at the center of the structure ($y = 0$) (the dashed line in Fig.3), in the waveguide, perturbations can take both maximum and minimum values owing to the interference nature of the waveguide field. Maximum perturbations to depth occur in the region of either constructive or destructive interference of modes. This is illustrated by Fig. 3b at $z = 100m$, where a minimum was formed in the unperturbed field. If the illumination field is incident on the screen at an angle, then partial diffraction structures can be separated in space. Consider the manifestation of this effect in the frequency plane. If the screen is shifted from the line connecting the source and the observation region, then the receiver will fall into different parts of the direction pattern of the diffracted wave when the illumination field frequency is scanned. On the whole, this will be manifested as modulation of the diffracted field along the frequency axis. Figure 4 shows the dependence of the
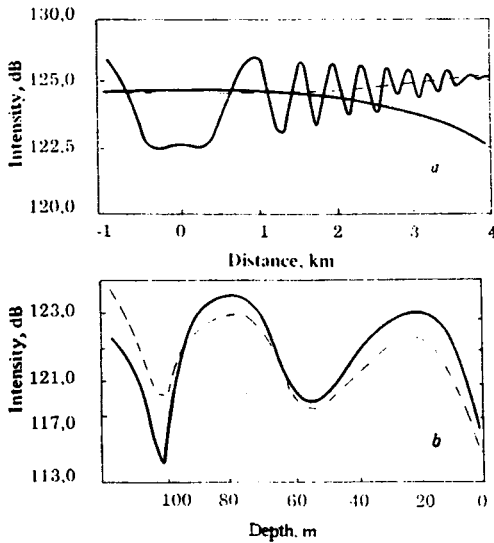
Fig. 3. The structure of horizontal and vertical perturbations (undisturbed field is shown by dashed line).

normalized matrix element $\sigma_{nm} = <|P_d|^2>/<|P_0|^2>$, showing how many times the intensity of the diffracted field is less than the intensity of the illumination signal for a receiving system having equal coefficients of excitation of the received mode m and the illumination mode with number n (it's supposed that one mode with number n is incident out the body and one mode with number m is received). Figure 4a shows the dependencies $\sigma_{nm}(f)$ for different displacements of the screen along the axis of frequencies f. Since frequency scanning occurs at fixed values of the vertical angles of illumination and observation, the numbers n and m depend on the frequency of the illumination field. The screen is located at a fixed depth and, therefore, when scanning the frequency of the incident field, the screen falls into the mode of the incident or diffracted mode for some frequencies. This is manifested as a set of zeroes of the function σ_{nm}, shown in Fig.4b (these features of the function σ_{nm} are not exhibiters in Fig.4a).

Up to a few hundred modes are excited in deep-water oceanic channels. Deep shadow zones and convergence zone emerge as the result of their constructive or destructive interference. If the dimensions of the perturbing body are small, then the latter can fall entirely into the shadow region. On the other hand, if the body is located in the focusing zone, it can be illuminated nonuniformly. Of course, if conditions (7) are satisfied, the field variation spectra will intersect and it will be problematic to isolate the diffracted field structure.
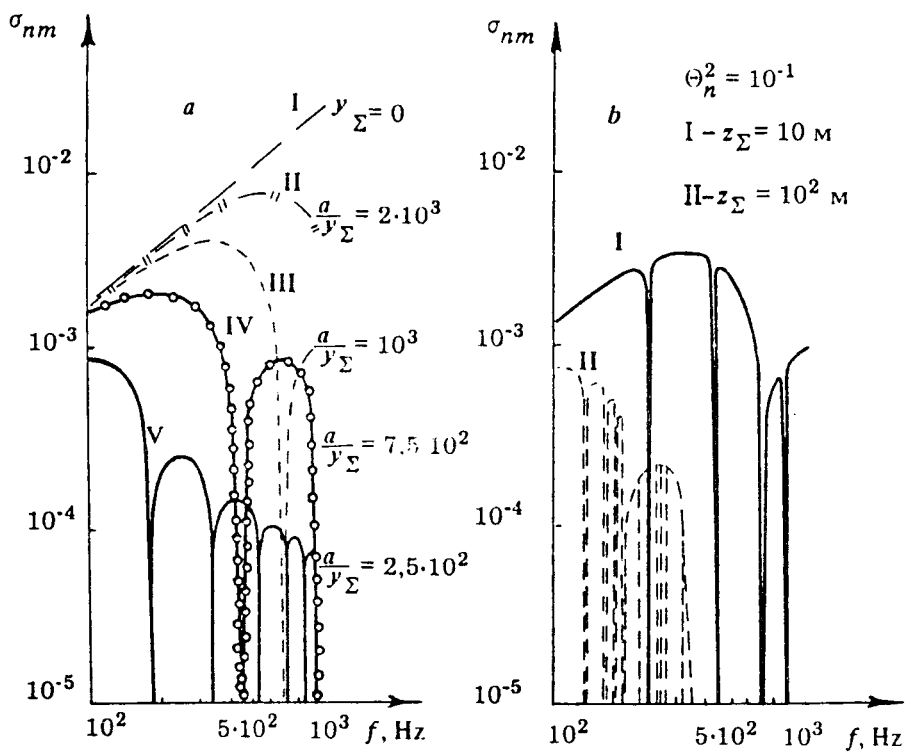
71

Fig. 4. The dependencies of normalized matrix element σ_{nm} on frequency.

OBSERVATIONS AND MEASUREMENTS OF DIFFRACTED FIELDS IN WAVEGUIDES.

Measurement of diffracted hydroacoustic fields in a small-angle approximation under field conditions is impeded by their relative smallness and time dependence and by the inhomogeneity of the hydroacoustic channels. A diffracted, relatively weak signal is observed against the background of a large fluctuating illumination signal. Thus, the accuracy of measurement will be limited considerably unless the measures are taken to lower the fluctuation level. A natural method of increasing the accuracy of measurement is the spatial-temporal filtering including the use of spatially developed receiving systems.

Vertically developed arrays. Papers [12,13] consider the possibilities of isolating a diffracted signal by vertical receiving-transmitting arrays in combination with quasiharmonic probing pulse of illumination (the differential method). The main principle of the differential method of measuring diffracted fields in waveguides consists on the use of the emitted mode with number n and the received mode with number m. By way of temporal gating of signals one isolates those diffracted in the layers of width Δx, into which the whole path of observation from the source to the observation region can be divided; the spatial resolution is $\Delta x = v_n v_m T |v_n - v_m|^{-1}$, where $v_{n,m}$ are the group velocities of the modes, and T is the duration of the probing pulse. The higher the intermode dispersion is, the more efficient the differential method is. Therefore, such a measurement technique should be used in shallow-water areas or in surface channels with a high sound velocity gradient in depth. The degree of mode selection is also defined by the dimensions of the arrays. Taking into account the technical difficulties in creating extended arrays one should use, where possible, the natural zones of mode shadow [14,15], or use complex pulses with their respective compression in the receiving system as illumination pulses to facilitate the isolation of mode pulses [16]. (It should borne in mind that such a method requires an a'priori value and correction of intramode dispersion).

Spatial filtering of signals by a horizontal array. Another method to single out a weak signal against the background of the fluctuation field of direct illumination is to image the perturbing body, which requires the use of a sufficiently large array for focusing [17]. If the source of the illumination field and the perturbing spatially localized inhomogeneity are spaced to a distance exceeding the spatial resolution of the horizontal array in defocusing, then the level of the illumination field in the perturbing region image will be reduced considerably. Obviously, for a further decrease of the direct illumination level it is

needed to use the dark field method, developed in optics, which is based on filtering the low-frequency part of the space spectrum forming the illumination background. These method allow the accuracy in measurement of diffracted signal to be increased by broadening the dynamical range in which the signal is measured. It should be noted that the fluctuations, the space scales of which coincide with the spectrum of the perturbing inhomogeneity, cannot be completely suppressed by space filtering, which uses a'priori information on the location of the illumination source (the dark field method). In order to suppress the noises of this kind, it is necessary to use also the a'priori information on the expected structure of the diffracted signal. However, matched of filtering impedes appreciably the measurements.

Temporal gating of signals. In the measurement of diffracted signals, an essential role is played by the possibility of detuning from the noises due to reverberation from the structure elements. In oceanic waveguides, such noises are caused by the reflection or scattering of the illumination field from the bottom irregularities. A possible way to isolate a useful signal can be the use of pulsed signals for illumination with a subsequent gating of required pulsed volumes. However, the use of quasiharmonic pulses for noise selection in the measurement of fields diffracted at small angles is not effective, since often the noises are located in the same pulsed volume as the scatterer. For higher efficiency of the temporal filtering of direct signal it is more preferable to use complex pulses in combination with their matched processing. Since the duration of an equivalent compressed pulse is small, its pulsed volume reduces and the efficiency of temporal selection increases [17]. The use of complex pulses in the measurement of fields diffracted by spatially localized inhomogeneities is connected with some difficulties due to the deterioration the pulse structure because of the inter- and intramode dispersion. Hence either the measurement conditions should be such that dispersion will not break considerably the pulse structure or filters should be used for compensation of the dispersion influence.

Synthesis of apertures. If the inhomogeneity in the waveguide is immobile, or the characteristic time of its steady state is small, then diffracted fields in the waveguides can be measured with the accuracy required by means of synthesis of apertures [26]. This method is based on sequential measurements of signals with shifting the source and or receiver relative to the localized inhomogeneity. This provides the same accuracy in measurement as that achieved when larger arrays are used by way of aposteriori joint processing of signals. Space resolution that is achievable by synthesis of apertures is defined by the dimensions of the synthesized aperture. It should be noted that the
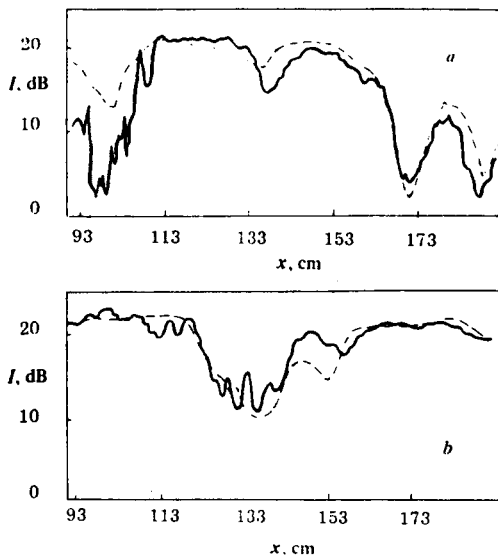
Fig. 5. The dependence of the field intensity variation when receding the point of observation.

source or receiver move at a finite velocity it is possible to isolate the signals of separate modes by filtering the respective Doppler shifts [18], but the latter are small in case of small-angle diffraction, which makes it difficult to determine the contribution of modes to the diffracted field.

The criterion of efficiency of the methods for calculation of the diffracted field structure in oceanic-type waveguides is based on the comparison of calculated and experimental data. Many works in electrodynamics, optics, and microwave engineering for two-dimensional bounded waveguides were devoted to such a comparison. However, it is seen from the literature that measurements of diffracted fields and comparison of experimental data with calculations, as applied to oceanic waveguides having specific features, were performed only in a few papers [19,20].

Figures 5,6 and 7 show the measurements of the horizontal and vertical structures of diffracted fields measured in an isovelocity layer of liquid $(c_1 = 1478,3 m/s, \rho_1 = 1 g/cm^3)$ of thickness 3 cm, resting on a rubber base $(c_2 = 1700 m/s, \rho_2 = 1.13 g/cm^3$, the tangent of the loss angle 0,28). The measurements were made at a frequency 512 kHz for the emitted pulse duration 100 ms. A steel cylinder of length 3,5 cm and a diameter 0,3 cm and 0,6 cm was used as a perturbing body. Figure 5 shows the dependencies of the field intensity variation as the point of observation recedes from the cylinder on the horizon 2,25cm (a) and 0,75 cm (b) when the emitter was at a depth 1,5 cm and the body was at a depth 2,5 cm at a distance 93 cm from the source. Field attenuation is observed directly behind the cylinder. This can be explained by the energy transformation to high-frequency modes as the
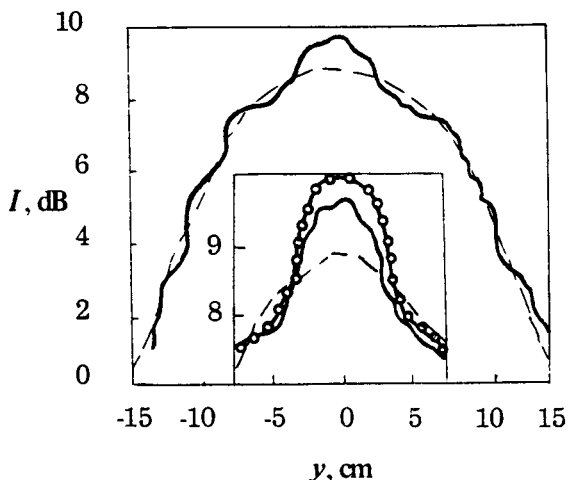
Fig. 6. The transverse distribution

result of diffraction and their subsequent damping in the absorbing bottom. Figures 6 and 7 show the measurements of the transverse and vertical distributions, respectively, at a depth 2,5 cm and 70 cm from the cylinder (the dashed line in Figs. 5,6 and 7 shows the unperturbed fields). The field decay as the receiver is displaced from the symmetry axis (Fig. 6) can be explained by the directive (the width of the direction pattern in a horizontal direction is 4.2°) of the source field and partly by the interference of the lower modes in the layer of liquid. Weak field variations under positive displacements of the receiver is a consequence of the incident field scattering due to local roughness of the bottom surface. Perturbations of the field, when a body is introduced into it, are defined by the directivity of the diffracted field, to a smaller extent, by the interference of modes. When receding from the cylinder, the field intensity at the center of the pattern changes from the maximum to the minimum with a quasiperiod, defined, as it must be, by the interference of modes. The vertical structure of an unperturbed field is formed mainly by the lower modes (shown by a dashed line in Fig.7), which is manifested as a decrease of field roughness when receding from the cylinder, where dissipation of higher modes in the bottom is stronger (Fig.7a). Diffraction of the field on the cylinder enriches the mode spectrum, which is seen as an increase of field roughness (shown by a solid curve in Fig. 7). A simple waveguide model adopted in the measurements allowed the measurements to be used for validation on the calculations within the framework of the short-wave model of
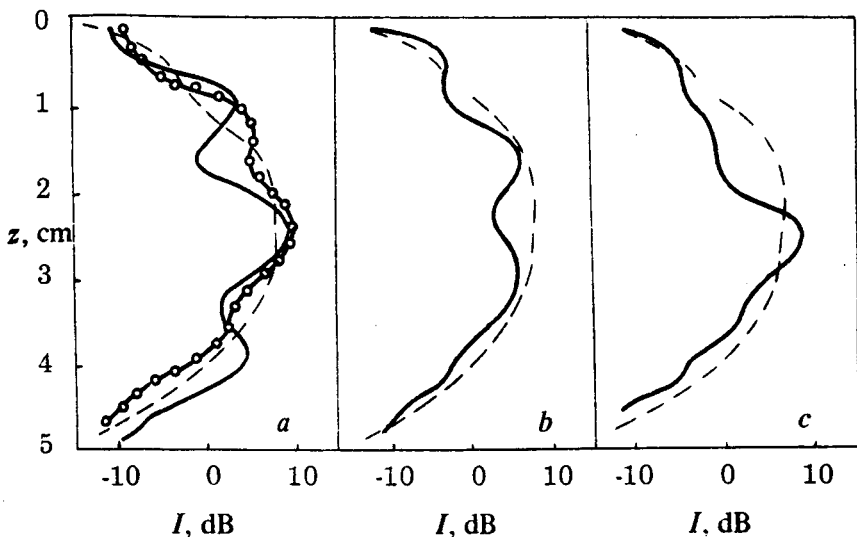
76

Fig. 7. The vertical field variations.

diffraction on bodies in waveguides [19]. Figures 6 and 7a (curve ○ ○ ○) show the calculations for a numerical model describing the conditions of measurements, in which the expressions obtained by Kronhausen-Renier [21] are used to take dissipation into account; the losses due to the excitation of transverse waves were taken into account by way of an equivalent increase of dissipation in the liquid half-space. Comparison of the measured and the calculated data shows good coincidence of the results. The observed differences are first of all due to the limitedness of the numerical model, owing to which the real conditions of measurements are not taken into account in sufficient detail. In particular, the model of a liquid bottom with losses is inaccurate. Control of all parameters of the problem in the measurements was limited to a 5 percent accuracy on the average. It influences the results of the comparison between theory and experiment.

The pulses diffracted on a vertically arranged cylinder of large radius, with linear frequency modulation in an isovelocity waveguide of depth 400λ, were measured [17,18].

The measurements showed the possibility of dividing the diffracted signal and the direct illumination signal, starting with certain angles of observation and illumination. In those experiments, an 8 percent frequency deviation was used and, therefore, the signals can be assumed to be narrow-banded. In waveguides with low dispersion in a small-angle approximation the effects due to the deterioration of

77

the pulse shape because of the dispersion can be neglected. This fact was clearly demonstrated in the experiments in which the pulse deterioration due to the intermode dispersion was observed only at large angles of observation. Paper [17] offers the measurements of diffracted fields on a plate with a sinusoidal relief in the waveguide modelling the shelf zone (the wedge connecting the shallow-water and the deep-water areas). These results show that a waveguide of such a structure forms a natural mode shadow when the illumination source is located in the shallow-water region. From the measurements given in [17] it follows that under such conditions diffracted fields can be measured against the background of the direct illumination field attenuated by 15 dB. Note that this is possible only for inhomogeneities broadening considerably the mode spectrum. Although, besides the measurements, investigation [17] also contains a theoretical calculations, only their qualitative comparison is possible. This is because the theoretical model is limited and does not take into account all details of the experiment, in particular the complex transformation of the field in the wedge.

CONCLUSION

This paper is an investigation of the diffraction of acoustic waves by spatially localized inhomogeneities in oceanic-type waveguides using the methods of a numerical and physical model experiment. This paper analyzes short-wave method of solving the internal boundary-value problem of diffraction by spatially localized inhomogeneities (in particular, by bodies) in oceanic-type waveguides. In our paper we have analyzed the structure of the fields diffracted at small angles in oceanic waveguides within t;he framework of a short-wave diffraction model and for a waveguide of a simple form. The last fact permitted us to compose the calculated and experimental data and, therefore, show the efficiency of the calculation technique. Comparison of the results of a numerical and a physical model experiment leads to the conclusion of practical feasibility of the formation of diffracted acoustic fields by optimizing the excitation of the waveguide, the arrangement of the receiving system and the choice of the signal processing algorithm.

REFERENCES

1. Kravtsov Yu.A., Kuz'kin V.M., Petnikov V.G. The approximate approach to the problem of diffraction of waves with smoothly varying parameters. Izv.VUZov - Radiofizika, 1983, v.26, No 4, pp. 440-446.

2. Ingenito F. Scattering from an object in a stratified medium,. JASA, 1987, v.82, pp.2051-2059. 12. Galishnikova T.N., Iljinsky A.S. Numerical methods in the diffraction problems. Moscow State University, Moscow, 1987.

3. Shenderov E.L. Emission and scattering of sound. Sudostroyeniye, Leningrad, 1989.

4. Waterman P.C. New formulation of acoustic scattering. JASA. 1969, v.45, No 6, pp. 1417-1430.

5. Gorskaya N.V., Gorsky S.M., Zverev V.A. et.al. Short-wave diffraction in a multi-mode layered waveguide. Akustichesky Zhurnal, 1988, v.34, No 1, pp.55-59.

6. Collins M.S., Verby M.F. A parabolic equation model for scattering in the ocean. JASA, 1989, v.85, No 5, pp.1895-1905.

7. Below V.E., Gorsky S.M., Khil'ko A.I. et. al. Diffraction of acoustic waves on an elastic cylinder in a multimode layered waveguide. Waves and Diffraction, issue 90. Physical Society, Moscow, 1990, v.1, pp.378-382.

8. Oboznenko I.L. Integral equations of the diffraction problems on bodies with mixed boundary conditions. Elektroarestika i Zvukotekhnika. Polytechnical Institute. Kiev, 1984, No 8, pp.15-18.

9. Hackman R.H., Sammelmann G.S. Acoustic scattering in an inhomogeneous waveguide: Theory JASA, 1986, v.80, pp.1447-1458.

10. Bostrom A. Transmission and reflection of acoustic waves by an obstacle in a waveguide. Wave Motion, 1980, No 2, pp. 167-184.

11. Tobocman W. Comparison of the T-matrix and Helmholtz integral methods for wave scattering calculation. JASA, 1985, v.77, No 2, pp.369-374.

12. Gorskaya N.V., Gorsky S.M., Zverev V.A. et.al. Features of short-wave diffraction of sound in multimode layered-inhomogeneous waveguides. Ocean Acoustics (in Russian). Ed. I.B.Andreyeva and L.M. Brekhovskikh. Nauka, Moscow, 1991, pp.97-110.

13. Kravtsov Yu.A., Kuz'kin V.M., Petnikov V.G. Wave diffraction on regular scatterers in multimode waveguides. Akustichesky Zhurnal, 1984, v.30, No 3, pp.339-343.

14. Zverev V.A. Radiooptics (in Russian). SovetskoyeRadio, Moscow, 1975.

15. Nechaev A.G., Khil'ko A.I. Differential acoustic diagnostics of random inhomogenieties in the ocean. Acustichesky Zhurnal, v.34, No 2, pp.285-289.

16. Nechaev A.G., Khil'ko A.I. Definition of the local characteristics of oceanic inhomogeneities distributed, along the acoustic path. Akustickesky Zhrnal, 1988, v.34, No 4, pp.694-699.

17. Borodina E.L., Gorskaya N.V., Gorsky S.M. et.al. The potential of shadow methods for study of diffracted sound fields in waveg-

uides. in book The Formation of Acoustical Fields in Oceanic Waveguides, ed. V.A. Zverev, Nizhny Nivgorod, IAP RAS, 1991, pp.174-199.

18. Gorskaya N.V., Gorsky S.M., Gurbatov S.N. et.al. Investigation of the possibility of using frequency- modulated waves for study of scattering in irregular waveguides. Akustichesky Zhurnal, 1991, v.37, No 5, pp.914-921.

19. Gorskaya N.V., Nikolayev G.N., Rychova T.A., Salin B.M. Spectral analysis in the investigation of harmonic source fields in acoustic waveguides. Akustichesky Zhurnal, 1981, v.27, No 2, pp.202-205.

20. Tolstoy I., Kley K.S. Ocean Acoustics (in Russian). Mir, Moscow, 1969.

21. Belyakova K.I., Gorskaya N.V., Kurin V.V. et al. Experimental investigation of the sound field structure in shallow sea using a physical model. Akustichesky Zhurnal, 1986, v.32, No 1, pp.107-111.

THE OCEAN TOMOGRAPHY AS AN INVERSE PROBLEM

V.A. Burov, S.N. Sergeev

In this article the questions to be discussed are connected with large ocean regions acoustical tomography based on wave theory of sound propagation and using of the vertical linear hydroacoustical antenna for data gathering.

The acoustic tomography methods for ocean researches were developed some later then, for example, X-ray diagnostics in medicine because the work in the ocean has some specific conditions and it is necessary to have deep water arrays as a tomographic investigations basic instrument with all problems of their location and control.

From other methods of search and diagnostics of 3-D structures the tomography ones are distinguished by that the information from every part of investigated object is obtained over and over again in different aspects relative to object [1]. During tomographic reconstruction the investigated object is illuminated from different directions and the measured characteristics of radiation passed over the object layer are recorded, than the spatial distribution of object's quantitative characteristics is found with help of computer.

It is not the only view on the tomography essence [2], but view that has probably the historic character. Nowadays the term "tomography" often means any method of volume structure reconstruction including as a component the solution of propagation and scattering inverse problems that allow to use the already developed inverse problems technics [3-4]. At the same time the 2-D one layer at a time representation of final results justify the using of the term.

The practical researches on the ocean tomography were begun after W. Munk and C. Wunch works [5-6], in which the sound speed reconstruction schemes were applied to the ocean and proceeded as a rule by using the rays methods [7].

In general case the tomographic scheme can be reduced to the solution

of the parametric manifold of Fredholm integral equations of 1 kind

$$\int P_\alpha(\mathbf{r}, \mathbf{r}')g(\mathbf{r}')d\mathbf{r}' = f(\mathbf{r}|\alpha), \qquad (1)$$

Here $\mathbf{r}$ and $\mathbf{r}'$ - the spatial coordinates, $P(\mathbf{r}', \mathbf{r})$ - integral transformation core, $f(\mathbf{r})$ - measured characteristics, $g(\mathbf{r}')$ -reconstructed image.

The physical sense of equation (1) is the following: the measured characteristics $f(\mathbf{r})$ are defined by the distribution $g(\mathbf{r}'$ along the whole way of exploring wave propagation. The information of the geometry of primary radiation is contained in the core structure $P(\mathbf{r}', \mathbf{r})$. If $P(\mathbf{r}', \mathbf{r})$ undepends on $g(\mathbf{r})$ the problem is linear.

The tomographic problem (1) is ill-posed. It is so because in real conditions only approximate values for functions f and P are known and for them the exact solution may not exist, and if it exists it may be unstable to small measure errors. So the solution of the equation (1) is built with using of some regularization methods that were developed for ill-posed problems [8].

For fixed source and receiver location the parameters contained in equation (1) have the following sense: $P(\mathbf{r}', \mathbf{r})$ determines the exploring ray trajectory, $f(\mathbf{r}) \rightarrow f_k = t_k$ - time delay of signal propagation on k-th ray, $g(\mathbf{r}) = 1/c(\mathbf{r})$ - reverse sound speed distribution. The ray trajectory itself is a function of $c(\mathbf{r})$, so the tomographic problem in this case is nonlinear that is also peculiar to the inverse wave's problems of strong inhomogeneity reconstruction. The problem is roughly linearized relative to the perturbations $\delta c(\mathbf{r})$ which have been determed by means of the choice of zero approximation of sound speed $c_0(\mathbf{r})$ closely spaced to the true one:

$$t_k - t_k^0 = \int\limits_{l_k^0} \frac{\delta c(\mathbf{r})}{c_0^2(\mathbf{r})} dl$$

where l_k^0 is the ray trajectory of k-th ray calculated for unperturbated sound speed profile. In this approach it is assumed that the single ray trajectories could be resolved (it takes place, for example, in the case with deep sound channel).

An opposite approach is the mode tomography that consists in the reconstruction of the characteristics of the propagating modes (for example, their phase velocities), from which the information about ocean inhomogeneities could be obtained. The question about relationship between rays and modes in the sense of production of information about sound speed profile perturbations in the ocean was studied in [9]. Different rays coming to receiver are corresponding to the interference maximum of mode groups that have close numbers. As a distance between source and observer's point increases the

number of constructive interfering modes in every group decreases and from definite distance even neighboring modes cease to constructively interfere. In this case the mode description of sound field should be preferable rather then ray description.

The use of mode description is most justified in the case of adiabatic approximation validity [10].

Let's assume that the region under investigation is surround with S radiating and R receiving vertical antennae, the number of them is approximately equals to each other ($S \approx R$) and $S \times R \geq M$ where M is the quantity of covered region under study spatial elements to be resolved (or number of parameters characterized this region). Account of radiating elements in each antenna can be small (1-3) because in definite depth locations even one element can excite all accounting modes in the wavequide.

If vertical receiving antennae make available separation of all accounting modes then for every mode number independent inverse problem is formed for reconstruction of phase speed "map" in investigated region, it's solution can be found by using general methods that have been developed for such tasks [3,11-12]. If the inhomogeneity under study is enough smooth so the maximum lateral size of ray tubes between any pairs of emitter-receiver systems less than spatial cell the next simplification can be done due to using of combined presentation of type "vertical modes, horizon rays" [13]. So the transition from wave to ray tomography takes place in horizon plane.

In the tasks in question such aspects as influence of scatter's force to the technique for solving of inverse tomographic problems, uniqueness of the solution, etc. have specific features.

A linearized Born approximation is valid when the perturbation to be determined is very small so that it's action changes receiving mode's phase to little quantity that doesn't act on the ray path. In this case the solution of the inverse problem can be done in monochrome regime. Manyfrequency measurements result to solution accuracy improvement due to the data redundancy increase but they are not necessary condition of uniqueness.

The use of monochrome regime is possible also in the case of receiving mode phase change in limits $\pm\pi$. This case is analogous with "medium force" scattering case [3]. For it the ray path distortion is essential and a correction of this path in the iteration cycle of solution: rays $\rightarrow$ receiving modes phase distortion $\rightarrow$ estimation of the perturbation $\rightarrow$ rays correction. The role of data redundancy be obtained in manyfrequency experiments now is more substantial because it results to the iteration speed increase and convergence region extendance.

Further scatterer force increase resulting to phase distortion of receiving modes more than 2π makes the estimated perturbation to be "strong" be-

cause field's distortion inside investigated region surpasses the original field in norm that results in "few revolutions" of phase. The ambiguity in the solution that arises in this case has evident form of phase ambiguity. A manyfrequency regime restores the uniqueness. Especially clear it is exhibited in pulse tomography where in the elementary case the group delay of modes propagation is measured. The time delay of n-th mode propagating time on the i-th trajectory equals to

$$\delta t_n = - \int\limits_{l_k^0} \frac{\delta v_n(x, y)}{v_n^2(x, y)} dl$$

where v_n is the group velocity, δv_n - it's perturbation caused by sound speed perturbation δc.

In a case of big frequency dispersion (in frequencies close to critical one) a blurring of receiving packet demands more complete data measuring in a form of more detailed frequency or time description estimation.

At the end of such many frequency measurements the obtained disperse data for the whole receiving mode set allow to reconstruct the hydrology profile by using the method similar to the one has been described in [14] for the internal waves.

Such sequence of reconstruction operations (measurement data $\rightarrow$ modes separation $\rightarrow$ hydrology reconstruction) is not absolutly necessary: the modes separation of the receiving signals can be excluded and the connection "hydrology perturbation $\rightarrow$ signal perturbation" can be used at once although mode representation retains useful for the correspondence operator construction.

The exclusion of modes structure reconstruction operation is necessary in case where the number of receiving hydrophones is less then the number of modes participating in sound field forming.

If a limit transition to the groups of neighboring modes on enough high frequencies can be done that is the transition to rays representation in a vertical plane and this returns us to the initial pulse-rays ocean tomography.

The obtained data can be used only if the space locations of each antenna elements are exactly known. So in the case of vertical antenna arrays employment it is assumed that they maintain straight line, but the real declination of antenna elements from vertical line can reach hundreds meters (Fig. 1). The data plotted in the picture were obtained during numeric calculations based on the hydrodynamic relationships for vertical hydroacoustic antenna by length 1 km that has been constructed as a rope by diameter 2 mm and buoyancy 0.5 N/m, loaded at the end by the ball with mass 40, 30 and 20 kg in a flow with constant velocity 0.2 m/s. The calculated declinations of such antenna from vertical are equal to the hundreds
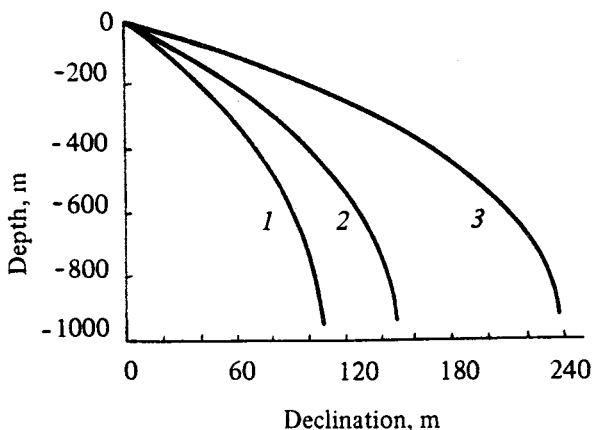
Figure 1: The profile of vertical antenna by length 1 km and diameter 2 mm in isospeed flow with velocity 0.2 m/s with cargo at the end by mass m=40(1), 30(2) and 20(3) kg

meters that is corresponds in order to the value in published data [15]. Standard methods for improvement of this disadvantage are the using of engineering ways for the antenna to straighten (bringing an antenna to an anchor, suspension of a big cargo etc. [16-17] that results into the whole installation weight increase and complication of its deployment. Another solving of this problem – the estimation of distorted antenna true profile. So, in the experiment that was conducted by the research group of Oceanology Institute (Russia) [18] the antenna units location was fixed with help of three receiver-radiator modules that have formed a triangle with side approximately equal to ship length on the depth 15-20 m. The principals of work are based on the measurement of propagation time intervals for every module and every antenna element. Than calculation of every receiver location was done in coordinate system connected with reference triangle so the antenna profile was defined. As a fundamentally new approach to the problem we have proposed "4-frequency" algorithm which allowed to compensate the unknown antenna distortions [19-20]. The essence of the method is following.

The deflection of k-th antenna element with unknown value Δx_k results to the appearance of additional phase of l-th mode $\kappa_l \delta x_k$, where κ_l - horizontal wave number. If the value of deflection is smaller then the distant resolution ability (which is defined for any frequency by the difference between reverse phase velocities of lowest and highest modes) than for this

distortion the difference of phase velocities of separate modes can be ignored and the phase factor is equal to

$$\exp\left(i\left(\kappa_l \triangle x_k\right)\right) \approx \exp\left(i\omega \triangle x_k/c\right),$$

where c is the some average phase velocity of the accounted modes. In this case the additional phase will be compensated by the combination of receiving fields magnitudes into the product of 4-th order for the 4 frequencies:

$$M_k = U_{\omega_{1k}} U^*_{\omega_{2k}} U^*_{\omega_{3k}} U_{\omega_{4k}},$$

where 3 frequencies are chosen arbitrary and the fourth is defined by the rule

$$\omega_1 + \omega_4 = \omega_2 + \omega_3,$$

where k is the vertical number of hydrophone.

The results are represented in Fig. 2 to illustrate the 4-frequency algorithm work for waveguide with depth 1 km and symmetric parabola sound speed profile wich has been chosen as a model (Fig. 3). The product of 4-th order that was built by the use of described method was compared with reference product M_4, calculated by the same way for some set of estimated parameters. The comparison was done by the correlation formula

$$R = \left|\sum_k M_{k_0} M^*_k\right| \bigg/ \left(\sum_k |M_k|^2 \sum_k |M_{k_0}|^2\right)^{1/2},$$

the closeness of this expression to the maximum value is the criterion of the correspondence of the estimated parameters to the true ones. The curves that are represented on Fig. 2a are corresponded to the frequency set 17, 20, 20, 23 Hz (1); 27, 30, 30, 33 Hz (2); 77, 80, 80, 83 Hz (3); 157, 160, 160, 163 Hz (4); 197, 200, 200, 203 Hz (5) and sound source location at the distance of 10 km from antenna. It is clear from the picture that as the chosen frequencies increas the result is less depends on the declination less then 0.5 km so the antenna distortions that result to its nodes shifts to hundreds meters (to be expected in practice, see Fiq. 1) don't cause the deterioration. But the averaged product is sensitive to the large distance mismatch, it can be seen from Fig. 2b where the dependence R having been averaged over pointed frequency set upon the distance is represented. The peak corresponding to the source location at a distance 10 km from antenna is well distinguished. This property of 4-th order product allows to use it for tomography task solving with reasonable precession of space resolution.

Analogous calculations demonstrate the good capacity for work of the algorithm during depth coordinate estimation.
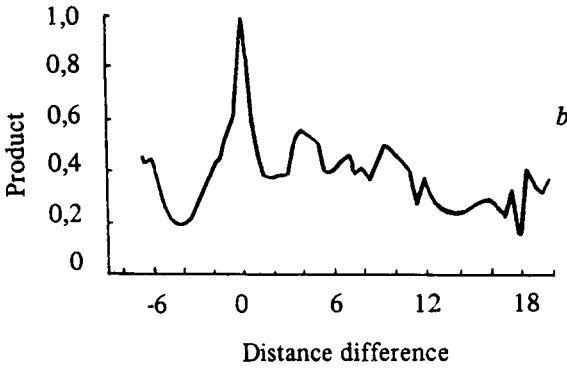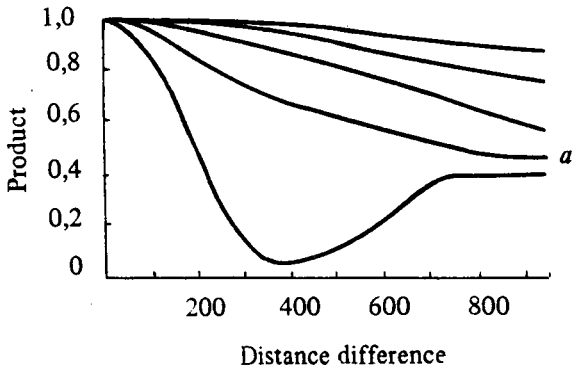
Figure 2: The illustration of using of the 4-frequency algorithm with small (a) and big (b) distance difference
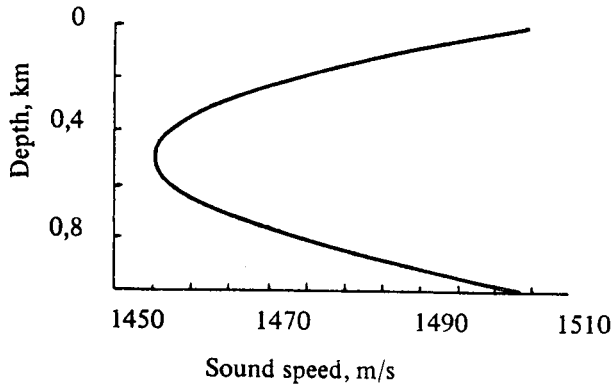
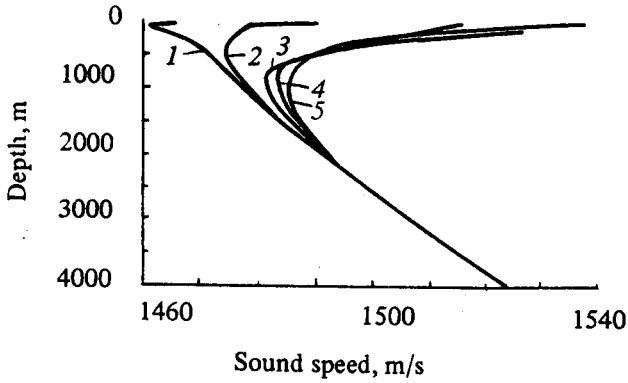Figure 3: The model waveguide with parabolic hydrology profile

Figure 4: The profile of sound speed: 1–arctic, 2–subarctic, 3–subtropics, 4–tropic, 5–equator type
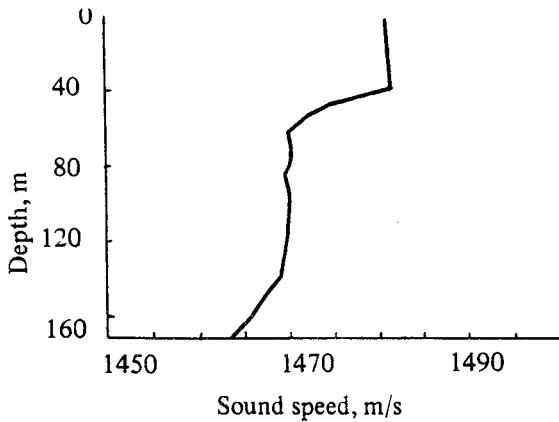
Figure 5: The profile of sound speed of shallow sea

In order to study the opportunity of practical use of 4-th order product the ambiguity function was calculated for base types of sound speed stratification in the ocean (Fig. 4) and shallow sea (Fig. 5). This function is the response to the source distance and depth mismatch (Fig. 6). The discrepancy in the distance from -5 to +5 km was plotted along axis X and the one in the depth from -0.25 to +2 km (from -50 to 200 m in the case of shallow water) along axis Y. The source was located in the point (0,0).

The analysis of obtained functions results to the conclusion that there is no principal differences between them that means that it is not necessary to adopt the algorithm to the specific conditions of experiment realization and about it's enough universality. It is important so that the main peak so is unique at least on the depth of practical interest because there aren't maximums higher than 0.5 of main one, moreover the ambiguity function is decreasing in general as the both distance and depth discrepancy is increasing. But the peak width becomes narrow along both coordinates in the case of shallow sea (Fig. 6f).

In order to construct the full scheme of ocean tomography first discuss the standard computer tomography scheme [21].

If in the cross section of the object under investigation its ability to attenuate the penetrating radiation is characterized by the 2-dimensional distribution $\mu(x, y)$ than the intensity of radiation passed through the object under the angle Φ along ray AB (Fig. 7) can be written in the kind
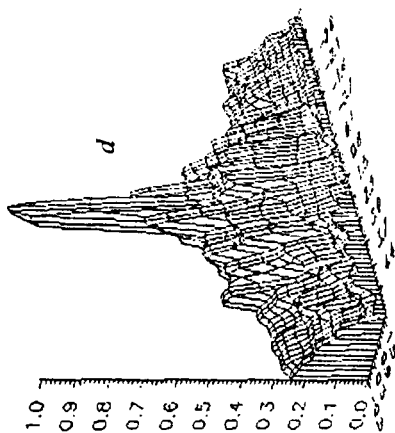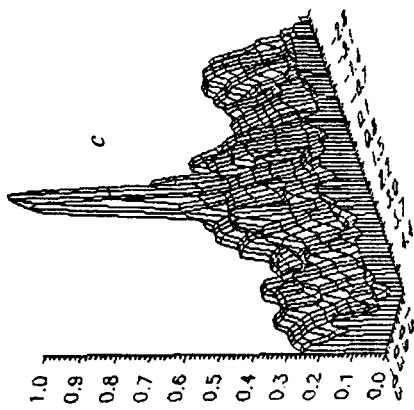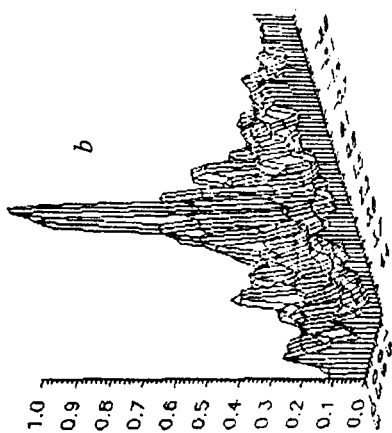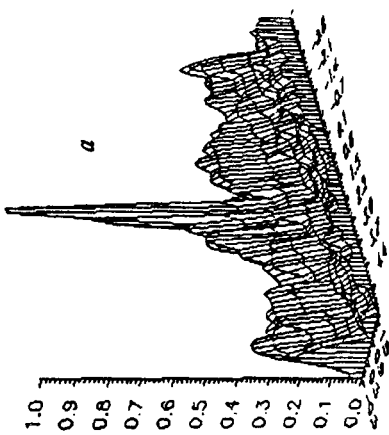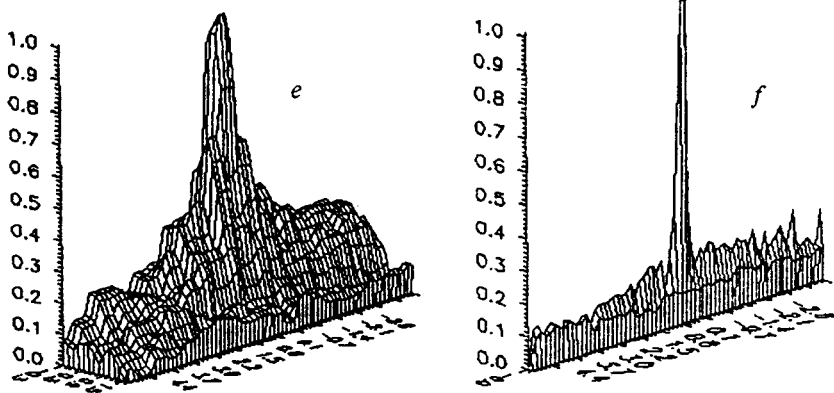
Figure 6: The ambiguity function for hydrology types: a–arctic, b–subarctic, c–tropic, d–subtropics, e-equator, f–sh..low sea
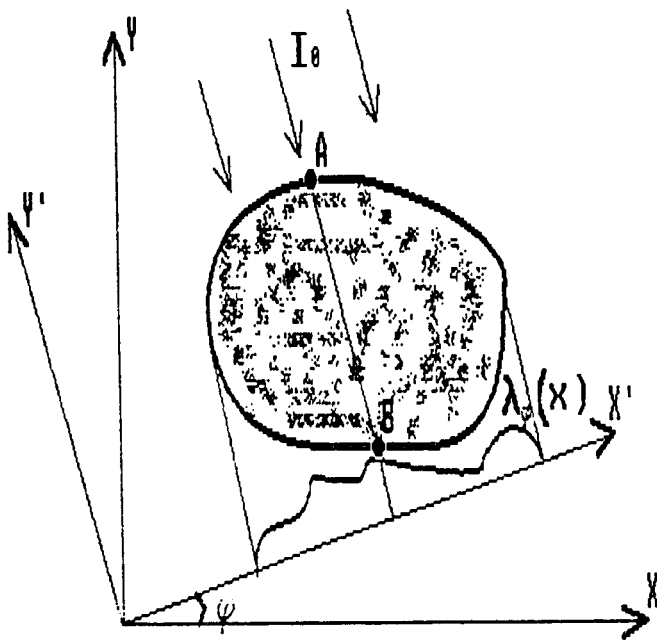

Figure 7: The scheme of the 2-D computer tomography of the scalar object

$$I_\Phi(x') = I_\Phi^0(x') \exp\left(-\int\limits_{AB} \mu(x,y)\,dy\right).$$

The function of separate projection of the object under angle Φ is

$$\lambda_\Phi(x') = -\log \frac{I_\Phi(x')}{I_\Phi^0(x')} = \int\int\limits_{-\infty}^{\infty} \mu(x,y)\delta(x\cos\Phi - y\sin\Phi - x')\,dx\,dy$$

(the line AB is mind by the equation $x' = x\cos\Phi + y\sin\Phi$).

The problem of image reconstruction consists in the reversal of this relationship that is in reconstruction $\mu(x,y)$ using set $\lambda_\Phi(x')$. For convenience let's see the projection under angle $\Phi = 0$. It's Fourier transform (FT)

$$\Lambda_0(\zeta) = \int\limits_{-\infty}^{\infty} \lambda_0(x)\exp(-2\pi\zeta x)\,dx = \int\int\limits_{-\infty}^{\infty} \mu(x,y)\exp(\zeta x + \eta y)\bigg|_{\eta=0} dx\,dy.$$

So the 1–D FT of projection Λ_0 is determed by the values of 2–D FT $M_0(\zeta, \eta)$ that are values $\mu(x,y)$ along the mind line. This line is the central cross section that is oriented along the direction $\Phi = 0$. This statement in the arbitrary oriented coordinate system makes up the content of the central projection theorem:

$$\Lambda_\Phi(\zeta) = M_\Phi(\zeta, \eta).$$

For image reconstruction some methods were developed, the most number of them are based on the central projection theorem. For example the essence of often quoted method of convolution and reverse projection reduces to the fact that every projection n $\lambda_\Phi(x')$ is convolved (filtered) with some function $p(x')$ that is determed by using equipment and every filtered projection is reversibly projected to the space (x, y) such that all single projections are used for obtaining the image $\mu(x, y)$.

The development of the convenient scheme in purposes of wave ocean tomography realization has a number of features, the main feature consists in an influence of hydrology over the whole ocean depth upon the sound speed propagation character that makes the problem 3–D in principal i.e. the task can be treated as a hydrology "map" reconstruction. In the other words in a difference from the traditional tomography of the plane section of a scalar object the ocean tomography is a vector-parametric problem.

Let's devide the investigated region of the ocean on vertical bars-cells and examine the sound field transformation during passing throw one bar.
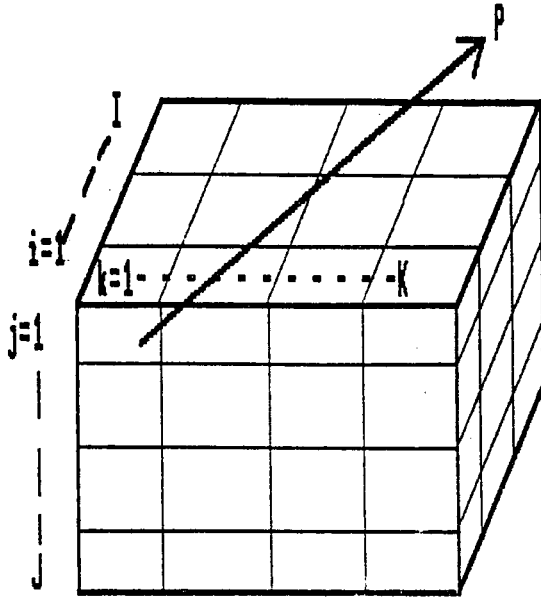
Figure 8: The scheme of the 3-D ocean tomography

If the bar contains only basic environment than the fields in its "exit" and "entrance" are connected by by means of propagation operator $\hat{A}^0$:

$$U(z_k, \mathbf{r} + \triangle \mathbf{r}) \cong U_k = \hat{A}^0_{ki} U(z_i, \mathbf{r}).$$

The summing by repeat indexes is implied.

The hydrology perturbation $\delta c(z_j)$ causes the operator's perturbation:

$$\delta \hat{A}_{ki} = \frac{\partial \hat{A}_{ki}}{\partial c(z_j)} \cdot \delta c(z_j) = \hat{B}_{kij} \cdot \delta c_j$$

Let the signal to pass throw P bars between radiating and receiving antenna. In this case the main field transformation is

$$U_k = \left[\prod_{p=1}^{P} \hat{A}^{0^p} \right]_{ki} U_i.$$

The perturbation presence results to observable profile distortion that in

93

the linearized case is

$$\delta U_k = \sum_i \sum_{p \in P_l} \left[\prod_{t \neq p}^{P} \hat{A}^{0^t} \sum_j \hat{B}_j^p \cdot \delta c_j^p \right]_{ki} U_i =$$

$$= \sum_i \left[\sum_{p \in P_l} \hat{D}_p \sum_j \hat{B}_j^p \cdot \delta c_j^p \right]_{ki} U_i = \qquad (2)$$

$$= \sum_{p \in P_l} \sum_j \sum_i \left[\hat{D}_p \hat{B}_j^p \right]_{ki} U_i \cdot \delta c_j^p = \sum_{p \in P_l} \sum_j \hat{F}_{kj}^p \delta c_j^p,$$

where the sense of introduced designations is seen from the transformation sequence, $\hat{D}$ in the adiabatic approximation and mode representation is the diagonal operator and P_l describes the l-th ray trajectory. In this equation the summing signs are represented in the evident form.

This expression - formula for tomographic ocean investigation and it is analogous to formula (1) in this sense. But in this formula the particularities of ocean tomography are reflected. The main one is "volumness" that means the necessity of account and reconstruction of vertical hydrology for description of each ocean cross section, that gives the second sum on the depth coordinate which appears in formula (2). That property is contrast to the convenient schemes of computer tomography to be used in medicine and other practical realizations because in the pointed cases the reconstruction of plane section of scalar object takes place by using results of penetrating of that section (Fig. 7).

The situation becomes simpler in the case of the adiabatic approximation in modes representation. The consideration analogous to having been done above gives the next relationship for the vector of complex amplitudes:

$$\delta \psi_k = \sum_{p \in P_l} \sum_i \sum_j \left[\hat{D}_p \hat{B}_j^p \delta c_j^p \right]_{ki} \psi_i,$$

i.e. the every vertical bar in such case introduces the equal contribution to the every ray wich passing throw it. This relation generalizes the scalar tomography case, where every cell contributes equally to the all passing rays, to the vector-parameter case.

The next important question touches the source of penetrating radiation. For the simulation and in practics we should use the finite and discrete modes representation. Due to the operator $\hat{A}$ is diagonal in the case of adiabatic approximation the $\hat{B}$ and $\hat{D}$ so become diagonal and it allows to get separate tomographic problem for phase velocity of each mode by use only one depth of source location such that all modes of investigated waveguide are excited. In general case the question is about the nonsingularity of

operator $\hat{F}$ but this is not guaranteed. It is possible to raise its due to data redundancy by using different radiator depth.

So the question is important about the choice of work frequencies in the case where the reconstruction is done with using mode representation. It is so because for one work frequency it is possible to reconstruct the map of mode's phase velocities but it is not possible to reconstruct the profile $c(z)$ because the perturbation in phase velocity of n-th mode $\delta v \sim \int \delta c(z)\psi_n^2(z)\,dz$ but the set $\{\psi_n^2\}$ doesn't form the full system on one frequency. So the reconstruction of $\delta c(z)$ is possible only by use of data recieved on several frequencies.

In general case for solving the direct problem and constructing the operator of correspondence (the matrix of translation from measured data to the hydrology characteristics) which is the base of inverse problem solving it is possible to employ the mode approach with use of first (linear) members of perturbation theory expansion. For this purpose it should be regarded the equation

$$\psi_l''(z) + k^2(z)\psi_l(z) = \kappa_l^2 \psi_l(z), \tag{3}$$

where κ_l^2 is the l-th eigenvalue (square of horizontal wave number), ψ_l - the corresponding to it eigenfunction (mode) and $k(z) = \omega/c(z)$, $c(z)$ - the sound speed profile. The field in the homogeneous waveguide on depth z and distance r from the source has been located on depth z_0 is represented in form

$$U(r,z) = \sum_{l=1}^{\infty} \sqrt{\frac{2}{\pi \kappa_l r}} \psi_l(z_0)\psi_l(z)\exp\left(i(\kappa_l r - \pi/4)\right). \tag{4}$$

The immediate calculation of sound speed by using this formula is difficult and the often situation is that the exact representation of eigenfunctions $\psi_l(z)$ is unknown because of only in limited number of occasions the equation (3) has the exact solution. For the fields to be calculated it is necessary to use the approximate methods. One of them that has the wide application in different branches of wave phisics is the perturbation theory method that is used when the square of wavenumber $k(z)$ is represented in the form:

$$k^2(z) = k_0^2(z) + k_1^2(z).$$

The profile of nonperturbated wavenumber $k_0(z)$ choosed so that the nonperturbated wave equation

$$\psi_l^{0\prime\prime}(z) + k_0^2(z)\psi_l^0(z) = \kappa_l^{0^2}\psi_l^0(z)$$

has the known (analytical or had been obtained before by numeric calculations) solution and perturbation $k_1^2(z)$ would give some corrections to the

solution of nonperturbated equation. The consistent calculation of these corrections results to the expansion into a series on some formal parameter λ. The first (linear) approximation of perturbation theory gives the next corrections to the eigenvalues and eigenfunctions:

$$\kappa_{1_l}^2 = \int_0^H k_1^2(z)\psi_l^{0^2}(z)\,dz,$$

$$\psi_l^1(z) = \sum_{m \neq l} \frac{\psi_m^2(z)}{\kappa_l^2 - \kappa_m^2} \int_0^H \psi_m(z)k_1^2(z)\psi_l(z)\,dz.$$

It is worth while to introduce the expansion with finite measure representation of values involving in the formulae by use of the sampling theorem or other functional basis:

$$k_{1_l}^2(z) = \sum_{j=1}^N k_{1_j}^2 \theta_j(z),$$

where N is the number of accounted members of series. By introducing the designation

$$\int_0^H \psi_l^0(z)\theta_j(z)\psi_m^0(z)\,dz = B_{lmj}$$

these formulae are transformed to the kind

$$\kappa_{1_l}^2 = \sum_{j=1}^N k_{1_j}^2 B_{llj},$$

$$\psi_l^1 = \sum_{j=1}^N k_{1_j}^2 \sum_{m \neq l} \frac{\psi_m^{0^2}(z)}{\kappa_l^2 - \kappa_m^2} B_{lmj}.$$

The small perturbation of wavenumber profile $k_1(z)$ results to the approximately proportional to it perturbation of sound field [22]:

$$\Delta U(r, z_k) = \sum_{j=1}^N k_{1_j}^2 Q_j(r, z_k), \tag{5}$$

where $Q_j(\mathbf{r}, z)$ is the matrix which calculated by use of perturbation theory formulae.

The formula (5) sets up the linearized relationship between given on such horizons perturbations of wavenumber and perturbations of mode wavenumbers and perturbation of acoustical field with using the elements of matrix

96

Q as translation coefficients that allows to solve inverse reflection problem immediately [23]: from measured sound fields to obtain the change of profile of stratified hydrology. Such formulation corresponds to the simplest tomographyc scheme for the volume consisting of one elementary bar.

It is necessary to point that nowadays the modification of perturbation theory has been developed that allows to exclude some disadvantages of standard form of theory such as necessarity to now all spectrum of nonperturbated operator for calculation of corrections to the every mode and the decision of question about rule for summing the series. The exclusion of these disadvantages is made by "delinearization" by the reduction equation (3) to the nonlinear first order equation

$$y_l' - y_l^2 = k^2 - \kappa_l^2$$

doing by means of substitution $y_l = -\psi_l'/\psi_l = -(\ln \psi_l)'$ into the primary equation. This approach called by "nonlinear perturbation theory" or "delinearization method" for hydroacoustical problems is described in detail in works [24-25]. The expansion upon the formal parameter λ results to the correction formulae every of which demands the knowledge only that nonperturbated eigenfunctions and eigenvalues to which the corrections are searched. Moreover, the result is represented in quadratures that makes the method be suitable for computer calculations.

Account only first linear corrections also results to the lineariezed relationship (5) with that difference that now the matrix Q is calculated with use of formulae of nonlinear perturbation theory. The solution of this lineariezed system gives the corrections to the local values of eigenvalues which are added to the values of choose as an initial profile of wavenumber $k_0(z)$ which corresponds to the $c_{init}(z)$ on the frequency ω. Such process can be repeated iterationly with the founded profile $k(z)$ taken as the new initial one. So the gradually precisive approximation to the right solution is built.

For modeling the described algorithm the program of numeric calculation was created. At the first step of program's work the initial data are assumed - the known parameters of the waveguide (depth, boundary conditions, the initial approximation of wavenumber $k_0(z)$ profile), the coordinates of source and antenna receiver elements. At the second step we have chosen the basis functions $\theta_j(z)$ as $\sin x/x$ and the discrete profile of hydrology is expanded upon them. At the third step the field that has to be "measured" by the vertical array is calculated. The simulation of measuring process carries out with assignment of true hydrology profile and calculating of corresponding field that means the solving of the direct problem. Then the iteration account begins. At the first stage of every iteration the solution of the direct problem for the initial eigenvalue profile was found

with the corrections had been found at the previous iterations. The Hunkel functions asymptotic values were determed, the initial field was formed. At the next stage the calculations and forming the matrix Q were made. Then system of linear equations (5) was solved, the corrections κ_1 in the points of hydrophones location were founded and the refined hydrology is rebuilt. The program begines the next iteration. The process of the convergence to the true profile was controlled by the discrepancy – sum of the squares of the reconstructed profile values declination from the true one:

$$S = \sum_{i=1}^{N} \left(c_{iter} - c_{init} \right)^2$$

Here N is the number of points where the field is "measured".

The results of the program processing for the model of ocean with depth 1 km, monochrome (50 rad/s) source located at the depth 250 m are present in the tab where profile values were taken during every 100 m.

Vertical profile of sound speed, km/s

True profile	Init. profile	1 iteration	2 iteration	3 iteration
1.50327	1.50523	1.50419	1.50365	1.50330
1.48505˙	1.48655	1.48560	1.48518	1.48510
1.47141	1.47250	1.47187	1.47149	1.47144
1.46199	1.46270	1.46242	1.46207	1.46202
1.45657	1.45691	1.45667	1.45665	1.45660
1.45502	1.45500	1.45503	1.45502	1.45501
1.45729	1.45691	1.45706	1.45705	1.45719
1.46344	1.46270	1.46304	1.46321	1.46331
1.47363	1.47250	1.47309	1.47356	1.47357
1.48810	1.48655	1.48746	1.48802	1.48806
1.50723	1.50523	1.50653	1.50715	1.50720
Discre-pancy	$1.6271 \cdot 10^{-5}$	$2.9596 \cdot 10^{-6}$	$3.0870 \cdot 10^{-7}$	$3.9200 \cdot 10^{-8}$

The convergence of the algorithm to the true value of hydrology during iterations account confirms normal operation of described gradient method based on the nonlinear perturbation theory.

Process including distorted antenna and use the 4-frequencies algorithm reduces the inverse refraction problem in the simplest form to the equation system

$$\triangle M_4(r, z_k) = \sum_{j=1}^{N} k_{1j}^2 A_j(r, z_k)$$

where A is the matrix determed by the matrix Q at chosen frequencies [20].

At the conclusion let's describe the complete scheme of ocean tomography with use the set of vertical antenna distorted by the ocean flows.

For this purpose determine at every cell of investigated region the hydrology profile $c_0(i, k, j)$. The presence of the inhomogeneous $\delta c(i, k, j)$ leads to the field perturbation at the "exit" of every bar which is calculated with help of perturbation theory:

$$\delta U(i, k, j) = \sum_{n=1}^{N} \delta k_n^2(i, k) Q_n(i, k, j) \approx$$
$$\approx -2 \sum_{n=1}^{N} k_0^2 Q_n(i, k, j) \frac{\delta c_n}{c_0},$$

where $n = 1, \ldots, N$ – index of functional basis, for example, the basis of sampling theorem. If there are P vertical bars with coordinates (i, k) between radiating and receiving antenna then the passed field has the perturbation

$$\delta U_P = \sum_{p=1}^{P} \left(-2 \cdot \sum_{n=1}^{N} \frac{k^{p^2}}{c_0} Q_n^p(j) \delta c^p(n) \right).$$

This formula represents by itself the analog of linearized computer tomography formula where field perturbation on P-th ray δU_p plays the role of single point in single cross section and $\delta c^p(j)$ - of reconstructed image.

This perturbation throw the P_l-ray trajection passes present the complete perturbation of 4-th order product along the ray. Radiating the region under investigation by intersecting rays results in these approach to the algebra equation system, the solution of which allows to reconstruct the inhomogeity. But it is only first step of iteration procedure. The next one begins from a new value $c_0^1(z) \rightarrow c_0^0(z) + \delta c_1(z)$.

It is necessary to note that the idea of acoustical monitoring surely will be developed at the nearest future at a number of directions of tomographic methods which nowadays represent possibly the unique class of methods of detailed investigation of large ocean regions, and the development to the ocean purposes the methods which have been extended initially for medicine aims is a reasonable way for solution of arising problems. Their main advantage is the quick increase of data information as the number of new sources and receivers are added into the net of sound ways intersecting trajectories. This property allows to investigate large regions with the help of relatively small number of devices.

A necessity of reconstruction of underwater flaws velocity map doesn't been involved in this discussion but note that the use of the "unreciprocity" theorem for moved mediums allows to reconstruct it.

Literature

1. A.N. Tikhonov, V.Ya. Arsenin, A.A. Timonov. The mathematical tasks of computer tomography, Nauka, Moscow, 1987 [in Russian].

2. Natterer F. The mathematics of computerized tomography, B.G. Teubner, Stuttgart, and John Wileys Sons Ltd, 1986.

3. V.A. Burov, A.A. Gorunov, A.V. Saskovets, T.V. Tikhonova. Inverse scattering tasks in acoustics (survey)//Sov. Phys. Acoust., v. 32, 1986.

4. V.A. Burov, M.N. Rychagov, A.V. Saskovets. Account of multiple scattering in diffraction tomography tasks: T-matrix approach//Moscow University Trans. Phys., v. 30, p. 44, 1989.

5. W. Munk, C. Wunch. Ocean acoustic tomography: a scheme for large-scale monitoring//Deep Sea Res., v. 26(A), p. 123, 1979.

6. W. Munk, C. Wunch. Up/down resolution in ocean acoustic tomography//Deep Sea Res., v. 29, p. 1415, 1982.

7. V.V. Goncharov, V.M. Kurtepov. The successes and problems of acoustical tomography of the ocean, Acoustical waves in the ocean, Nauka, Moscow, 1987 [in Russian].

8. A.N. Tikhonov, V.Ya. Arsenin. The methods of solving of the ill-posed tasks, Nauka, Moscow, 1979 [in Russian].

9. W. Munk, C. Wunch. Ocean acoustic tomography: Rays and modes// Rev. of Geoph. and Space Phys., v. 21, p. 777, 1983.

10. E.S. Shang. Ocean acoustic tomography based on adiabatic mode theory//J. Acoust. Soc. Am., v. 85, p. 1531, 1989.

11. V.A. Burov, M.N. Rychagov, A.V. Saskovets. Account of multiple scattering in acoustic inverse problems of tomographic type//Acoust. Imaging, v. 19, p. 35, 1992.

12. V.A. Burov, M.N. Rychagov, A.V. Saskovets. Iteractive methods for the reconstruction of characteristics of strong inhomogeneities by the data of acoustic scattering//Proc. Ultrason. Int. Conf., p. 201, 1991.

13. R. Barrige, T. Veinberg. Horizontal rays and vertical modes, Wave propagation and underwater acoustics.

14. S.V. Baykov, V.A. Burov. The estimation of buoyancy frequency profile by dispersive characteristics of the internal waves//Marine hydrophys. mag., N3, p. 35, 1983 [in Russian].

15. A demonstration of ocean acoustic tomography//Nature, v. 299, p. 121, 1982.

16. R.C. Swenson. Suspended Kelvar array technology//Oceans-79: 5-th Annu. Comb. Conf., p. 54, 1979.

17. Sotirin B.J., Hildebrand J.A. Large aperture digital acoustic array//IEEE J. Oceanic Eng., v. 13, p. 271, 1988.

18. S.A. Dremuchev, V.N. Kuznetsov, A.V. Kulikov. The distributed acoustical array with system of determination of its spatial configuration//Oceanology, v. 29, p. 326, 1989 [in Russian].

19. V.A. Burov, S.N. Sergeev. The acoustical fields treatment in the ocean waveguides with compensation of unknown profile distortion of a linear vertical antenna, The formation of acoustic fields in oceanic waveguides, N.Novgorod, 1991.

20. V.A. Burov, S.N. Sergeev, N.P. Sergievskaya. Acoustical tomography of the ocean using data from vertical mode antenna distorted by the underwater flows//Sov. Phys. Acoust., v. 38, 1992.

21. The physics of Medical Imaging, Adam Hilger, Bristol and Philadelphia, 1990.

22. V.A. Burov, S.N. Sergeev. The up-to-day methods of perturbation theory using for calculation of hydroacoustical fields//Moscow University Trans. Phys., v. 33, 1992.

23. V.A. Burov, S.N. Sergeev. Solution of an inverse refraction problem by nonlinear perturbation theory// Sov. Phys. Acoust., v. 37, p. 221, 1991.

24. I.V. Gindler. Perturbation theory for nonmating waveguide task// Sov. Phys. Acoust., v. 33, p. 584, 1987.

25. I.V. Gindler, A.R. Kozel'skii. The use of "nonlinearizing" procedure for foundation of the eigenvalues of Pekeris problem//Sov. Phys. Acoust., v. 34, p. 356, 1988.

FORMATION OF MULTI-VIEW IMAGES IN OCEANIC WAVEGUIDES BY DARK FIELD METHOD

E.L. Borodina, N.V. Gorskaya, S.M. Gorsky, V.A. Zverev,
G.N. Nikolaev, A.I. Khil'ko, V.N. Shirokov

INTRODUCTION

The problem of visualization of primary and secondary sources of acoustic fields, i.e. forming the spatial light intensity distribution pattern, has independently arisen in a large number of practical fields, such as underwater engineering, ecologic monitoring of extensive oceanic region state, navigation. It allows to obtain the acoustical information by visual channels of perception using imaging mentation mechanisms. There is no necessity to prove the efficiency of the method, well known in various fields of technical acoustics (from medicine and nondestructive testing of samples to vibroscopy of the Earth). This method is known as "the acoustic vision" [1,2]. Here the spatial distribution of acoustic fields is screened on a monitor in a form of a brightness pattern.

Usually the acoustic images are obtained using numerical or similar methods (including scanning and reconstruction into the observation area). Such images are essentially informative, that allows successive interpretation of observation data. However, one can not expect a direct analogy between acoustic and optic images because these fields have the different physical nature. That makes acoustic images unusual for perception, for example, some internal peculiarities of an acoustically transparent object can be visible [3]. The interference structure of a secondary source field also can cause the significant singularities of sonovision images (for example, the speckle-noise) [4].

In this paper we propose to transfer the sonovision methodology to geophysical waveguide conditions (it is assumed, that the distances of observation are large enough, such that the waveguiding conditions of the sound propagation are fully shown). It should be mentioned, firstly, that the oceanic medium in common is inhomogeneous (if one can avoid rough and complex boundaries, a water layer can be described using smoothly-inhomogeneous layered waveguide model). These circumstances complicate the process of a local inhomogeneity inverse reconstruction, because such medium is not isoplanar and does not "transmit" images [5].

Secondly, the oceanic medium is unsteady and randomly inhomogeneous. It results in illuminating source fluctuations, that prevents

the use of sonovision methods, developed for homogeneous media. And, thirdly, usually observed objects have large wave dimensions (for example, an intrathermocline lens), so that the most part of scattered field energy is concentrated in a small angle around the illumination direction. It is important both because of a noise and a signal decrease due to a signal propagation in natural conditions, and difficulties of design of a power illuminating source field.

The previous consideration lets us suppose that the scheme in which the observed inhomogeneities are situated between the source and the receiving array (or distributed scanning system) is an optimal hydroacoustic vision scheme (this proposition has a theoretical and experimental proof). This scheme is analogous to optical schemes of spatial filtration. But in the acoustic scheme the spatially-distributed receiving system (the array consisting of remote hydrophones or the antenna of synthesized aperture) plays a role of an image forming lens in coupling with the system of reconstruction forming optical images and displaying them as brightness pattern.

The described circumstances significantly complicate the process of hydroacoustic image reconstruction concerning the free space imaging, thus it is necessary to take into account waveguiding conditions in a reconstruction algorithm. Moreover the important part of the algorithm is the dark field method, that provides a filtration of a strong illumination source field [6].

In previous papers [7,8] we showed, that under the above conditions oceanic inhomogeneity images can be reconstructed in a way similar to "shadow" images, which contain information of only one projection of inhomogeneities. In this paper we study the possibilities of the common processing of a number of inhomogeneity projections to get more complete information on the inhomogeneity spatial distribution in a vision area of a hydroacoustic system. In addition to analytic and numerical results the experimental data on physical modeling in the ultrasonic range are given.

ANALYSIS OF THE ONE-VIEW FRESNEL IMAGES RECONSTRUCTION IN THE OCEAN

In a large number of papers devoted to the tomography inhomogeneity reconstruction algorithms are described using a combination of projections [9], the broad concept of "projection" is determined here as one field distribution on an array aperture for one fixed position of a source and a receiver (it is assumed here that a received source wave is plane, and an amplitude or phase or propagation time

of a scattered plane wave vary [10]). In this case the inhomogeneity considered is weak and large-scale [11,12].

In diffraction tomography for each illuminating source position there is a number of projections of diffracted signal [13]. And we can conditionally consider this combination characterizing the scattered fields at one angle of illumination as one projection. This concept of projection is especially convenient for inhomogeneities of large wave dimensions, when a scattered signal spectrum is in a small interval of scattering angles, and the small array aperture is enough for measurements. In this case we assume that Fresnel approximation for the aperture dimensions is realized, i.e. the array aperture contains few Fresnel zones for the observed inhomogeneities. Here we also obtain only one projection, and although aperture dimensions allow to reconstruct two-dimensional inhomogeneity distribution by focusing of a measured signal, the longitudinal resolution is small [14]. The obtained pseudo-image is a "shadow" image, and it is similar to a single projection in the tomographic method (at the same time this image contains information on a longitudinal structure of an inhomogeneity). Below we will call it the one-view image. In our previous paper [14] the properties of such images were investigated and, in particular, certain methods of spatial filtration of a direct illuminating source signal were developed.

For more complete reconstruction of two-dimensional horizontal distribution of inhomogeneities the common processing of projections or pseudo-images is required. It allows to obtain more complete reconstruction of an inhomogeneity shape even for a few projections, for example, for two ones.

It should be mentioned that this scheme is similar to the human eyesight, i.e. to the binocular system consisting of two lenses at a small angle to each other. The multi-view image reconstruction will be considered in the next section. Here we analyze the one-view image taking into account the influence of the waveguiding conditions on the formation of acoustic images in the ocean.

We use the analogy of the image formation by the lens and the antenna in the Fresnel zone. In addition to that we assume, that the observed rigid inclusion of horizontal and vertical dimensions L_h and L_v, respectively, is situated in the waveguide between the source and the receiving system (i.e. horizontally and vertically stretched array of hydrophones), see Fig. 1.

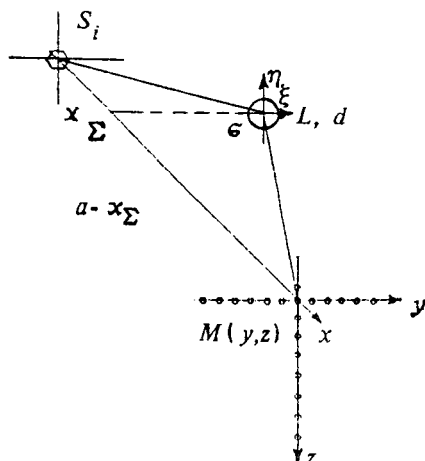The common velocity potential $u(\vec{R})$ in the region of observation

Fig. 1. Basic scheme of the hydroacoustical vision system and the measurement geometry

$\vec{R}(x, y, z)$ is determined from the Helmholtz-Kirchhoff equation [15]:

$$u_0(\vec{R}) + \frac{1}{4\pi} \oint_S \left[\frac{\partial u(\vec{R}_s)}{\partial n} G(\vec{R}_s, \vec{R}) + u(\vec{R}_s) \frac{\partial G(\vec{R}_s, \vec{R})}{\partial n} \right] d\vec{R}_s = u(\vec{R}) \quad (1)$$

where $u_0(\vec{R})$ - is the velocity potential of the direct illumination field, n - is the outer normal of an inhomogeneity surface S, $G(\vec{R}_s, \vec{R})$ - is the Green function of the undisturbed medium. The problem consists in the reconstruction of an inhomogeneity location and shape (by a spatial distribution of secondary sources $\frac{\partial u(\vec{R}_s)}{\partial n}$ and $u(\vec{R}_s)$) from fields $u(\vec{R}_s)$ measured on an array aperture $M(y, z)$. The measurements are carried out in the presence of noise.

As follows from (1) the problem of hydroacoustic vision is the inverse problem of scattering (IPS), because the integral equation with the known right-hand side is solved with respect to spatial distribution of secondary sources on the surface S of unknown shape. From this point of view the problem of vision is the particular problem of IPS, that is more general and complete problem of the reconstruction of both an internal structure and physical characteristics of inhomogeneities. But the aim of vision is to restore images of investigated objects convenient for visual observation.

For the further analysis of imaging in oceanic waveguides some

105

approximations are necessary. It is assumed that the inhomogeneity is remote far from waveguide surfaces, so that the multiple scattering can be neglected [16]. In addition to that we assume: 1) the horizontal wave dimension of the inhomogeneity is large $L_h \gg \lambda$ (λ - is the wavelength of the illuminating source); 2) the small angle approximation is realized; 3) distances between the source, the inhomogeneity and the receiver are large concerning the waveguide thickness. In this case the equation (1) given in a simplified form is [17]:

$$u_0(\vec{R}) - \frac{1}{2\pi} \int_\sigma \int \sigma(\xi, \eta) \frac{\partial u_0(\xi, \eta)}{\partial n} G(\vec{R}_s, \vec{R}) d\xi \, d\eta = u(\vec{R}) \qquad (2)$$

where $\sigma(\xi, \eta)$ - is a part of plane limited by a line dividing light and dark sides of the inhomogeneity situated at a distance x_Σ from the source and $a - x_\Sigma$ from the receiver (see Fig. 1). Further we use the mode approach of the acoustic field in the oceanic waveguide [15]. Thus, we get the expression for the incident field and Green function:

$$u_0(x, y, z) = \sum_{n=1}^{N} A_0 \varphi_n(z) \varphi_n(z_i) \frac{\exp\left[i(ah_n - \frac{\pi}{4})\right]}{(ah_n)^{1/2}} \exp\left[i\frac{y^2}{2a} h_n\right] \qquad (3)$$

$$G(\xi, \eta, 0, x, y, z) = \sum_{m=1}^{N} \varphi_m(y) \varphi_m(\eta) [h_m(a - x_\Sigma)]^{-1/2} \times$$

$$\exp\left[i(a - x_\Sigma) h_m + i\frac{\eta^2 + y^2}{2(a - x_\Sigma)} h_m - i\frac{y\eta h_m}{(a - x_\Sigma)} - i\frac{\pi}{4}\right] \qquad (4)$$

where N - is a number of propagated waveguide modes, h_n and φ_n - are eigenvalues and eigenfunctions of the waveguide, respectively, the distances are represented by Taylor decomposition including square components because we take into account the spherical character of incident and scattered fields, $A_0 = const$.

Combining (3), (4) and (2), we obtain the integral equation with respect to the location and shape of an inhomogeneity. For the arbitrary shape σ the vertical and horizontal coordinates (ξ, η) in (2) are interrelated, that complicates the analysis. Thus it is convenient to investigate these dependencies separately, because they contain the different physical information. In the vertical direction at large distances only waveguide modes take part in the scattering, in which a transformation of a spectrum occurs [18]. In the horizontal direction

the diffraction of each mode on the inhomogeneity is analogous to the diffraction in the free space.

For the simplification of our investigations we assume that for the observed inclusion shape $\sigma(\xi, \eta) = L(\eta) \times T(\xi)$. Then the integral equation (2) discounting (3) and (4) is shown by the relationship:

$$u(a, y, z_A) \simeq A_0 \sum_{n=1}^{N} \varphi_n(z_A)\varphi_n(z_i)\frac{\exp\left[i(r_0 h_n - \frac{\pi}{4})\right]}{(r_0 h_n)^{1/2}} - $$

$$\frac{A_0}{2\pi} \sum_{m=1}^{N} \varphi_m(z_A) \sum_{n=1}^{N} \varphi_m(z_i)(-ih_n)T_{nm} \times$$

$$\frac{\exp\left[i\left(h_n x_\Sigma + h_m(a - x_\Sigma) + h_m\frac{y^2}{2(a-x_\Sigma)} - \frac{\pi}{4}\right)\right]}{(h_n h_m r' s')^{1/2}} \times$$

$$\int_{-\infty}^{\infty} L(\eta) \exp\left[-i\left(\frac{y_i}{s'}h_n + \frac{y}{r'}h_m\right)\eta\right]d\eta \tag{5}$$

where $r_0 \simeq a + \frac{y^2}{2a}$, $r' \simeq a - x_\Sigma + \frac{y^2}{2(a-x_\Sigma)}$, $s' = x_\Sigma + \frac{y^2}{2x_\Sigma}$ and the matrix element T_{nm} is equal:

$$T_{nm} = \int_{-\infty}^{\infty} T(\xi)\varphi_n(\xi + z_\Sigma)\varphi_m^*(\xi + z_\Sigma)d\xi \tag{6}$$

It is evident that the first component of the sum (5) represents the incident field in the observed region in mode presentation. The second component corresponds to the scattered field. Examine at first the possibilities of inhomogeneity vertical distribution reconstruction. As follows from (5), the scattering in vertical direction is described by mode spectrum transformation and is defined by matrix component (6). If the vertical inhomogeneity dimensions are small, so that the characteristic scale of the field fluctuations is much more than L_v, for the isovelocity waveguides the expression takes place: $\varphi_n(z) = sin(q_n z) = (\exp(iq_n z) - \exp(-iq_n z))/(2i)$. Then defining the function $T_{n\pm m} = \frac{1}{2\pi}\int_{-\infty}^{\infty} T(\xi)\exp(i\xi(q_n \pm q_m))d\xi$ we obtain the expression for the matrix T_{nm}:

$$T_{nm} = \mp\frac{\pi}{2}[T_{n\pm m} - T_{n\mp m}] \tag{7}$$

The spatial filtration of waveguide modes is described (as in free space) by the convolution of an "input" discrete mode spectrum and

the mode filter T_{nm} (6):

$$\varphi_m(z) = -\sum_{n=0}^{N} \frac{\pi}{2}\varphi_n(T_{n+m} - T_{n-m})L_{nm} \tag{8}$$

where $L_{nm} = ih_n \int_{-\infty}^{\infty} L(\eta)\exp\left[-i\left(\frac{y_i}{s'}h_n + \frac{y}{r'}h_m\right)\eta\right]d\eta$ If the waveguide surfaces are remote to the infinity, the expression (8) transforms into the convolution integral corresponding to the spatial filtration in a free space [19]. As seen from (8), the estimation of the inhomogeneity vertical structure is possible if we solve (8) by the deconvolution method [20]; however a prior information on an incident field mode spectrum and a measured mode spectrum of the field is required. From the physical point of view the situation is illustrated by the example, where the inclusion is illuminated by a single mode of the acoustic field, the scattered field consists of many modes, and each scattered mode is measured. In this case the envelop curve of the mode spectrum represents the scattering pattern, which allows to estimate the vertical dimension of the inhomogeneity by an inverse Fourier transform. However, this way of reconstruction requires a waveguide mode selection that demands the use of vertical arrays, time gating, etc. All of the required methods are connected both with technical difficulties and a complication of processing algorithms [21,22].

We do not discuss this problem and consider in detail the reconstruction of inhomogeneity horizontal distribution. As it follows from (5), for the given indexes n, m the field distribution along the receiving aperture is presented by Fourier transform of an unknown function, which determines an inhomogeneity shape in a horizontal plane in transfer direction, where the distance between the object and the observation region includes a square item. The multi-mode structure is displayed in a complementary field modulation within the observed region (in the form of mode summation). In papers [17,18] the conditions are obtained when the interference modulation spatial spectrum and the spatial spectrum of the inhomogeneity variations substantially differ:

$$\left(\frac{4\pi r_0}{\Delta h_{ij}}\right)^{\frac{1}{2}} \approx \frac{r_0\pi}{\langle h_{ij}\rangle L} \tag{9}$$

where $r_0 = a - x_\Sigma$, δh_{ij} - is the difference of horizontal projections of mode wave vectors, $<h_{ij}>$ - is the average value. For fixed parameters of a waveguide and inhomogeneities the distance of observation r_0 plays an important role: for $r_0 \gg r_0$ (where r_0 satisfies the condition (9)) the frequency of an interference modulation is more, and

for $r_0 \ll r_0$ - it is less then the "useful" variations, that allows easy filtration of each item. However, when (9) is satisfied, the interfering modulation may be filtered only using prior information both on waveguide parameters and on inhomogeneities, so that the image reconstruction without taking into account the mode structure may be significantly altered. At middle distances (see (9)) images corresponding to different modes overlap each other, that often makes the summary image interpretation impossible. At large distances restored images are multiplied.

Observe now one mode imaging in detail, where $n = m$. To this end we assume that the mode selection is carried out, or one mode is differentiated due to the dissipation loss in a waveguiding propagation, or the mode interference component is filtered in the imaging process [7]. In one-mode approximation (5) is equivalent to:

$$u(a, y, z_A) \simeq S_n^0 e^{i\frac{y^2}{2a}h_n} - S_n e^{i\frac{y^2}{2(a - x_\Sigma)}} \int_{-\infty}^{\infty} L(\eta) e^{-i(\frac{y_0}{s'} + \frac{y}{r'})h_n\eta} d\eta \qquad (10)$$

where

$$S_n^0 = A_0 \varphi_n(z_A) \varphi_n(z_i)(r_0 h_n)^{-1/2} \exp[i(ah_n - \frac{\pi}{4})],$$

$$S_n = \frac{A_0}{2\pi} \varphi_n(z_A) \varphi_n(z_i)(-ih_n) T_{nn}(h_n^2 r's')^{-1/2} \times$$

$$\exp[i(h_n x_\Sigma + h_n(a - x_\Sigma) - \frac{\pi}{2})] \ .$$

Assumption $y_0 = 0$ yields the expression for the second component in equation (10):

$$S_n \int_{-\infty}^{\infty} L(\eta) \exp\left[i\left(-h_n\frac{\eta}{r'}y + h_n\frac{y^2}{2(a - x_\Sigma)}\right)\right] d\eta.$$

The exponential factors in Fresnel integral represent the complete orthonormal basis [23]. To solve the integral equation (10) concerning $L(\eta)$, it is necessary to multiply both parts of the equation by $\exp[i(h_n y \sin \alpha - h_n y^2/R)]$ (where α, R - are polar coordinates of the point (x, y)) and to integrate the expression over the whole range of definition of Fresnel functions. Than in the right-hand side of (10) we obtain the Fresnel transform of the field measured on the infinite aperture. The left-hand side contains two images of a point illuminating source: at $\alpha^0 = 0$, and $R^0 = 2a$ (the first item) and image determined by $L(\alpha r')$ when $R = 2(a - x_\Sigma)$. However, it is a formal solution, because we did not take into account the finiteness of the measuring aperture. Denoting this aperture as the function $M(y_A)$,
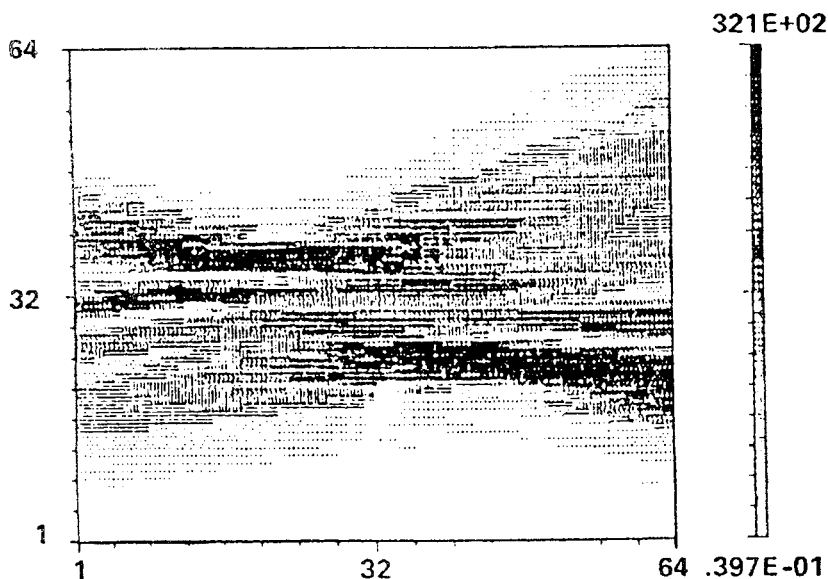
109

Fig. 2. Fresnel image of point sources distributed in a horizontal plane from one projection. Sources are situated at different angles and distances $(a - x_\Sigma = D, \ D = 30\lambda)$

we multiply both sides of (10) by $M(y_A)exp[i(h_n y_A \sin\alpha - h_n \frac{y_A^2}{R})]$ and integrate it within infinite limits. Than in the right-hand side we obtain the function $\Phi_n(\alpha, R)$, determining the image reconstruction algorithm using the measured data. Two components in the left-hand side of (10) can be written as:

$$S_n^0 F_n(\alpha, (1/(2a) - 1/R)^{-1} - S_n \int_{-\infty}^{\infty} L(\eta) F_n(\alpha - \frac{\eta}{r'}, \varepsilon^{-1}) d\eta \qquad (11)$$

where $\varepsilon = 1/(2(a - x_\Sigma)) - 1/R$ - is the parameter of vision system focusing, $\sin\alpha \simeq \alpha$, and F_n - is the pulse-transient characteristic of the reconstructing system (that is the image of primary or secondary point source):

$$F_n(\alpha, R) = \int_{-\infty}^{\infty} M(y_A) e^{ih_n[(\frac{\eta}{r'} - \alpha)y_A + \varepsilon y_A^2]} dy_A \qquad (12)$$

As known from the image reconstructing systems theory (for example, optical systems), a quality of imaging is characterized by the

110

pulse- transient function [19]. In many cases this characteristic appears to be independent on a point source position within a vision area. However, in the observed case it does not occur because an image of a discrete point object essentially depends on a source location. As seen from (12), this dependence is vividly displayed at large distances between the observation point and the measurement area. For the rectangular aperture when $M_n(y_A) = \begin{cases} 1, & |y_A| \leq D/2 \\ 0, & |y_A| > D/2 \end{cases}$ at $\varepsilon = 0$ (for the focused image) $F_n(\alpha, a - x_\Sigma) = DSinc(h_n \alpha D)$, and the transverse dimension (on x axis) is described as $\Delta x = (\lambda(a - x_\Sigma))/(2D)$.

The point source image is much wider in the longitudinal direction: $\Delta y \sim (5 \ldots 10)\Delta x$ (it can be estimated by Fresnel integral). As an observed object moves from the array, the separate elements of resolution increase along y-axis. As follows from (11), the structure of point source images determines the number of independent elements in the object image resolution. In Fig. 2 the images of sources situated at different angles and distances are shown. The image of a far remote source is displayed in the observation area as a quasi-uniform background. It is caused by finiteness of the antenna aperture and, therefore, a weak focusing of these source fields.

It should be noted, that the number of independent image elements is determined not only by the size of the point source image, but also by limitness of a vision area. This circumstance is explained by an inapplicability of the Fresnel approximation near the antenna and the resolution decrease at large distances and large displacements on x-axis. As seen from (11), the receiving system registers both the scattered field from the observed inhomogeneities and the direct illumination field. The first term in (11) defines the source image. Again, if the source is far remote from the receiver, its image occupies in common the whole vision area. As mentioned, the strong direct signal fluctuations overlap inhomogeneity images. In addition to that the strong direct signal decreases the dynamic range of signal registration.

To overcome these difficulties the general dark field method of source field suppression was developed [6-8,14]. This method is based on a selection of scattered and direct signal spectra, corresponding the sources differently remote from an array. In the first realization of the dark field method the signals of two neighboring receivers are subtracted and resulting spatial components of masked source signal are filtered [7]. This operation realizes a spatial mask in a focal plane matched according to prior information of the source location. Another way is based on spatial filtration of Fresnel images by two-dimensional filters adjusted to a source image [7,8]. Both methods

require prior information on the source location, however, the second way may be readily used in complex-structure media, when a filter is constructed using the empirical data in the absence of inhomogeneities. An example of diffracted signal differentiation from high background (when the direct signal is by 15 dB larger than the diffracted signal) is given in Fig. 3. Fig. 3b shows the scatterer image obtained using a two-dimensional spatial spectrum filter $\theta(\xi_x, \xi_y) = |F^0(\xi_x, \xi_y)|^{-1}$, where $F^0(\xi_x, \xi_y)$ - is a source spectrum, ξ_x, ξ_y - are spatial frequencies. In the considered example the aperture dimension is about 10 Fresnel zones for the source.

In paper [7] this method was applied to image reconstruction of the vertical steel rod in the water layer. The interference of waveguide modes in these experiments resulted in a strong distortion of the source image, that led to almost complete masking of the cylinder image. The spatial filter obtained by inversion of the source spectrum amplitude component (including a mode interference) was used to localize the cylinder. As seen from analysis of various kinds of one-view images, for complicated spatial distributions a significant part of information may be lost, that leads to some uncertainty of the observed objects shape and location definition. To illustrate this fact the images of the letter П and a rectangle (situated in a transverse plane (x, y)) of the same dimensions on y-axis are given in Fig. 4.

As seen from the numerical simulation, an adequate interpretation of various objects by one-view images is difficult. By the recent time tomographic methods [10] providing more complete reconstruction of the spatial distribution by the combined processing of projections fixed at different angles are developed. However, a consequent measurements of signals in the ocean at numerous angles is long-time process, that is unsuitable for nonstationary inhomogeneity observations. The creation of simultaneous schemes is very expensive and also unacceptable. Apparently, a possible way to be adopted is an application of scanty-view schemes, which allow to solve this problem, although, not to the full. In addition to that, taking into account technical and other difficulties arising in far sonovision scheme creation (when waveguide peculiarities become significant), it is important to organize a location of each source according to natural conditions. Thus, it appears impossible to make large horizontal antennas of continuous aperture including many Fresnel zones. The more acceptable way is to construct an array of sparse hydroacoustic receivers.

Some realizations of sonovision schemes by means of sparse transducer arrays and also the scheme of reconstruction from two projections ("binocular scheme") are discussed in the next section. And pre-
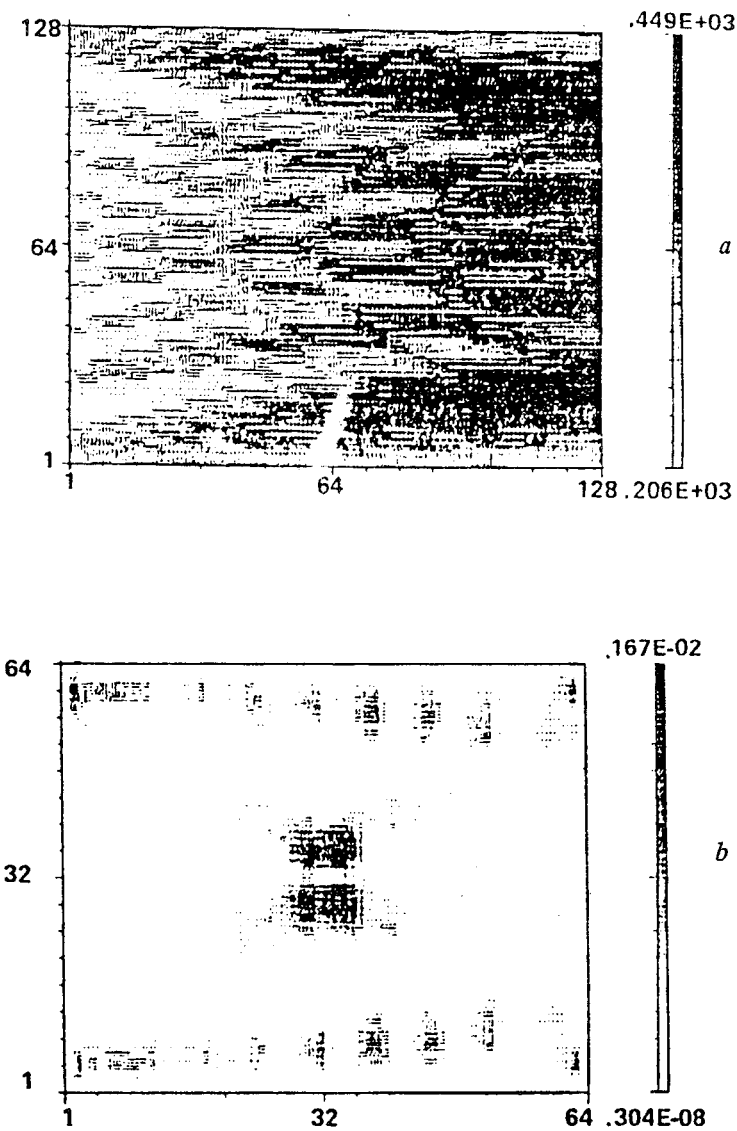
Fig. 3. Unfiltered summary signal (a): only the illuminating source is seen; the filtered signal (b): the scattered image appears
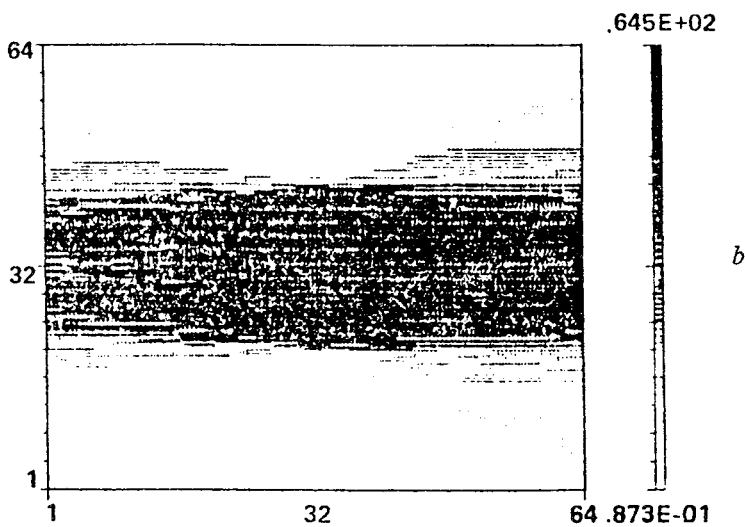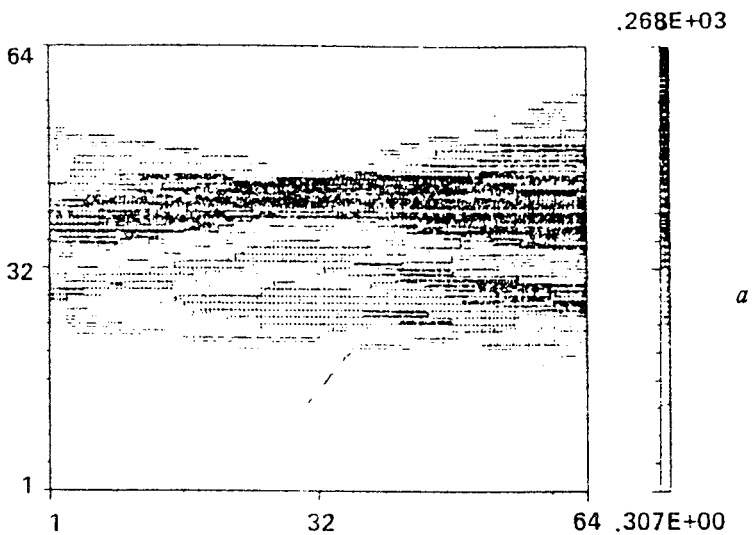
Fig. 4. Images of the sign Π (a) and the transverse rectangle (b) reconstructed from one projection. Direct illumination field is suppressed

viously it is necessary to pay attention to the influence of waveguiding conditions on the depth distribution of receivers. In papers [13,21] the differential diagnostics methods are proposed for a reconstruction of an inhomogeneity spatial structure reconstruction between the source and the receiving system using vertical radiating and receiving arrays. In this way the arrangement of receivers providing matched radiation and reception of waveguide modes far remote in a mode spectrum is optimal. Generally, the problem of optimization of source and receiver situation in the hydroacoustic vision scheme is considered in [23,24], where translation characteristics of inhomogeneities are introduced and special optimization algorithms are derived.

BINOCULAR SCHEME OF ACOUSTIC VISION

Return to scanty-view schemes using stated above one mode approximation. However, we assume now that measurements are carried out by a finite set of far remote receivers. Before the analysis of the binocular scheme consisting of two far remote arrays we consider briefly one view reconstruction by discrete array. The aperture function $M(y_A)$ for a finite number of receivers can be written as:

$$M(y_A) = \sum_{n=1}^{N} A_0 \delta(nd - y_A) \Pi_{y_A} \tag{13}$$

where $A_0 = const$, $\Pi_{y_A} = \begin{cases} 1, & |y_A| \leq D/2 \\ 0, & |y_A| > D/2 \end{cases}$, $d = D/N, N$ - is a number of hydrophones.

As it is known, the fewness of an array results in the multiplication of images [7]. Fig. 5a shows the resulting multiplied images of the point scatterer and the source in the scatterer plane.

The received signal is processed to focus the source image, leaving the scatterer image unfocused. Combining (12) and (13) for $r = 2a$ we obtain the focused image of the illuminating source $S_n^0 \sin[Nkyd/(2a)]$ $\sin^{-1}[kyd/(2a)]$, where $k = 2\pi/\lambda$.

For the direct signal suppression a filter enclosing main and two neighboring maxima of each source image is used, and the obtained signal is focused into each point of vision area (Fig. 5b). Besides that more successive filtration is possible, when a matched filter multiplier is $\theta = \sin(\frac{kyd}{2a})$. Taking off the spectral components of number $\pm N$ we obtain a pure scatterer signal (Fig. 5c). It should be mentioned for image reconstruction by rarefied antennas, that the fewness of an array limits the vision area and makes it possible to fix an inhomogeneity situation within a multiplication period. In the considered case
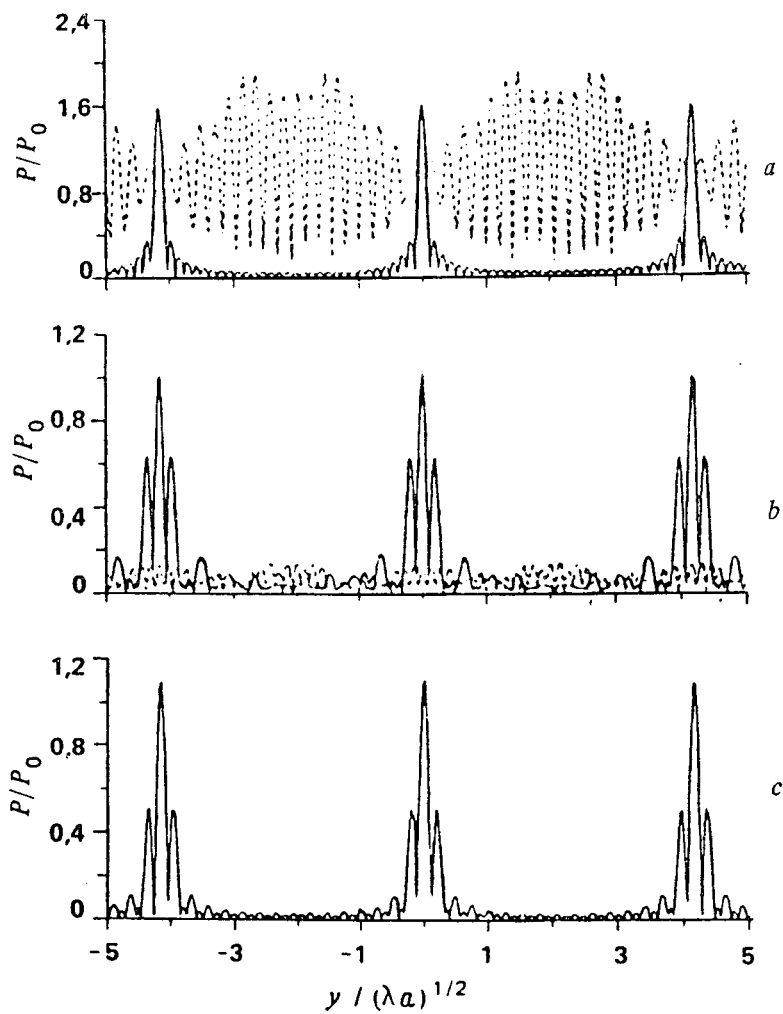
Fig. 5. Reconstruction of point source image in a scatterer plane before (a) and after filtration by the meander mask (b) and the sinusoidal mask (c) using 16-element array
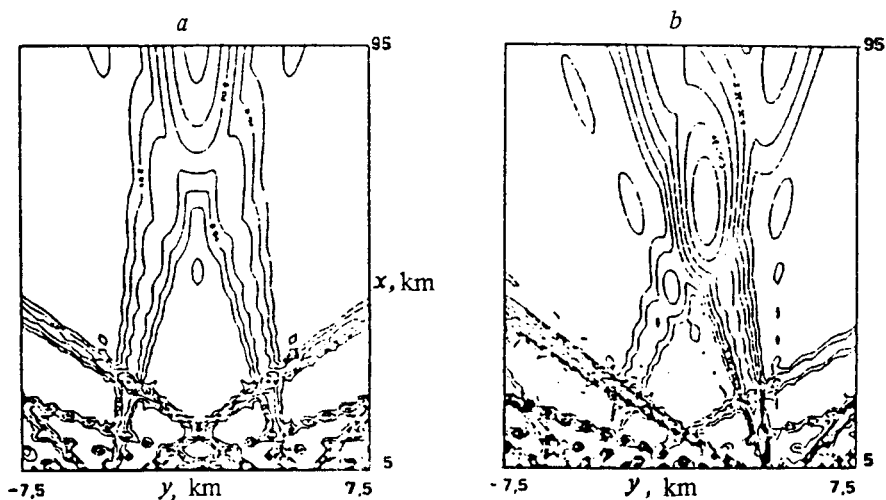
Fig. 6. Binocular image reconstruction by two 8-element arrays of length 20λ separated by 800λ before (a) and after (b) the filtration

the number of individual elements of the image in transverse direction along y-axis is of order $\frac{D}{d}$. Apparently these simplified schemes are useful for observations of small objects. For definition of the real object location using the same receiving array a set of images at different frequencies, not multiple, is required. A true image in obtained patterns stays on its place, and we obtain the desired source image as a result of summation. The resolution in the longitudinal direction is limited both by dimensions of the region of measurement (as for the continuous aperture) and by a multiplication effect. As it was mentioned in the section 1, to increase the spatial resolution in the longitudinal direction (on x-axis) it is necessary to increase the receiving aperture dimensions, that is difficult to realize in practice.

However, one can avoid these difficulties by using the registration system of two remote antennas. Then the vision is realized as if it is carried out in two directions, that can provide some advantages, for example, the increase of the longitudinal resolution. According to (11) and taking into account (12) and (13) the character of images reconstructed by each array is similar to those shown in Fig. 5, and the resulting image can be obtained by coherent or incoherent summation of these images. As a result of coherent summation the obtained signal is modulated by the interference component (characterized by different spatial periods for different distances from the antenna). In
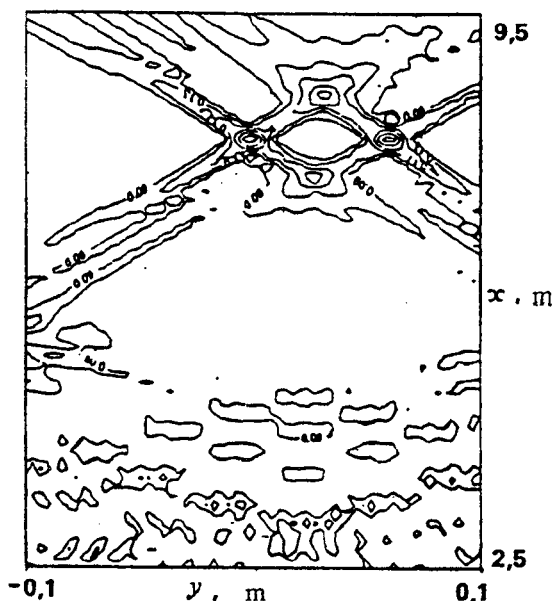
Fig. 7. Filtered image of the transverse rectangle reconstructed from two projections

particular, the spatial frequency of modulation decreases as the source moves from the array. Moreover, the modulation frequency increases with the angle displacement augmentation. Such spatial modulation allows in certain cases to define the distance from the scattering inhomogeneity, but it requires either observations at several frequencies or an inspection of an inhomogeneity transference.

Examine closely the incoherent summation of images. Such kind of processing can be used when the signals in each reception region are incoherent. If the distance between the receiving antennas is large enough (more than the interval of coherence depending on randomly distributed inhomogeneities of the oceanic medium), the interference modulation does not enter the images. As it is shown in Fig. 6a, the unfiltered source signal masks the image of the point scatterer almost completely, and after the filtration the scatterer is clearly seen (Fig. 6b). Only one of multiplied images of a small spatial resolution is shown in Fig. 6, because small arrays $\sim 10\lambda$ were used.

However, each separate array does not allow to determine a distance from the inhomogeneity and its configuration in the certain vision area. For this purpose the system of two arrays is used, be-

cause the accuracy of distance definition depends rather on the interval between antennas then on the antenna length. In this case the spatial resolution is determined by vertical and horizontal projections of direction pattern lobes in a certain region of the vision area. The spectral filtration can cause the image distortion, because low frequencies in the inhomogeneity spectrum are suppressed. Fig. 7 shows the binocular image of the rectangle extended in a transverse direction as a result of such filtration.

Here the original contouring takes place, i.e. only ends of the rectangle are visible (because these regions are formed by high-frequency components of the spatial signal, which was not filtered).

As stated above, the reconstruction of the spatial distribution using rarefied arrays at few observation angles can be carried out within certain limits.

Apparently, it is possible to observe spatially-localized inhomogeneities moving in the vision area. The reconstruction of complex shaped objects or a distribution of a number of objects requires registration of larger amount of data. So that, consider possibilities of the hydroacoustic imaging by means of common processing of few images at various observation angles.

MULTI-VIEW IMAGES

Contrary to the binocular scheme of reconstruction using only one illuminating source, further we consider schemes where the angle of illumination and the receiving array location angle shift at the same pitch in opposite directions. In an observation of stationary distributions the sequence of partial images at each view may be fixed in succession, in the opposite case simultaneous measurements are required. As mentioned, the resulting image can be obtained both by coherent and incoherent summation of separate projections. The coherent summation is connected with interference effects, which can essentially distort the observed object image [25]. At the same time this way of processing allows the summation with correcting complex weight multipliers, that improves the image characteristics. For randomly distributed inhomogeneities it is convenient to carry out an incoherent summation to decrease the speckle-noise. Fig. 8 shows a multi-view image of a rectangle as a result of coherent (a) and incoherent (b) summation of twelve images reconstructed at various angles uniformly spaced within the interval $0° \ldots 90°$.

In the coherent image, firstly, the significant interference structure masks the rectangle. (Such structure is stipulated by the circumstance, that two of all images are salient by theirs brightness.

.132E+04

64

32

1

1   32   64   .994E+01

a

.132E+04

64

32

1

1   32   64   .103E+03
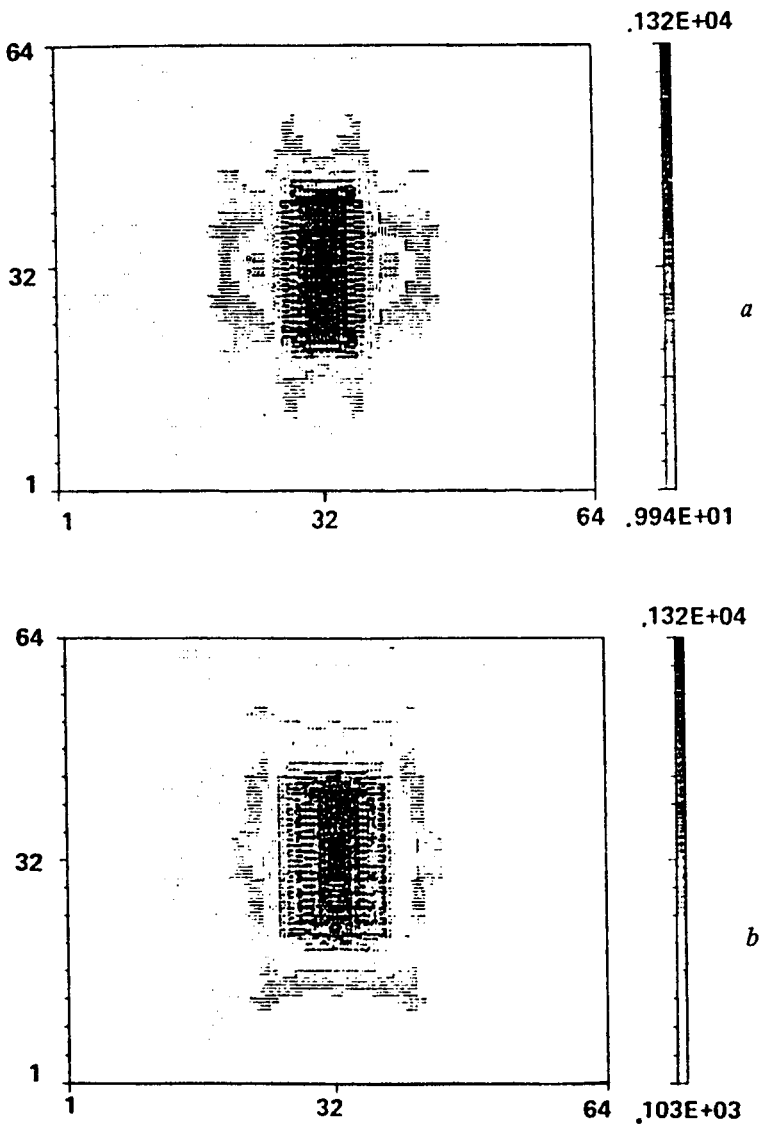
b

Fig. 8. Reconstruction of the horizontal rectangle of length 7λ and width 1λ as a result of coherent (a) and incoherent (b) summation of 12 projections after the illumination field suppression

And these two images, corresponding to the observation from longer sides of the rectangle, interfere as in binocular scheme.) Secondly, the spatial interference of the summary image is caused by the complex structure of each item. And, finally, the interference from numerous separate image details of approximately equal brightness produces the speckle-noise [4] well known not only in acoustics, but in optical reconstruction in laser light [19]. These phenomena can be used in special methods of sonovision, in particular, in ultrasonic medical diagnostics. However, in certain cases, when the estimation of average inhomogeneity distribution is required, or partial images are incoherent due to random inhomogeneities, the incoherent summation is carried out. In this case interference component is absent and an image looks more smooth. However, one loses the opportunity of coherent signal processing.

Observe now the characteristics usually used for the description of an image quality, namely, the spatial resolution and the vision area. As seen from (11)-(13), the Fresnel images are nonisoplanar, i.e. the spatial resolution significantly depends on the position in the vision area. In the multi-view imaging the best resolution appears in the area center (Fig. 9a), because all partial images are identical. With the displacement from center an individual element of resolution becomes more indistinct and decreases in its amplitude (Fig. 9b).

It occurs, because for several angles where the object is farther from antenna, its image is extended in the corresponding direction. Thus, the resulting image becomes illegible. Numerical estimations show that the best multi-view reconstruction in Fresnel zone, apparently, is obtained in the circle of the diameter $0.75a$ and the center $(0.5a, 0)$. The images of the letter Π are given in Fig. 10 for coherent (Fig. 10a) and incoherent (Fig. 10b) summation of images at 32 angles of observation uniformly spaced within the interval $0° \ldots 180°$.

The illuminating object is considered in the given example, that allows to obtain the Fresnel images do not taking into account the problem of source field suppression. It is seen, that the restoration of source spatial distribution is more adequate using the incoherent summation. In the opposite case one of lines forming the letter is weakly visible. This suppression is evidently caused by the interference of partial projections, because this effect disappears with the transfer of the object. A comparison of these two images shows, that in the case of incoherent summation the noise is displayed in the form of some averaged "halo", which can be removed by a low frequency filter. In another case, when partial images are summed in a coherent way an interference speckle-noise appears whose wide spatial spectrum hinders the filtration.
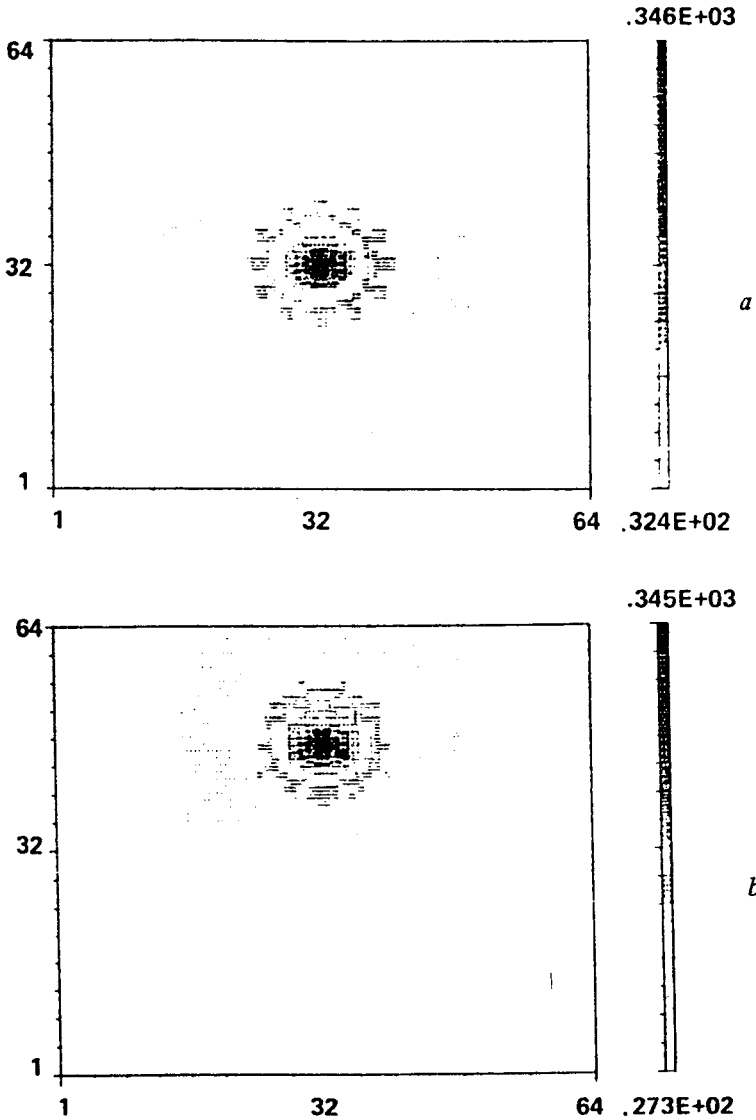
Fig. 9. Image of the point source reconstructed from 12 projections when the source was situated in the centre (a) and near edge (b) of the vision area
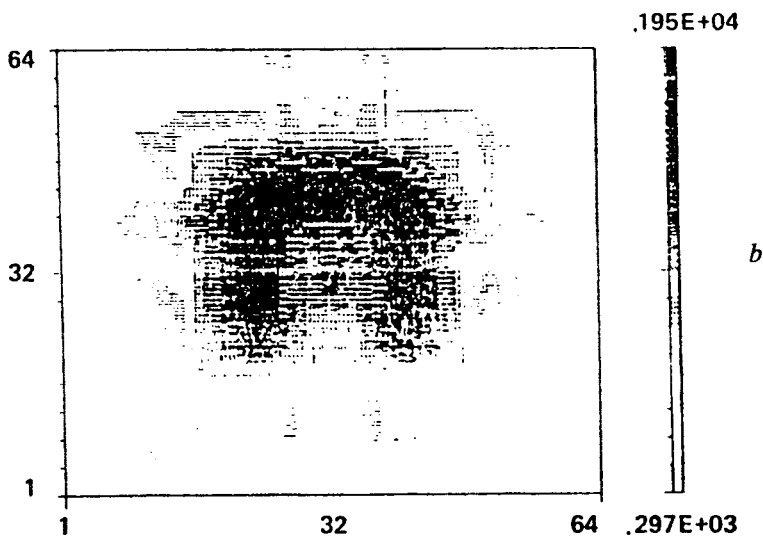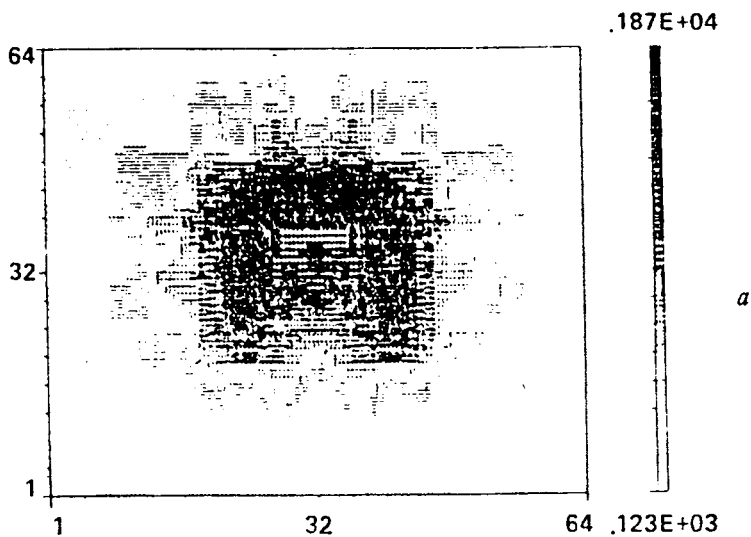
.187E+04

64

32

1

1   32   64 .123E+03

a

.195E+04

64

32

1

1   32   64 .297E+03

b

Fig. 10. Coherent (a) and incoherent (b) multi-view images of a sign II

123

EXPERIMENTAL RECONSTRUCTION
OF SCANTY-VIEW IMAGES

For the verification of hydroacoustic image reconstruction algorithms the ultrasonic experimental set modeling the propagation and scattering of hydroacoustic signals in oceanic waveguides was designed. The measurement system includes a homogeneous water layer with a thickness 3 cm and a sound velocity 1485 m/s on a rubber bottom. A piezoceramic source has a direction pattern specially arranged in a horizontal plane, that allows to avoid the reflection from basin walls. We realized the conditions of scanty mode propagation for the pulse signals 300 mcs in duration at frequencies 140 Hz and 512 Hz. Waveguide modes were weakened due to losses in the rubber layer (a tangent of a loss angle in the rubber was 0.28). Signals were recorded by two quadrature channels for a latter processing and image reconstruction using the computer system (Fig. 11).

Fig. 12a shows the image of the vertical steel cylinder 0.25 cm in diameter reconstructed from one projection. Evidently, the image mainly presents the illuminating source, here the waveguide mode interference is clearly depicted as vertical strips fully masking the image of the cylinder. The scatterer image after the spatial filtration is given in Fig. 12b.

The filter was formed inversely to the amplitude spectrum of the source 7 cm in length accounting the mode interference. Such filter was obtained from the experimental data in the absence of the cylinder. This allows to define only the object position (dimensions of the cylinder are less then the wavelength, that makes the reconstruction of inhomogeneity shape practically impossible).

Observe now possibilities of the multi-view reconstruction. In the experiment we assumed the equality of the situations when: 1) the source and receiving array rotate around the inhomogeneity situated in the center and 2) the inhomogeneity turns in the opposite direction. Three scattering vertical cylinders with diameters 1 cm, 2 cm and 3 cm were mounted on a mechanical rotatable frame, so that the distances between them were 9 cm, 5 cm, 6 cm. The length of the antenna synthesized by moving at the depth $z_A = 0.3$ cm receiver was 36.5 cm. The depth of the source was 1.7 cm. The results of reconstruction of the inhomogeneity spatial distribution from 32 projections are given in Fig. 13 (note, that in these experiments the inhomogeneity was located not in the middle of the acoustic track, where $x_\Sigma = \frac{a}{2}$, but closer to the antenna at $a - x_\Sigma = 25$ cm, $a = 152$ cm, that was taken into account in summation of partial images).

As it is seen from the shown images, significant distortions appear in the reconstruction process (among them an interference in spatial
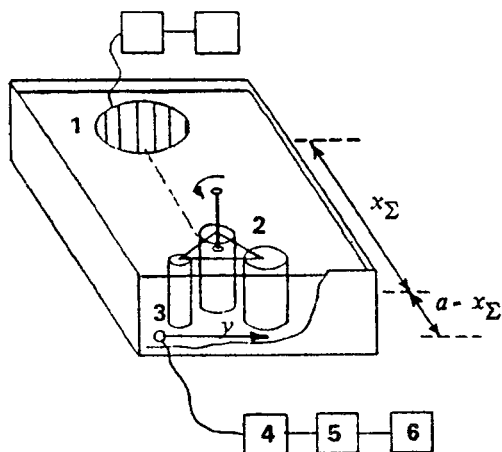
Fig. 11. Basic scheme of the experimental set (1 - a pulse source, 2 - the object of observation, 3 – moving receiver, 4 - an amplifier, 5 - a filter, 6 - a computer). Observation region is limited by dashed line

frequency range comprising the useful signal). It does not allow to suppress the interference by simple methods.

CONCLUSION

In this work the possibilities of image reconstruction of oceanic large-scale inhomogeneities by scanty-view systems (when an incident field and scattered field were registered in limited range of angles) were investigated. The peculiarities of the hydroacoustic imaging in Fresnel zone were analyzed in waveguiding conditions. From the practical point of view the particular attention was paid to vision systems consisting of a few sparse hydrophones (a binocular system among them). Then, the schemes using multi-view observations were investigated. These schemes were analyzed both in theory (analytically and numerically) and in experiment by physical modeling.

The observed particular problem is one in more general field of inverse problems of scattering (including tomographic methods). In this paper we investigated only the problem of vision, i.e. the reconstruction of secondary source spatial distribution on an inhomogeneity surface without reconstruction of its physical structure. Thus,

Fig. 12. Image of the vertical steel cylinder at the distance 20 cm from the source ($a = 44.6$ cm, $L = 28.6$ cm, $f = 140$ kHz) before (a) and after (b) the filtration

only the information on inhomogeneity localization in the observation area and its shape can be obtained.
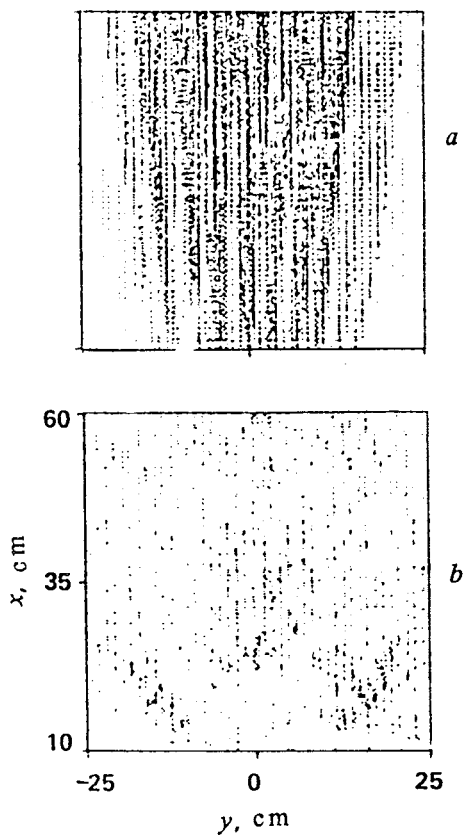
Now sum up the results:

- it was shown, that for measurements by a horizontal antenna (the length of which is more than a few Fresnel zones for observed inclusions) the inhomogeneity distribution reconstruction is possible by consecutive angle scanning and focusing into each point of a vision field. The spatial resolution and vision field limits were estimated.

- it was shown, that the dark field method is required to improve image characteristics (in particular, in the form of a posterior spatial two-dimensional filtration of the resulting image).

- it was found, that an application of the binocular observation scheme (consisting of two receiving arrays) leads to the improvement of image spatial resolution in the longitudinal direction.

- limitations of the spatial resolution and vision field dimensions were estimated for receiving arrays consisting of a few scanty hydrophones.

- limits of the resolution of spatial inhomogeneity distribution were estimated for coherent and incoherent summation of 32 images at different angles, and also for the elimination of the source image by the dark field method.

The efficiency of image reconstruction methods was examined by the experimental image reconstruction. The experimental results confirmed, firstly, the efficiency of the used methods and algorithms and, secondly, allowed to estimate their applicability limitations. Thus, distortions of the complex scatterer image (three steel cylinders) appear, apparently, due to the diffraction on "strong" scatterers (according to the classification used in [12]), for which multiple scattering effects are significant. The reconstruction of such inhomogeneities becomes substantially complicated and requires the use, for example, of iteration algorithms [12]. Another important cause of distortions is the interference, arising from the scattering on random inhomogeneities in the medium and basin walls and also from waveguide mode interference. The weakening of random inhomogeneities influence can be attained by an averaging of random data (if their spatial spectra do not intersect). For weakening of other disturbances in a signal processing the priory information on oceanic waveguide construction and observed inhomogeneities is necessary.

The analysis of possibilities of spatial inhomogeneity distribution reconstruction is of peculiar scientific interest. For an illumination by low frequency sources (when a few modes approximation is realized), the reconstruction in a vertical direction is practically impossible. In the case of high frequency illumination (when numerous waveguide modes propagate) the vertical distribution can be reconstructed, but
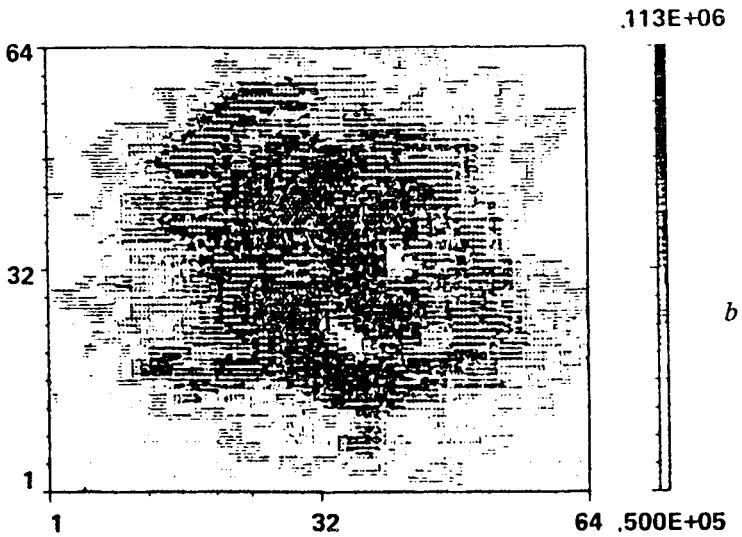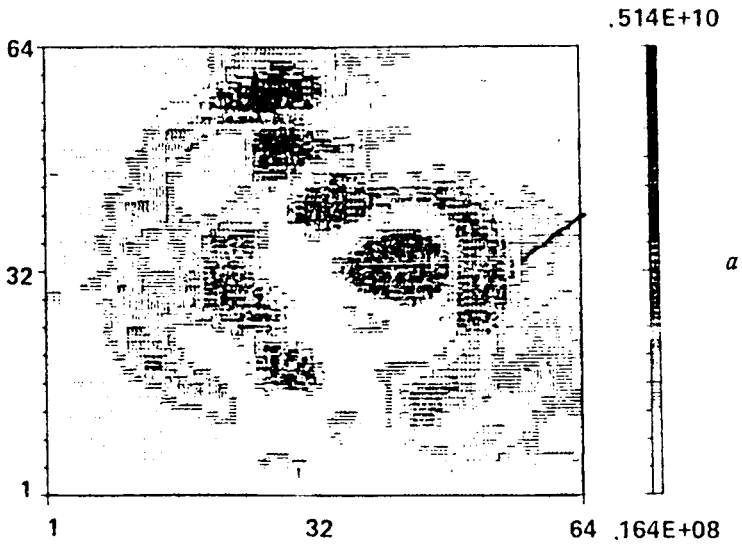
.514E+10

a

.164E+08

.113E+06

b

.500E+05

Fig. 13. Image of three cylinders reconstructed from experimental data as a result of coherent (a) and incoherent (b) summation after illumination source suppression

it requires special methods of matched filtration using both vertical arrays and vertical illuminating systems. Such methods of angle selection and weight sorting by vertical radiating and receiving antennas are developed in [21,24].

REFERENCES

1. *Greguss P.* Ultrasonic Imaging. Focal Press Limited. London, Focal Press Inc. New York, 1980.

2. *Makovski A.* Ultrasonic imaging using arrays // Proc. IEEE. 1979. V. 67. P. 484-495.

3. *Maguer P., Gelly J. F. , Maerfeld C. and Grall G.* An underwater focused acoustic imaging system // Acoustical Imaging. V.10. NY: Plenum Press, 1967. P. 607-617.

4. *Goodman J. W.* Film - Grain, Noise in wavefront-reconstruction imaging // JOSA. 1967. V. 57. P. 493.

5. *Kravtsov Yu. A., Kuz'kin V. M. and Petnikov V. G.* Diffraction of waves on regular scatterers in multimode waveguides // Sov. Phys. Acoust. 1984. V. 30. N 3. P. 339-343. (in Russian).

6. *Borodina E. L., Gorskaya N. V., Gorsky S. M., et al.* Possibilities of shadow methods for studying diffracted sound fields in waveguides // Forming of Acoustic Fields in Oceanic Waveguides / Ed. Zverev V. A. Nizhny Novgorod: IAP RAS, 1991. P. 174-200. (in Russian).

7. *Borodina E. L., Gorskaya N. V., Gorsky S. M., et al.* Spatial filtration of images in ultrasonic visualization of large inhomogeneities // Sov. Phys. Acoust. 1992. V. 38, N 6, P. 1004-1013. (in Russian).

8. *Borodina E. L., Gorskaya N. V., Gorsky S. M., et al.* Reconstruction of the noise "soiling" of inhomogeneous media by dark field methods // Proc. I Symp. RAS. 1992. Moscow: ACIN. P. 19-22. (in Russian).

9. *Mueller R. K., Kaveh M. and Wade G.* Reconstructive tomography and applications of ultrasonics" // Proc.IEEE. 1979. V. 67. N 4. P. 567-587.

10. Image reconstruction from projections / Ed. Herman G. T. NY: Springer-Verlag, 1979. ·

11. *Munk W., Wunch C.* Ocean acoustic tomography: a scheme for large-scale monitoring // Deep Sea Res. 1979. V. 26(A), P. 123-161.

12. *Burov V. A., Rychagov M. N., Sackovets A. V.* Interactive methods for the reconstruction of characteristics at strong inhomogeneities by the data of acoustic scattering // Proc. Ultrason. Int. Conf. 1991. P. 201-206.

13. *Nechaev A. G., Khil'ko A. I.* Acoustical diffraction tomography of the ocean // Dynamic and Stochastic Wave Phenomena, Proc. of the Inter. Scien. School-Seminar, 1992. N.Novgorod: N.Univ. P. 177-181.

14. *Gorskaya N. V., Zverev V. A., Nikolaev G. N., et al.* On reconstruction of the spatial localization of secondary hydroacoustic sources // Proc. XI All-Union Acoust. Conf., 1991. Moscow: VNIIFTRI. Section T. P. 16-18. (in Russian).

15. *Brechovskich L. M. and Lysanov Yu. P.* Theoretical Principles of the Oceanic Acoustics. Moscow: Gidrometeoizdat. 1982. (in Russian).

16. *Morita N. and Kumagai N.* Scattering and mode conversation of guided modes by a spherical object in an optical filter // IEEE Trans. on Microwave Theory. 1980. V.MTT-28. N 2. P. 137-141.

17. *Gorskaya N. V., Gorsky S. M., Zverev V. A., et al.* Short - wave diffraction in a multimode layered waveguide // Sov. Phys. Acoust. 1988. V. 34, N 1, P. 55-59. (in Russian).

18. *Gorskaya N. V., Gorsky S. M., Zverev V. A., et al.* Peculiarities of short-wave diffraction of sound in multimode layered waveguides // Acoustics in the Ocean / Ed. Andreeva I. B., Brechovskich L. M. Moscow: Nauka, 1992. (in Russian).

19. *Born M., Wolf E.* Principles of Optics. Moscow: Nauka, 1973. P. 415-416. (in Russian).

20. Underwater Acoustics and Signal Processing / Ed. Bjorno L. Moscow: Mir, 1985. (in Russian).

21. *Nechaev A. G., Khil'ko A. I.* Differential acoustical diagnostics of random oceanic inhomogeneities // Sov. Phys. Acoust. 1988. V. 34. N 2. P. 285-289. (in Russian).

22. *Gorskaya N. V., Gorsky S. M., Gurbatov S. N., et al.* Investigation of a possibility of frequency modulated wave approximation for studying of the scattering in inhomogeneous waveguides // Sov. Phys. Acoust. 1991. V. 37. N 5. P. 914-921. (in Russian).

23. *Khil'ko A. I., Smirnov I. P. and Zorin A. Yu.* Characteristics of the energetic coupling of the inhomogeneous medium points // Dynamic and stochastic wave phenomena: Proc. of the Int. Scien. School-Seminar, N.Novgorod: N. Univ., 1992. P. 51-53.

24. *Khil'ko A. I., Smirnov I. P. and Zorin A. Yu.* On choosing parameters of acoustical imaging systems in inhomogeneous media (see pres. collect.).

25. *Adams M. F. and Anderson A. P.* Tomography from multiview ultrasonic diffraction data: comparison with image reconstruction from projections // Acoustical Imaging. 1980. V. 10, P. 365-380.

TOMOGRAPHICAL PROBING OF BOTTOM STRUCTURE BY DOPPLER METHOD

M. M. Slavinsky, Yu. V. Petukhov, and I. B. Burlakova

This paper investigates the method of Doppler tomography of the ocean bottom, developed and tested under natural conditions, combines the aperture synthesis and the Doppler effects. This method makes it possible to determine the angular dependencies of the reflectivity, the effective values of sound velocity C and ρ density, as well as the scattering indicatrix of bottom sediments in the low frequency range. The method is based on the analysis, on the frequency-range plane, of the spectral dependencies (dopplerograms) of the spectral power density of bottom - reflected and scattered acoustic signals, separated by Doppler shift, when a high-stability tone source of emission is towed along the path. By the spectral power densities along the trajectories of bottom reflections of different multiplicity, normalized to the geometric divergence, it is possible to find the spatial (angular) dependencies of the reflectivity modules and the effective values of ρ and C in the soil. The scattering characteristics are measured by making spectral cuts of the dopplerograms on given distances with averaging over the space region. The angular coordinates of the scattering indicatrix are identified using the calculated dependencies of the Doppler shifts corresponding to the rays, incident to the bottom at definite angles. The proposed technique was successfully used in measuring the acoustic characteristics of the soil in the frequency range 100–400 Hz in the deep-water regions of the Indian ocean with a smooth and strongly cut bottom relief on acoustic paths up to 80 km. The experimental results on defining the scattering characteristic, as well as the sound velocity and density of bottom sediments agree with the known geophysical data.

The class of tomographic systems differing from those described in [12] includes the system which is based majorly on the works of the author [13] and combines the principles of reconstruction tomography with Doppler effects [14]. The method of Doppler tomography developed in [14] and know now as the method of the synthesized radar aperture [1-3], was used for the first time to map the Moon reflectance [14], and later, in ultrasound techniques; of late this method has been widely used in ocean acoustics [5-7,15-17].

The present paper demonstrates the potentials of Doppler tomography for determination of, first, angular dependence of the reflection coefficient for the even bottom, which yields the sound speed

and sediment density; and, second, angular dependence of acoustic signals scattered by the uneven bottom; the authors have made some use of the results obtained in [5-7].

To illustrate our method, we consider first the simplest waveguide, i. e. , a uniform layer of fluid with depth H, density ρ_0, and sound velocity in it, c_0. It lies on the uniform fluid half-space with corresponding acoustic characteristics c and ρ. If a tonal source with radiation frequency $f_0 = \omega_0/2\pi$ moves in a well-defined horizontal direction $r = vt$ $(t \geq 0)$ at the depth z_s with speed v $(v/c_0 \ll 1)$, dependence of pressure perturbation $P(t)$ on time $t(r)$ at a stationary receiver placed at the depth z_r is defined by the signals propagating along a pair of "water" rays and fours of rays with various multiplicities $m = 1, 2 \cdots$ of bottom reflections; correspondingly, signal frequencies depend on r (see [5,6]). Since further we will consider bottom reflections only, then in the case of $z_s/H \ll 1$ and $z_r/H \ll 1$ being most convenient for their separation by frequency Doppler shifts, each reflection will be formed by fours of rays with the same multiplicity m. Hence, after "current" spectral analysis of the signal $S(\omega, r) = \frac{1}{T} \int\limits_{t}^{t+T} P(\tau) \exp(i\omega\tau)d\tau$ and averaging T with respect to time, we find, unlike [18-20], the following equation for spectral density of the power current $|S^{(m)}(\omega, r)|^2$ within the approximation of the false source pattern (see [8]):

$$|S^{(m)}(\omega, r)|^2 = R_0^2 |S_{1m}(\omega)V^m(\Theta_{1m})e^{i\omega t_{1m}}/R_{1m}$$

$$- S_{2m}(\omega)V_m(\Theta_{2m})e^{i\omega t_{2m}}/R_{2m} - S_{3m}(\omega)V^m(\Theta_{3m})e^{i\omega t_{3m}}/R_{3m} \qquad (1)$$

$$+ S_{4m}(\omega)V^m(\Theta_{4m})e^{i\omega t_{4m}}/R_{4m}|^2,$$

where

$$t_{jm} = R_{jm}/c_0, \qquad \Theta_{jm} = \arcsin(r/R_{jm}), \qquad R_{jm} = \sqrt{r^2 + (2mH + h_j)^2},$$

$$j = [1, 4], \qquad h_1 = -(z_s - z_r), \qquad h_2 = -(z_s - z_r),$$

$$h_3 = -h_2, \qquad h_4 = -h_1,$$

$$\omega_{jm} = \omega_0(1 - \frac{v}{c_0}\frac{r}{R_{jm}}), \qquad S_{jm} = \frac{1}{2\sqrt{\pi}\Omega_{jm}} \exp\left\{-\left(\frac{\omega - \omega_{jm}}{\Omega_{jm}}\right)^2\right\}$$

$$V(\Theta_{jm}) = \frac{\mu\cos(\Theta_{jm}) - \sqrt{n^2 - \sin^2(\Theta_{jm})}}{\mu\cos(\Theta_{jm}) + \sqrt{n^2 - \sin^2(\Theta_{jm})}} \qquad (2)$$

$$n = c_0/c, \qquad \mu = \rho/\rho_0.$$

Here $S_{jm}(\omega)$ is spectrum of the signal at a small distance R_0, and Ω_{jm} is parameter characterizing the spectrum width of the signal propagating along the corresponding ray. When a signal is emitted or received near free surface $((h_j/2mH)^2 \ll 1)$, Eq.(2) yields the following dependencies for the parameters:

$$t_{jm} \simeq t_m = \frac{R_m}{c_0}\left(1 + \frac{2mHh_j}{R_m^2}\right), \qquad R_{jm} \simeq R_m = \sqrt{r^2 + (2mH)^2},$$

$$\Theta_{jm} \simeq \Theta_m = \arcsin(r/R_m), \qquad \omega_{jm} \simeq \omega_m = \omega_0(1 - \frac{v}{c_0}\frac{r}{R_m}), \qquad (3)$$

$$\Omega_{jm} \simeq \Omega_m, \qquad S_{jm}(\omega) \simeq S_m(\omega) = \frac{1}{2\sqrt{\pi}\Omega_m}\exp\left\{-\left(\frac{\omega - \omega_m}{\Omega_m}\right)^2\right\},$$

Using them we find an apparent dependence for $|S^{(m)}(\omega, r)|^2$:

$$|S^{(m)}(\omega, r)|^2 = 4\left(\frac{R_0}{R_m}\right)^2 |S_m(\omega)|^2 |V(\Theta_m)|^{2m} \times$$

$$\left\{1 - \cos\left[\frac{\omega_m}{c_0}\frac{4mHz_s}{R_m}\right] - \cos\left[\frac{\omega_m}{c_0}\frac{4mHz_r}{R_m}\right] + \qquad (4)\right.$$

$$\left. + \frac{1}{2}\cos\left[\frac{\omega_m}{c_0}\frac{4mHh_2}{R_m}\right] + \frac{1}{2}\cos\left[\frac{\omega_m}{c_0}\frac{4mHh_4}{R_m}\right]\right\}.$$

Two points should be emphasized here. First, to separate frequencies of neighboring reflections m and $m+1$ by frequency Doppler shifts one needs synthesize aperture $D = vT > L = \frac{c_0}{f_0 r}\frac{R_m R_{m+1}}{R_{m+1} - R_m}$, whose size should be considerably large at large distance $(2mH/r)^2 \ll 1$ since parameter $L \simeq \frac{c_0}{2(2m+1)f_0}\left(\frac{r}{H}\right)^2$ grows rapidly as r increases. Second, when deriving Eq.(4), variations of frequency Doppler shifts in fours of signals characteristic for every m (see Eq.(3)) have been neglected because, when $z_s/H \ll 1$ and $z_r/H \ll 1$ separation of the $f_{jm} = \omega_{jm}/2\pi$ $(j = [1,4])$ is rather complicated for the whole region $0 < r < \infty$. This separations is possible only when the following conditions are met: $\sigma_1 = |\delta f_{jm}/\Delta \bar{f}| > 1$ and $\sigma_2 = |\delta f_{jm}/\Omega_m| > 1$; (here $\delta f_{jm} \simeq -f_0\frac{v}{c_0}\frac{r}{R_m^3}4z_j mH$ stands for variations of frequency Doppler shifts in fours of signal, $\Delta \bar{f} = -f_0\frac{v}{c_0}\frac{D}{R^3}(2mH)^2$ is range of averaging with respect to frequency Doppler shift when aperture D is synthesized; $z_1 = z_s$, $z_2 = z_r$, $z_3 = |h_2|$, $z_4 = h_4$). Assuming $\Omega_m = \Omega = const$ and $D \simeq L$, we evaluate σ_1 and σ_2 as follows:

$$\sigma_1 = \frac{f_0 z_j r^2}{c_0 mH}\frac{R_{m+1} - R_m}{R_{m+1}R_m}, \qquad \sigma_2 = \frac{v}{c_0}\frac{\omega_0}{\Omega}\frac{4mHrz_j}{R_m^3}, \qquad (5)$$

These formulas easily yield simple dependencies for two boundary cases:

$$\sigma_1 \simeq \frac{f_0 z_j}{c_0} \frac{2}{m+1} \left(\frac{r}{2mH}\right)^2, \quad \sigma_2 \simeq \frac{v}{c_0} \frac{\omega_0}{\Omega} \frac{r z_j}{2(mH)^2}, \quad \left(\frac{r}{2mH}\right)^2 \ll 1;$$

(6)

$$\sigma_1 \simeq \frac{f_0 z_j}{c_0} \frac{2(2m+1)}{m} \frac{H}{r}, \qquad \sigma_2 \simeq \frac{v}{c_0} \frac{\omega_0}{\Omega} \frac{4mH z_j}{r^2}, \qquad \left(\frac{r}{2mH}\right)^2 \gg 1.$$

It follows from Eq. (5),(6) that separation with respect to Doppler shifts $\Delta f_{jm} = f_{jm} - f_0$ with $m = const$ is possible only for high frequencies $f_0 z_j / c_0 \gg 1$ and in the intermediate region of distances $r \simeq 2mH$.

Taking these considerations into account, let as go back to analyzing Eq.(4). It can be previously simplified for the case of $z_s = z_r = z$:

$$|S^{(m)}(\omega, r)|^2 = 16 \left(\frac{R_0}{R_m}\right)^2 |S_m(\omega)|^2 |V(\Theta_m)|^{2m} |sin^4 \left[\frac{\omega_m}{c_0} \frac{4mH z}{R_m}\right]. \quad (7)$$

As follows from Eq.(7), dependence of $J_m(\omega, r) = \left(\frac{R_m}{R_0}\right)^2 |S^{(m)}(\omega, r)|^2$ on r a function oscillating with a period which increases as the distance grows; maxima of the function correspond to the spatial (angular) dependence of the reflection coefficient modulus in the degree equal to doubled reflection multiplicity. Comparing Eqs.(4) and (7), it is obvious that the latter is more convenient to determine the angular dependence $|V(\Theta_m)|^{2m}$, since all the interference maxima characterized by the last multiplier in Eq.(7) have the same amplitude, unlike in Eq.(4).

Thus, having obtained the experimental dependence $J_m(\omega_m, r)$ we can find its maxima and, consequently, develop a corresponding angular dependence $|V(\Theta_m)|^{2m}$, whose accuracy for given H grows with increase of the emission frequency, depth of corresponding points, and bottom reflection multiplicity; that is , their increase causes the oscillation period $J_m(\omega_m, r)$ to decrease with respect to r, and angular dependence of the reflection coefficient is defined in more detail. Using $|V(\Theta_m)|^{2m}$ to determine the angle full internal reflection Θ_r and $W_0 = 1 - V(\Theta_m = 0)$ we find the looked for parameters:

$$n = \sin\Theta_r, \qquad \mu = (2 - W_0)n/W_0.$$

Taking into account stratification of sound velocity $c(z)$ with respect to depth z in a water layer has little effect on the proposed

method of determining n and μ. Within the geometric-acoustic approximation of field presentation as multiple scattering similar to Eq.(1), we obtain the following expression:

$$|S^{(m)}(\omega, r)|^2 = R_0^2 |S_{1m}(\omega) V^m(\Theta_{1m}) \exp(i\frac{\omega}{c_s}\varphi_{1m}) / \Sigma_{1m}^{0.5}$$

$$-S_{2m}(\omega) V^m(\Theta_{2m}) \exp(i\frac{\omega}{c_s}\varphi_{2m}) / \Sigma_{2m}^{0.5} -$$

$$-S_{3m}(\omega) V^m(\Theta_{3m}) \exp(i\frac{\omega}{c_s}\varphi_{3m}) / \Sigma_{3m}^{0.5} +$$

$$+ S_{4m}(\omega) V^m(\Theta_{4m}) \exp(i\frac{\omega}{c_s}\varphi_{4m}) / \Sigma_{4m}^{0.5}|^2 \qquad (8)$$

where

$$\Sigma_{jm} = \sqrt{n^2(z_s) - \sin^2 \Theta_{jm}^{(0)}} \sqrt{n^2(z) - \sin^2 \Theta_{jm}^{(0)}}$$

$$\times \left(\sin \Theta_{jm}^{(0)} / r_{jm} \left| \frac{\partial r_{jm}}{\partial \sin \Theta_{jm}^{(0)}} \right| \right),$$

$$r_{jm} = 2mD(H) - r_j, \qquad r_1 = D(z_s) + D(z_r),$$

$$r_2 = D(z_r) - D(z_s), \qquad r_3 = -r_2, \qquad r_4 = -r_1;$$

$$\varphi_{jm} = 2mJ(H) + \sin\Theta_{jm}^{(0)} r - x_j, \qquad x_1 = J(z_s) + J(z_r),$$

$$x_2 = J(z_r) - J(z_s), \qquad x_3 = -x_2, \qquad x_4 = -x_1;$$

$$D(z) = \int\limits_0^z \frac{\sin\Theta_{jm}^{(0)} dz}{\sqrt{n^2(z) - \sin^2\Theta_{jm}^{(0)}}}, \qquad J(z) = \int\limits_0^z \sqrt{n^2(z) - sin^2\Theta_{jm}^{(0)}} dz,$$

$$\omega_{jm} = \omega_0 \left[1 - \frac{v}{c_s} \sin\Theta_{jm}^{(0)} \right].$$

Here $n(z) = c(z_s)/c(z)$ - is refraction coefficient for acoustic waves, $c_s = c(z_s)$, $\Theta_{jm}^{(0)} < \arcsin[n(H)]$ - is angle at which the corresponding ray leaves the source (it can be called "outlet angle and is the solution of the equation for the point of stationary phase $r_{jm}(\Theta_{jm}^{(0)}) = r$); $\Theta_{jm} = \arcsin[\sin\Theta_{jm}^{(0)}/n(H)]$. When $z_s = z_r = z$, Eq.(8) yields the following formula similar to Eq.(7):

$$|S^{(m)}(\omega, r)|^2 = 16\frac{R_0^2}{\Sigma_m} |S_m(\omega)|^2 |V(\Theta_m)|^{2m} \sin^4 \left[\frac{\omega}{c(z_s)} 2J(z) \right], \qquad (9)$$

where

$$\Sigma_m = \sqrt{n^2(z_s) - \sin^2 \Theta_m^{(0)}} \sqrt{n^2(z) - sin^2\Theta_m^{(0)}} / \left(\sin \Theta_m^{(0)} / r_m \left| \frac{\partial r_m}{\partial \sin \Theta_{jm}^{(0)}} \right| \right) ,$$

$r_m = 2mD(H)$, and outlet angle $\Theta_m^{(0)}$ is a solution of the equation $r_m = r$. Comparison of Eqs.(7) and (9) shows that sound speed stratification in a water layer does not change the algorithm for determination of angular dependencies $|V(\Theta_m)|^{2m}$.

Taking into account stratified structure of bottom sediments makes the analysis more complicated, of course; for example, if we assume multilayer sediment structure, the expression for $|S^{(m)}(\omega, r)|^2$ is not that simple (see Eq.(1),since behavior of this value for given m is the characterized by interference of a considerable number of rays $(max\{j\} \gg 4)$ with complex combinations of reflection coefficient from media interfaces, corresponding to each ray. If the sediment layer thickness h is small comparison with the ocean depth $(h/H \ll 1)$ it is possible to use in the equations for $|S^{(m)}(\omega, r)|^2$ the plane wave reflection coefficients, and this way is demonstrated in [9]. However, it does not simplify determination of sound speed and density stratification in sediments.

Nevertheless, for the majority of practically important cases, account of stratified bottom structure is reduced to consideration of one layer with thickness h, sharp lower boundary of media interface and the depth-depending sound speed in it [10]. It makes determination of acoustic properties of sediments much easier blending the method proposed in [11] and in the present paper. It is evident that Doppler frequency shift separation of signals reflected by lower and upper boundaries of a comparatively thin layer $(h/H \ll 1)$ is complicated if $z_s/H \ll 1$ and $z_r/H \ll 1$ due to the same reason as for the signals reflected from one of these boundaries only (see earlier Eq.(5),(6)); it can be realized only if a bottom receiver $z_r \to H$ picks up signals not reflected from ocean free surface and $z_s \to H$, but the last condition is hardly realized in practice. Hence, determination of angular dependencies of reflection coefficient from the upper and lower boundaries of the layer is possible only using comparison of theoretical and experimental dependencies $J_m(\omega, r)$ with respect to r. This method is similar to one proposed in [11]; within that method one needs to compare dependencies of $| \sum\limits_{m=1}^{M} S^{(m)}(\omega, r)|^2$ on the depth of corresponding points at various distances r; (here $M = max\{m\}$ is number of reflections taken into account when making calculations).

For practice a simpler but "inaccurate" approach is possible; it

consists in introducing some effective uniform liquid bottom with certain acoustic characteristics c_{ef} and ρ_{ef}. The advantages of the method are that $|V(\Theta_m)|^{2m}$, c_{ef} and ρ_{ef} can be determined using also conclusions yielded by Eq. (7) and (9), i.e., by maxima of the dependence $J_m(\omega_m, r)$. Of course, when obtaining experimental dependencies $J_m(\omega_m, r)$ it is necessary to average

$J_m(\omega, r) = (\Delta\omega)^{-1} \int\limits_{\omega_m - \Delta\omega/2}^{\omega_m + \Delta\omega/2} J_m(\omega, r)d\omega$ with respect to a certain fre-

quency band $\Delta\omega > \delta f_{jm} 2\pi$ including Doppler frequency shifts for the four signals with the corresponding reflection multiplicity.

Now we will consider experiment testing of the proposed method for determining $V(\Theta)$ and ground parameters c_{ef} and ρ_{ef}. Similar to [5-7], experimental investigations were made in a deep-water ($H = 3500$ m) region of the Indian Ocean (Arabic Sea) with typical dependence of sound speed $c(z)$ on depth z (see Fig.1a) and even bottom whose upper sediment layer consists of silt and sand. The source emitted low - ($f_0 = 146$ Hz) and high - ($f_0 = 392$ Hz) frequency signals and was towed with velocity $v \simeq 3.5 - 4$ m/s at depth $z_s = 70 - 80$ m along two paths in turn. Azimutal angles of the paths differed by $\pi/2$, and the distance between the initial points was $\simeq 10$ km. Acoustic signals were received at the depth $z_r = 100$ m. When experimental dependencies on the distance of Doppler frequency shifts $\Delta f_m = \omega_m/2\pi - f_0$ and corresponding to them $J_m(\omega_m, r) = J_m(r)$ were determined for bottom reflection of various multiplicities $m = 1, 2 \cdots$, the received signal $p(t)$ was recorded in parallel to the reference one, heterodyned over intermediate frequency $f_p = 1$ Hz and filtered within the frequency band $\Delta f_f = 2$ Hz. The treated signal $p_f(t)$ was digitized and entered into the computer; frequency digitization was $f_d = 5$ Hz. Spectral analysis was made with no weight processing and with duration of each realization $T = 100$ s and time step $\Delta T = 25$ s.

Dependence $W(\Delta f, r) = \left| \frac{1}{T} \int\limits_{t}^{t+T} P_f(t)e^{i\Delta\omega t}dt \right|^2$ shown in Fig.2 only

at high frequency $f_0 = 392$ Hz - for the sake of ease of interpretation yields the following: in the plane $\Delta f - r$ (Doppler frequency shift - distance) trajectories $\Delta f_0(r)$, $\Delta f_1(r)$, and $\Delta f_2(r)$ are identified; the trajectories correspond to signals propagating along "purely" water rays ($m = 0$) and bottom reflections with various multiplicities $m = 1$ and $m = 2$.

Dependence $J_1(\omega_1, r)$ and $J_2(\omega_2, r)$ on r found after integration along corresponding trajectories $\Delta f_1(r)$ and $\Delta f_2(r)$ for both frequencies in two paths, are presented in Fig.3,4. Maxima of the dependen-
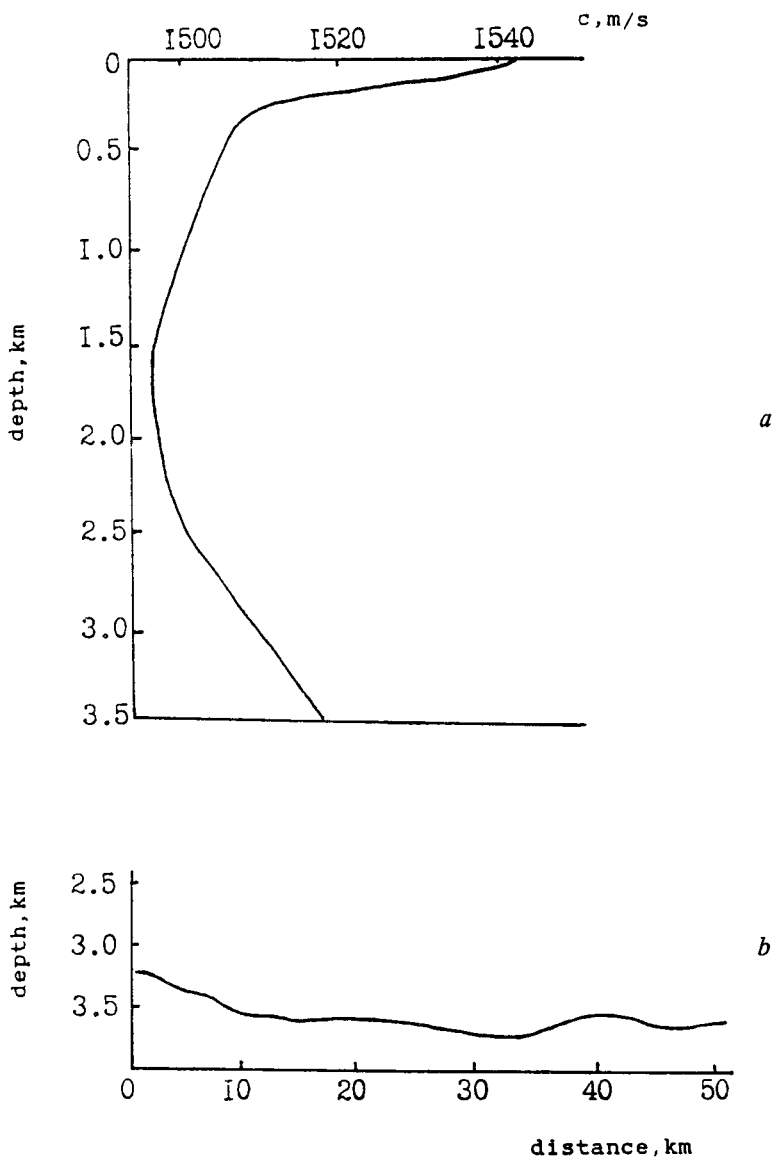
Fig. 1. Typical dependence of sound speed $c(z)$ on depth z in the regions of experimental investigations - (a) and variations of water layer depth $H(r)$ with distance r in the region with uneven bottom - (b).

Fig. 2. Spectral density of acoustic signal power flow $W(\Delta f, r)$ presented by brightness form on the plane Doppler frequency shift - distance along the first path for radiation frequency $f_0 = 392$ Hz. Trajectories 0,1,2 correspond to Doppler frequency shifts $\Delta f_m(r)$ in water signals ($m = 0$) and signals of corresponding multiplicity of bottom reflections ($m = 1, 2$).
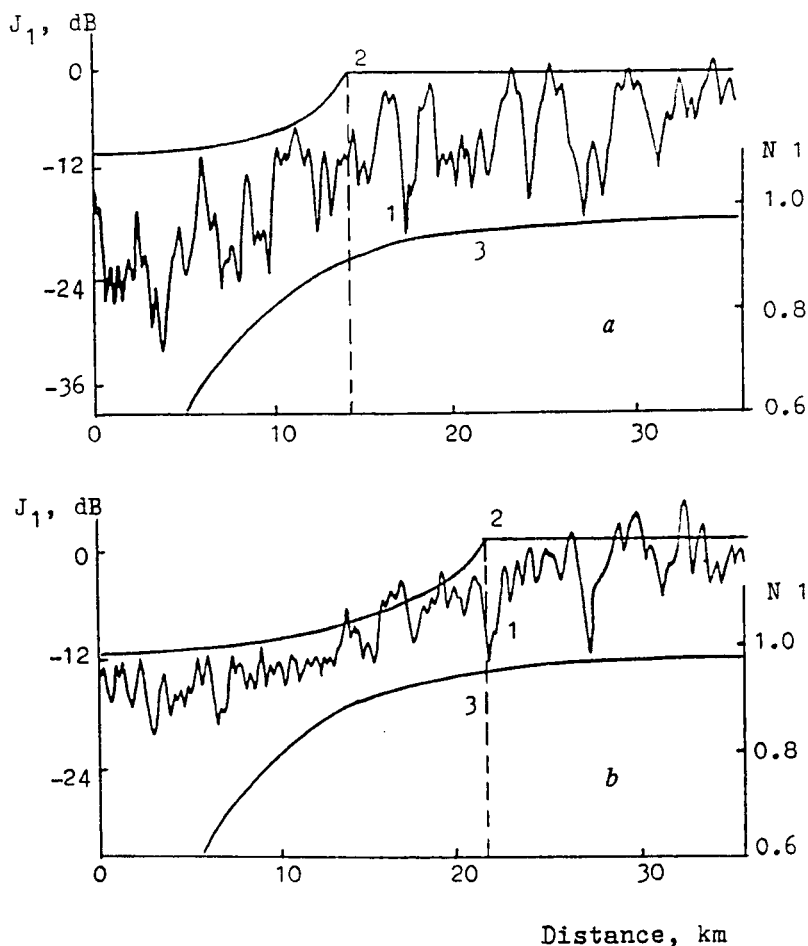
Fig. 3. Experimental dependence on distance r of the spectral density of power flow of the first bottom reflection signal $J_1(r)$, averaged with respect to Δf_m and normalized over geometric divergence - curve 1: a) - $f_0 = 146$ Hz, $\delta f = 0.015$ Hz, b) - $f_0 = 392$ Hz, $\delta f = 0.05$ Hz at the first path; c) - $f_0 = 146$ Hz, $\delta f = 0.015$ Hz, d) - $f_0 = 392$ Hz, $\delta f = 0.05$ Hz at the second path. Curve 2 corresponds to approximation dependence $10 \lg |V(\theta_1)|^2$; curve 3 - to $N_1(r) = \sin\Theta_1$.
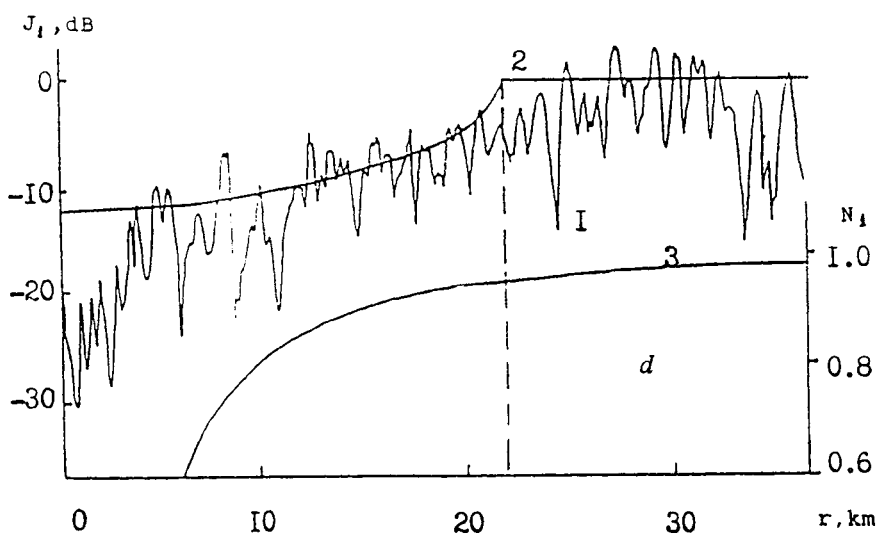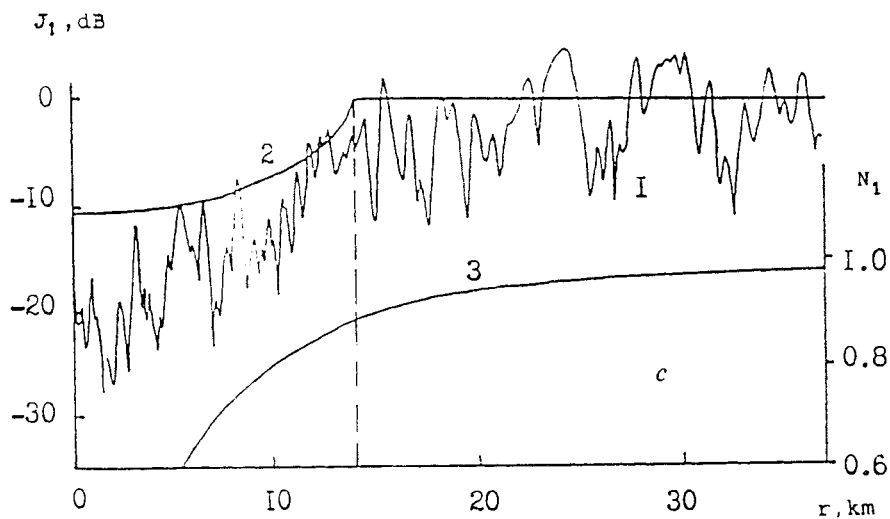
Fig. 3
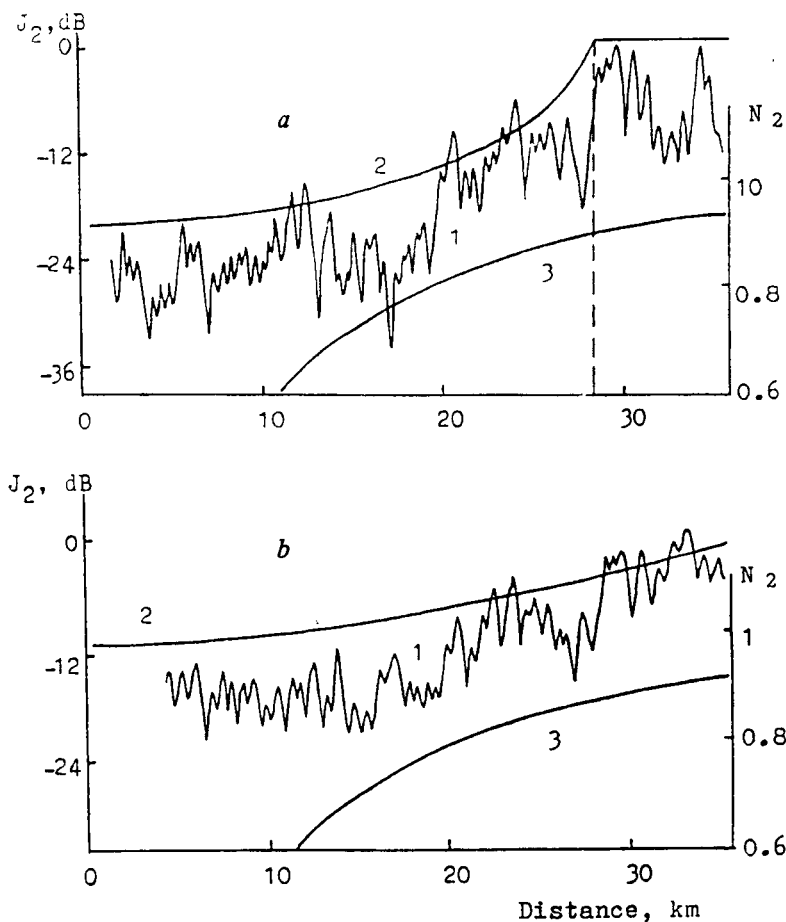
Fig. 4. Experimental dependence on distance r of the spectral density of power flow of the second bottom reflection signal $J_2(r)$, averaged with respect to Δf_m and normalized over geometric divergence - curve 1: a) $f_0 = 146$ Hz, $\delta f = 0.015$ Hz, b) - $f_0 = 392$ Hz, $\delta f = 0.05$ Hz at the first path; c) - $f_0 = 146$ Hz, $\delta f = 0.015$ Hz, d) - $f_0 = 392$ Hz, $\delta f = 0.05$ Hz at the second path. Curve 2 corresponds to approximation dependence $10 \lg |V(\Theta_2)|^2$; curve 3 - to $N_2(r) = \sin \Theta_2$.
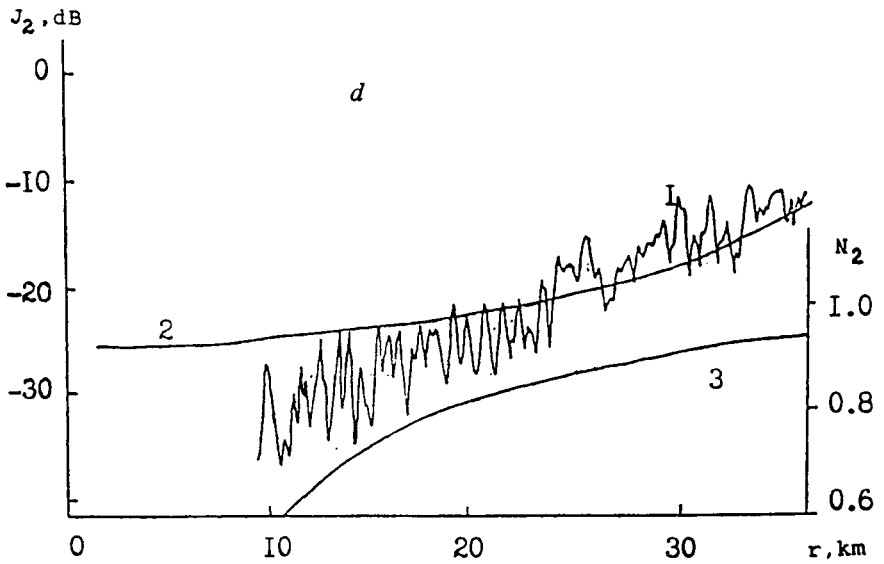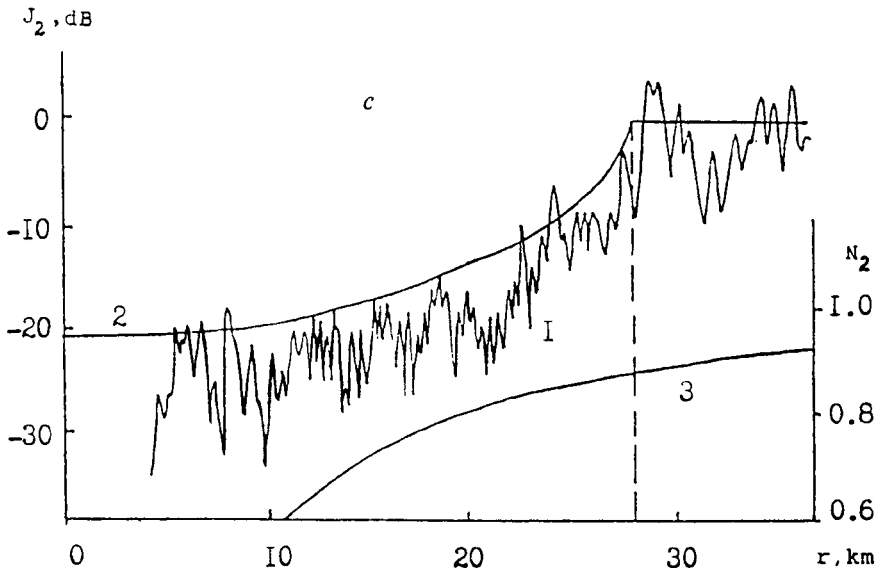
Fig. 4

cies shown in those figures have been used to approximate the angular dependencies $|V(\Theta_m)|^{2m}$ to be found. We determined the following acoustic parameters of the bottom : $\rho_{ef}/\rho_0 \simeq 1.66$, $c_0/c_{ef} \simeq 0.89$ at low frequency and $\rho_{ef}/\rho_0 \simeq 1.6$, $c_0/c_{ef} \simeq 0.95$ at high frequency. They are in good agreement for $m = 1$ and $m = 2$ and seem to be sufficiently close to reality for both paths in this region of the ocean. The ration ρ_{ef}/ρ_0 and c_{ef}/c_0 considerably decrease with increasing frequency; evidently, it is caused by the influence on reflection of higher-frequency sound of less deep layers of sediment thickness, on the average, with smaller c_{ef} and ρ_{ef} (see [21]). Presented theoretical and experimental results are a proof for successful use of Doppler tomography combining aperture synthesis with Doppler effects, for determination of angular dependence of the bottom reflection coefficient, as well as of sound speed and density in sediments of deep-water ocean regions.

Now we proceed to demonstrate the possibility of applying the Doppler tomography method for investigation of patterns of angular dependence for acoustic signals scattered by an uneven bottom at various distances between corresponding points. We immediately pass to the analysis of the experimental data also obtained in a deep-water region of the Indian ocean with similar (see Fig.1a) dependence of the sound speed $c(z)$ on depth z (other experimental conditions are also identically) but with a considerably uneven bottom (see Fig.1b). Fig.5 shows the results of spectral analysis of the heterodined and filtered signal. The spectral density of signal power $W(\Delta f, r)$ presented by brightness form on the plane $(\Delta f - r)$; it is seen from the analysis that only two lines $\Delta f_0(r)$ and $\Delta f_1(r)$ are noticeably prominent. They correspond to "purely" water signals and the mirror component of the first bottom reflection easily discernible in the background of scattered components $\Delta f_s(r)$ on its both sides. Due to pronounced bottom roughness the analogous of $\Delta f_1(r)$ line corresponding to the signal of the second bottom reflection is hardly discernible in the distance range $r \geq 10$ km, being slightly higher than $\Delta f_1(r)$. Hence, one can expect the scattered field to be determined majorly by signals only once reflected by the ocean bottom.

Of the data presented in Fig.5, particularly interesting is considerable asymmetry in location of the components $\Delta f_s(r)$ in relation to $\Delta f_1(r)$. The range of their values is noticeably extended to the region $\Delta f_1(r) < \Delta f(r) < |\Delta f_1(r)|$ up to distances $r_1 \simeq 18 - 20$ km. To explain the revealed asymmetry in the behavior of dopplerograms $W(\Delta f, r)$ (of signals $\Delta f_s(r)$ scattered by the ocean bottom) we use easy representations of the ray theory. According to it,
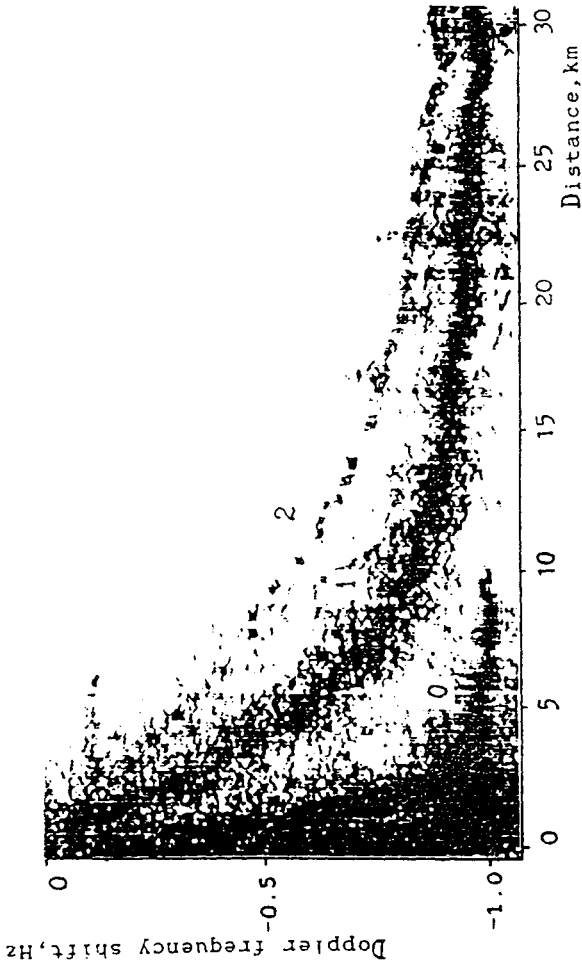
$$\Delta f_s = -f_0 \frac{v}{c(H)} \sin \Theta,$$
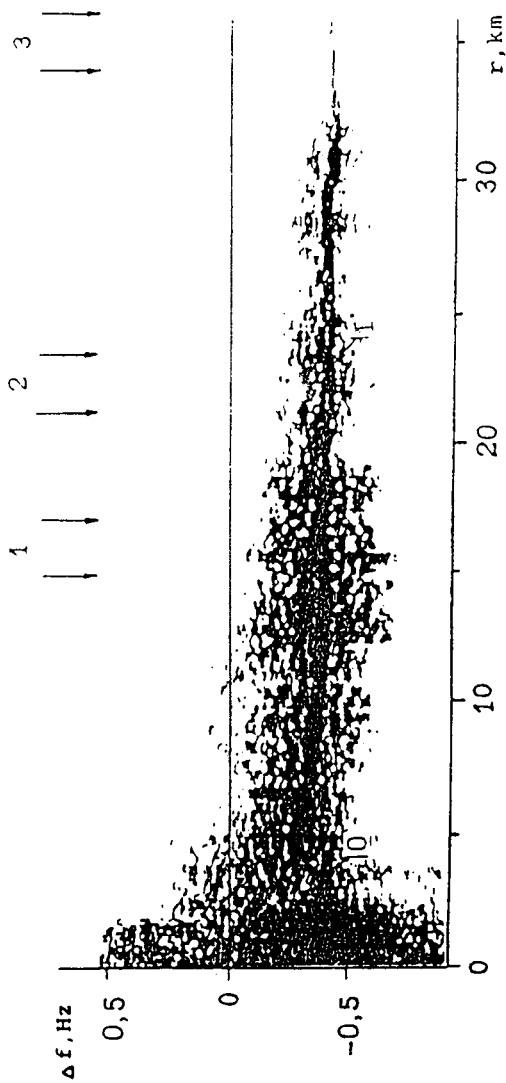
Fig. 5. Spectral density of acoustic signal power flow $W(\Delta f, r)$ presented by brightness form on the plane Doppler frequency shift - distance for radiation frequency $f_0 = 392$ Hz along the path with an uneven bottom (see Fig. 1b). Line 0 corresponds to water signals, line 1 - to mirror component of the first bottom reflection signal; on its both sides components corresponding to the scattered signals are shown. Vertical arrows show regions of r used to obtain mean values of $\bar{W}(\Delta f, r)$ presented in fig. 7.

where $\Theta = \arcsin\frac{c(H)\sin\Theta^{(0)}}{c(z_s)}$ is the angle at which signals come to the bottom, depending on the profile of sound speed $c(z)$, water layer depth H and outlet angle $\Theta^{(0)}$, which is positive when corresponding rays are directed into the backward (in relation to the emitter motion) hemisphere, and negative when they are directed into the forward hemisphere. For present values of $c(z)$, $H \simeq 3500$ m, z_s and z_r the bottom region insonified by the signals propagating along "purely" water rays is $0 \leq r \leq D(z_s, z_r)/2 \simeq 16$ km, i. e., half of the maximum length on the ray cycle $D(z_s, z_r)$. Scattered signals propagating along "purely" water rays at outlet angles $-\frac{\pi}{2} \leq \Theta_s^{(0)} \leq \frac{\pi}{2}$ from secondary sources placed at height $h = 2 - 200$ m over the average bottom depth $H = 3500$ m, come directly to the receiver if the distance to it is up to $r = D(H - h, z_r)/2 = 18 - 20$ km. Therefore, in the region $0 \leq r \leq D(H - h, z_r)$ the range $-\frac{v}{c(z_s)}f_0 \leq \Delta f_0 < \Delta f_1(r)$ becomes narrower with increasing r and if $r = D(H - h, z_r)/2$, its width is only 10% of its initial value when $r = 0$ (see Fig.6). Of course, the range $\Delta f_1(r) < \Delta f_s \leq 0$ becomes wider in the distance region $0 \leq r \leq D(H - h, z_r)/2$. If the range of positive $0 \leq \Delta f_s \leq \frac{v}{c(H)}f_0 \sin\Theta_b(r)$ when $0 \leq r \leq D(H - h, z_r)/2$ (here $\Theta_b(r)$ is the boundary angle at which signals come to the bottom, depending on the distance) is taken into consideration, then asymmetry in the location of $\Delta f_s(r)$ on the both sides of the mirror component $Delta f_1(r)$ must be more discernible in the distance region 4 km $\simeq [D(H - h, z_r) - D(z_s, z_r)]/2 \leq r \leq D(H - h, z_r)/2 \simeq 20$ km. It follows from the calculation results (see Fig.6) and is in good agreement with the experimental data (see Fig.5).

To obtain angular dependence of bottom-scattered signals it is quite sufficient to make spectral "sections" in the plane $\Delta f - r$ at certain values of r (see Fig.5). By this, to exclude possible non-informative fluctuations of the spectrum analysis results, it is of use to average $\bar{W}(\Delta f, r) = R^{-1} \int_r^{r+R} W(\Delta f, r)dr$ with respect to a certain region of distances R. At it follows from the results shown in Fig.7, asymmetry in the spectra of scattered signals is discernible only when $r < 20$ km. Besides, in the spectra of scattered signals, along with the absolute maximum $\Delta f(r) = \Delta f_1(r)$ which corresponds to the mirror component of the first bottom reflection, a relative maximum is easily discernible at the opposite in sing frequency Doppler shift $\Delta f(r) = |\Delta f_1(r)|$ when $r > 20$. Calculation show (see Fig.6) that this maximum corresponds to the backward-scattered signals produced when the signals of the first bottom reflection come to an uneven bottom at the angles close to $\Theta \simeq \arcsin\{|\Delta f_1(r)|/[v f_0/c(H)]\}$ and again reflected by
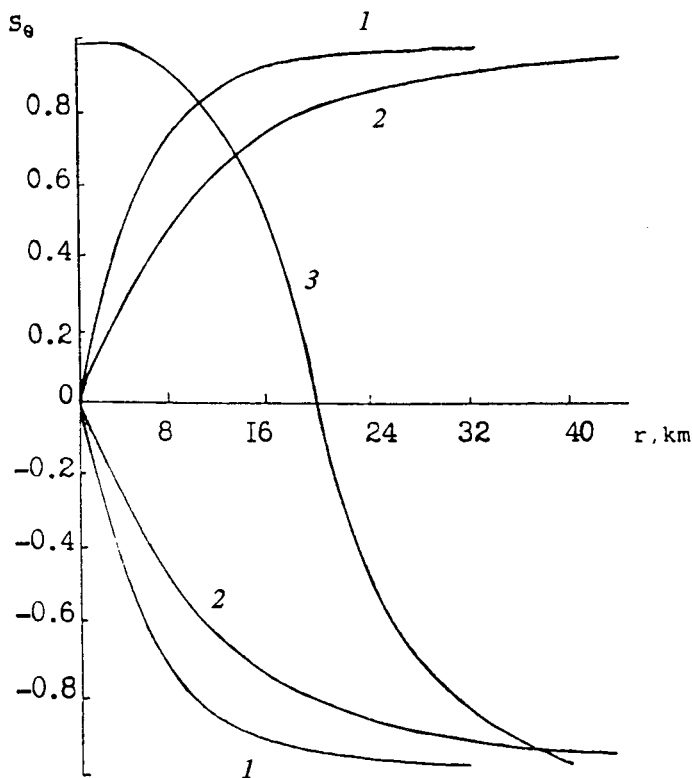
Fig. 6. Theoretical dependencies on distance r of $S_\Theta = \Delta f(r)c(H)/f_0 v = -\sin \Theta$ characterizing the angle Θ at which signals come to the bottom. Curves 1 and 2 correspond to mirror components of signals of the first ($m = 1$) and second ($m = 2$) bottom reflection; curves 1' and 2' - to components of corresponding backward-scattered signals; curve 3 shows the (left) boundary of observation region of scattered signals formed after the first bottom reflection and propagating towards the receiver along "purely" water rays with no secondary bottom reflections.
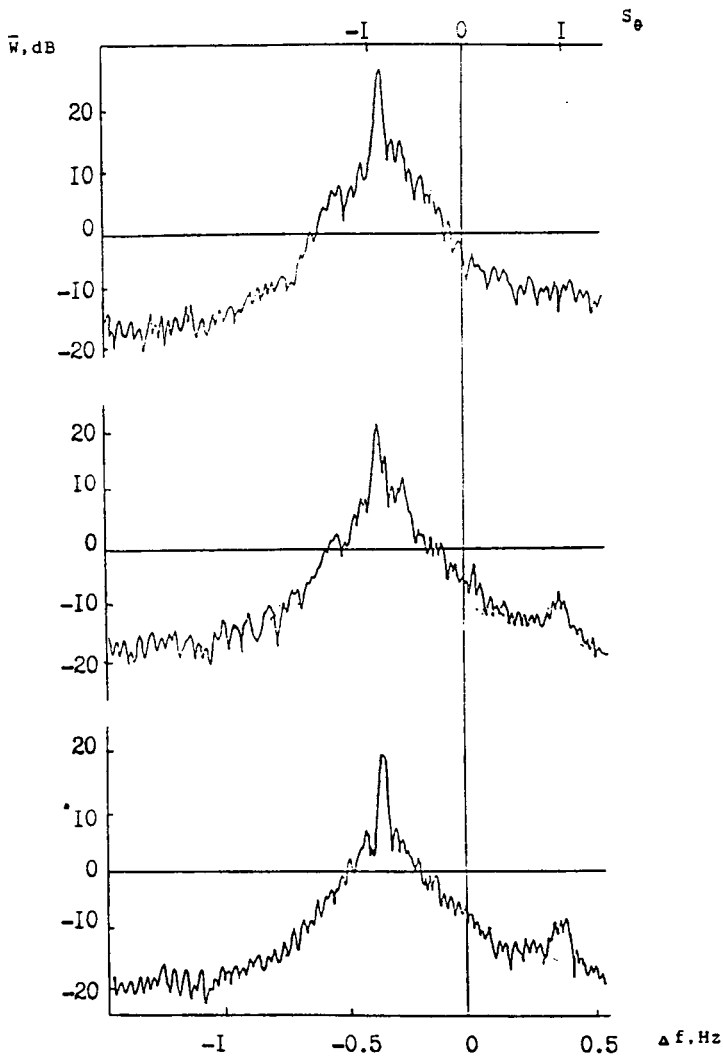
Fig. 7. Experimental dependencies of power flow spectral density $\bar{W}(\Delta f, r)$ of bottom-scattered acoustic signals on Doppler frequency shift Δf and value $S_\Theta = -\sin\Theta$ (Θ is the angle at which signals come to the bottom); when $r = 15$ km - (a), $r = 21.5$ km - (b), $r = 34.5$ km - (c); averaging scale of $R = 2$ km.

the bottom. Since, the maximum of $\bar{W}(\Delta f, r)$, when $\Delta f = |\Delta f_1(r)|$ is 30-35 dB lower than the basic maximum, i.e., when $\Delta f = \Delta f_1(r)$, the corresponding line in Fig.5 is not visible due to the narrow dynamic range of visualization; calculations show (see Fig.6) that in the region $0 \leq r \leq 12$ km the signals with $\Delta f = |\Delta f_1(r)|$ must be hidden by straight scattered signals propagating along "purely" water rays with no additional bottom reflection.

To obtain spatial (angular) dependence for the bottom-scattered signals produced when initial pressure waves come to the bottom at certain angle $\Theta = -\arcsin[\Delta f c(h)/f_0 v]$, it is sufficient to make a horizontal section of the dopplerogram in the plane $\Delta f - r$ (see Fig.5) for the given Δf. However, the dependencies $W(\Delta f, r)$ on r obtained for various Δf give no new information and are not presented here.

Thus, it was shown that the method of Doppler tomography allows us to study also angular dependence of an acoustic field scattered at a rough bottom. Besides, using this method we managed to reveal the effects which are of great interest to us. These effects are: at first, asymmetry in angular dependence of signals scattered at the bottom in a definite region of distances; this asymmetry can be explained by stratification of sound velocity affecting the wave propagation in a water layer. At second, existence of a maximum in the spectrum of a scattered field; this maximum corresponds to a backward-scattered signal.

REFERENCES

1. *Katrona L.J.* Radiolocation stations with aperture synthesis / Reference book on radiolocation/ Ed. by Skolnik M., Moscow, Sov.Radio 1977, v.2, p.337-362.

2. *Karavaev V.V., Sazonov V.V.* Basis of the synthesized antenna theory. Moscow, Sov.Radio 1974, p.168.

3. *Tomiyasu K.* Radiolocation stations with aperture synthesis and their application for ocean surface mapping. Methodological Review// IEEE. 1978.

4. *Muller R.K., Kaveh M., Wade J.* Reconstruction tomography and its application in ultrasonic technique.// IEEE. 1979, v.67, N.7, p.146-170.

5. *Burlakova I.B., Golubev V.N., Zharov A.I., Nechaev A.G, Petukhov Yu.V.,Slavinsky M.M.* Doppler tomography in ocean acoustic // Acoust.Journal, 1988, v.34, N4, p.756-758.

6. *Burlakova I.B., Petukhov Yu.V., Slavinsky M.M.* Determination of acoustic characteristics for oceanic waveguide bottom using Doppler tomography // Acoust. Journal 1989, v.35, N6, p.1015-1020.

7. *Burlakova I.B., Petukhov Yu. V., Slavinsky M.M.* Angular dependence of tonal acoustic signal scattered by the bottom in a deep-water oceanic waveguide // Preprint of the Gorky Radiophysical Research Institute 1990, N.305, p.11.

8. *Brekhovskikh L.M.* Waves in Laminar media. Moscow, Nauka, 1973. 343p.

9. *Golubev V.N., Orlov E.F., Petukhov Yu. V.* Spectral characteristics of pulse signals multiply scattered at a laminar bottom and oceanic surface // Acoust. Journal 1986, v.32, N.4. p. 462-467.

10. *Gamilton E.L.* Geoacoustic models of the sea bottom // Acoustics of sea depositions Ed. by Hampton L., Moscow, Mir. 1977, p. 176-210.

11. *Antakol'sky L.M., Volovov V.I.* On deteːrmination of reflection coefficient for low-frequency sound reflected at the shallow-water bottom// Acoust. Journal 1986, v.32, N.3, p.365-366.

12. *Munk W.H., Wunsch C.* Ocean acoustic tomography: rays and modes / Rev. Geophys. and Space Phys. 1983, v.21, N.4, p.777-793.

13. *Bracewell R.N.* Strip integration in radioastronomy // Aust. J. Phys. 1956,v.9, N.1, p.198-217.

14. *Ponsonbly J.E.B., Thomson J.H.* Two-dimension aperture synthesis in lunar radar astronomy // Proc. Roy. Soc. ser. A 1968, v.303,N.3, p.477-491.

15. *Williams R.* Creating an acoustic synthetic aperture in ocean // J. Acoust. Soc. Amer. 1976, v.60, N.1, p.60-73.

16. Comparison of sonar system performance achievable by more conventional means // J. Acoust. Soc. Amer

17. *Carey W., Jen N.-C.* Application of synthetic - aperture processing to toward-array data // J. Acoust. Soc. Amer. 1989, v.86,N.2, p.754-765.

18. *Fitzgerald R.M., Guthrie A.N., Nutile D.A., Shaffer J.D* Long-range low-frequency CW propagation in the deep ocean: Antigua - newfoundland // J. Acoust. Soc. Amer. 1974,v.56, N.1, p.58-69.

19. *Clark J.G., Flagan R.P., Weinberg N.L.* Multipath acoustic propagation with a moving source in a bounded deep ocean channel // J. Acoust. Soc. Amer. 1976,v.60, N.6, p.1274-1284.

20. *Hawker K.E.* A normal mode theory of acoustic Doppler affects in the oceanic waveguide // J. Acoust. Soc. Amer. 1979,v.65, N.3, p.675-681.

21. *Tucholke B.E.* Acoustic environment of the Hatteras and Nares Abyssal Plains, Western North Atlantic Ocean, determined from velocities and physical properties of sediment cores // J. Acoust. Soc. Amer. 1980,v.68, N.5, p.1376-1390.

ON CHOOSING PARAMETERS OF ACOUSTICAL IMAGING SYSTEMS IN INHOMOGENEOUS MEDIA

A.I. Khil'ko, I.P. Smirnov, A.Yu. Zorin

The direction of energetic coupling the source with the receiver in a homogeneous medium and the signal propagation time in this case are easily foretold. However, the energy propagates along the curve trajectories (rays) in smoothly inhomogeneous that, and, therefore, such predicting becomes more difficult. This fact is demonstrated by rays, forming coupling channels with the complex structure in natural waveguides (such as the ocean and the atmosphere). The complicate of the spatial structure of energy propagation channels display itself also in temporal characteristics of signals. The set of pulses is received after propagating through an inhomogeneous medium instead of the single one. It results from the difference of lengths of trajectories. Such pulses can be both selected and mixed, thus received signals, having the complex temporal distribution, are formed. Mentioned phenomena play a great role, if reconstructing parameters of inhomogeneities is dealt with. That is carried out, for instance, by tomogrphical monitoring systems in atmospherical and oceanic waveguides. The disposition of sources and receivers is determined by the comfort and the monitoring system embodiability. The problem of choosing this position becomes more difficult in weakly inhomogeneous medium of refractional type. The coupling channels have the complicated structure in this case, and positions of sources and receivers, viewing the given region, must be chosen with taking this fact in account. The shadow regions (both for the source and for the receiver), existing in the ocean really, give the good example,confirming this conclusion. The localized inhomogeneities, situated in such regions don't disturb received signals. Thus one can suppose, the field of view of an imaging system is nonuniform. Knowing the propagation path loss, characterizing atmospherical and oceanic waveguides permit to estimate the form of the field of view [6,7]. At the same time, the distribution of such loss, calculated for the source and for the receiver, must be combined, to receive the detailed information about that [8]. However, the difficulty of such estimation grows with increasing the number of devices, that takes place with developing tomographical viewing systems in atmospherical and oceanic waveguides [9-11]. It is still more difficult to describe the interconnection between the spatial structure of the field of view and the temporal structure of received signals [12,13].

The "differential" tomography, rejecting the disturbances, coming

into being due to non-stationarity and existence of random inhomogeneities, and "dark field" method for oceanic waveguides [14,16] use such estimations and co-processing responses of a few receivers and sources.

Discussing the development of acoustical imaging systems helps to word the problem of optimal choosing parameters of the ones. The smoothly-inhomogeneous waveguides are, for example, the geophysical, the planar ones, being dealt with in microwave technique. Note, the synthesis and the analysis of the field structure in the waveguide are equivalent to designing optimal configurations of emitting and receiving systems, focusing the energy at given region of the medium and picking out the algorithm of processing. It provides the good spatial resolution in the range of spatial parameters [17,18]. Such investigations are applied to viewing and tomographical systems, generally. It is profitable, to carry out viewing along the direction of transmitting, if the wave size of the inhomogeneities, situated in the refractional waveguide, is great. It is necessary to solve the internal diffraction problem for such inhomogeneity, placed in the inhomogeneous layered waveguide, in order to estimate possibilities of systems [21]. The best disposition of sources and receivers is searched, basing on received results.

Methods of optimal choosing parameters of acoustical imaging systems in refractional layered waveguides are suggested in this paper. In particular, some optimization problems are worded and classified. Solving the problem of scattering fields by inhomogeneities is discussed. The transferal characteristics of the inhomogeneous medium are defined and computing their spatial distributions is analyzed. The ones can be used as the prior information. The method and results of optimizing the model of the imaging system are presented. The limitations, the possible applications and the improvement of suggested methods are discussed in the conclusion.

1. SOLVING THE FIELD SCATTERING PROBLEM IN SMOOTHLY -INHOMOGENEOUS LAYERED WAVEGUIDES.

As it is noted above, the sensibility of the coupling channel structure concerning to variations of inhomogeneity parameters and the location should be estimated in order to analyze the efficiency of the acoustical imaging system. The spatial distribution of transferal characteristics can be used in this case. Different regions of the field of view are "tested" by means of the touch-body. The field calculation is made, basing on the geometrical theory of diffraction (GTD) [1-3].

Note briefly, that developed methods can be applied also with the mode approximation [3].

Let the point source S, the point receiver R and the hard localized inhomogeneity P (its size is less than the scale of the field variation) be placed in a smoothly-inhomogeneous medium. The total received field can be expressed in the follow way:

$$u = \sum A_{n_1} e^{ik S_{n_1}} + k^{-1} \sum \vec{A}_{n_2} e^{ik S_{n_2}} + (k^{-1})^2 [...] = u_0 + u_1 + ... \quad (1)$$

The first group of addenda u_0 describes the field as in the geometrical optics (A_n is the amplitude, S_n is the phase and k is the wave index). This group includes both the ordinary waves, propagating along the curve trajectories and the waves, reflected from the inhomogeneity. The second, u_1 describes diffractional amendments of the first degree concerning to k^{-1} . There are two subgroup in this group. The 1st describes the diffractional effects in the ordinary wave (the transverse amplitude diffusion, the diffraction at the bounds of the waveguide etc.). The 2nd is associated with the diffraction on the localized inhomogeneity and includes diffractional waves of different types [1-3].

1.1 The problem of aiming .

It is necessary to trace curve trajectories (rays) in order to calculate fields, mentioned above. Looking over all rays can be made, but this method is often unfit because it requires the great amount of the calculation for small inhomogeneity. Approximate estimations (confirmed by the practice) show, it grows proportionally to x/R where x is the length of the propagation route, R is the scale of the inhomogeneity.

Special methods of aiming are more effective in the case of small inhomogeneities. The one of these methods is described below. Outside of the inhomogeneity the ray submits to rules of geometrical optics (Fermat's principle). Thus the problem of aiming consists in selecting the pairs of rays, coupling points S and R with the point of the scatterer surface. These pairs must satisfy to conjugation conditions at given point of the surface. The ones are determined by the ray type.

The conjugation condition for the wave I (see Fig. 1), reflected from the inhomogeneity surface is:

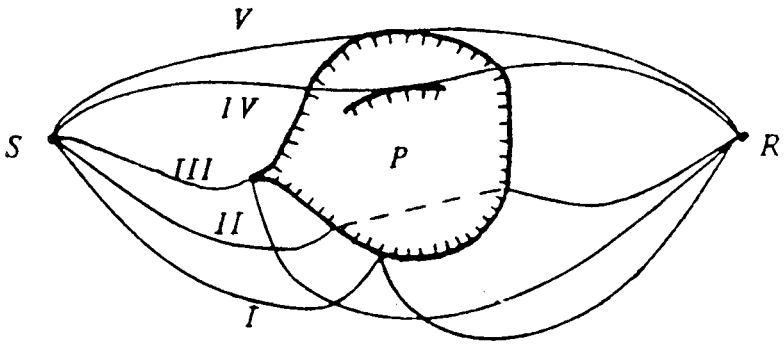$$\vec{N} = -\frac{(\vec{t}_S + \vec{t}_R)}{\sqrt{2\left(1 + <\vec{t}_S, \vec{t}_R>\right)}}, \quad (2)$$

Fig. 1. The disposition of the source S, the receiver R and the scatterer P. Rays, corresponding to reflected (I), refracted (II), diffractional (III, IV) and sliding (V) waves are shown.

where $\vec{t}_{S,R}$ are ray orts, drawn at the point of reflection, $\vec{N}$ is the external normal at this point, $< ., . >$ is the scalar product of vectors.

One-time refracted by the inhomogeneity wave is characterized by means of following set of conditions:

$$\vec{N}_1 = \frac{\frac{1}{n_1}\vec{t}_1 - \vec{\tau}_1}{\left\|\frac{1}{n_1}\vec{t}_1 - \vec{\tau}_1\right\|}, \vec{N}_2 = \frac{\frac{1}{n_2}\vec{t}_2 - \vec{\tau}_2}{\left\|\frac{1}{n_2}\vec{t}_2 - \vec{\tau}_2\right\|} \tag{3}$$

where $\vec{N}_{1,2}$ are external normals of the surface, $n_{1,2}$ are ratios of refractive indexes, calculated at the ray exit point.

And the ones for the wave III, coming into being at the edge L, are

$$< \vec{e}, \vec{t}_S > + < \vec{e}, \vec{t}_R >=< \vec{e}, \vec{t}_S + \vec{t}_R >= 0 \tag{4}$$

where $\vec{e}$ is the edge orth, drawn at the ray touching point.

Lastly, such conditions for the sliding wave IV, concerned with the diffraction on the surface of the smooth body, are expressed as follows:

$$< \vec{N}, \vec{t}_S >= 0 < \vec{N}, \vec{t}_R >\geq 0 < \vec{N}, \vec{t}_S, \vec{t}_R >= 0$$

where $\vec{N}$ is the external normal of the surface at the point of sliding, $< ., ., . >$ is the mixed product of vectors. The normal is easily found from this formula:

$$\vec{N} = \frac{-\vec{t}_S < \vec{t}_S, \vec{t}_R > +\vec{t}_R}{\left\|[\vec{t}_S, \vec{t}_R]\right\|}$$

One can draw the normal at the point of touching and limit the set of points of the surface, where the given wave can appear. It is possible, if ray orts $\vec{t}_{S,R}$ are known. In the case of the refracted wave II the normals $\vec{N}_{1,2}$ can be found from equations (3) after excluding unknown vectors $\vec{\tau}_{1,2}$. However, the supplementary information about the internal inhomogeneity structure is needed. The equation (4) limits the set of permissible edge orts $\vec{e}$ and, therefore, the set of points, where the wave III can be discovered. Analogously, the "sharp" points of the surface, where conjugation conditions are right, can be easily selected. Solving the problem can be accelerated essentially by means of confining the set of points, where the given wave appears. It is enough to aim at the suspicious point and check the necessary conditions for given pair of rays.

However, there is no universal algorithm of drawing orts of $\vec{t}_{S,R}$ at the point of touching for arbitrary inhomogeneous media and localized inhomogeneities. None the less, these orts can be approximated by the ones $\vec{t}_{S,R}^{\,*}$ of rays, connecting points S and R with fixed point P^* of the inhomogeneity. It is possible if the size of the inhomogeneity is essentially less, than the scale of variations of the field, produced by sources, placed to points S and R, near the inhomogeneity. (It is right for inhomogeneities, placed far from caustic surfaces and waveguide bounds) The details, concerned with limits of the application of mentioned approximation, are analyzed in [1,22]. However, the general way of reasoning doesn't change with taking these especialities in account. The procedure of aiming at the inhomogeneity can be summarized as follows: 1) tracing rays, coupling points S, R with P^* ; 2) drawing ray orts $\vec{t}_{S,R}^{\,*}$ at this point; 3) searching the approximated normal or $\vec{e}^{\,*}$ at the touching point, basing on $\vec{t}_{S,R}^{\,*}$; 4) selecting points of the surface with found normals; 5) aiming at selected points and checking necessary conditions for each pair of rays. The parameters of rays become the next approximation, if these conditions are done.

Aiming at points of the surface of the small ellipsoid is discussed below. It is supposed, the interior of that is acoustically homogeneous $n_1 = n_2 = n$, $\vec{\tau}_1 = -\vec{\tau}_2$. The central point of the ellipsoid, called P^*, is the zero of the cartesian coordinate system. Coordinates of a point of the ellipsoid are expressed by means of components of the normal $\vec{N}$, drawn at this point:

$$\vec{r} = \vec{g}\left(\vec{N}\right) = (a^2 N_x \vec{i} + b^2 N_y \vec{j} + c^2 N_z \vec{k})(a^2 N_x^2 + b^2 N_y^2 + c^2 N_z^2)^{-\frac{1}{2}},$$

where $\vec{i}, \vec{j}, \vec{k}$ are the orts of cartesian coordinate system, a, b, c are the half-sizes of the ellipsoid. The orts of rays, reaching the point P^* are called $\vec{t}_{S,R}^{\,*}$. One can find the point of the surface, where the reflected wave come into being, using the formula (2):

$$\vec{r}_0 \simeq \vec{g}\left(-\frac{(\vec{t}_S^{\,*} + \vec{t}_R^{\,*})}{\sqrt{2\left(1+ < \vec{t}_S^{\,*}, \vec{t}_R^{\,*} >\right)}}\right)$$

The sliding point of diffractional wave is (from (5)):

$$\vec{r}_s \simeq \vec{g}\left(-\frac{\vec{t}_R^{\,*} + \vec{t}_S^{\,*} < \vec{t}_S^{\,*}, \vec{t}_R^{\,*} >}{||\,[\vec{t}_S^{\,*}, \vec{t}_R^{\,*}]\,||}\right)$$

The point, corresponding to the refracted wave, is located, if the expression (3) is supplemented by the follow equation:

$$\vec{\tau} = \frac{\vec{g}\left(\vec{N}_2\right) - \vec{g}\left(\vec{N}_1\right)}{\left\|\vec{g}\left(\vec{N}_2\right) - \vec{g}\left(\vec{N}_1\right)\right\|} \equiv \vec{F}\left(\vec{N}_1, \vec{N}_2\right)$$

This equation shows, the orth $\vec{\tau}$ of the vector, connecting points of the surface, depends on normals $\vec{N}_1$, $\vec{N}_2$. Finally, we have the system of equations:

$$\vec{N}_1 \left\|\frac{1}{n}\vec{t}_S^{\,*} - \vec{F}\left(\vec{N}_1, \vec{N}_2\right)\right\| = \frac{1}{n}\vec{t}_S^{\,*} - \vec{F}\left(\vec{N}_1, \vec{N}_2\right)$$

$$\vec{N}_2 \left\|\frac{1}{n}\vec{t}_R^{\,*} - \vec{F}\left(\vec{N}_1, \vec{N}_2\right)\right\| = \frac{1}{n}\vec{t}_R^{\,*} - \vec{F}\left(\vec{N}_1, \vec{N}_2\right)$$

and can locate the ray exit points $\vec{r}_{1,2} \simeq \vec{g}\left(\vec{N}_{1,2}\right)$.

The numerical experiments were made for bilinear waveguide. They display the practical fit of discussed algorithm. The iterrative process converges with geometrical speed, if the searched ray exists. The algorithm becomes circular, if there is no solution. This fact is easily noted. The time gain of aiming is inversely proportional to the ellipsoid size.

1.2 Calculating field amplitudes.

The next stage of calculating the scattered field is searching amplitudes of waves, propagating along rays [24]. In accordance with GTD [1,2] these amplitudes can be found from formulae:

$$A_d = A_{ord}S\left(\vec{t}_S, \vec{t}_R\right) \frac{1}{\sqrt{|J|}}$$

where A_{ord} is the amplitude of the ordinary wave, J is the Jacobi's determinant of the transform, that is proportional to the area of the transverse section of the beam, bringing the field from the point of falling to the receiver, $S(.)$ is the diffractive index. The fields of reflected and refracted waves are expressed analogously.

Let's consider, for example, the smooth curve surface, placed in horizontally stratified inhomogeneous waveguide (Fig. 2) and calculate the intensity of the wave, reflected from this surface. It is supposed, the source S is situated at the zero of coordinate system. The ray coordinates are the azimuthal ϕ and polar θ angles of the ray
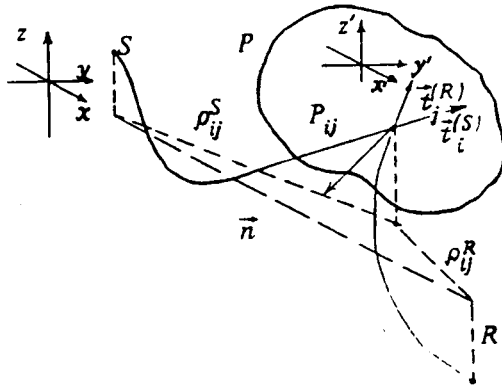
Fig. 2. Towards the calculation of fields, scattered by the curve surface.

orth and natural parameter l , being equal to the length, counted out along the ray to the current point $\vec{r}(\theta, \phi, l)$. This coordinate system is conformed with the form of the beam, but not with that of the surface. The function $\vec{R}(M, \vec{r}, l) \equiv (X, Y, Z)$, called the ray function, describes the trajectory, going out from the point $M(X, Y, Z)$ along the direction $\vec{r} = (\cos\beta\cos\gamma, \cos\beta\sin\gamma, \sin\beta)$. The derivative of this function must be calculated, to trace the beam:

$$\vec{R}'_l = \vec{t}, \ \ \vec{R}'_z = \left(\vec{k} - t_z\vec{t}\right)\left(\frac{\partial z^{(\rho)}}{\partial z} - 1\right)$$

(6)

$$\vec{R}'_\beta = \left(\vec{k} - t_z\vec{t}\right)\frac{\partial z^{(\rho)}}{\partial z}, \ \ \vec{R}'_\gamma = \rho\vec{e}_\gamma$$

where $\rho = \sqrt{x^2 + y^2}$ is the ray orth at the current point, $e_\gamma = \frac{1}{\rho}(-Y, X, 0)$ is the vector, being orthogonal to the ray plane, $z^{(\rho)}$ is the vertical coordinate of the point of ray, being on the surface $\rho = const$. Then the set of reflected rays is given by the formula:

$$\vec{r}(\theta,\phi,l) = \vec{R}(\theta,\phi) + \vec{R}(P(\theta,\phi),\vec{\tau}(\theta,\phi),l-l(\theta,\phi)) \qquad (7)$$

where $\vec{R}(\theta,\phi) = R(0,\vec{t}^0,l(\theta,\phi))$ is the radius-vector of the point $P(\theta,\phi)$ of the ray reflection from the surface.

Let the wave I be reflected from the surface and reach the receiver. Then the intensity of this wave is (W means th power of the point source):

$$I = |\Gamma|^2 \frac{W}{4\pi} \frac{t_1^0}{|D|}, D = \left\langle \vec{r}'_\theta, \vec{r}'_\phi, \vec{r}'_l \right\rangle \qquad (8)$$

where Γ is the Fresnel's coefficient at the reflection point . The expression of Jacobi's determinant follows from (7), (8) and has the form of the mixed product of vectors:

$$D = \left\langle \vec{r}'_\theta, \vec{r}'_\phi, \vec{r}'_l \right\rangle$$

$$\vec{r}'_\theta = \vec{f}_1 \frac{\partial z^{(\rho)}}{\partial z} + \vec{k}\left[f_{1z}\frac{\partial z^{(\rho_1)}}{\partial \theta}\left(\frac{\partial z^{(\rho_2)}}{\partial z}-1\right) + \frac{\partial z^{(\rho_2)}}{\partial \beta}\frac{\left\langle \vec{\tau}'_\theta, \vec{k}\right\rangle}{\vec{\tau}_1} \right] +$$

$$+ \rho_2 \vec{e}_\gamma \frac{\left\langle \vec{\tau}'_\theta, \vec{e}_\gamma \right\rangle}{\tau_\perp}$$

$$\vec{r}'_\phi = \rho_1 \vec{f}_2 + \vec{k}\left[f_{2z}\rho_1\left(\frac{\partial z^{(\rho_2)}}{\partial z}-1\right) + \frac{\partial z^{(\rho_2)}}{\partial \beta}\frac{\left\langle \vec{\tau}'_\phi, \vec{k}\right\rangle}{\vec{\tau}_\perp} \right] + \rho_2 \vec{e}_\gamma \frac{\left\langle \vec{\tau}'_\phi, \vec{e}_\gamma \right\rangle}{\tau_\perp}$$

$$\qquad (9)$$

$$\vec{r}'_l = \vec{T}$$

where

$$\vec{f}_1 = \vec{k} - \frac{n_z}{n_t}\vec{t},\ \vec{f}_2 = \vec{e}_\phi - \frac{n_\phi}{n_t}\vec{t}$$

are tangential orts of lines of the intersection of coordinate planes $\phi = C_1$, $\theta = C_2$ and the surface, drawn at the reflection point, $\vec{t}$, $\vec{\tau} = \vec{t} - 2n_t\vec{n}$ are orts of the ordinary ray and the reflected ray, accordingly. Basing on Weingarten's derivation formulae, one receives:

$$\frac{\partial \vec{n}}{\partial \theta} = k_{11}^* \vec{R}'_\theta + k_{12}^* \vec{R}'_\phi = k_{11}\vec{f}_1 + k_{12}\vec{f}_2,\ k_{11} = k_{11}^*\frac{\partial z^{(\rho_1)}}{\partial \theta},\ k_{12} = k_{12}^*\rho_1$$

$$\frac{\partial \vec{n}}{\partial \phi} = k_{21}^* \vec{R}_\theta' + k_{22}^* \vec{R}_\phi' = k_{21}\vec{f}_1 + k_{22}\vec{f}_2, \, k_{21} = k_{21}^* \frac{\partial z^{(\rho_1)}}{\partial \theta}, \; k_{22} = k_{22}^* \rho_1$$

Parameters k_{11}^* - k_{22}^* are expressed by means of coefficients of 1st and 2nd quadratic forms of the surface. Thus the derivatives, used in (9), are:

$$\vec{\tau}'_\theta = \mp \left(\frac{1}{t_1} - f_{1t}\frac{d}{dz}(\ln C)\frac{\partial z^{(\prime,\,\prime)}}{\partial \theta} \right) \left(\vec{f}_1 - f_{1t}\vec{\tau} \right) - 2(k_{11}\vec{m}_1 + k_{12}\vec{m}_2),$$

$$(10)$$

$$\vec{\tau}'_\phi = t_\perp \left(\vec{f}_2 - f_{2t}\vec{\tau} \right) + \rho_1 f_{2t}\left(f_{1t}\vec{\tau} - \vec{f}_1 \right)\frac{d}{dz}\ln C - 2(k_{21}\vec{m}_1 + k_{22}\vec{m}_2)$$

where $\vec{m}_1 = n_t\vec{f}_1 + f_{1t}\vec{n}$, $\vec{m}_2 = n_t\vec{f}_2 + f_{2t}\vec{n}$.

The needed intensity at the point of receiving can be found after inserting (10) to (8) and (9).

The general expression has the unwieldy form, that is why only the simplest examples are discussed below. á) Scattering by the azimuthally symmetrical surface (thorum) This surface is given by the equations: $F(\rho, z) = 0$, vectors $\vec{n}, \vec{t}, \vec{r}, \vec{T}$ are at the ray plane $\phi = const$, if reflecting from such surface takes place. Thus, vectors $\vec{f}_1$, $\vec{f}_2$ are oriented along main surface curvature directions, $k_{11}^* = -k_1$, $k_{12}^* = k_{21}^* = 0$, $k_{22}^* = -k_2 = n_\perp\rho_1^{-1}$, k_1 is the curvature of the normal surface section, made by the ray plane. Then, after inserting this expression in (8), that takes the following form:

$$I = |\Gamma|^2 \frac{W}{4\pi}\frac{t_\perp^0}{T_\perp}\frac{1}{\rho\left| \frac{\partial z^{(\rho)}}{\partial \theta} \right|}, \; \rho = \rho_1 + \rho_2$$

One can foretell this fact, taking the symmetry in account. On the other hand, there is the asymptotical with $k_1 \to \infty$ expression for the ray, having small sliding angle:

$$I = |\Gamma|^2 \frac{W}{8\pi}\left| \frac{\tau_n}{\tau_\perp} \right| f_1 f_2 \frac{1}{\rho_1\rho_2}\frac{1}{\rho|k_1|} \tag{11}$$

where

$$F_1 = \frac{c_S\rho_1}{c\left| \frac{\partial z^{(\rho_1)}}{\partial \theta} \right|}, \; F_2 = \frac{c\rho_2}{c_R\left| \frac{\partial z^{(\rho_2)}}{\partial \beta} \right|}$$

are factors of vertical focusing of rays, reaching the reflection point from points S and R. The intensity of the wave, falling on the surface, equals to $\frac{W}{4\pi}\frac{F_1}{\rho_1^2}$. The Jacobi's determinant of the transform equals to $\frac{\rho_2^2}{F_2}$ for the beam, connecting points R and P. (11) is presented as follows:

$$I = I_{ord}S^2\frac{1}{|J|}$$

where the multiplier

$$S^2 = \frac{1}{2}|\Gamma|^2\left|\frac{\tau_n}{\tau_\perp}\right|\frac{1}{\left(\rho_1^{-1}+\rho_2^{-1}\right)|k_1|} \tag{12}$$

is analogous to the diffractive index for the reflected wave (it is called the coefficient of the reflection from the curve surface).

b) Scattering by an arbitrary inhomogeneity in a homogeneous medium. One has in this case: $\frac{\partial z^{(\rho_2)}}{\partial z} = 1$ $\frac{\partial z^{(\rho_1)}}{\partial z} = \frac{\rho_1}{t_\perp^2}$ $\frac{\partial z^{(\rho_2)}}{\partial \beta} = \frac{\rho_2}{\tau_\perp^2}$ Then (8) can be written:

$$I = |\Gamma|^2\frac{W}{4\pi}\frac{1}{\left|(l_1+l_2)^2 + 2l_1 l_2(l_1+l_2)\left(\frac{k_1}{\tau_n}+k_2\tau_n\right)+4l_1^2 l_2^2 k\right|} \tag{13}$$

k_1 is the curvature of the normal surface section, made by plane, containing vectors $\vec{t}, \vec{\tau}$. k_2 is that of the section, made by the orthogonal plane, K is the Gaussian curvature of the surface, calculated at the reflection point. $l_{1,2}$ are lengths of segments $[SP]$ and $[RP]$, accordingly. The intensity of the falling field equals to $\frac{W}{4\pi}\frac{1}{l_1^2}$ and the Jacobi's determinant J equals to l_2^2. Then the coefficient of the reflection is:

$$S^2 = |\Gamma|^2\left|\left(l_1^{-1}+l_2^{-1}\right)^2 + 2\left(l_1^{-1}+l_2^{-1}\right)\left(\frac{k_1}{\tau_n}+k_2\tau_n\right)+4k\right|^{-1} \tag{14}$$

Note, that the formula (13) was written in the first time by Fock [1] for the intensity of the wave, reflected from the curve surface.

c) Reflecting from the surface, having the great curvature. There is asymptotical expression for the intensity of the received wave in a stratified medium with $k \to \infty$. The approximate equation follows from (8) and (10):
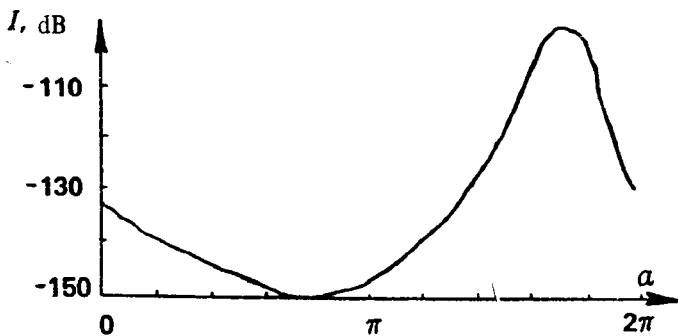
Fig. 3. The dependence of the intensity of the field, scattered by the ellipsoid, on the orientation of that. The source and the receiver are fixed. The bilinear waveguide is dealt with.

$$I \simeq |\Gamma|^2 \frac{W}{4\pi} \frac{F_1 F_2}{4\rho_1^2 \rho_2^2} \frac{1}{|k|} \qquad (15)$$

It shows, the asymptotical formula

$$S^2 \simeq \frac{|\Gamma|^2}{4|k|} \qquad (16)$$

is right for the coefficient of the reflection. The same expressions take place also for refracted waves [3,23]. Fig. 3 shows the dependence of the intensity of the scattered field on the orientation of the ellipsoid, placed into bilinear waveguide. (It is supposed, the source and the receiver are fixed). This figure illustrate the capacity for the work of suggested method.

The methods of calculating signals, scattered by touch-body are developed above for layered waveguides of refractional type. However, some details haven't been dealt with because of the limited size of the paper. They are, for instance, scattering by the body, placed near

to the waveguide bound, accurate calculating the field near caustics etc. But general conclusions don't change in this case. Received expressions optimize imaging systems with using transferal maps, computed on the basis of calculating fields, scattered by isotropical touch-bodies.

2. WORDING AND ANALYZING SOME PROBLEMS OF OPTIMAL CHOOSING PARAMETERS OF IMAGING SYSTEMS.

This section is devoted to the consideration of some optimization problems of acoustical imaging. Solving these problems, uses the maps of spatial distribution of transferal characteristics of the medium, such as EC and AC (see below). It should be noted, general wording, given below, doesn't exhaust all conceivable situations. The problems, concerned with temporal characteristics of signals, aren't dealt with in the matter, for example. Such temporal parameters are, for instance, mean time of reaching the receiver (MTR), the probability of "ordinary reaching" the receiver (POR), the probability of distinguishing the ordinary and scattered signals (PD) [8,12].

2.1 The total intensity of the reflected wave.

The total intensity of the wave, reflected from the localized inhomogeneity is expressed as follow:

$$ I(P, S, R) = \frac{W}{4\pi} \sum_{i,j} \frac{F_{ij}^{(1)} S_{ij} F_{ij}^{(2)}}{\left(\rho_{ij}^{(1)} \rho_{ij}^{(2)} \right)^2} \tag{17} $$

where incoherent summing the field over all rays, reaching the receiver after the reflection from the surface of the inhomogeneity is made. S_{ij} is the coefficient of the reflection, calculated at according point.

If the inhomogeneity has a small size, then $\rho_{ij}^{(1)} \simeq \rho_1$, $\rho_{ij}^{(2)} \simeq \rho_2$. Besides of that, the set of all rays, coupling the source S with the body surface, can be divided into a few classes of rays, not intersecting with each other. The class includes rays, differing unsignificantly. It comes into being as the result of splitting the ray, connecting S with the central point P^* of the body. The analogous dividing can be carried out for the receiver rays, Then, factors of focusing are: $F_{ij}^{(1)} \simeq F_i^{(1)}$, $F_{ij}^{(2)} \simeq F_i^{(2)}$. $F_i^{(2)}$, $F_i^{(2)}$ are parameters of "central" rays. Let the fixed coordinate system $X'Y'Z'$ be fastened with the body. n_1', n_2', n_3' are coordinates of the orth of this system. The function

$S(\vec{n}) = S(n'_1, n'_1, n'_1)$ characterizes the scattering surface. Its arguments are mentioned coordinates. (If there are a few points of the surface, where the normal equals to $\vec{n}$, then this function results from summing coefficients of the reflection over all such points). Inserting this function in (1), one can express the intensity (17) ($|\Gamma_{ij}| \equiv 1$). U is the unitary matrix of the transform the medium coordinate system XYZ to $X'Y'Z'$. Then

$$S_{ij} = S(U\vec{n}_{ij}), \quad \vec{n}_{ij} = \frac{\vec{t}_i^{(1)} + \vec{t}_j^{(2)}}{\sqrt{2\left(1 + \left\langle \vec{t}_i^{(1)}, \vec{t}_j^{(2)} \right\rangle\right)}},$$

$\vec{t}_i^{(1)}, \vec{t}_j^{(2)}$ are ray orts, drawn at the point of the reflection. Finally, the expression of the total intensity of the reflected wave is:

$$I = \frac{W}{4\pi} \frac{1}{\rho_1^2 \rho_1^2} \sum_\alpha F_\alpha S(U\vec{n}_\alpha), \qquad (18)$$

where $\alpha = (i, j)$, $F_\alpha = F_i^{(1)} F_j^{(2)}$

The intensity, determined by means of this formula, is the function of problem parameters:

$$I = I\left(\vec{R}_S, \vec{R}_R, \vec{R}_P, S(.), U\right),$$

$\vec{R}_{S,R,P}$ are radius-vectors of the source, the receiver, and the inhomogeneity, accordingly. $S(.)$ is the function, describing the orientation of the reflector. Let's consider some problems of optimal choosing mentioned parameters. It provides the maximality of the received intensity. The goals of the consideration are mathematical wording, classifying and analyzing these problems. The greatest attention is paid to factors, influencing on the solution essentially.

2.2 Choosing the optimal scatterer form.

It is supposed here, all parameters except the function $S(.)$ are given and fixed.

$$I = I(S(.)) \longrightarrow extr_{S(.)}$$

Obviously, the function $S(\vec{n})$ is easily expressed by means of that $f\left(U^{-1}\vec{n}\right)$. Thus the problem is equivalent to the following:

$$\sum_\alpha F_\alpha f(\vec{n}_\alpha) \longrightarrow extr_{f(.)\in F}$$

Here $\{F_\alpha, \vec{n}_\alpha\}$ is the given set of parameters, F is the class, containing functions, being permissible as solutions. This class should have quite many elements, to provide the existence of the solution, on other hand it should be hardly limited, to provide the physical realizability of the one. It should be also in accordance with limits, given by problem wording. The approximation (16) can be used to give wording of the problem. The one can be summarized as follows:

it is needed to find the smooth, convex, closed surface $\vec{r} = \vec{r}(u, v)$, maximizing the sum

$$\sum_\alpha F_\alpha |K_\alpha|^{-1}$$

K_α is the total curvature of the surface, calculated at the point where the external normal equals to $\vec{n}_\alpha$. It is supposed, the surface area is constant and ots curvature satisfies to the two-sided limitations: $0 < \delta_1 \leq K_\alpha \leq \delta_2$, $\delta_{1,2}$ are given values. This is the nonclassical problem of the calculus of variations (the optimal control problem). There is no prior information about points of the surface, where the reflection takes place. This especiality makes solving more difficult. General wording of the problem (for a plane) is:

$$\rho_1' = \rho_2$$

$$\rho_2' = \rho_1 + 2\rho_1^{-1}\rho_2^2 - \left(\rho_1^2 + \rho_2^2\right)^{\frac{3}{2}}\rho_1^{-1}u$$

$$\int_0^{2\pi} \sqrt{\rho_1^2 + \rho_2^2}\,d\phi = l$$

$$\rho_1 \cos\phi - \rho_2 \sin\phi - \left(\rho_1^2 + \rho_2^2\right)\cos\phi n_\alpha^{(1)} = 0, \ \phi = \phi_\alpha$$

$$\rho_2 \cos\phi - \rho_1 \sin\phi - \left(\rho_1^2 + \rho_2^2\right)\sin\phi n_\alpha^{(2)} = 0, \ \phi = \phi_\alpha$$

$$\rho_1(0) = \rho_1(2\pi), \ \rho_2(0) = \rho_2(2\pi)$$

$$\sum F_\alpha u^{-1}(\phi_\alpha) \longrightarrow extr$$

$$0 \leq \phi_\alpha < 2\pi, \ \alpha = 1..\alpha_0, \ 0 < \delta_1 \leq u \leq \delta_2, \ 0 \leq \phi < 2\pi$$

$\rho = \rho_1(\phi)$ is the equation, giving the scatterer bound (polar coordinates are used), $\{\vec{n}_\alpha^{(1)}, \vec{n}_\alpha^{(2)}\}$ is the set of normals, l is the bound length.

2.3 Optimal controlling the scatterer orientation.

This problem consists in choosing the unitary matrix U, that determines the orientation of the scatterer

$$I = I(U) \longrightarrow extr_{\{U\}}$$

This is the problem of mathematical programming. The orientation can be described by means of two scalar parameters t_1, t_2 (Euller's angles, for instance). The follow system of equations gives the necessary conditions of the extremum:

$$\frac{\partial I}{\partial t_1} = \sum_\alpha \langle U_1^*, \nabla S, F_\alpha \vec{n}_\alpha \rangle = 0$$

$$\frac{\partial I}{\partial t_2} = \sum_\alpha \langle U_2^*, \nabla S, F_\alpha \vec{n}_\alpha \rangle = 0$$

$U_{1,2} = \frac{\partial U}{\partial t_{1,2}}$ and $*$ means the transposing operation. Note, if the absolute value of the vector $\sum_\alpha F_\alpha \vec{n}_\alpha$ is small, (with given scatterer location), the gradient of the function

$$(\nabla I)_i = \sum_\alpha \langle U_i^*, \nabla S, F_\alpha \vec{n}_\alpha \rangle \simeq \left\langle U_i^*, \nabla S^*, \sum_\alpha F_\alpha \vec{n}_\alpha \right\rangle \simeq 0, \; i = 1, 2$$

is also small. (∇S^* is the value of that, calculated at an intermediate point). It means, the intensity (18) depends on the scatterer orientation unsignificantly. In the opposite case, if the value of the $\sum_\alpha F_\alpha \vec{n}_\alpha$ is great, the absolute value of the gradient depends on the orientation essentially, therefore, relative variations of the intensity are great with changing the scatterer one. Thus, the scalar parameter

$$\delta = \left| \frac{\sum_\alpha F_\alpha \vec{n}_\alpha}{\sum_\alpha F_\alpha} \right|$$

taking its values from segment [0,1], can be a measure depending of the intensity on the scatterer orientation. The more δ, the harder this dependence. The parameter δ, called the "Anisotropy Coefficient" (AC) [3] is determined by medium properties and not by the ones of the scatterer. It characterizes the nonuniformity of illuminating the reflector from different sides.

Let's consider choosing the parameter, defined above, more concretely. The spherical surface is illuminated from directions, giving by means of $\vec{n}_1, \vec{n}_2, .., \vec{n}_k$. The intensity of the flow, falling along the direction $\vec{n}_j$ is proportional to F_j. The illuminativity of the point is: $\Phi \left| \sum_\alpha F_\alpha \chi(< \vec{n}_\alpha, \vec{S} >) \right|$, here $\vec{s}$ is the external normal, drawn at this point, $|\chi(u)| \le |u|$ is given function. Therefore, $\Phi \le \sum F_\alpha$ and the relative illuminativity of the point of sphere $\vec{S}$ can be defined as follows:

$$\delta\Phi\left(\vec{S}\right) = \frac{\Phi\left(\vec{S}\right)}{\sum F_\alpha} = \left| \frac{\sum\limits_\alpha F_\alpha \chi\left(\left\langle \vec{n}_\alpha, \vec{S}\right\rangle\right)}{\sum\limits_\alpha F_\alpha} \right|$$

$\vec{n}_1, \vec{n}_2, ..., \vec{n}_k$ are direction of illuminating. The nonuniformity of the illuminativity is defined analogously:

$$\delta = max_{\vec{S}}\delta\Phi\left(\vec{S}\right) - min_{\vec{S}}\delta\Phi\left(\vec{S}\right) \qquad (20)$$

Then AC (19) follows from this expression with $\chi(u) = -u$. But it is more naturally to suppose, that $\chi(u) = -u1(u)$, where $1(u)$ is the indicative function of the negative half-axes. So, AC (19) equals to 0, if the sphere is illuminated from all sides and the flow intensity doesn't depend on the ones. However, (20) shows, δ decreases monotonously, if $N \to \infty$. This expression is in better accordance with realizing the nonuniformity of the illuminativity. The parameter (19) describes the situation rightly and is the most simple for calculation. Preliminary computing the distributions of transferal characteristics (such as AC) should be made before solving practical optimization problems. It is useful, for example, with optimizing the imaging systems in inhomogeneous media, and provides, in the first, the visible presentation of the properties of the waveguide. In the second, the maps of these distributions give the prior information for such solving.

Fig. 4 shows the spatial distribution of AC, computed for practically important case of the bilinear waveguide. The one has the follow profile of the sound velocity (z[km.]/c[km.p.s.]): (0.0/1.500), (-0.2/1.470), (-3.0/1.550). The source is situated at the depth of 200 m. the receiver- at the depth 200 m (fig. 4a, 4c), 2850 m (fig. 4b, 4d). The distance between the source and the receiver is 100 km. The maps have 16 grades of the brightness. The more AC value, the darker this point in the map. (The details of the structure of distributions of transferal characteristics for different inhomogeneous waveguides are analyzed in [3,12]).
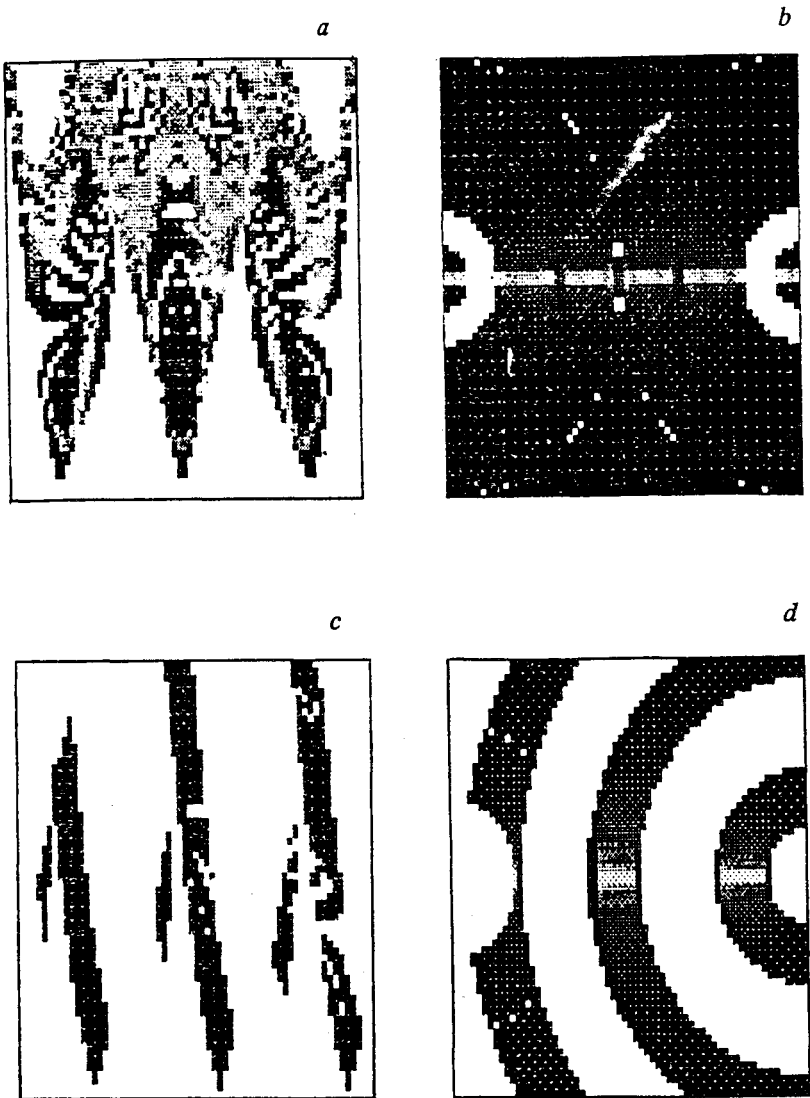
Fig. 4. The spatial distributions of the Anisotropy Coefficient at the vertical c) and the horizontal (b, d) plane. The bilinear waveguide is dealt with.

a

b

c

d
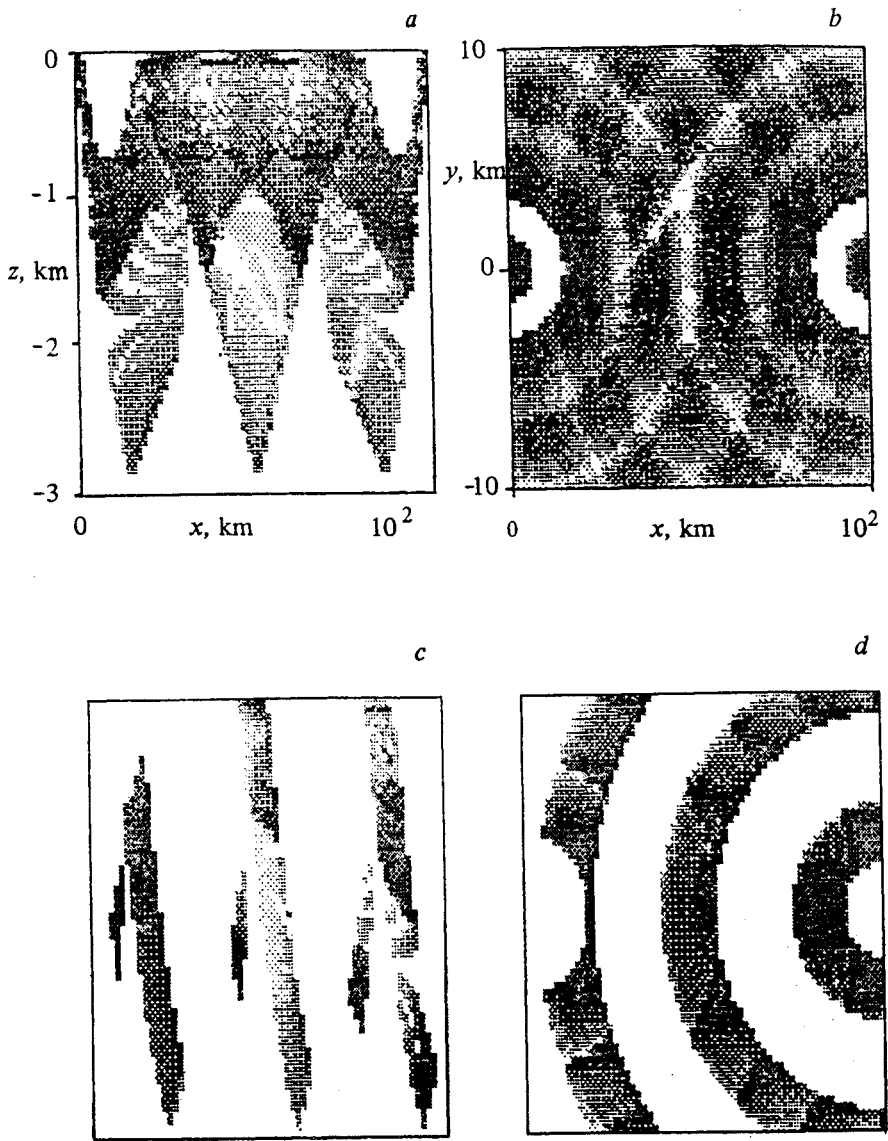
Fig. 5. The spatial distributions of Energetic Coupling.

2.4 Optimal disposing the reflector.

The problem is choosing the position of the scatterer in the region Ω:

$$I = I\left(\vec{R}_P\right) \longrightarrow extr_{P_0 \in \Omega}$$

If thee coefficient of the reflection is limited: , then the intensity is estimated:

$$I \leq \frac{W}{4\pi} S_0 \frac{1}{\rho_1^2 \rho_1^2} \sum_\alpha F_\alpha$$

The parameter $V(P)$

$$V(P) = \frac{1}{\rho_1^2 \rho_1^2} \sum_\alpha F_\alpha, \tag{21}$$

is determined by the medium properties. It characterizes the capacity of points of the region to transfer the energy, reflected from the inhomogeneity, placed at the one. The less V, the less this ability. This coefficient is called "Energetic Coupling" (EC) of points S and R "by means of" the point P, EC is proportional to the intensity of the wave, reflected from the sphere:

$$S = S_0, \ I = \frac{W}{4\pi} \frac{1}{\rho_1^2 \rho_1^2} \sum_\alpha F_\alpha S\left(U\vec{n}_\alpha\right) = \frac{W}{4\pi} S_0 V$$

Therefore, EC informs about the optimal position of symmetrical scatterer. However, if the scatterer isn't symmetrical, the great value of V doesn't provide the one of the received intensity. The supplementary guarantee is given by the uniformity of illuminating the reflector from different sides. It is characterized by δ, defined above. That is why, the scalar parameter $\gamma = V(1 - \delta)$ gives more detail information.

The coefficients δ, V and γ don't take the reflector properties in account. However, they can be used with solving an optimization problem. That is why, calculating the parameters δ, V of the medium is the desirable stage of this procedure.

Fig. 5 shows the maps of spatial distribution of EC for the same conditions, which take place for AC in fig. 4.

3. OPTIMIZING THE ACOUSTICAL IMAGING SYSTEM.

The model of the imaging system, dealt with in this section, consists of arrays of sources S_i, $i = 1..n$ and receivers R_j, $j = 1..m$ of acoustical waves, viewing the given region of the inhomogeneous medium.

The quality of viewing, carried out by the pair $P_{ij} = (S_i, R_j)$, can be characterized by the scalar parameter $\alpha_{ij} \geq 0$. Meaning of that is determined by the system functions. So, if the goal is locating the inhomogeneities, appearing in this region, the natural measure of the quality of viewing is the averaged coupling of points S_i, R_j of medium "by means of" the ones of given region

$$\alpha_{ij}^V = \int\limits_\Omega V(P) dP$$

where $V(P)$ is EC, calculated at the point P of the region.

The better characteristic of the quality is the parameter

$$\alpha_{ij}^D = \int\limits_\Omega D(P) dP$$

if the goal is locating the inhomogeneities, changing their orientation fastly. Here $D(P)$ is the "Anisotropy Coefficient".

The quality of viewing can be defined also on the basis of temporal parameters (the "Probability of Distinguishing the ordinary and the reflected pulse" (PD), the "Probability of Ordinary Reaching the receiver" (POR), etc.), if pulsed probing the medium is dealt with.

Besides of $\alpha_{ij} \geq 0$, giving the estimation of the quality of viewing, other parameters, characterizing sets of sources and receivers, should be used with problem wording. More concretely, let $\beta_i \geq 0$ be the cost of placing the source S_i at its position, $\gamma_i \geq 0$ be that for the receiver R_j. Let $\delta_{i'j'}^{ij}$, $(|i - i'| + |j - j'| > 0)$ be the cost of the noise immunity of the pair P_{ij}, concerning to other pairs $P_{i'j'}$.

Then the quality of imaging system is determined by follow:

$$Q = \sum_{i,j} \alpha_{ij} - \sum_i \beta_i - \sum_j \gamma_j - \sum_{i,j} \sum_{i',j'} \delta_{i',j'}^{i,j}, \ (|i' - i| + |j' - j| > 0)$$

One can deal with forming the system, having the maximal quality.

Some supplementary limitations are also conceivable. For example, the number of pairs can be limited and fixed, or the set of device positions can be confined. Therefore, the subsystem, having the maximal quality, must be chosen.

This is the problem of discrete mathematical programming. It has a solution (possibly, not single). That can be found by means looking over (sorting) all variants. But the number of the ones grows proportionally to 2^{n+m} with growing n and m. This fact makes the ordinary sorting unfit. Let's consider some methods of accelerated sorting. The ones require less amount of the calculation. Two algorithms, realizing alternative strategies, are suggested. They are "Excluding Groups" (EG) and "Sorting Groups" (SG). The co-operation of these algorithms is possible and gives quite good results. EG begins working and confines the set of permissible subsystems. If the solution is not reached, SG continues approaching to that. It is supposed below, sources and receivers don't interact with each other and $\delta_{i',j'}^{i,j} = 0$. Suggested methods of optimizing imaging systems and achieved results are discussed below.

3.1 EG algorithm.

Here $\alpha_{ij} \geq 0, \beta_i \geq 0, \gamma_j \geq 0, i = 1..n, j = 1..m$ are given values. The problem is to maximize the follow function Q. Its domain is the set Π of all non-empty subsegments I, J of segments $1..n, 1..m$, accordingly.

$$Q(I,J) = \sum_{i \in I} \sum_{j \in J} \alpha_{ij} - \sum_i \beta_i - \sum_j \gamma_j, \; I \subset 1..n, J \subset 1..m$$

In other words, the goal is to select the subgroup of rows (from n first, the last is included without fail) and the subgroup of columns (from m first, the last is included without fail) of the follow matrix:

$$\alpha_{11} \;\; \alpha_{12} \ldots \alpha_{1m} \; - \beta_1$$

$$\alpha_{12} \;\; \alpha_{22} \ldots \alpha_{2m} \; - \beta_2$$

$$\alpha_{11} \;\; \alpha_{12} \ldots \alpha_{1m} \; - \beta_1$$

$$-\gamma_1 \; - \gamma_2 \ldots - \gamma_m \; *$$

The sum of selected elements of submatrix must be maximal. Let I^* and J^* be optimal subsegments. Discussed method is based on the simple conclusion: the sum of elements of ith row is positive for any $i \in I$, if I^* includes more than 1 row. All rows, which don't satisfy to this rule, can be excluded from the original matrix. This procedure results in increasing the criterion function f. Obviously, the analogous conclusion is right for the subset of column numbers. Thus, the first stage of this algorithm can be summarized as follows: the input is the original matrix of maximal size. All rows, having the negative
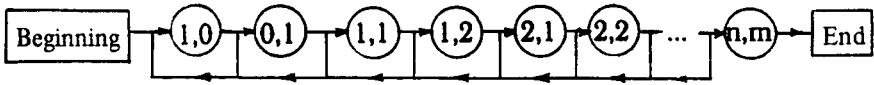
The EG algorithm scheme.

sum of elements, are excluded, because they aren't contained in the solution. This procedure is called "step $(1,0)$" or "$(1,0)$" briefly. After that, all columns, having the negative sum of elements, are excluded. This is "step $(0,1)$. If the last results in coming into being of the "negative" rows , the algorithm returns to step $(1,0)$. This stage is repeated, while the "negative" rows and columns appear. The next stage is called "step $(1,1)$". In this case one row and one column, having the negative common sum, are struck off simultaneously. The solution doesn't contain such combinations. Really, the common sum is negative, therefore, this row and this column must be excluded from the matrix. However, the own sum of the row is positive, because it was kept at previous stages. It means, the sum of the column without the element, belonging to this row, is negative, therefore, these elements must be excluded too. After this stage the "negative" rows and columns can come into being, the algorithm must return to step $(1,0)$. The combinations "one row-two columns", "two rows- one column","two rows- two columns", etc. are deleted at next stages.

Thus suggested algorithm is the sequence of stages (as it is shown below).

Returning to step $(1,0)$ takes place, if excluding rows and columns at the current step $(k,l), k \geq 0, l \geq 1$ is completed. The work is ended, if there are no striking off at any stage right up (n_1, m_1), where $n_1 + 1$, $m_1 + 1$ are achieved sizes of matrix (numbers of kept rows and columns). It is this submatrix, that is the solution of the problem. The needed number of operations depends hardly on the difference of the original matrix and the solution. The most unfavorable case is that of coinciding the ones. Then the amount of calculation of

EG algorithm equals to that of ordinary looking over. However, the number of operations becomes times as less with each excluding a row or a column. This fact results in essential increasing the speed of computation.

3.2 The SG method.

Here the alternative algorithm, called "Sorting Groups", is considered briefly. The process includes a kind of gradiental drawing near the solution. That increases the speed of computation essentially. The essence of the algorithm is summarized briefly below. At first the easier problem is dealt with. Let's fix the subset of rows $I = \{i_1, i_2, ..i_k\}$ of original matrix and consider submatrixes, formed by that and all possible subsets of columns $J = \{j_1, j_2, ..j_l\}$ (the subrow $-\beta_i, i \in I$ and the subcolumn $-\gamma_j, j \in J$ are taken into consideration, certainly). Then the submatrix, having the maximal quality, amongst described above, should be found. The columns, forming that, is united in subset J^*. Obviously, the quality of considered subsystems is written as follow:

$$Q(I, J) = \sum_{i \in I} \sum_{j \in J} \alpha_{ij} - \sum_{i \in I} \beta_i - \sum_{j \in J} \gamma_j = \sum_{j \in J} \left(\sum_{i \in I} \alpha_{ij} - \gamma_j \right) - \sum_{i \in I} \beta_i$$

And, defining

$$\delta_j(I) \equiv \left(\sum_{i \in I} \alpha_{ij} - \gamma_j \right)$$

$$Q_0(I) \equiv \sum_{i \in I} \beta_i = const \geq 0$$

one can receive:

$$Q(I, J) = \sum_{j \in J} \delta_j(I) - Q_0(I)$$

Searching the solution is based on the theorem, formulated below.

Let $I = \{i_1, i_2, .., i_l\}$, $k \in 1..n$, $I \subset I_0$, $I_0 \equiv 1..n$ be the fixed subset of rows, determining considered matrixes. Then the set of columns J^* of submatrix, having the maximal quality contains:

a) all columns, having positive value of $\delta_j(I)$ and only the ones, if such columns exist.

That is:

If $j^* \in J_0, J_0 \equiv 1..m : \delta_{j^*}(I) > 0$, then $J^* = \{j_1^*, j_2^*, ...j_p^*\} : \delta_{j_p^*}(I) > 0, \delta_j(I) \leq 0, \forall j \in J_0 - J^*$.

174

b) the single column, having the maximal value of $\delta_j(I)$, if the demand of the paragraph (a) is not fulfilled.

That is:

If $\forall j \in J_0 : \delta_j(I) \leq 0$, then $J^* = \{j^*\} : \delta_{j^*}(I) \geq \delta_j(I), \forall j \in J$

Then the solution of the original problem can be found in the follow way: the subsystem, having the maximal quality is searched for each possible subset I of rows, and "globally maximal" subsystem is picked out from these subsystems.

Estimating the speed of the computation (confirmed by practice) shows, that only $nm2^m$ machine's operations are needed in this case. If the FLOP duration is 20 μs (this value is real for i287 co-processor, for example) and n=m=10, then the computation time is easily evaluated. It is about 2-4 s. Note, that the ordinary looking over requires 3-4 min.

Co-operating of considered algorithms is desirable. The EG algorithm carries out fast decreasing the size of the matrix. It operates successfully, if the one contains the negative combinations of rows and columns. However, the SG algorithm is more effective, if there are no such combinations in the achieved matrix. Co-operating is carried out in the follow way: EG begins working. Let the negative combinations be absent at ith stage. The jump function $f(i, \tau_{next}, T_{SG})$ is calculated in this situation. Here τ_{next} is the summary duration of a few next stages of EG algorithm, T_{SG} is the time of processing achieved matrix by means of SG algorithm. The jump to SG takes place, if the function f is positive or zero: $f \geq 0$. The jump function can be, probably, defined in the follow way:

$$f(i, \tau_{next}, T_{SG}) = (\tau_{next} - T_{SG}) + \sigma(i, i_0)((T_{SG} - \tau_{next}) + \epsilon), \epsilon > 0$$

$$\sigma(i, i_0) = 0, \ i < i_0$$

$$\sigma(i, i_0) = 1, \ i \geq i_0$$

where i_0 is the bound step number, calculated with comparing productivities of algorithms.

Operating of optimizing algorithms and the computation of positions of 5 sources and 5 receivers for the bilinear waveguide with parameters, given above, and for the follow receiving region (x_0, x_1, z_0, z_1):(35 km., 38 km., -2.46 km.,-2.67 km.) are shown.

Fig. 6 shows the original sets (positions) of sources and receivers and the optimal sets of the ones. It is visible, the intensity of transferal coefficients is maximal in given region for the optimal configuration of system.
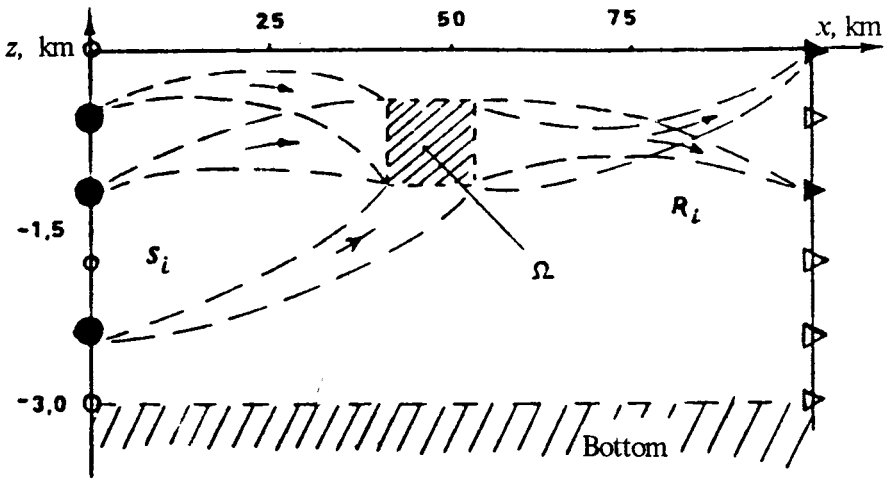
Fig. 6. The results of optimizing the hydroacoustical imaging system. Arrays consist of 5 sources and 5 receivers.

4. DISCUSSION AND CONCLUSIONS.

The principles of optimal choosing parameters of imaging systems are investigated. In particular, the transferal characteristics of the medium such as EC and AC have been defined and analyzed. These parameters were defined in the first time in the papers [3, 8, 12], the applying the ones for solving practical problems (forming acoustical imaging systems in inhomogeneous media, for example) were recommended. In this paper the maps of mentioned coefficients have been used for solving problem of optimizing the number and positions of elements of imaging systems. That provides the maximal sensitivity of the system. Note, that accurate defining the cost and analyzing limitations of these systems aren't dealt with.

The general scheme of wording, analyzing and solving the simplest problems was rather interesting for authors. This fact is concerned both with the weak masterativity of discussed problems and with the great amount of the computation, needed for solving the ones.

Some limitations of applying of methods, developed here, are:

1) The geometrical optics is used to calculate the transferal characteristics. This fact limits the field of applications of suggested methods. Only high frequency approximation is dealt with. However, both the mode approximation and the parabolic approximation can be used. The approximation is determined, certainly, by the comfort of calculating. Analyzing shows, the distributions of EC and AC become simpler in the case of the fields, having only a few modes, in the low frequency approximation [3].

2) Besides of transferal characteristics (EC and AC), considered above, other parameters (concerned with the temporal signal structure, in particular) should be put to the foundation of optimizing imaging systems in inhomogeneous media. Such coefficients ("Mean Time of Reaching the receiver" (MTR), the "Probability of Ordinary Reaching the receiver" (POR), the "Probability of Distinguishing the ordinary signal and the reflected one" (PD), etc.) were investigated in papers [8, 12]. First of all, basing on temporal characteristics is preferable with monitoring non-stationary objects or media. On the other hand, the problems of noise rejection becomes solvable with using such parameters. This noise can come into being due to fluctuations of the ordinary illuminating signal (the "dark field" method, developed for the inhomogeneous medium [9, 12]). One deals with optimizing acoustical imaging in this case, but the non-stationarity should be taken into consideration [25,26]. Note, that the geometrical dispersion has influence over temporal parameters (unlike EC and AC) at the low frequency approximation, that results in destroying the temporal pulse structure [27] and in being the optimal periods,

when viewing is the best.

3) The problem of acoustical imaging (like the problem of tomographical monitoring) is the inverse scattering problem. It is known, regularizing, basing on a prior information, can be needed for solving such problem. Optimizing positions of elements of the imaging system is on its essence the such procedure, because it excludes unsteady solutions. Analyzing these conclusions is interesting for authors and will be carried out in the future.

4) Incoherent summing fields was made. That permit us to avoid considering effects, concerning with the fine interferrential structure of the field in smoothly-inhomogeneous media. The possibility to apply this approximation depends on properties of real inhomogeneous media, such as atmospherical and oceanic waveguides. There are spatially distributed random inhomoogeneities in such waveguides. Therefore, it should be supposed the fields, propagating in the ones, are partially-coherent. The coherency is determined both the spatial and temporal spectra of random medium variations and the scale of the ones of smooth inhomogeneities [28]. Limitations of scale of the inhomogeneity are declared at this paper. Basing on this declaration and on results of experiments and computations, incoherent summing was suggested. It make the problem simpler. Mention must be made, coherent or partially-coherent summing doesn't change the general way of solving.

5) Let's consider briefly the problem, concerned with the matter. The viewed region (the resolution element of the field of view) was fixed with optimizing positions of sources and receivers. Thus, the optimal aperture for viewing given element of the field of view, was estimated. The optimal set of devices and the optimal aperture are changed with varying the region. Thus, the set of optimal apertures, corresponding to the set of elements of the field of view can be received after solving a few problems of optimizing. This set is a kind of generalized basis and permit to carry out spatial scanning the inhomogeneous medium. Each solution is the tomogrphical projection, like to that, being dealt with at differential monitoring [10].

6) Possible applications of received results can be briefly summarized as follows. First of all, they can be used with electromagnetic wave probing the atmosphere. The same problems are solved in seismic prospecting, in nondestructive monitoring, and tomography, in medicine.

REFERENCES.

1. *Kravtsov Yu.A., Orlov Yu.I.* Geometrical optics of inhomogeneous

media. Nauka, Moscow, 1980.

2. *Brekhovskikh L.M., Lysanov Yu.P.* Theoretical fundamentals of ocean acoustics. Gidrometeoizdat, Moscow, 1982.

3. *Zorin A.Yu., Smirnov I.P., Khil'ko A.I.* The characteristics of energetic coupling of the inhomogeneous medium points. Izv.VUZov - Radiofizika, 1993, v.16, No 5.

4. *Nechaev A.G., Khil'ko A.I.* Acoustic diffraction tomography of the ocean. Proc. of the Int. Scien. School-Seminar "Dynamic and stochastic wave phenomena". Nizhny Novgorod: UNN, 1992, p. 177-188.

5. *Borodina E.L., Gorskaya N.V., Gorsky S.M., et al.* The image spatial filtering for ultrasonic visualization of large inhomogeneities. Akustichesky Zhurnal, 1992, v.38, No 6.

6. *Borodina E.L., Khil'ko A.I., Shirokov V.N.* The peculiarities of excitation of shallow waveguide from air. Akustichesky Zhurnal, 1992, v.38.

7. *Borodina E.L., Khil'ko A.I., Shirokov V.N.* Formation of acoustic fields by modes as well as by shear and side waves in small-mode stratified inhomogeneous ocean waveguides. In book: "The Formation of acoustic Fields in Oceanic Waveguides". Nizhny Novgorod: IAP RAS, 1991, pp. 66-82.

8. *Smirnov I.P., Zorin A.Yu., Khil'ko A.I.* The characteristics of energetic coupling of the inhomogeneous medium points. Proc. of the Int. Scien. School-Seminar "Dynamic and stochastic wave phenomena". Nizhny Novgorod: UNN, 1992, pp. 51-52.

9. *Borodina E.L., Gorskaya N.V., Gorsky S.M. et.al.* The potential of shadow methods for study of diffracted sound fields in waveguides. In book: "The Formation of acoustic Fields in Oceanic Waveguides". Nizhny Novgorod: IAP RAS, 1991, pp.174-199.

10. *Nechaev A.G., Khil'ko A.I.* The reconstruction of ocean inhomogeneities along acoustic path by differential diagnostics method. Proc. of IAP RAS N 178, Nizhny Novgorod, 1987, 23 p.

11. *Nechaev A.G., Khil'ko A.I.* The waveguide inhomogeneity diagnostics by ** of pulse signal intensity. Izv.VUZov - Radiofizika, 1991, v.33, No 1., pp. 65-71.

12. *Zorin A.Yu., Smirnov I.P., Khil'ko A.I.* The temporal characteristics of coupling channels of source and receiver in inhomogeneous medium. Izv.VUZov - Radiofizika, 1993, v.16, No 12.

13. *Zorin A.Yu., Smirnov I.P., Khil'ko A.I.* The noise suppression by screens in inhomogeneous medium. Collected Papers of the I Session of Russian Acoustic Society. Moscow: OI, 1992.

14. *aya N.V., Zverev V.A., Nicolaev G.N., et al.* About the reconstruction of spatial localization of secondary hydroacoustic sources. Collected Papers of IX Acoustic Conference. Moscow: OI, 1991, sec. T.

15. *Khil'ko A.I., Shirokov V.N.* The use of mode shadow for acoustic tomography of ice in shallow sea. Collected Papers of V Symposium on

Numerical Tomography. Moscow: VNIIFTRII, 1991, pp. 217-218.

16. *Nechayev A.G., Khil'ko I.A.* Differential acoustic diagnostics of random inhomogenieties in the ocean. Acustichesky Zhurnal, v.34, No 2, pp.285-289.

17. *Gorodetskaya E.Yu., Malehanov A.I., Talanov V.I., Fiks I.Sh.* Synthesis and analysis of acoustic field in the ocean. In book: "The Formation of acoustic Fields in Oceanic Waveguides". Nizhny Novgorod: IAP RAS, 1991, pp. 9-32.

18. *Danilov V.Ya., Kravtsov Yu.A., Nakonechnyi A.G.* Mathematical methods of controlling hydroacoustic fields. In book: "The Formation of acoustic Fields in Oceanic Waveguides". Nizhny Novgorod: IAP RAS, 1991, pp. 32-55.

19. *Gorskaya N.V., Gorsky S.M., Zverev V.A. et.al.* Features of short-wave diffraction of sound in multimode layered-inhomogeneous waveguides. Ocean Acoustics (in Russian). Ed. I.B.Andreyeva and L.M. Brekhovskikh. Nauka, Moscow, 1991, pp.175-189.

20. *Nechaev A.G., Khil'ko I.A.* Definition of the local characteristics of oceanic inhomogeneities distributed, along the acoustic path. Akustickesky Zhrnal, 1988, v.34, No 4, pp.694-699.

21. *Gorskaya N.V., Gorsky S.M., Zverev V.A. et.al.* Short-wave diffraction in a multi-mode layered waveguide. Akustichesky Zhurnal, 1988, v.34, No 1, pp.55-59.

22. *Zhidko Yu.M.* The scattering of electromagnetic waves by ideally reflecting bodies placed in inhomogeneous medium. Izv.VUZov - Radiofizika, 1969, v.12, No 8, 1205 p.

23. *Smirnov I.P., Khil'ko A.I.* About "aim problem" in the problem of sound field calculation in inhomogeneous medium with localized inhomogeneities. Vesti KPI. Electroacoustics and sound-techniques. 1992, issue 16, pp. 9-12.

24. *Smirnov I.P., Khil'ko A.I.* Structure of high frequency acoustic fields in stratified inhomogeneous medium with curvilinear surfaces. Vesti KPI. Electroacoustics and sound-techniques. 1992, issue 16, pp. 9-12.

25. *Karetnikova I.R., Nechaev A.G., Khil'ko A.I.* The features of diagnostics of waveguide random inhomogeneities changing in time by using complex pulse signals. Izv.VUZov - Radiofizika, 1990, v.13, No 12, pp. 1370-1378.

26. *Gorskaya N.V., Gorsky S.M., Gurbatov S.N. et.al.* Investigation of the possibility of using frequency- modulated waves for study of scattering in irregular waveguides. Akustichesky Zhurnal, 1991, v.37, No 5, pp.914-921.

27. *Petuhov Yu.V., Khil'ko A.I.* The estimation of seismoacoustic source sizes in layered-inhomogeneous medium. Proc. of NIRFI N 352, Nizhny Novgorod, 1992, 42 p.

28. The sound propagation in fluctuating ocean. Ed. by S. Flate. Moscow: MIR, 1982.

THE NEAR–FIELD ACOUSTIC MEASUREMENTS

I.Sh.Fiks, V.I.Turchin

1. Introduction

The technique of the near-field measurements is used widthly nowadays for the testing and control the microwave antennas. Since 70–th years the methods of the far-field and aperture field determining from electromagnetic field measured near the antenna have been developed and the detail analysis of method's possibilities and errors has been executed [1-3]. Last time the near-field technique was used in the acoustic measurements [4-9], in which its advantages (a possibility to measure with small values of radiated power, a decreasing of reverberation influence) are more important than in the microwave measurements.

The main area of the near-field method applications may be offer in the diagnostics of the moving broad-band sound sources: transport, ships, etc. The final purpose of the diagnostics is the far-field reconstruction for the correct sound levels determining and the reconstruction of elementary sources (monopoles, dipoles) distribution along the radiator - so-called acoustic imaging of radiator as well as in microwave technique.

The development of the near-field technique in acoustics must consist in the following.

In the majority of cases we must operate with the random broad-band acoustic signals, which sources are the noises of mechanisms, streaming etc. So, the procedure of the far-field reconstruction or the acoustic imaging must combine with the estimation of the frequency spectra. A multielement antenna array must be used for the signal receiving, unlike the situation when the radiator exites by the known signal, and the receiving may perform by single receiver which is moving along the radiator [1].

Then, in most of the practically important cases the size of a radiator along one coordinate excels the other sizes strongly (for example, a vessel building). In this case the linear antenna array can be used for the measurements. The far-field reconstruction algorythms and the imaging algorythms are changing correspondingly (generally, this case will be consider below).

---

[1] Usually the measurements by the moving probe are used in the microwave technique.

The results of a radiator movement relative the receiving antenna give two effects. Firstly, it is the complicated transformation of the frequency spectra if the movement is fast. Secondly, it is the changing of the visual angle at wich the radiator is observed from the center of the receiving antenna. The first effect must be taken into account in reconstruction algorythms or for its neglecting the above limitations of the radiator velocity must be formulated. The second effect is very important for the spectral estimation forming of the far field or acoustical image for all radiator trajectory because the resolution interval is changed in the process of radiator movement.

In this paper, at first, the signal processing algorythms are developed using the integral transform technique. This approach (as it will be shown below) allows to analyze the possibilities of the near-field method for the moving broad-band radiators very effectively.

2. Integral transform method: theoretical concept.

We assume that the initial result of near–field measurements is a set of momentary values of the pressure $\{p_n(t)\}$, measured by sensors with numbers $n = 1, ... N_a$. The sensors are placed at the points with coordinates denoted by the vectors $\vec{r_{n,s}}$ The configuration of the sensor disposition has such a form that the surface S stretched on the points $\vec{r_{n,s}}$ surrounds the investigated broad-band radiator or closes at infinity (see Fig. 1).

If the distance between sensors is small enough, we can consider the measurement results as a function of continuous coordinates $\vec{r_s}$ on the surface S: $\{p_n(t)\} \to p(t, \vec{r_s})$. Let us assume that the radiator is fixed relative to sensors and surrounding medium is homogeneous free space.

The $p(t, \vec{r_s})$ transformation into the designed characteristics can be made in time domain or in frequency domain after Fourier transformation of $p(t, \vec{r_s})$ into spectral components $p(f, \vec{r_s})$:

$$p(f, \vec{r_s}) = \int_{-\infty}^{+\infty} p(t, \vec{r_s}) e^{2\pi i f t} dt \tag{1}$$

At the beginning we consider the transformation in frequency domain. The method of the $p(f, \vec{r_s})$ decomposition by a complete set of the partial solutions of the homogeneous equation orthogonal on the surface S with the compensation of probe direction pattern [3]
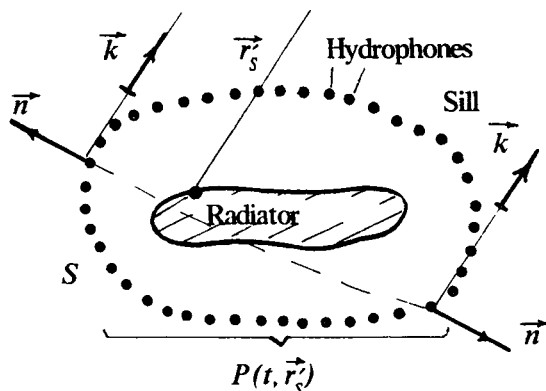
Fig. 1 The disposition of the radiator and the receiving elements (hydrophones). The surface S is stretched on the receiving elements, the vector $\vec{n}$ denotes the normal to the surface, the unit vector $\vec{k}$ shows the current direction in the far-field zone, the dashed line separates the "illuminated" part S_{ill} of the surface. The vector $\vec{r_s}$ denotes the point of the stationary phase corresponded to the given vector $\vec{k}$ and any point on the radiator.

and the integral transformation method using, in particular, a surface Green's function [2] have been well devised for the diagnostics of the microwave antennas. These methods are broadly used for the $p(f, \vec{r_s})$ transformation into far-field. Both methods generalized for acoustic problems give identical result in many acoustic cases because the sensor direction pattern can be considered as isotropic. Below we shall mainly use the technique of the integral transformations.

If the spectral component of pressure $p(f, \vec{r_s})$ is known on the surface S, the spectral component $p(f, \vec{r})$ at an arbitrary point $\vec{r}$ outside the surface S is given by the integral transformation:

$$p(f, \vec{r}) = \int \int_S p(f, \vec{r_s}) \Gamma_f(\vec{r}, \vec{r_s}) dS \qquad (2)$$

where Γ_f is so-called surface Green's function (see, for instance, Ref. [2]). For the reconstruction of far field we denote $\vec{r} = \left| \vec{r} \right| \vec{k} = r \vec{k}$, where $\vec{k}$ is an unit vector ($\left| \vec{k} \right| = 1$) defining the orientation of the observation point in far zone when $r \to \infty$. So,

$$p(f, \vec{r}) \to R_f(\vec{k}) \frac{e^{ik_o r}}{r},$$

183

where $R_f(k)$ is a direction pattern of radiator for frequency $f, k_o = 2\pi\frac{f}{c}$, c is a sound velocity. Thus, we obtain:

$$R_f(\vec{k}) = \int\int_S p(f, \vec{r_s})\gamma_f(\vec{k}, \vec{r_s})dS \qquad (3)$$

where $\gamma_f(\vec{k}, \vec{r_s}) = \lim_{r\to\infty}(re^{-ik_o r}\Gamma_f(\vec{k}r, \vec{r_s}))$

The kernel of the transformation (3) γ_f can be constructed as the decomposition by the complete set of functions which are partial solutions of the homogeneous Helmholtz equation for the plane, cylindrical or spherical surface S (see Ref. [3]).

For the plane surface we have:

$$\gamma_f(\vec{k}, \vec{r_s}) = -i\frac{\left(\vec{n}, \vec{k}\right)}{\lambda}e^{-ik_o\left(\vec{k}, \vec{r_s}\right)}, \qquad (4)$$

where $\vec{n}$ is a normal vector to the surface $S, \lambda = c/f$ is a wave length.

For the cylindrical surface of radius a this function is:

$$\gamma_f(\vartheta, \varphi, x_s, \varphi_s) = \frac{e^{-ik_o x_s \sin\vartheta}}{2i\pi^2 a} \sum_{n=-\infty}^{\infty} \frac{e^{-in(\varphi-\varphi_s-0,5\pi)}}{H_n^{(1)}(\omega)},$$

$$\omega = k_o a\cos\vartheta \qquad (5)$$

where x_s, φ_s are the current coordinates of the point on a cylinder, the angle φ_s defined in a plane perpendicular to the cylinder axis, x_s is an coordinate along the cylinder axis, $dS = ad\varphi_s dx_s$. Angles ϑ, φ are angles of far-field observation point. The angle φ is defined the same way as the angle φ_s, ϑ is an angle between the vector $\vec{k}$ and the plane perpendicular to the cylinder axis. $H_n^{(1)}$ is the Hankel's function of the first kind and order n.

For an arbitrary smooth surface S the function γ_f is a result of the solution of the following integral equation:

$$e^{ik_o(\vec{k}, \vec{r_s})} = k_o\frac{\partial}{\partial n}\int\int_S \gamma_f(\vec{k}, \vec{r_s})\frac{e^{ik_o\left|\vec{r_s}-\vec{r_s'}\right|}}{\left|\vec{r_s}-\vec{r_s'}\right|}dS', \qquad (6)$$

where $\frac{\partial}{\partial n}$ is a derivation along normal to the surface S.

If the curvative radius of the surface S is much more than the wave length, we can use a high frequency approximation of the solution of

184

equation (6):

$$\gamma_f(\vec{k},\vec{r_s}) \to \gamma_f^{(HF)}(\vec{k},\vec{r_s}) = \begin{cases} -i\dfrac{\left(\vec{n},\vec{k}\right)}{\lambda} e^{-ik_o\left(\vec{k},\vec{r_s}\right)}, & \vec{r_s} \in S_{ill} \\ 0 & \vec{r_s} \in S_{shade} \end{cases}$$

(7)

where S_{ill} is the part of the surface S with a bound determined by the equation $\left(\vec{n},\vec{k}\right) = 0$ (Fig. 1), S_{shade} is an additional part to the surface S_{ill}. The estimate of the limits of the applicability of expression (7) have been given in Ref. [2].

We would like to notice that the procedure (3) using (4)-(5) is accurate and doesn't depend on the radiator disposition inside the area bounded by the surface S, on the radiator sizes and the type of elementary sources (monopoles, dipoles, etc.) describing the radiator.

However, other way is possible too [7]. In this case the radiator field is wholly determined by some a priori unknown function of the distribution of the elementary sources of the given type $m_f(\vec{r})$ (for instance, monopoles) concentrated on the given finite surface S_r (see Fig. 1), where $\vec{r}$ is a position-vector of current point on the surface S_r. All elements of the surface S_r lie inside the volume bounded by the surface S. In this case we have:

$$p(f,\vec{r_s}) = \int\int_{S_r} m_f(\vec{r}) \frac{e^{ik_o|\vec{r_s}-\vec{r}|}}{|\vec{r_s}-\vec{r}|} dS_r,$$

(8)

$$R_f\left(\vec{k}\right) = \int\int_{S_r} m_f(\vec{r}) e^{ik_o\left(\vec{k},\vec{r}\right)} dS_r$$

(9)

Substituting (8) and (9) in (3), we can obtain that the function γ_f must satisfy to the following integral equation:

$$e^{-ik_o\left(\vec{k},\vec{r}\right)} = \int\int_{S_r} \gamma_f\left(\vec{k},\vec{r_s}\right) \frac{e^{ik_o|\vec{r_s}-\vec{r}|}}{|\vec{r_s}-\vec{r}|} dS,$$

(10)

where $\vec{r} \in S_r$ and any unit vector $\vec{k}$ which is a parameter in equation (10). For instance, if S and S_r are two parallel planes, it can be shown that the solutions of the equations (6) and (10) are the same for coinciding coordinate axes of the vectors $\vec{r_s}$ and $\vec{r}$.

In the real situation the sensors can be disposed on the finite part of the surface S forming the receiving aperture S_a of finite sizes. The

correspondence among the receiving aperture sizes S_a, the radiator sizes S_r and the set of unit vectors $\vec{k}$ in the far zone where the far field can be correctly reconstructed for any distribution of $m_f(\vec{r})$ can be obtained from equation (10). Substituting (7) in (10), we can show that the main term of the asymptotical decomposition of integral (10) relative to a large parameter k_o (this term is defined by a point of the stationary phase $\vec{r_s}$ of the integral) coincides with the left side of expression (10). Thus, the point of the stationary phase must belong to the receiving aperture S_a: $\vec{r_s} \in S_a$. The location of the point $\vec{r_s}$ is deduced from simple geometrical construction. The point $\vec{r_s}$ is a point of the intersection of the surface S and a ray from the current point $\vec{r}$ in the direction $\vec{k}$ (see Fig. 1):

$$\vec{r_s} - \vec{r} = \left| \vec{r_s} - \vec{r} \right| \vec{k}, \quad \vec{r} \in S_r \tag{11}$$

The condition $\vec{r_s} \in S_a$ should be true for all $\vec{r} \in S_r$. The angular sector where $\vec{r_s} \in S_a$ can be obtained by geometrical construction for the concrete mutual disposition S_a and S_r. Within this sector the radiation pattern can be correctly reconstructed with an error termined by next terms of asymptotical decomposition of equation (10) (see Ref. [2]). Notice that the real angular sector is more narrow than at constructed in accordance with (11), because $\vec{r_s}$ must belong to the surface S_a together with its Fresnel's zone. The sizes of the Fresnel's zone are determined by the second derivatives of phase in under-integral expression (10). This problem has been investigated in [2].

Expression (8) can be also considered as an integral equation for the determination of the distribution of the elementary sources of definite type (in our case - monopolar sources) on a radiator. Unlike the problem of far field reconstruction which can be solved exactly, the problem of source distribution reconstruction is non-correct and its solution depends on the choice of the surface S_r and the type of elementary sources. The corollary of non-correct statement problem is a determination of smoothed estimate instead of function $\widehat{m_f}(\vec{r})$:

$$\widehat{m_f}\left(\vec{r}\right) = \int \int_{S_r} m_f(\vec{r'}) F_f\left(\vec{r}, \vec{r'}\right) dS_r \tag{12}$$

where F_f is a function with well-outlined global maximum in the enviroment of the point r: $\left| \vec{r} - \vec{r'} \right| < \Delta, \quad \Delta \geq \lambda/2$. A linear integral

transformation of the spectral component of near-field data corresponds to equation (12):

$$\widehat{m_f}\left(\vec{r}\right) = \int\int_S p\left(f,\vec{r_s}\right) G_f\left(\vec{r},\vec{r_s}\right) dS, \tag{13}$$

$$F_f\left(\vec{r},\vec{r}\right) = \int\int_S G_f\left(\vec{r},\vec{r_s}\right) \frac{e^{ik_o\left|\vec{r'}-\vec{r_s}\right|}}{\left|\vec{r'}-\vec{r_s}\right|} dS \tag{14}$$

The type of the kernel G_f is set in from the obvious requirements to the function F_f. These ones are a minimum width of the main maximum and low level of sidelobes. Besides that, the normalization condition should be satisfied, for instance:

$$\int\int_{S_r} F_f\left(\vec{r},\vec{r'}\right) dS_r' = 1 \quad for\ all\ \vec{r}\in S_r \tag{15}$$

Consider the plane surface $S(z = 0)$ in the Cartesian coordinate system (x, y, z) as an example. Assume that all sources of the monopolar type are concentrated in the semi-infinite space $z \geq z_o$. The Fourier transformation of the pressure $p_f(x, y)$ measured on the plane $z = 0$ can be presented as:

$$\int\int_{-\infty}^{+\infty} p_f(x,y) e^{-i(k_x x + k_y y)} dx dy = 2\pi M_f(k_x, k_y, -K) \frac{e^{iz_oK}}{iK}$$
$$k_x^2 + k_y^2 < k_o^2 \tag{16}$$

where $K = \left(k_o^2 - k_x^2 - k_y^2\right)^{1/2}$ is a positive branch of the root, $M_f(k_x, k_y, k_z)$ is a three-dimensional Fourier transformation of the three-dimensional distribution of the sources in the semi-infinite space. As it follows from (16), inside the circle $k_x^2 + k_y^2 < k_o^2$ the measured data contain the information only about the values of M_f on the sphere $k_x^2 + k_y^2 + k_z^2 = k_o^2$. Thus, the three-dimensional distribution of sources can't be reconstructed by a single way. Outside the circle $\left(k_x^2 + k_y^2 > k_o^2\right)$ the Fourier transformation of p_f decreases exponentially if $|M_f|$ is finite. It means that for $k_o z_o \gg 1$ the measured data don't contain the information about the m_f components which oscillate with a period less than λ. Then the external sources of acoustic field can be both the scalar sources (mass sources in the Euler equation) and the external forces $\vec{f_f}$. Having been composed the Fourier image of monopolar sources

and a scalar product $\left(\vec{k}, \vec{F}_f \left(\vec{k} \right) \right)$ (where $\vec{F}_f \left(\vec{k} \right)$ is a Fourier-image of the three-dimensional distribution of the external forces), $M \left(\vec{k} \right)$ can't be separated into four components. Thus, the additional a priori information about the surface S_r, where elementary sources are disposed, and about the types of elementary sources must be used for the acoustic image reconstruction.

Choose a plane $z = z_o$ as a surface S_r. In this case this function M_f doesn't depend on k_z: $M_f \left(k_x, k_y, k_z \right) \to M_f \left(k_x, k_y \right)$ and the Fourier image $P_f \left(k_x, k_y \right)$ of the function $M_f \left(k_x, k_y \right)$ can be considered as a estimate $\widehat{m_f}$:

$$
P_f \left(k_x, k_y \right) = \left\{ \begin{array}{ll} 1, & k_x^2 + k_y^2 \le k_o^2 \\ e^{-2z_o \sqrt{k_x^2 + k_y^2 - k_o^2}}, & k_x^2 + k_y^2 > k_o^2 \end{array} \right. \tag{17}
$$

Then,

$$
G_f \left(\vec{r}, \vec{r}_s \right) = -\frac{1}{4\pi^2} \frac{\partial^2}{\partial z^2} \left\{ \frac{e^{-ik_o \left| \vec{r}_s - \vec{r} \right|}}{\left| \vec{r}_s - \vec{r} \right|} \right\}_{z=z_o}
$$

$$
\simeq \frac{k_o}{4\pi^2} \frac{z_o^2}{\left| \vec{r}_s - \vec{r} \right|^4} \frac{e^{-ik_o \left| \vec{r}_s - \vec{r} \right|}}{\left| \vec{r}_s - \vec{r} \right|},
$$

$$
k_o z_o \gg 1 \tag{18}
$$

and $F_f \left(\vec{r} - \vec{r}' \right)$ which is a Fourier transformation of the function $P_f \left(k_x, k_y \right)$ correspond to this estimate. For $k_o z_o \gg 1$ we have:

$$
F_f \left(\vec{r} - \vec{r}' \right) \simeq \frac{k_o^2}{2\pi} \frac{J_1 (v)}{v}, \quad v = k_o \left| \vec{r} - \vec{r}' \right| \tag{19}
$$

where $J_1 (v)$ is a Bessel function of the first order. The main lobe width of the function F_f (for the level half as much as maximum value) is $\Delta = 0,7\lambda$.

For arbitrary smooth surfaces S and S_r G_f can be choosen as:

$$
G_f \left(\vec{r}, \vec{r}_s \right) = k_o B \left(\vec{r}, \vec{r}_s \right) \frac{e^{-ik_o \left| \vec{r}_s - \vec{r} \right|}}{\left| \vec{r}_s - \vec{r} \right|}, \tag{20}
$$

where the function B is a smoothly changing function depending on the coordinates $\vec{r}, \vec{r}_s$. The required type of smoothing function F_f can be synthesized from the function B. Notice that formula (20) presents a well-known principle of focusing on source displaced near receiving aperture (see Ref. [2]).

The above-mentioned measured data processing procedure in the frequency domain can be transformed into the time domain. For instance, for the plane surface S the following equation can be used instead of the equations (1), (3) with substituting (4) (see Ref. [8]):

$$q(t, \vec{k}) = \frac{\left(\vec{n}, \vec{k}\right)}{2\pi c} \frac{d}{dt} \int \int_S \mathrm{p}\left(t - t_o + \frac{1}{c}\left(\vec{k}, \vec{r}_s\right), \vec{r}_s\right) dS,$$

$$R_f\left(\vec{k}\right) = \int q(t, \vec{k}) e^{2\pi i f t} dt, \qquad (21)$$

where t_o is some constant time delay. The analogous transformation can be deduced for the approximation (18) or for the estimate of time distribution of the monopolar sources on a radiator $\widehat{m}\left(t, \vec{r}\right)$:

$$\widehat{m}\left(t, \vec{r}\right) =$$

$$\frac{1}{2\pi c^2} \frac{d^2}{dt^2} \int \int_S B\left(\vec{r}, \vec{r}_s\right) \mathrm{p}\left(t - t_o + \frac{1}{c}\left(\left|\vec{r} - \vec{r}_s\right|\right), \vec{r}_s\right) \frac{\cdot dS}{\left|\vec{r} - \vec{r}_s\right|} \qquad (22)$$

The estimate $\widehat{m}\left(t, \vec{r}\right)$ can be decomposed into the spectral components $\widehat{m}_f\left(\vec{r}\right)$ (12) by the Fourier transformation. However, the estimate $\widehat{m}\left(t, \vec{r}\right)$ has independent scientific interest for the investigation of non-stationary processes, such as the process of short duration.

The transformations (21) and (3), (1),(4) are equivalent but the structure of the signal processor realizing (21) differs from realizing (1), (3). Thus, the choice of the transformation type can be made from the avaliability of hardware and software. Besides that, we shall show below that in the time domain the signal processing procedures can be generalized for moving radiators more easily.

In general case, for instance, for cylindrical surface the transformations in time domain do not correspond to the procedures with time delays (as in (21) or (22)) because of complex frequency dependence of (5). In similar cases we do not need to in time domain.

In many practical situation the received acoustic signals are random and stationary. So the second statistical moment must be determined as:

$$Q\left(\vec{k}\right) = E\left\{\left|R_f\left(\vec{k}\right)\right|^2\right\}, \; K_f\left(\vec{r},\vec{r'}\right) = E\left\{m_f\left(\vec{r}\right)m_f^*\left(\vec{r'}\right)\right\}, \quad (23)$$

where $E\{...\}$ is a expectation operator (we assume that $E\{R_f\} = E\{m_f\} = 0$). We also assume that the processes are ergodic so that we can average in time domain. Expression (1) is replaced by:

$$p_j\left(f,\vec{r_s}\right) = \int_0^T \mathrm{p}\left(t + jT_1, \vec{r_s}\right)e^{2\pi i f t}dt, \quad j = 0, 1, ...J - 1 \quad (24)$$

where T defines a resolution in frequency domain, $T_1 \approx (0, 5...1)T$. Then, the functions $R_{f,j}\left(\vec{k}\right)$, $\widehat{m_{f,j}}\left(\vec{r}\right)$ are estimated and averaged:

$$\widehat{Q}\left(\vec{k}\right) = \frac{1}{J}\sum_{j=0}^{J-1}\left|R_{f,j}\left(\vec{k}\right)\right|^2,$$

$$\widehat{K_f}\left(\vec{r},\vec{r'}\right) = \frac{1}{J}\sum_{j=0}^{J-1}\widehat{m}_{f,j}\left(\vec{r}\right)\widehat{m}_{f,j}^*\left(\vec{r'}\right) \quad (25)$$

We would like to add that the resolution for the estimates $\widehat{Q}$, $\widehat{K}$ in frequency domain is determined by not only the time interval T but also receiving system sizes, distance between radiator and antenna and so on.

3. The case of an essentially oblong radiator

Consider a radiator which is essentially oblong along one of the coordinate axes and sensors which are disposed on a streight line. In this case the exact solution is possible if the radiator field has an axial symmetry or if elementary sources of known type are disposed, for example, on a segment of the streight line.

Assume that the radiator field has an axial symmetry relative to axis which is parallel to a line of sensor disposition and is y_o distant away from sensors. The field spectral components on the line of sensor disposition $p(f, x)$ can be connected with the far field $R_f(\vartheta)$ by the relation analogous to (3):

$$R_f(\vartheta) = \int p(f, x)\gamma_f(\vartheta, x)dx \quad (26)$$

where x is a coordinate on the sensor line, the angle ϑ is measured from a normal to the field symmetry axis. The function γ_f is defined by (5) because the field can be continued on the cylindrical surface S of radius y_o through the axial symmetry: $p(f, x) \rightarrow p(f, x, \varphi_s)$, where $p(f, x, \varphi_s)$ doesn't depend on the angle φ_s. Substituting (5) in (3) and integrating over φ_s, we obtain [8]:

$$\gamma_f(\vartheta, x) = e^{-ik_o x \sin \vartheta} / \left(i\pi H_o^{(1)}(\omega) \right), \quad \omega = k_o y_o \cos \vartheta \qquad (27)$$

For the perpendicular disposition of symmetry axis and sensor line, cutting at the point $x = 0$, the field p_f can be continued on the plane S which is perpendicular to the symmetry axis: $p_f \rightarrow p(x, \varphi_s)$, where $x > 0, \varphi_s$ is an angle in a polar coordinate system. Substituting (4) in (3) and integrating over φ_s, we have:

$$\gamma_f(\vartheta, x) = ik_o x |\sin(\vartheta)| J_o(k_o x \cos \vartheta), \quad x > 0 \qquad (28)$$

where $J_o(z)$ is a Bessel function of the zero order. Notice that an additional field symmetry relative to the anfle $\vartheta = 0$ follows from (28). The kernel of the transformation (26) can be changed if it is assumed that all elementary sources are concentrated on the symmetry line on the same side from the cutting point $x = 0$.

Expressions (26), (27) can be used when the radiator field has no circular symmetry. In this case the calculated function $R_f(\vartheta)$ is a radiation pattern section by the plane where radiator axis and parallel sensor line lie. For the radiators with sizes $L_r \times L_\perp$ (where L_r is a size along sensor line, $L_\perp$ is a size across sensor line, $L_r \gg L_\perp$) $R_f(\vartheta)$ is a direction pattern section if the following condition is satisfied:

$$2L_\perp^2/\lambda \leq y_o \qquad (29)$$

It means that sensors are in far zone relative to cross radiator size. If the small cross size radiator has multipole sources, for low-order multipoles the condition $\lambda \leq y_o$ must be satisfied instead. In particular, if radiator is a dipole oriented perpendicularly to the sensor line, it may be shown that the calculated section:

$$|R_f(\vartheta)|^2 = P_f \cos^2 \vartheta \left| H_1^{(1)}(\omega) / H_o^{(1)}(\omega) \right|^2 \qquad (30)$$

where P_f is a constant proportional to the radiation power for the frequency f, differs from the exact section of the dipole radiation pattern $\left| R_f^{(d)}(\vartheta) \right|^2 = P_f \cos^2 \vartheta$. For $\omega \geq 2...3$ we have:

$$\left| H_1^{(1)}(\omega) / H_o^{(1)}(\omega) \right|^2 = 1 + \frac{1}{2\omega^2} + o\left(\frac{1}{\omega^4} \right) \qquad (31)$$
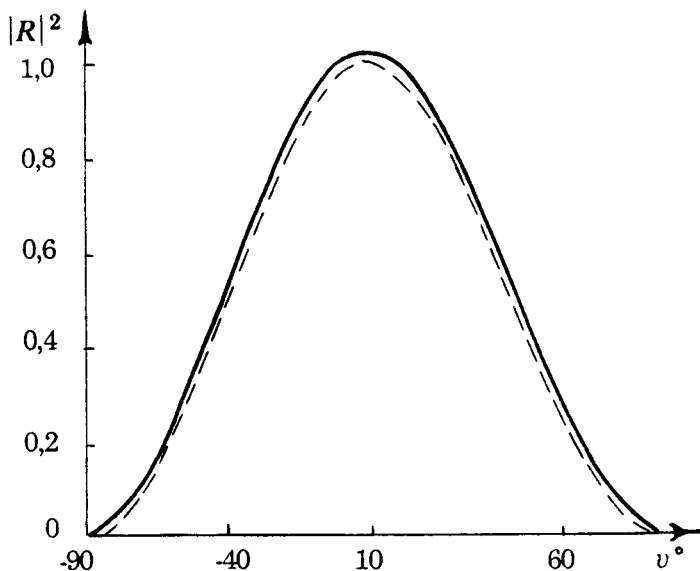
Fig.2 The radiation pattern of the dipole: reconstructed (———) and exact (— — — —).

and can neglect a difference between $|R_f(\vartheta)|$ and $\left|R_f^{(d)}(\vartheta)\right|$. Figure 2 shows the functions $|R_f(\vartheta)|^2$ and $\left|R_f^{(d)}(\vartheta)\right|^2$ as functions of the angle ϑ for $y_o/\lambda = 1$. We can see a good coincidence.

The analogous relations can be easily deduced for multipoles of any orders. The analysis of quadropole relations has shown that the good reconstruction accuracy is reached for $y_o \geq (0,6...1)\lambda$. See Fig. 3 for quadropole with the axis perpendicular to the sensor line and $y_0/\lambda = 0,4$.

Apparently, the cases of parallel and perpendicular dispositions of sensor line and symmetry axis exhaust the possibilities of the deduc-
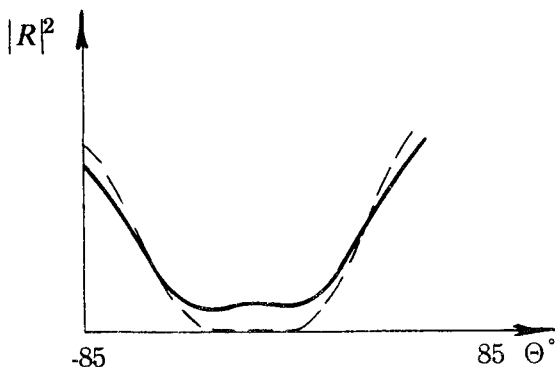
$|R|^2$

-85   85 Θ°

Fig.3 The radiation pattern of the quadropole with the axis perpendicular to the sensor line: reconstructed (_____) and exact (— — ——).

tion of the exact formulae for γ_f. However, for practical goals it is important that the function γ_f be known for an arbitrary disposition of radiator and the sensor line. Consider the analogy of Eq. (10) for a priori unknown distribution of monopole sources on the streight line:

$$\int \gamma_f(\vartheta, x) \frac{e^{ik_o\rho(x,y)}}{\rho(x,y)} dx = e^{-ik_o y \sin \vartheta}, \qquad (32)$$

where y is a current coordinate along the source disposition line, $\rho(x, y)$ is a distance between the point with the coordinate x on the sensor line and the point with the coordinate y on the source line.

Introduce two parallel planes P_1 (where the source line L_1 is disposed) and P_2 (where the sensor line L_2 is disposed) which are Δh apart. Introduce also the Cartesian coordinate system (x, y) in the plane P_2. The axis x coincides with the line L_2 (see Fig. 4). Then, the distance $\rho(x, y)$ is:

$$\rho(x,y) = \left[\Delta h^2 + (y - \omega)^2 + z^2\right]^{1/2},$$
$$w = x \cos \alpha - (y_o \sin \alpha + x_o \cos \alpha), \qquad (33)$$
$$z = x \sin \alpha + (y_o \cos \alpha - x_o \sin \alpha)$$

where α is an inclination angle of the projection of line L_1 into the
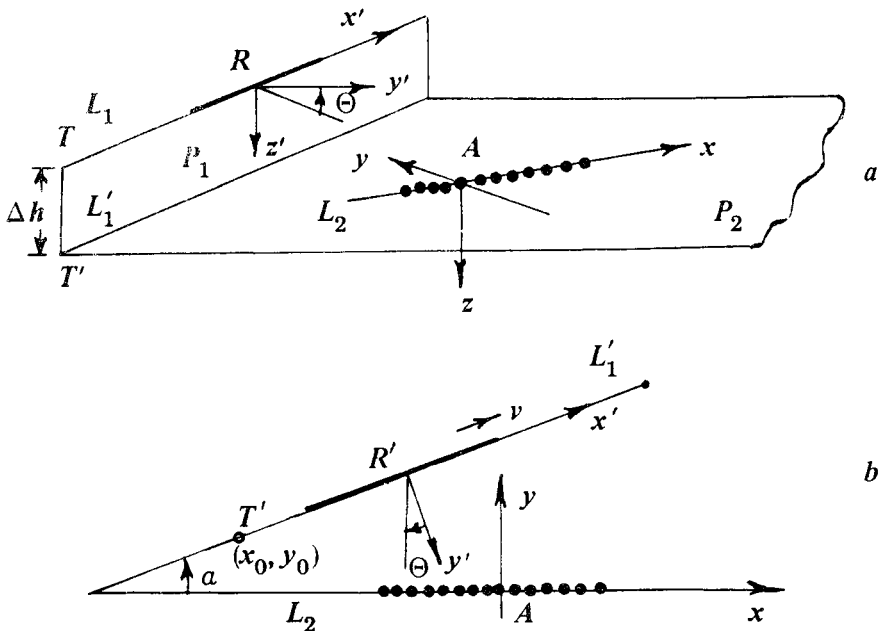
Fig.4 The mutual disposition of the radiator R and antenna A: general view (a) and the projection on the plane P_2.

plane P_2 to the line L_2. The angle ϑ is measured from the normal to the line L_1 in the plane which is parallel to the plane P_2.

Using the method of the approximate solution of the integral equation (32) (see Ref.[6]), we obtain:

$$\gamma_f(\vartheta, x) \simeq \gamma_f^{(HF)} = \sqrt{\frac{\beta(\vartheta, x)}{\lambda}} e^{-ik_o l(\vartheta, x) - i\pi/4}, \tag{34}$$

where

$$\beta(\vartheta, x) = \frac{\left(z \sin\vartheta \sin\alpha - \cos\vartheta \cos\alpha\sqrt{z^2 + \Delta h^2}\right)^2}{\cos\vartheta\sqrt{z^2 + \Delta h^2}}, \tag{35}$$

$$l(\vartheta, x) = w \sin\vartheta + \cos\vartheta\sqrt{z^2 + \Delta h^2} \tag{36}$$

Note the following prorerties of the obtained solution. Function (34) is not changed and independent on x item appears in function (34) if the substitution $x_o \to x_o + r\cos\alpha$, $y_o \to y_o + r\sin\alpha$ (i.e. the slip of coordinate beginning along the line L_1) occurs. Thus, if $|R_f(\vartheta)|^2$ is determined, the transformation (26), (34) doesn't depend on the position of coordinate beginning on the line L_1. For $\alpha = 0^o$ the expression (34) and (27) are the same, if the Hankel's function in (27) $H_o^{(1)}(\omega) \simeq \sqrt{2/\pi\omega}\exp(i\omega - i\pi/4)$, y_o is replaced by $\sqrt{z^2 + \Delta h^2}$ and $x_o = 0$. The property allow to estimate the applicability limits for (34). Using (34) and (32), we can find an angular sector where the direction pattern is correctly reconstructed for finite number of sensors.

Assume that the sensors are disposed on a segment $[-L_a/2, L_a/2]$ of the line L_2, where L_a is a receiving antenna length. Also assume that the elementary sources are disposed on a segment of the line L_1 with length L_r (L_r is a radiator length). The radiator center is displaced for the distance d relative to the coordinate beginning. Realizing the geometrical construction described in the Section 2, we obtain that $\vartheta_1(d) < \vartheta < \vartheta_2(d)$, where:

$$\tan\vartheta_1(d) = \left(r_1^2 - r_{1_b}^2 + L_r^2\right) / \sqrt{2r_{1_b}^2\left(r_1^2 + L_r^2\right) - r_{1_b}^4 - \left(r_1^2 - L_r^2\right)^2}$$
$$\tan\vartheta_2(d) = \left(r_{2_b}^2 - r_2^2 - L_r^2\right) / \sqrt{2r_{2_b}^2\left(r_2^2 + L_r^2\right) - r_{2_b}^4 - \left(r_2^2 - L_r^2\right)^2}$$
$$r_1^2 = \Delta h^2 + \left(x_o + (d - L_r/2)\cos\alpha + L_a/2\right)^2 + \left(y_o + (d - L_r/2)\sin\alpha\right)^2$$
$$r_{1_b}^2 = \Delta h^2 + \left(x_o + (d + L_r/2)\cos\alpha + L_a/2\right)^2 + \left(y_o + (d + L_r/2)\sin\alpha\right)^2$$
$$r_2^2 = \Delta h^2 + \left(x_o + (d + L_r/2)\cos\alpha - L_a/2\right)^2 + \left(y_o + (d + L_r/2)\sin\alpha\right)^2$$
$$r_{2_b}^2 = \Delta h^2 + \left(x_o + (d - L_r/2)\cos\alpha - L_a/2\right)^2 + \left(y_o + (d - L_r/2)\sin\alpha\right)^2$$
$$(37)$$

If $\vartheta_1 > \vartheta_2$, the point of the stationary phase does not belong to the interval $[-L_a/2, L_a/2]$, so that the direction pattern can not be reconstructed. Formula (37) is essentially simplified for $\alpha = 0$. Substituting $x_o = 0$ and $y_1 = \sqrt{y_o^2 + \Delta h^2}$, we obtain:

$$\tan\vartheta_{1,2} = \left(d \mp (L_r - L_a)/2\right)/y_1 \qquad (38)$$

Angles ϑ_1, ϑ_2 are shown in Fig. 5. It follows from (37) and Fig. 5, that the receiving antenna must be longer than the radiator: $L_a > L_r$ (in the opposite case the condition $\vartheta_1 < \vartheta_2$ is not satisfied). The area of the plane (d, ϑ) limited by curves $\vartheta = \vartheta_1(d)$ and $\vartheta = \vartheta_2(d)$ is shown in Fig. 5. Let us assume that the radiator moves along the line L_1. We can conclude from Fig. 5 that the angular sector $[\vartheta_1, \vartheta_2]$ displaces such a way that it overlaps almost all angular sector $[-90^o, 90^o]$ for

ample length of radiator trajectory. On the other hand, some interval $[d_1, d_2]$ of the radiator center positions within the line L_1, for which the direction pattern $R_f(\vartheta)$ can be correctly reconstructed, corresponds to each angle ϑ. If the radiator moves with a constant velocity v, a time interval $(d_2 - d_1)/v$ can be divided into a time windows T (see (24)) for the spectral analysis and calculation of $|R_{f,j}(\vartheta)|^2$ (j is a number of the time windows) can be averaged over j.

In Section 2 we have remarked that the angular sector where the direction pattern is reconstructed with a small error is more narrow than that determined by the geometrical construction, because the point of the stationary phase for the integral (10) and its enviroment must belong to the integration region $[-L_a/2, L_a/2]$. More precise definition of the angular sectors has been fulfilled by numerical simulation. Integral (26) has been replaced by a sum:

$$|R_{f,j}(\vartheta)|^2 = \left|\overrightarrow{\gamma}_f^T(\vartheta)\,\overrightarrow{p}_f\right|^2, \tag{39}$$

where $\overrightarrow{p}_f = \|p_f(x_n)\|^T$, $\overrightarrow{\gamma}_f(\vartheta) = \Delta_a\|\gamma_f(x_n,\vartheta)\|^T$ are column-vectors with length N_a, superscript T denotes transpose, x_n is a coordinate of sensor n, Δ_a is a sensor distance (in our numerical simulation $\Delta_a = 0,5\lambda$). The vector $\overrightarrow{p}_f$ has been calculated for a set of discrete monopole sources with complex amplitudes $m_{f,n}$ disposed at the points y_n of the line L_1, where $n = 1,...N_r$, a distance between point y_{n+1} and y_n is $\Delta_r \ll \lambda$. Then, $\overrightarrow{p}_f = G_f\,\overrightarrow{m}_f$, $\overrightarrow{m}_f = \|m_{f,n}\|^T$, $G_f = \|\exp(ik_o\rho(x_n,y_n))/\rho(x_n,y_n)\|$ is a $N_a \times N_r$-matrix and $\rho(x,y)$ is determined by (33). The calculations have been fulfilled for the following types of the covariance matrixes of complex amplitudes:

$$M = \begin{cases} I & (a) \\ \overrightarrow{m}_o\,\overrightarrow{m}_o^H & (b) \end{cases} \tag{40}$$

where I is an identical matrix, $\overrightarrow{m}_o = \|\exp(-ik_o y_n \sin\vartheta)\|^T$, superscript H denotes conjugate-transpose. The case (a) corresponds to the spatially non-coherent radiator, the case (b) corresponds to spatially coherent radiator phased relative to the angle ϑ. Obviously, the exact value $|R_f(\vartheta)|^2$ is a constant: N_r for the case (a) and N_r^2 for the case (b). The areas of the plane (ϑ, d) where the difference between reconstructed and actual $|R_f(\vartheta)|^2$ is less than 10% are shown in Fig.5.

It can be shown that these areas practically coincide for the models (a) and (b) and slightly differs from the limits obtained from geomet-
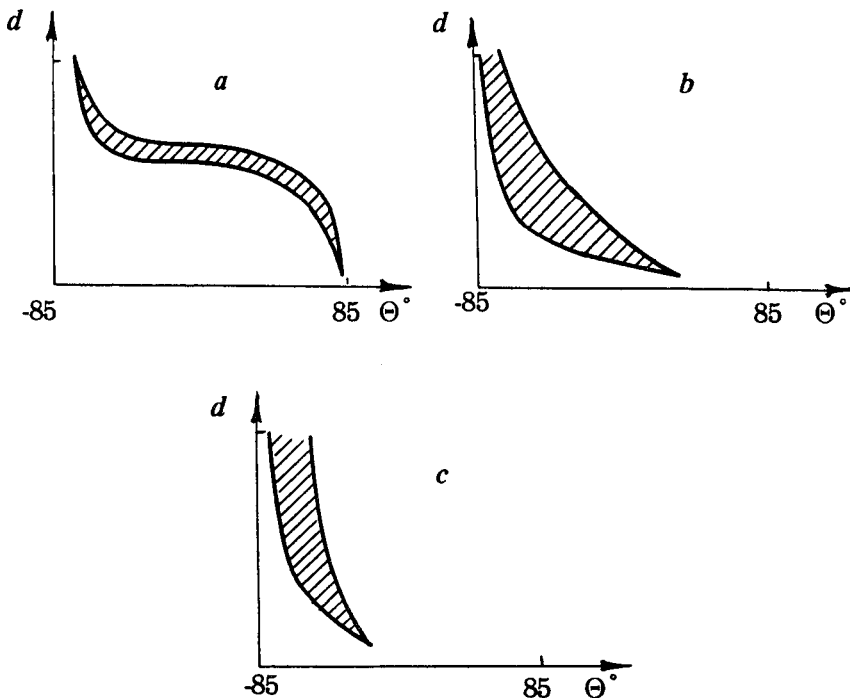
Fig.5 The dependence of the angles ϑ_1 (left curve) and ϑ_2 (right curve) on the current position of the radiator center d: $\alpha = 0°$ (a), $\alpha = 45°$ (b), and $\alpha = 90°$ (c). The difference between ϑ_2 and ϑ_1 representes the angular sector in which the far–field pattern are reconstructed correctly. The areas where the difference between reconstructed and actual far–field pattern is less then 10% are shown in a dark color.

rical expantions (37) even for $L_r < 3\lambda$. The difference decreases if the ratio L_r/λ increases.

Finally, the method of the direction pattern measurement by a linear array for the moving radiator with an arbitrary frequency spectrum is realized by the following way. For each angle ϑ in far zone the interval of radiator center dispositions $[d_1, d_2]$ relative to the receiving antenna is found (see Fig. 5). The time interval corresponding to $[d_1, d_2]$ is divided into the analysis windows T. Each spectral component of the near field is transformed in $R_{f,j}(\vartheta)$ (where j is a number of time window) by (24), then $|R_{f,j}(\vartheta)|^2$ is averaged over j.

The estimation of the intensity distribution of the monopole sources can be obtained by analogy with (18). It has been shown in the case of $\alpha = 0$ (see Ref. [4]) that the spatial resolution interval Δx_r is estimated as

$$\Delta x_r = \frac{\lambda}{|\sin \Psi_1 - \sin \Psi_2|} \tag{41}$$

where $\sin \Psi_{1,2} = (L_a/2 \mp d)/\sqrt{y_1^2 + (L_a/2 \mp d)^2}$. This result is in a good agreement with (38) because if the harmonic component in the spatial monopol distribution on the radiator is unresolved then the contribution of this component in the reconstructed far-field is negligible small.

Conclusion

The integral transform methods were developed for the far–field reconstruction and source distribution determining from the near–field measurements in the case of broadband acoustic radiator. It has been shown that the developed technique is highly effective when various limitations of the near–field method are investigated. The dependence of the reconstruction quality on the kernel approximations and finite length of the receiving array was considered. The radiator movement was allowed as the mutual displacement of the receiving array and radiator only: the frequency spectra transformation was not taken into account but this effect can be considered using the same integral transform technique. Some experimental results see, for example, in Ref. [9].

Finally, by ending the paper, one remarks, that the other approach of the near–field–far–field transform exists. The integral equation (8) connects the source distribution and the near–field data can be rewritten into a linear equation system which solvs by the various statistic methods [6,7]. The results of the reconstruction must be in a

good agreement but an arbitrary form of the linear equations permits the more realistic propagation model as the free space. However the analysis of the method limitations is not obvious in comparison with the integral transform technique. So, the both approaches can supplement each other.

REFERENCES

1. *D.M.Kerns* Plane–wave scattering–matrix theory of antennas and antenna-antenna interactions. NBS Monograph. 162, U.S.Gouvt. Printing Office, Washington, DC, 1981.
2. *L.N.Zakharjev, A.A.Lemansky, V.I.Turchin etc.* The microwave antenna measurement methods. /Ed. by N.M.Zeitlin. Moscow: Radio i swjaz', 1985 (in russian).
3. *A.D.Yaghjian* An Overview of Near–Field Antenna Measurement //IEEE Trans. on Ant. and Prop., vol.AP-34, N 1, January 1986, p.30.
4. *A.L.Fogel', A.I.Knafel', B.M.Salin, L.R.Semenova, V.I.Turchin* Holographic methods for measuring characteristics of acoustic source radiation /Vibroacoustic fields of complex objects and their diagnostics. Inst. of Appl. Phys., Gorky, 1989, p.118 (in russian).
5. *V.I.Turchin, I.Sh.Fiks* The remote measurements of the radiators with the complex spatial–temporal structure. Pt.1. Basic physical principles and signal processing methods in high frequency approximation. //The tomographical methods in the physical and technical measurements. Moscow, Sci. Res. Inst. Phys. Techn. Radio Measur. (VNIIFTRI), 1990, p.159 (in russian).
6. *G.V.Borgiotti, E.M.Rosen* The determination of the far field of an acoustic radiator from sparse measurement samples //J. Acoust. Soc. Am. 92(2), Pt.1, August 1992, p.807.
7. *R.Stoughton* Optimal near–field measurements in the presence of noise and reflections //Ibid., p.831.
8. *B.M.Salin, V.I.Turchin* Holographic reconstruction of wave field with arbitrary time dependence //Akust. Jurn., 1992, v.38, N 1, p.150. (in russian).
9. *I.Sh.Fiks, N.A.Sidorovskaia and V.I.Turchin* Reconstruction of spatial-time structure of complex acoustical sources from near–field measurements // Proc. Third Int. Congress on Air- and Structure–borne Sound and Vibration, June 13-15, 1994, Montreal, Can., p.1701.